Development of Molecular System with Efficient Fluorescence On/Off Switching Behavior Based on Photochromism of Diarylethenes

March 2019

Tatsumoto Nakahama

Development of Molecular System with Efficient Fluorescence On/Off Switching Behavior Based on Photochromism of Diarylethenes

(ジアリールエテンのフォトクロミズムに基づく効率的な

蛍光オン/オフスイッチング挙動を示す分子システムの開発)

March 2019

Graduate School of Engineering

Osaka City University

Tatsumoto Nakahama

中濱　龍源

Contents

General Introduction

1. Photochromic Compounds

Photochromism is defined as a reversible transformation between two isomers having different absorption spectra upon photoirradiation. Compounds which undergo the photochromic reaction are called photochromic compounds. A photochromic compound was first reported for tetracene by M. Fritzsche in 1867.[1] It becomes colorless upon photoirradiation and it is recolorized by heating. After that, various types of artificial photochromic compounds have been synthesized and investigated.

Photochromic compounds are classified into two types, T-type (thermally reversible type) and P-type (photochemically reversible type) according to thermal stability of the photogenerated colored isomer at room temperature.[2] Figure 1a shows a typical example of T-type photochromic compounds. Azobenzene, spiropyran, salicylideneaniline, hexaarylbiimidazole, naphthopyran, and so on are classified into T-type photochromic compounds. The photogenerated colored isomers return to the initial colorless isomers by not only photoreaction but also thermal reaction at room temperature because the photogenerated isomers are thermally unstable. T-type photochromic compounds are suitable for photomodulated materials such as photochromic ophthalmic lenses.[3] However, thermal instability of colored isomers makes it difficult to quantitatively evaluate their photophysical and photochemical properties. On the other hand, P-type photochromic compounds undergo reversible photochromic reaction by only

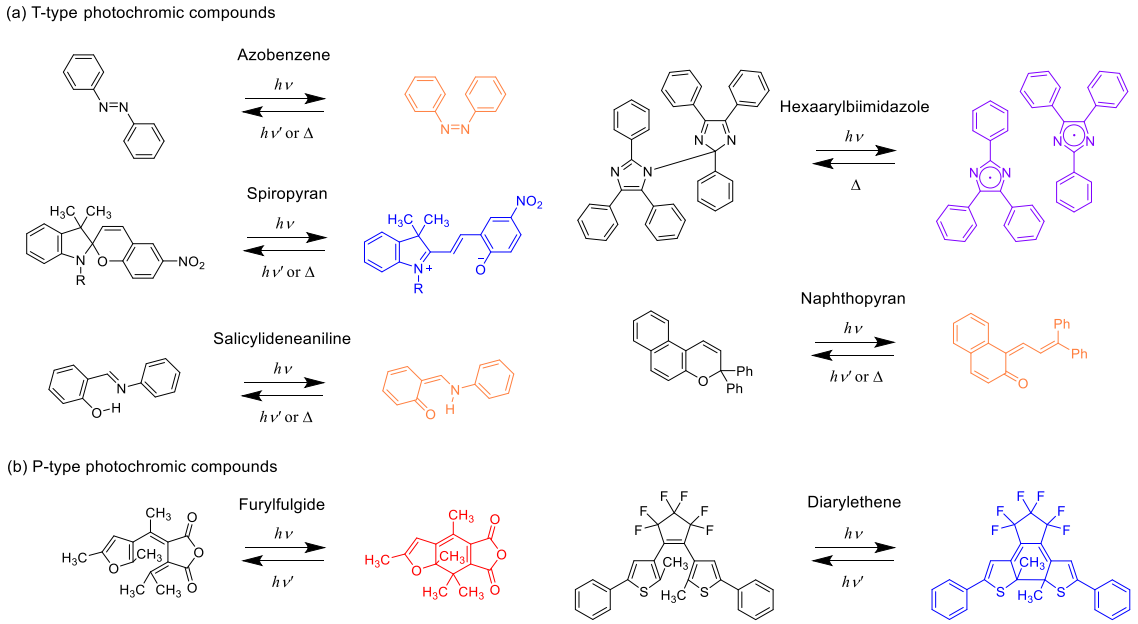

Figure 1. Typical (a) T-type and (b) P-type photochromic compounds.

photoirradiation because both the colorless and colored isomers are thermally stable at room temperature. The finding of the P-type photochromic compound leads to the development of fundamental and application researches on photochromism. In the 1980's, Irie *et al*. and Heller *et al*. reported diarylethene[4] and furylfulgide[5] classified into P-type photochromic compounds, respectively (Figure 1b). Especially, diarylethene is known as one of the most promising P-type photochromic compounds because of their excellent properties such as high durability, high sensitivity, rapid response, and reactivity in the solid state.[6] Thus, diarylethenes have potential applications as optical memories and switches,[7] and photoactuators.[8]

2. Photochromism of Diarylethenes

As mentioned above, diarylethene was first reported as P-type photochromic compound by Irie *et al*. in 1988.[4] It was serendipitously discovered in course of study on photoresponsive polymers. Diarylethene derivatives are composed of two heterocyclic aryl moieties connected to ethene moiety. Although diarylethene has a maleic anhydride in the ethene bridge in the first report, the most commonly used diarylethenes are diarylperfluorocyclopentenes which show high fatigue resistance property and can be easily synthesized. Diarylethenes undergo thermally irreversible photochromism between a colorless open-ring isomer and a colored closed-ring isomer upon alternating irradiation with ultraviolet (UV) and visible light. The photocyclization and photocycloreversion reactions are based on the Woodward-Hoffmann rule for 1,3,5-hexatriene/cyclohexadiene.[9]

The color change is due to the electronic structure change of the diarylethenes from the open-ring isomer to the closed-ring isomer.[6a] π-Conjugation of the open-ring isomer localizes in each thiophene ring, which gives the absorption spectrum in the ultraviolet region. On the other hand, in the closed-ring isomer, the HOMO-LUMO gap is small compared with the open-ring isomer because the π-conjugation delocalizes throughout the molecule. As a result, the closed-ring isomers have the absorbance in the visible light

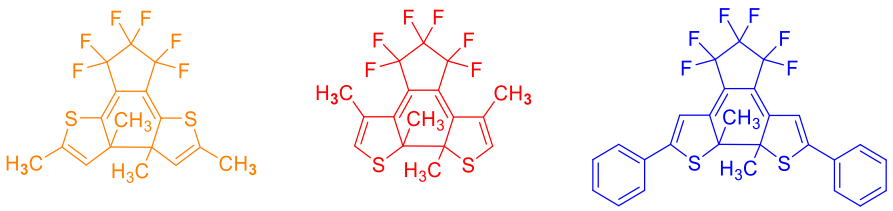

λ_{abs} = 425 nm λ_{abs} = 534 nm λ_{abs} = 575 nm

Figure 2. Molecular structures of the closed-ring isomers with different absorption maximum wavelength (λ_{abs}).

region. The color of the closed-ring isomer can be controlled by changing the molecular structure or introducing various substituent. Figure 2 shows the molecular structures of the closed-ring isomers having the different absorption maximum wavelength. When thiophene rings are connected to the ethene bridge at 2-position, the color of the closed-ring isomer is yellow with λ_{abs} at 425 nm due to the short π-conjugation localized in the central part. On the other hand, the π-conjugation delocalizes throughout the molecule in the closed-ring isomer by connecting thiophene rings to the ethene bridge at the 3-position. The long π-conjugation results in red color with λ_{abs} at 534 nm. The closed-ring isomer of the diarylethene introduced phenyl groups at the 5-position of thiophene rings shows blue color with λ_{abs} at 575 nm.

Figure 3 shows potential energy surfaces of the ground state and the excited state of diarylethene. The photocyclization reaction processes are explained by reaction paths through conical intersection.[10] The transient spectroscopic studies revealed that the photocyclization reaction takes place in less than 10 ps in solution.[11] Diarylethene open-ring isomer has two stable conformations, parallel and antiparallel conformations with the two aryl rings in mirror symmetry and in C_2 symmetry, respectively, as shown in Figure 4.[12] Only from antiparallel conformation, the conrotatory photocyclization can proceed.[9, 13] The two conformers interconvert with each other in solution. In most cases, the ratio of the antiparallel conformer relative to the parallel one is ca. 50%. In addition, the photocyclization quantum yields for most diarylethene derivatives are ca. 0.5 in solution. Therefore, improving the proportion of the antiparallel conformation can increase the photocyclization quantum yield. Various approaches to increase the

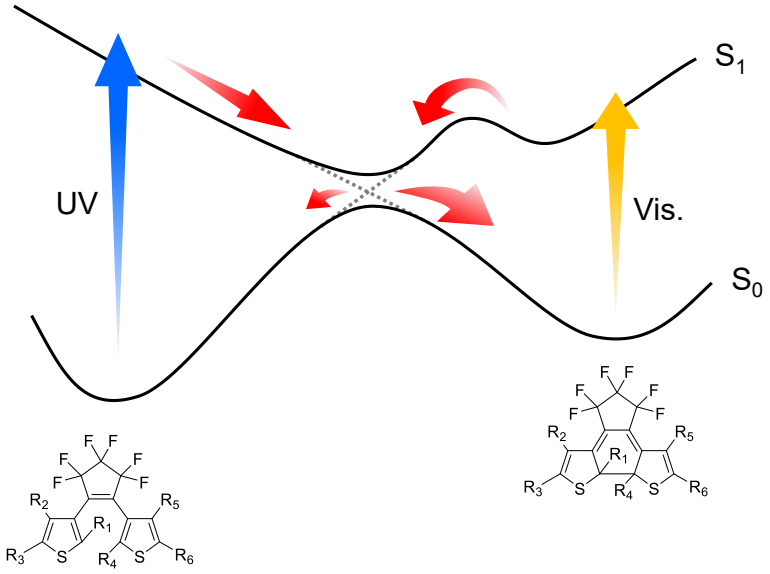

Figure 3. Potential energy surfaces of the ground state (S_0) and the excited state (S_1) of diarylethene molecule.

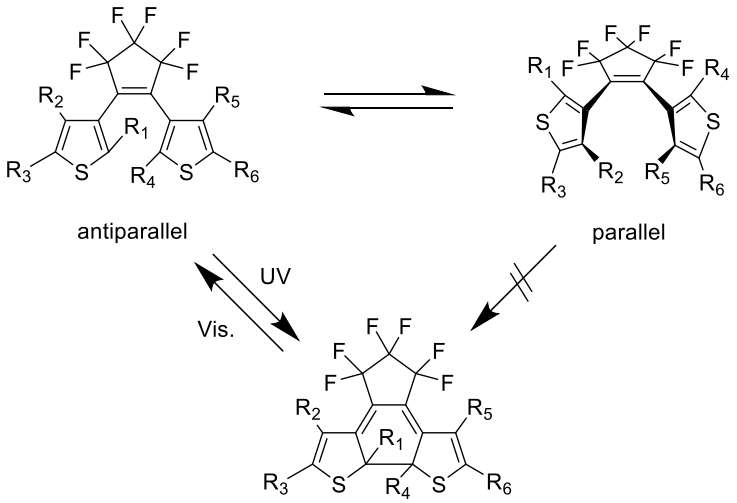

Figure 4. Two conformations of diarylethene open-ring isomer with two aryl moieties in mirror symmetry and C_2 symmetry, which are called parallel and antiparallel conformations, and photochromic reaction of diarylethene. Reprinted with permission from ref. 6b. Copyright 2014 American Chemical Society.

proportion of the antiparallel conformer, such as by introducing bulky substituents at the reactive carbons[14] and including diarylethene derivatives into cyclodextrin cavities,[15] were reported.[16] Especially, Kawai and co-workers achieved the photocyclization quantum yield of 100% by using the diarylethene derivative fixed in an antiparallel conformation by multiple intramolecular interactions including weak CH···N hydrogen-bonding interaction and S···N interaction.[17]

Photocycloreversion process of diarylethenes was studied in detail by theoretical methods, which revealed that the photocycloreversion reaction has an energy barrier in the excited state as shown in Figure 3.[18] The photocycloreversion reaction has to overcome an energy barrier to reach the conical intersection. The photocyclization quantum yield can be controlled by introducing specific substituents to the aryl groups. Diarylethenes having electron-donating substituents at the reactive carbons[19] or long π-conjugated aryl groups[20] show low photocycloreversion quantum yields. In addition, the photocycloreversion quantum yields of diarylethenes having *S*,*S*-dioxide thiophene or benzothiophene rings is strongly suppressed.[21]

Although most of the diarylethene derivatives are classified as P-type photochromic compounds, the thermal stability of a colored closed-ring isomer can be tuned by three factors:[22] (i) aromatic stabilization energy of the aryl groups,[9] (ii) electron-withdrawing substituents in the aryl groups,[23] and (iii) steric hindrance of the substituents at reactive positions[24] as shown in Figure 5. The thermal stability of the colored closed-ring isomer relates to the energy difference (ΔE) between the colored closed-ring isomer and colorless open-ring isomer in the ground state;[23b, 25] a larger ΔE leads to an increase in the thermal

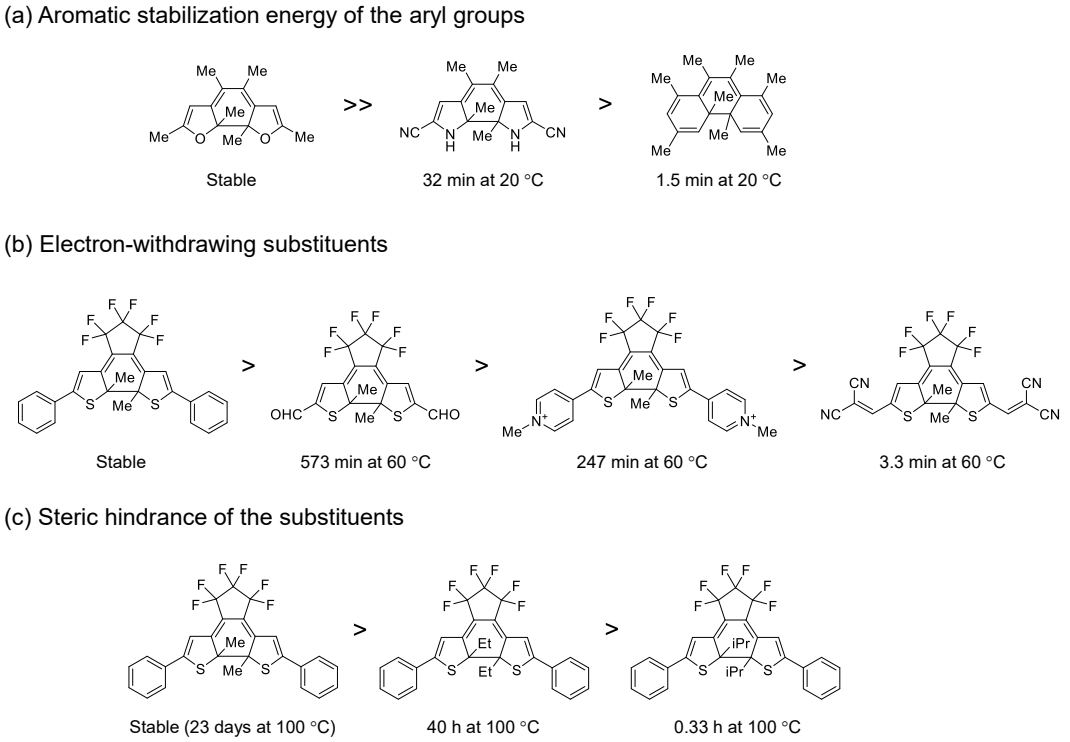

Figure 5. Thermal stability of diarylethene closed-ring isomers. The values below the molecular structures show the half-life of thermal cycloreversion. Adapted with permission from ref. 22. Copyright 2016 Wiley-VCH Verlag GmbH & Co. KGaA, Weinheim.

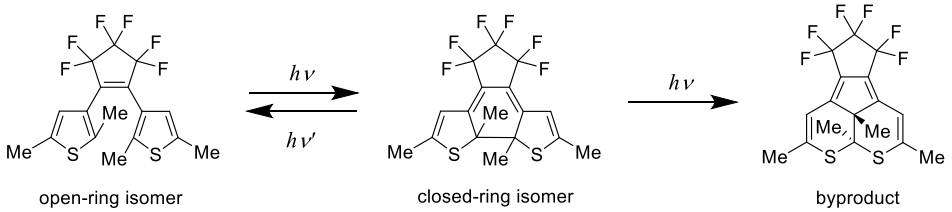

Figure 6. Byproduct formation of diarylethene upon irradiation with UV light.

cycloreversion reactivity.

Fatigue resistance is necessary for practical use of diarylethene in various application. The fatigue resistance of 1,2-bis(2-methyl-5-phenyl-3-thienyl)perfluorocyclopentene, which is one of the typical diarylethene derivatives, is high compared with the non-fluorinated diarylethene.[26] Thus, the fatigue resistance property of the diarylethene could be improved by replacing hydrogens with fluorines in the cyclopentene ring. In addition, the diarylethene derivatives substituted methyl groups at the 4-position of thiophene rings or the electron withdrawing groups at of *p*- or *m*-positions of the phenyl rings shows the higher fatigue resistance property compared with the non-substituted diarylethene.[27] However, these diarylethenes cannot repeat the photochromic reaction more than 1000 times. On the other hand, a series of diarylethenes which have benzothiophene rings as

the aryl moieties shows the high fatigue resistance property.[6a] When diarylethene closed-ring isomers are irradiated with UV light, byproducts are fabricated through radical migration (Figure 6).[28] Bianco *et al*. reported that the fatigue resistance depends on the amount of light absorbed by the closed-ring isomer rather than on the molecular structure.[29] In other words, the smaller the ratio of the absorption coefficient of the closed-ring isomer relative to that of the open-ring isomer at the excitation wavelength is, the better the fatigue resistance becomes.

Diarylethene can undergo the photochromic reaction even in solid states, such as in the crystal and the polymer film. Figure 7 shows the diarylethene crystals which can undergo photochromic reaction in the crystalline phase.[30] Upon irradiation with UV light, the colorless crystals change to yellow, red, blue, or green, depending on the molecular structure of the diarylethenes. The colors remain stable in the dark but disappear by irradiation with visible light. When the diarylethenes are packed in the antiparallel conformation and the distance between the reactive carbons is less than 4.0 Å, the photocyclization reaction in crystals takes place.[31] The cyclization quantum yields in the crystal become close to 1 (100%).[32] On the other hand, polymers bearing diarylethene derivatives in the main chain[16a, 33] or side chain,[34] and polymer films in which diarylethene derivatives are dispersed or embedded[35] are useful in terms of practical

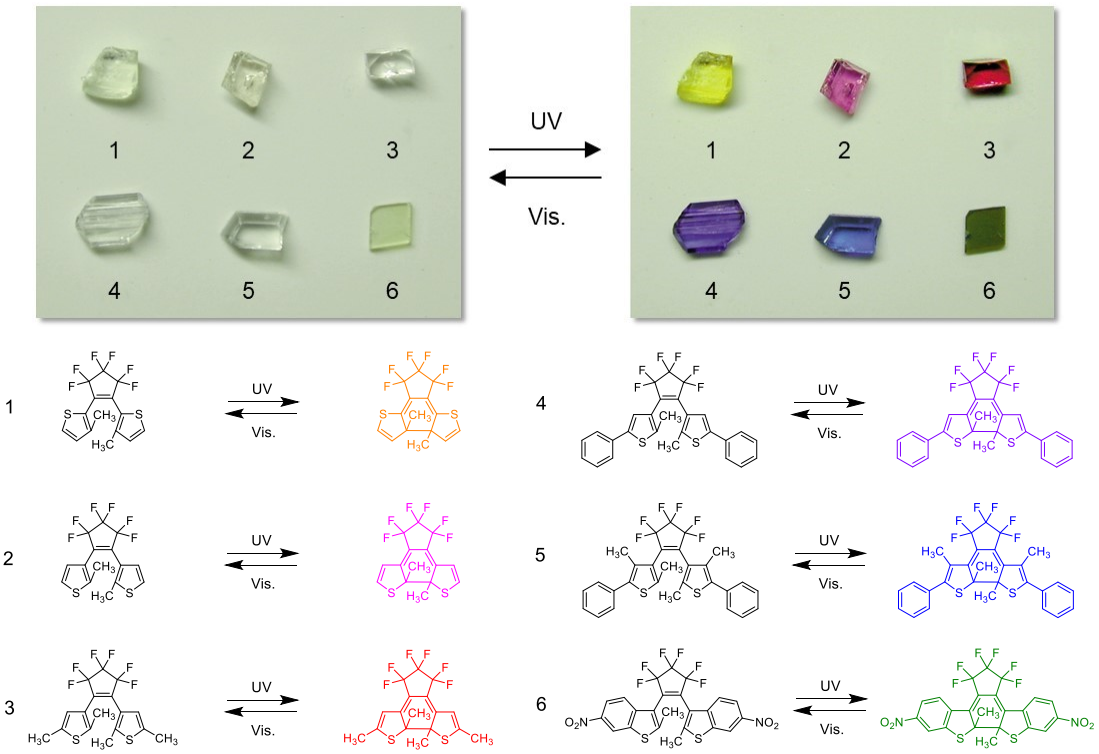

Figure 7. Photochromism of diarylethene derivatives in the single crystal. Adapted with permission from ref. 6b. Copyright 2014 American Chemical Society.

application.

As described above, a large number of researches for the photochromic properties of diarylethenes have been performed since Irie and co-workers first reported P-type photochromism of diarylethene in 1988.[4] Diarylethene derivatives can switch not only their color but also their molecular geometry,[36] fluorescence,[37] magnetism,[38] conductivity,[39] refractive index,[40] catalytic activity,[41] cytotoxicity,[42] and so on. The reversible changes of the physical or chemical properties upon the photochromic reactions can be applied to optical memory media, various photoswitching devices, and light-driven actuators.[6b]

3. Fluorescence Photoswitching of Diarylethenes

Among various fundamental and application researches on the photochromic reaction of diarylethene derivatives, fluorescence photoswitching using the diarylethene derivatives is one of the most widely investigated research fields because of the high sensitivity and ease of the observation, and the practical application such as optical memory and bioimaging.[43] Some of the diarylethenes exhibit fluorescence although most of the diarylethenes are non-fluorescent. As shown in Figure 8, the fluorescent diarylethenes are classified into three types, diarylethenes exhibiting fluorescence (i) in

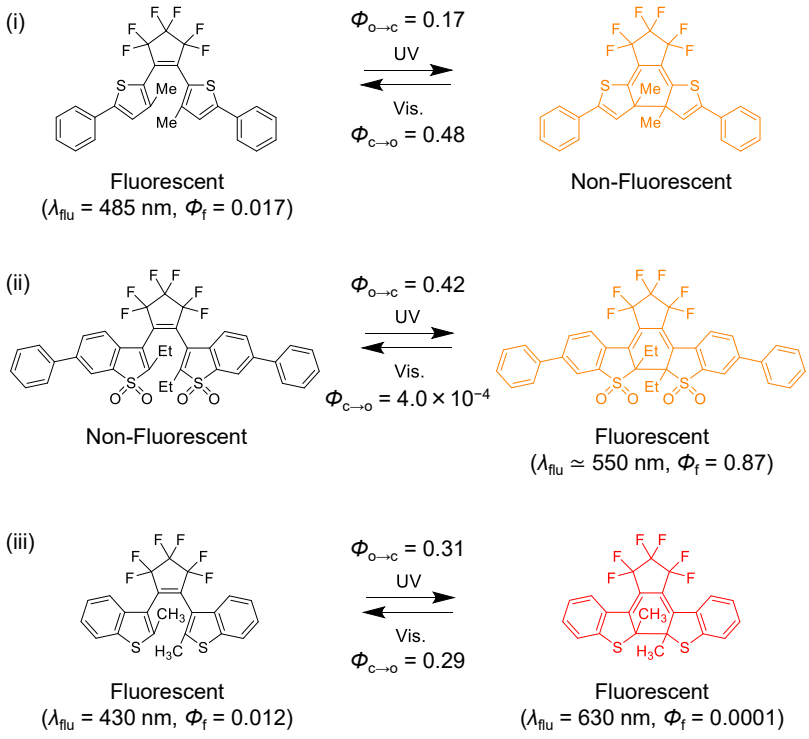

Figure 8. Diarylethenes exhibiting fluorescence (i) in the open-ring isomer, (ii) in the closed-ring isomer, and (iii) in both open- and closed-ring isomers.

their open-ring isomers, (ii) in their closed-ring isomers, and (iii) in both open- and closed-ring isomers. Their fluorescence intensity or spectrum changes upon alternating irradiation with UV and visible light, because the fluorescence properties between their open- and closed-ring forms are significantly different. As shown in Figure 9a, diarylethene open-ring isomers which have the fluorescent molecular structures in ethene bridge unit exhibit the fluorescence.[44] Moreover, diarylethene open-ring isomers also exhibit fluorescence by introducing fluorescent molecular structures, such as indole, oxazole, and pyrazole, to the aryl moiety (Figure 9b).[45] On the other hand, 1,2-bis(2-thienyl)ethenes also are one of the typical fluorescent diarylethenes as shown in Figure 9c.[37, 46] They have slightly red-shifted absorption spectra due to long π-conjugation compared with 1,2-bis(3-thienyl)ethenes in their open-ring forms, and emit blue fluorescence with λ_{flu} around 500 nm. Most of the fluorescent diarylethene open-ring isomers exhibit blue fluorescence with the fluorescence maximum wavelength (λ_{flu}) of 350-500 nm because the open-ring isomers have the absorption spectrum in the UV region

(a) Diarylethenes having the fluorescent molecular structures in the ethene moiety

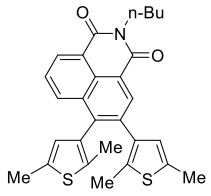

λ_{flu} = 420 nm
Φ_f = n.d.

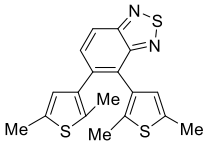

λ_{flu} = 470 nm
Φ_f = 0.077

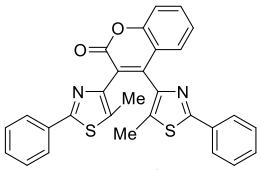

λ_{flu} = n.d.
Φ_f = 0.0025

(b) Diarylethenes having the fluorescent molecular structures in the aryl moiety

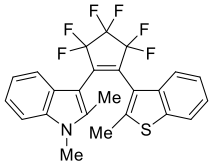

λ_{flu} = n.d.
Φ_f = 0.046

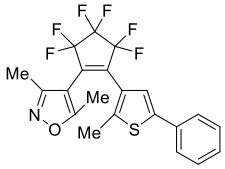

λ_{flu} = 496 nm
Φ_f = n.d.

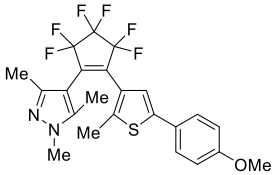

λ_{flu} = 414 nm
Φ_f = n.d.

(c) Diarylethenes with thiophene rings connected to the ethene moiety at the 2-position

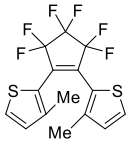

λ_{flu} = 500 nm
Φ_f = 0.01

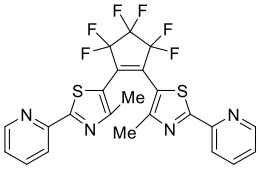

λ_{flu} = 500 nm
Φ_f = 0.005

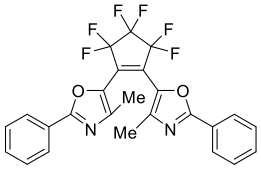

λ_{flu} = 470 nm
Φ_f = 0.19

Figure 9. Molecular structures of the diarylethenes which exhibit fluorescence in the open-ring isomer. (n.d. = no data available).

(< 400 nm). The fluorescence intensity of the open-ring isomers decreased upon irradiation with UV light. Upon irradiation with visible light, the fluorescence intensity returned to its initial one. Various types of the fluorescent diarylethene open-ring isomers were reported by a large number of researchers. However, the fluorescence quantum yields (Φ_f) of the most diarylethenes are quite low ($\Phi_f < 5\%$), which is a serious problem as a fluorescent molecule. The decrease is due to competition between the radiative process and the photocyclization or photocycloreversion reaction processes. Therefore, the high photocyclization quantum yield leads to the low Φ_f value.

The number of reports on the fluorescent closed-ring isomers is small compared with

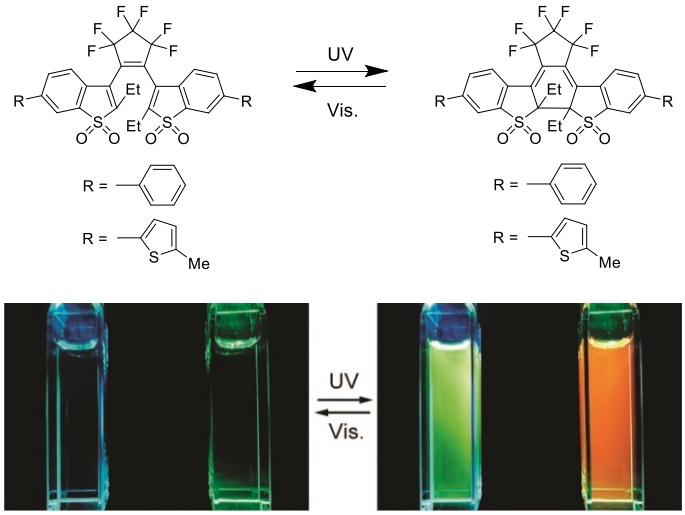

Figure 10. Molecular structures of the diarylethene derivatives which exhibit fluorescence in their closed-ring isomers and photograph of the fluorescence photoswitching upon irradiation with UV and visible light. Adapted with permission from ref. 21b. Copyright 2011 American Chemical Society.

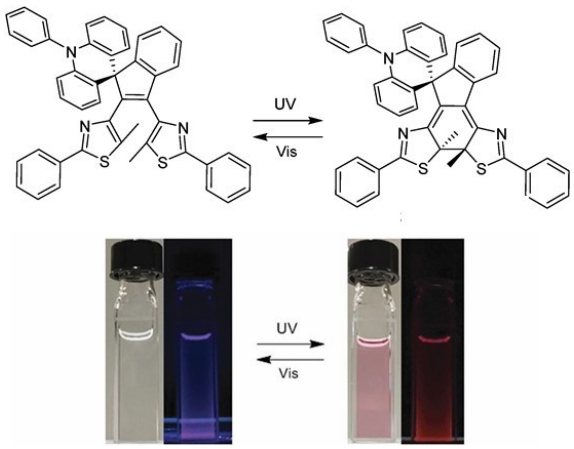

Figure 11. (a) Molecular structure of the diarylethene derivative which exhibits fluorescence in both open- and closed-ring isomers and (b) photograph of the fluorescence photoswitching upon irradiation with UV and visible light. Reprinted from ref. 52 with permission from The Royal Society of Chemistry.

the fluorescent open-ring isomers.[47] The diarylethene derivatives exhibit no fluorescence at the initial state. The fluorescence of the closed-ring isomers can be observed upon irradiation with UV light. The fluorescence spectra of the closed-ring isomer typically red-shifted in comparison with that of the open-ring isomers because the closed-ring isomers have an absorbance in the visible light region. As in the case of the fluorescent open-ring isomers, the fluorescence of the most closed-ring isomers is very weak. Ahn and co-workers reported that the Φ_f value of a diarylethene derivative, 1,2-bis(2-methyl-1-benzothiophen-3-yl)perfluorocyclopentene, closed-ring isomer was much enhanced from 0.0001 to 0.011.[48] In addition, the fluorescence of the oxidized diarylethene closed-ring isomer was further increased by replacing the methyl groups at the reactive carbons with the *n*-heptyl groups, and by introducing the acetyl groups to the 6- and 6'-positions of the *S*,*S*-dioxidized benzothiophene rings. In 2011, Irie *et al*. reported that the fluorescence performance of the oxidized diarylethene derivatives was dramatically improved by introducing both ethyl groups to 2- and 2'-positions (at the reactive carbons) and phenyl or thiophene rings to 6- and 6'-positions of the *S*,*S*-dioxidized benzothiophene groups (Figure 10).[49] The Φ_f values of the closed-ring isomers increased to ca. 0.9. However, the photocycloreversion quantum yields ($\Phi_{c\rightarrow o}$) of the oxidized diarylethenes were quite low ($\Phi_{c\rightarrow o} = 10^{-4}$-$10^{-5}$). A series of diarylethenes having benzothiophene rings as the aryl groups exhibit fluorescence in both open- and closed-ring isomers.[50] A small number of the other diarylethenes which exhibit fluorescence in both isomers were reported.[51] As shown in Figure 11, the open-ring isomer exhibits blue fluorescence. The fluorescence color changes from blue to red upon irradiation with UV light.[52]

It is difficult to obtain the fluorescent diarylethene with both high photochromic reactivity and high fluorescence quantum yield because of the competition between the radiative process and the photochromic reaction process. To overcome this point, molecular systems consisting of diarylethene and fluorophore moieties that are linked with each other through non-conjugated bonding are proposed. Diarylethene derivatives linked to fluorophore exhibit reversible fluorescence on/off switching accompanying the photochromic reactions. When diarylethene is in the open-ring form, the fluorophore exhibits fluorescence. On the other hand, when diarylethene is converted to the closed-ring form, the fluorescence is quenched. The process is based on intramolecular electron transfer (IET) or Förster resonance energy transfer (FRET) mechanism.[53]

The IET mechanism is based on changes in oxidation and reduction potentials of the diarylethene moiety.[43c] When the oxidation or reduction potential differences are large enough to induce the electron transfer between the fluorophore moiety and the open- or closed-ring isomer of the diarylethene moiety, the fluorescence on/off switching

accompanying the photochromic reaction was observed. The quenching by IET to the closed-ring isomer can avoid an undesirable photocycloreversion reaction by separating the absorption spectra of both isomers of the diarylethene and the fluorophore. Fukaminato and co-workers accomplished in designing a diarylethene-perylenebisimide dyad, which can completely avoid the photocycloreversion reaction induced by the energy transfer and exhibit the efficient reversible fluorescence on/off switching based IET mechanism.[54] However, it is difficult to design the molecular system exhibiting the fluorescence on/off switching based on the mechanism. The number of the reports on the fluorescence on/off switching by the electron transfer was limited compared with that on the FRET mechanism.[53b, 55]

Figure 12 shows a typical example of the diarylethene derivative linked to the fluorophore and schematic illustration of fluorescence on/off switching by an energy transfer.[56] When diarylethene is in the open-ring isomer, the fluorophore exhibits fluorescence. On the other hand, when diarylethene is converted to the closed-ring form, the fluorescence is quenched because of FRET process from the excited-state fluorophore to the diarylethene closed-ring isomer. Therefore, high FRET efficiency (*E*) can result in improving the fluorescence on/off switching properties such as the switching speed and the fluorescence on/off contrast. The *E* can be expressed as follows:[57]

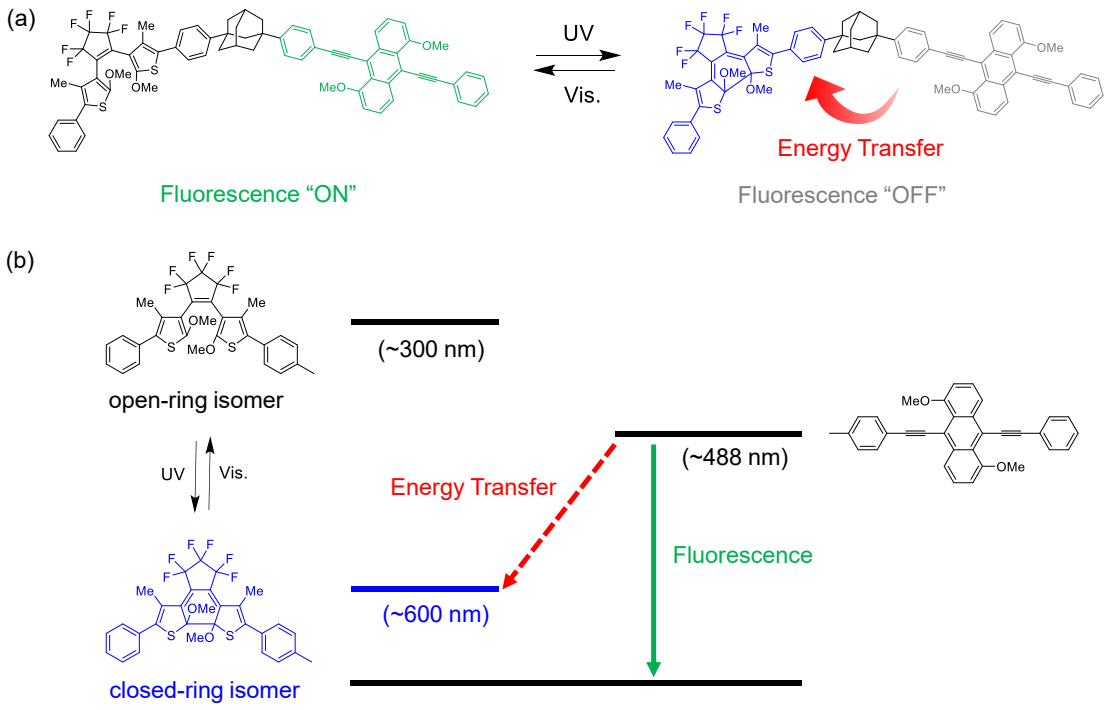

Figure 12. (a) Molecular structure and (b) schematic illustration of fluorescence on/off switching by an energy transfer. Adapted with permission from ref. 56. Copyright 2004 American Chemical Society.

$$E = \frac{k_{ET}}{k_f + k_{ET} + \sum k_i} = \frac{1}{1 + (\frac{r}{R_0})^6}$$

(1)

where k_{ET}, k_f, and k_i are rate constant on the energy transfer, radiative decay process, and any other non-radiative decay process, respectively. In addition, r is donor-to-acceptor separation distance and R_0 is Förster distance. The R_0 is defined as the distance at which the E is 50%. As shown in the equation described above, the E depends on the r with an inverse 6th-power law. The R_0 value can be described as follows:

$$R_0{}^6 = \frac{9Q_0(ln10)\kappa^2 J}{128\pi^5 n^4 N_A}$$

(2)

where Q_0 is the fluorescence quantum yield of the donor in the absence of the acceptor, κ^2 is the orientation factor, N_A is the Avogadro constant, and n is the refractive index of the medium. J is an overlap integral and is estimated by using the following equation:

$$J = \int f_D(\lambda)\varepsilon_A(\lambda)\lambda^4 d\lambda$$

(3)

where λ is the wavelength of the light, $\varepsilon_A(\lambda)$ is the molar extinction coefficient of the acceptor, and $f_D(\lambda)$ is the normalized fluorescence spectrum of the donor. As described above, the fluorescence on/off switching behavior on the FRET process depends on various factors: the distance between the diarylethene and the fluorophore moieties, diarylethene-fluorophore orientation, the fluorescence quantum yield of the fluorophore, and an overlap integral between the absorption spectrum of the diarylethene closed-ring isomer and the fluorescence spectrum of the fluorophore. It is important to select the diarylethene and the fluorophore pair in consideration of these factors.

Various diarylethene derivatives linked to the fluorophores were synthesized and investigated.[58] However, in the case of dyad systems consisting of a diarylethene derivative and a fluorophore, a low on/off contrast is often observed in a solution because the system remains still at a few of diarylethene open-ring forms at the photostationary state (PSS). In addition, high photocyclization conversion upon UV irradiation is required to quench the fluorescence completely because the fluorescence intensity decreases in proportion with the photocyclization conversion of diarylethene. To improve their

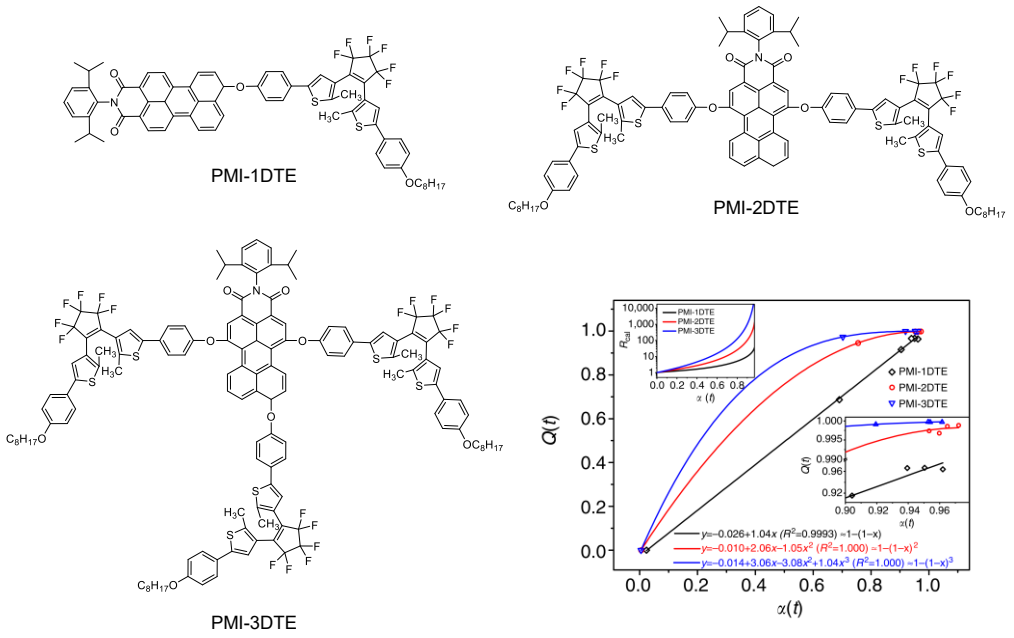

Figure 13. Molecular structures of perylenemonoimide dye-modified diaryleythenes (PMI-1DAE, PMI-2DAE and PMI-3DAE), and the polynomial fitting of the fluorescence quenching efficiency $Q(t)$ versus photocycloconversion yield $\alpha(t)$. Adapted with permission from ref. 62. Copyright 2014 Nature Publishing Group.

fluorescence on/off contrast, molecules bearing one fluorophore and multiple diarylethenes have been reported. Bis(phenylethynyl)anthracene,[59] porphyrin,[60] and perylenediimide[61] linked to multiple diarylethenes have been investigated for their fluorescence on/off switching properties. In particular, Zhu and co-workers reported that a perylenemonoimide dyad modified with triple diarylethenes exhibited a high fluorescence on/off switching speed; its fluorescence on/off contrast is the highest reported to date (Figure 13).[62]

Moreover, aggregates such as silica nanoparticles,[63] organic nanoparticles,[64] and polymers[65] have been proposed as alternative approaches to improve fluorescence on/off switching properties. Recently, Fukaminato, Métivier, and co-workers achieved extremely rapid and high fluorescence on/off contrast with full reversibility and high fatigue resistance using nanoparticles consisting of a diarylethene linked to a benzothiadiazole derivative (Figure 14).[64a] In the nanoparticles, a large number of the excited state fluorophores are quenched by a single diarylethene closed-ring form because of the close intermolecular distance in high density. As a result, the fluorescence intensity dramatically decreased even in low photocyclization conversion of diarylethenes, which resulted in highly efficient fluorescence on/off switching properties. As described above, the aggregate consisting of the multiple diarylethene and fluorophore moieties is a useful approach to obtain the highly efficient fluorescence on/off switching properties.

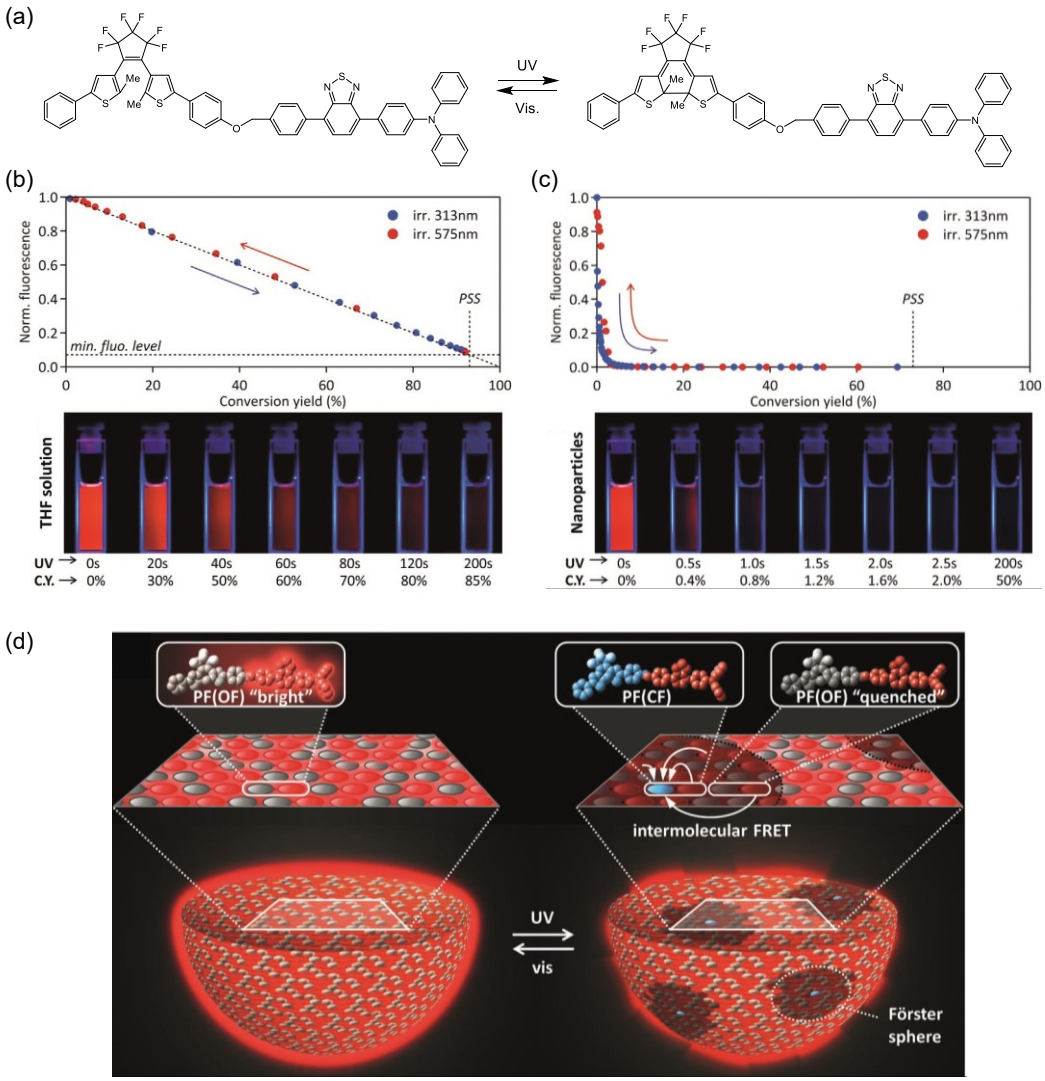

Figure 14. (a) Molecular structure and photochromic reaction of diarylethene-benzothiadiazole dyad. (b,c) Fluorescence intensity versus photocyclization conversion yield and photographs of sample in solution (b) and in nanoparticle suspension (c) under irradiation with UV light. (d) Illustration of the fluorescence on/off switching based on FRET in the nanoparticles. Adapted with permission from ref. 64a. Copyright 2016 Wiley-VCH Verlag GmbH & Co. KGaA, Weinheim.

4. Scope of This Thesis

The fluorescence photoswitching using the diarylethenes has been widely studied in the past decades. Especially, various types of single molecules or the aggregates consisting of the multiple diarylethene and fluorophore moieties were recently reported to improve the fluorescence on/off switching properties. The purpose of this thesis is to provide design and strategy of novel molecular system for the highly efficient fluorescence on/off switching using the diarylethenes and the fluorophores. To accomplish the purpose, the author constructed the novel molecular design of the

fluorescence on/off switchable system, and synthesized the diarylethenes and the fluorophores suitable for the molecular system.

This doctoral thesis consists of General Introduction and 6 chapters which are divided into two parts, Parts I and II. General Introduction describes the backgrounds of the photochromic and fluorescence properties of diarylethene derivatives and the scope of this thesis.

The author focused on two topics for the development of the fluorescence on/off switchable molecular system. Part I which consists of Chapters 1 and 2 deals with the first topic about the aggregate structures showing the fluorescence on/off switching. Although various systems of the aggregates containing the diarylethenes and the fluorophores have been proposed, there are few reports on the effect of the aggregate structures such as a molecular sequence and a ratio of the diarylethenes and the fluorophores for the fluorescence on/off switching properties, such as the fluorescence on/off contrast and switching speed. Clarifying these effects is expected to lead to systems bearing more efficient fluorescence on/off switching properties even if the same diarylethene and fluorophore moieties are used.

In Chapter 1, the fluorescence properties of fluorene derivatives bearing phenylthiophene or benzothiophene, and their *S*,*S*-dioxidized compounds are investigated to obtain the fluorophore suitable for the proposed molecular system. 9,9-Dioctyl fluorene was selected as the fluorescent unit in the fluorescence on/off switchable system because alkyl chains at the 9-position of the fluorene framework suppress concentration quenching by interfering with intermolecular π-π stacking. π-Extended fluorene derivatives introducing phenylthiophene or benzothiophene at the 2- and 7-positions and their *S*,*S*-dioxidized compounds were synthesized, and the fluorescence properties in the solution were investigated. In addition, the solvatofluorochromism was also discussed.

Chapter 2 describes the fluorescence on/off switching in polymers bearing diarylethene and fluorene in their side chains. The fluorene derivative, which has the highest fluorescence quantum yield among the fluorene derivatives synthesized in the previous chapter, was selected as the fluorophore unit. In addition, a diarylethene derivative having the absorption spectrum overlapping with the fluorescence spectrum of the fluorene derivative was adopted. A diarylethene-fluorene dyad connected by an ester bond, and random and alternative copolymers bearing the diarylethene and the fluorene in their side chains were synthesized. The effects of monomer sequence and ratio for the fluorescence on/off switching properties were investigated by using the random and alternative copolymers bearing the diarylethene and the fluorene in their side chains.

Part II which consists of Chapters 3-6 deals with the second topic about the

fabrication methods for the molecular systems with the highly efficient fluorescence on/off switching properties. Although the highly efficient fluorescence on/off switchable systems consisting of the diarylethenes and the fluorophores have been reported as mentioned in the previous section, a complicated multistep synthesis is required to construct the fluorescence switchable systems. If a more convenient system with the highly efficient fluorescence on/off switching properties can be constructed, it will lead to the development of the fluorescence on/off switchable system and a great contribution to the practical applications.

In Chapter 3, solid-state fluorescence properties of a diarylethene, 1,2-bis(3-methyl-5-phenyl-2-thienyl)perfluorocyclopentene, are described. To accomplish the purpose in Part II, the fluorophore showing the strong fluorescence even in the aggregate state, such as in the crystalline phase and in the amorphous phase, is needed. It was found that the diarylethene has two polymorphs which show the strong orange or yellow fluorescence. The optical properties of the diarylethene in the solid states were investigated. Furthermore, the thermodynamic solid-state polymorphic phase transition was found, and the process was directly visualized by a fluorescence color change.

Chapter 4 deals with the fluorescence behavior induced by the photochemical ring-opening reaction of crystal consisting of the diarylethene closed-ring isomer used in the previous chapter upon irradiation with visible light. The diarylethene open-ring isomer shows the different fluorescence color depending on the intermolecular π-π interactions in the crystal. It is considered that different fluorescence behavior can be observed by using the open-ring isomer crystal produced by the ring-opening reaction of the closed-ring isomer crystal. The crystals of the diarylethene closed-ring isomer were fabricated and the fluorescence properties induced by the photochemical ring-opening reaction of the crystal upon irradiation with visible light were investigated.

Chapter 5 describes the fluorescence properties of diarylethenes, 1,2-bis(3-methyl-5-(4-alkylphenyl)-2-thienyl)perfluorocyclopentenes, having various alkyl chains at the *p*-position of phenyl rings. In Chapter 4, the characteristic green fluorescence was observed from the open-ring isomer crystal produced by the ring-opening reaction of the closed-ring isomer crystal. However, the relationship between the fluorescence properties and the crystal structure was not obtained due to the lack of crystallinity after the ring-opening reaction. It was assumed that the introduction of alkyl substituents to the phenyl rings may modulate the intermolecular π-π interactions to result in a dramatic change in the solid-state luminescence properties. The solid-state fluorescence properties of diarylethenes introducing various alkyl chains at the *p*-position of phenyl rings were investigated. Moreover, the crystallization with mechanical scratching followed by

heating was found and the reversible fluorescence recording based on the crystallization process was demonstrated.

Chapter 6 deals with fabrication and fluorescence on/off switching properties of nanoparticles consisting of two types of diarylethenes. 1,2-Bis(3-methyl-5-phenyl-2-thienyl)perfluorocyclopentene was selected as the fluorophore unit owing to the orange fluorescence with the highest fluorescence quantum yield in the crystal among the diarylethenes investigated in Chapters 3-5. In contrast, 1,2-bis(2-methyl-5-phenyl-3-thienyl)perfluorocyclopentene, which undergoes a photochromic reaction involving a color change from colorless to blue in solution and in the crystal, was adopted as the photochromic molecular unit. The nanoparticles of two types of the diarylethenes were fabricated by a reprecipitation method. The dependence of the fluorescence on/off switching properties on Förster distance and the molar fraction was quantitatively evaluated.

5. References

[1] M. Fritzsche, *Comp. Rend.* **1867**, *64*, 1035-1037.

[2] H. Dürr, H. Bouas-Laurent, *Photochromism: Molecules and Systems*, Elsevier, **2003**.

[3] J. C. Crano, T. Flood, D. Knowles, A. Kumar, B. Van Gemert, *Pure Appl. Chem.* **1996**, *68*, 1395-1398.

[4] M. Irie, M. Mohri, *J. Org. Chem.* **1988**, *53*, 803-808.

[5] H. G. Heller, S. Oliver, *J. Chem. Soc., Perkin Trans. 1* **1981**, 197-201.

[6] a) M. Irie, *Chem. Rev.* **2000**, *100*, 1685-1716; b) M. Irie, T. Fukaminato, K. Matsuda, S. Kobatake, *Chem. Rev.* **2014**, *114*, 12174-12277.

[7] a) M. Irie, T. Fukaminato, T. Sasaki, N. Tamai, T. Kawai, *Nature* **2002**, *420*, 759; b) K. Matsuda, M. Irie, *J. Photochem. Photobiol. C* **2004**, *5*, 169-182.

[8] S. Kobatake, S. Takami, H. Muto, T. Ishikawa, M. Irie, *Nature* **2007**, *446*, 778-781.

[9] S. Nakamura, M. Irie, *J. Org. Chem.* **1988**, *53*, 6136-6138.

[10] M. Boggio-Pasqua, M. Ravaglia, M. J. Bearpark, M. Garavelli, M. A. Robb, *J. Phys. Chem. A* **2003**, *107*, 11139-11152.

[11] N. Tamai, H. Miyasaka, *Chem. Rev.* **2000**, *100*, 1875-1890.

[12] K. Uchida, Y. Nakayama, M. Irie, *Bull. Chem. Soc. Jpn.* **1990**, *63*, 1311-1315.

[13] A. Staykov, K. Yoshizawa, *J. Phys. Chem. C* **2009**, *113*, 3826-3834.

[14] a) K. Uchida, E. Tsuchida, Y. Aoi, S. Nakamura, M. Irie, *Chem. Lett.* **1999**, 63-64; b) T. Yamaguchi, M. Irie, *J. Photochem. Photobiol. A* **2006**, *178*, 162-169.

[15] a) M. Takeshita, C. N. Choi, M. Irie, *Chem. Commun.* **1997**, 2265-2266; b) M. Takeshita, N. Kato, S. Kawauchi, T. Imase, J. Watanabe, M. Irie, *J. Org. Chem.*

1998, *63*, 9306-9313; c) M. Takeshita, M. Yamada, N. Kato, M. Irie, *J. Chem. Soc., Perkin Trans. 2* **2000**, *4*, 619-622.

[16] a) F. Stellacci, C. Bertarelli, F. Toscano, M. C. Gallazzi, G. Zotti, G. Zerbi, *Adv. Mater.* **1999**, *11*, 292-295; b) K. Matsuda, Y. Shinkai, T. Yamaguchi, K. Nomiyama, M. Isayama, M. Irie, *Chem. Lett.* **2003**, *32*, 1178-1179; c) M. K. Hossain, M. Takeshita, T. Yamato, *Tetrahedron Lett.* **2005**, *46*, 431-433.

[17] a) S. Fukumoto, T. Nakashima, T. Kawai, *Angew. Chem. Int. Ed.* **2011**, *50*, 1565-1568; b) W. Li, C. Jiao, X. Li, Y. Xie, K. Nakatani, H. Tian, W. Zhu, *Angew. Chem. Int. Ed.* **2014**, *53*, 4603-4607.

[18] a) Y. Asano, A. Murakami, T. Kobayashi, A. Goldberg, D. Guillaumont, S. Yabushita, M. Irie, S. Nakamura, *J. Am. Chem. Soc.* **2004**, *126*, 12112-12120; b) D. Guillaumont, T. Kobayashi, K. Kanda, H. Miyasaka, K. Uchida, S. Kobatake, K. Shibata, S. Nakamura, M. Irie, *J. Phys. Chem. A* **2002**, *106*, 7222-7227; c) A. Goldberg, A. Murakami, K. Kanda, T. Kobayashi, S. Nakamura, K. Uchida, H. Sekiya, T. Fukaminato, T. Kawai, S. Kobatake, M. Irie, *J. Phys. Chem. A* **2003**, *107*, 4982-4988; d) S. Nakamura, T. Kobayashi, A. Takata, K. Uchida, Y. Asano, A. Murakami, A. Goldberg, D. Guillaumont, S. Yokojima, S. Kobatake, M. Irie, *J. Phys. Org. Chem.* **2007**, *20*, 821-829.

[19] a) K. Shibata, S. Kobatake, M. Irie, *Chem. Lett.* **2001**, 618-619; b) K. Morimitsu, S. Kobatake, S. Nakamura, M. Irie, *Chem. Lett.* **2003**, *32*, 858-859.

[20] a) M. Irie, T. Eriguchi, T. Takada, K. Uchida, *Tetrahedron* **1997**, *53*, 12263-12271; b) A. T. Bens, D. Frewert, K. Kodatis, C. Kryschi, H. D. Martin, H. P. Trommsdorff, *Eur. J. Org. Chem.* **1998**, 2333-2338.

[21] a) Y. C. Jeong, J. P. Han, Y. Kim, E. Kim, S. I. Yang, K. H. Ahn, *Tetrahedron* **2007**, *63*, 3173-3182; b) K. Uno, H. Niikura, M. Morimoto, Y. Ishibashi, H. Miyasaka, M. Irie, *J. Am. Chem. Soc.* **2011**, *133*, 13558-13564; c) M. Taguchi, T. Nakagawa, T. Nakashima, T. Kawai, *J. Mater. Chem.* **2011**, *21*, 17425-17432; d) H. Shoji, S. Kobatake, *Chem. Commun.* **2013**, *49*, 2362-2364.

[22] D. Kitagawa, S. Kobatake, *Chem. Rec.* **2016**, *16*, 2005-2015.

[23] a) S. L. Gilat, S. H. Kawai, J. M. Lehn, *Chem. Eur. J.* **1995**, *1*, 275-284; b) S. Nakamura, S. Yokojima, K. Uchida, T. Tsujioka, A. Goldberg, A. Murakami, K. Shinoda, M. Mikami, T. Kobayashi, S. Kobatake, K. Matsuda, M. Irie, *J. Photochem. Photobiol. A* **2008**, *200*, 10-18.

[24] a) S. Kobatake, K. Shibata, K. Uchida, M. Irie, *J. Am. Chem. Soc.* **2000**, *122*, 12135-12141; b) S. Kobatake, K. Uchida, E. Tsuchida, M. Irie, *Chem. Lett.* **2000**, 1340-1341; c) D. Kitagawa, K. Sasaki, S. Kobatake, *Bull. Chem. Soc. Jpn.* **2011**, *84*, 141-

147.

[25] D. Z. Chen, Z. Wang, H. H. Zhang, *J. Mol. Struct. (Theochem)* **2008**, *859*, 11-17.

[26] J. J. D. de Jong, L. N. Lucas, R. Hania, A. Pugzlys, R. M. Kellogg, B. L. Feringa, K. Duppen, J. H. van Esch, *Eur. J. Org. Chem.* **2003**, 1887-1893.

[27] M. Herder, B. M. Schmidt, L. Grubert, M. Patzel, J. Schwarz, S. Hecht, *J. Am. Chem. Soc.* **2015**, *137*, 2738-2747.

[28] a) K. Higashiguchi, K. Matsuda, S. Kobatake, T. Yamada, T. Kawai, M. Irie, *Bull. Chem. Soc. Jpn.* **2000**, *73*, 2389-2394; b) K. Higashiguchi, K. Matsuda, T. Yamada, T. Kawai, M. Irie, *Chem. Lett.* **2000**, 1358-1359; c) M. Irie, T. Lifka, K. Uchida, S. Kobatake, Y. Shindo, *Chem. Commun.* **1999**, 747-748.

[29] D. Mendive-Tapia, A. Perrier, M. J. Bearpark, M. A. Robb, B. Lasorne, D. Jacquemin, *Phys. Chem. Chem. Phys.* **2014**, *16*, 18463-18471.

[30] S. Kobatake, M. Irie, *Bull. Chem. Soc. Jpn.* **2004**, *77*, 195-210.

[31] S. Kobatake, K. Uchida, E. Tsuchida, M. Irie, *Chem. Commun.* **2002**, 2804-2805.

[32] K. Shibata, K. Muto, S. Kobatake, M. Irie, *J. Phys. Chem. A* **2002**, *106*, 209-214.

[33] a) J. Biteau, F. Chaput, K. Lahlil, J. P. Boilot, G. M. Tsivgoulis, J. M. Lehn, B. Darracq, C. Marois, Y. Levy, *Chem. Mater.* **1998**, *10*, 1945-1950; b) H. Cho, E. Kim, *Macromolecules* **2002**, *35*, 8684-8687.

[34] a) E. Kim, Y. K. Choi, M. H. Lee, *Macromolecules* **1999**, *32*, 4855-4860; b) H. Nakashima, M. Irie, *Macromol. Chem. Phys.* **1999**, *200*, 683-692; c) T. J. Wigglesworth, N. R. Branda, *Chem. Mater.* **2005**, *17*, 5473-5480; d) H. Tian, H. Y. Tu, *Adv. Mater.* **2000**, *12*, 1597-1600; e) A. J. Myles, N. R. Branda, *Macromolecules* **2003**, *36*, 298-303; f) H. Nishi, T. Namari, S. Kobatake, *J. Mater. Chem.* **2011**, *21*, 17249-17258; g) S. Kobatake, H. Kuratani, *Chem. Lett.* **2006**, *35*, 628-629; h) S. Kobatake, I. Yamashita, *Tetrahedron* **2008**, *64*, 7611-7618.

[35] a) A. Fernandez-Acebes, J. M. Lehn, *Adv. Mater.* **1999**, *11*, 910-913; b) D. H. Kwon, H. W. Shin, E. Kim, D. W. Boo, Y. R. Kim, *Chem. Phys. Lett.* **2000**, *328*, 234-243.

[36] a) T. Yamada, S. Kobatake, K. Muto, M. Irie, *J. Am. Chem. Soc.* **2000**, *122*, 1589-1592; b) T. Yamada, S. Kobatake, M. Irie, *Bull. Chem. Soc. Jpn.* **2000**, *73*, 2179-2184.

[37] a) T. Fukaminato, S. Kobatake, T. Kawai, M. Irie, *Proc. Japan Acad., Ser. B* **2001**, *77*, 30-35; b) T. Fukaminato, T. Kawai, S. Kobatake, M. Irie, *J. Phys. Chem. B* **2003**, *107*, 8372-8377.

[38] a) K. Matsuda, M. Irie, *J. Am. Chem. Soc.* **2000**, *122*, 7195-7201; b) K. Matsuda, M. Irie, *J. Am. Chem. Soc.* **2000**, *122*, 8309-8310; c) K. Matsuda, M. Irie, *J. Am. Chem. Soc.* **2001**, *123*, 9896-9897.

[39] a) T. Kawai, Y. Nakashima, M. Irie, *Adv. Mater.* **2005**, *17*, 309-314; b) H. Choi, H. Lee, Y. J. Kang, E. Kim, S. O. Kang, J. Ko, *J. Org. Chem.* **2005**, *70*, 8291-8297; c) E. Kim, H. W. Lee, *J. Mater. Chem.* **2006**, *16*, 1384-1389; d) P. Zacharias, M. C. Gather, A. Kohnen, N. Rehmann, K. Meerholz, *Angew. Chem. Int. Ed.* **2009**, *48*, 4038-4041.

[40] T. Kawai, N. Fukuda, D. Gröschl, S. Kobatake, M. Irie, *Jpn J. Appl. Phys. Part 2* **1999**, *38*, L1194-L1196.

[41] a) D. Sud, T. B. Norsten, N. R. Branda, *Angew. Chem. Int. Ed.* **2005**, *44*, 2019-2021; b) B. M. Neilson, C. W. Bielawski, *Organometallics* **2013**, *32*, 3121-3128.

[42] J. Okuda, Y. Tanaka, R. Kodama, K. Sumaru, K. Morishita, T. Kanamori, S. Yamazoe, K. Hyodo, S. Yamazaki, T. Miyatake, S. Yokojima, S. Nakamura, K. Uchida, *Chem. Commun.* **2015**, *51*, 10957-10960.

[43] a) T. Fukaminato, *J. Photochem. Photobiol. C* **2011**, *12*, 177-208; b) D. Kim, S. Y. Park, *Adv. Opt. Mater.* **2018**, *6*, 1800678; c) T. Fukaminato, S. Ishida, R. Métivier, *NPG Asia Materials* **2018**, *10*, 859-881.

[44] a) X. L. Meng, W. H. Zhu, Q. Zhang, Y. L. Feng, W. J. Tan, H. Tian, *J. Phys. Chem. B* **2008**, *112*, 15636-15645; b) W. H. Zhu, X. L. Meng, Y. H. Yang, Q. Zhang, Y. S. Xie, H. Tian, *Chem. Eur. J.* **2010**, *16*, 899-906; c) C.-T. Poon, W. H. Lam, H.-L. Wong, V. W.-W. Yam, *J. Am. Chem. Soc.* **2010**, *132*, 13992-13993; d) K. Suzuki, T. Ubukata, Y. Yokoyama, *Chem. Commun.* **2012**, *48*, 765-767.

[45] a) K. Yagi, M. Irie, *Bull. Chem. Soc. Jpn.* **2003**, *76*, 1625-1628; b) S. Z. Pu, H. Li, G. Liu, W. J. Liu, S. Q. Cui, C. B. Fan, *Tetrahedron* **2011**, *67*, 1438-1447; c) S. Z. Pu, T. S. Yang, J. K. Xu, B. Chen, *Tetrahedron Lett.* **2006**, *47*, 6473-6477; d) S. Z. Pu, G. Liu, L. Shen, J. K. Xu, *Org. Lett.* **2007**, *9*, 2139-2142.

[46] a) M. Giraud, A. Léaustic, M.-F. Charlot, P. Yu, M. Césario, C. Philouze, R. Pansu, K. Nakatani, E. Ishow, *New J. Chem.* **2005**, *29*, 439-446; b) J. Piard, R. Métivier, M. Giraud, A. Léaustic, P. Yu, K. Nakatani, *New J. Chem.* **2009**, *33*, 1420-1426; c) K. Shibata, L. Kuroki, T. Fukaminato, M. Irie, *Chem. Lett.* **2008**, *37*, 832-833; d) K. Uchida, T. Matsuoka, S. Kobatake, T. Yamaguchi, M. Irie, *Tetrahedron* **2001**, *57*, 4559-4565.

[47] a) M. Cipolloni, F. Ortica, L. Bougdid, C. Moustrou, U. Mazzucato, G. Favaro, *J. Phys. Chem. A* **2008**, *112*, 4765-4771; b) Z. Y. Li, J. L. Xia, J. H. Liang, J. J. Yuan, G. J. Jin, J. Yin, G. A. Yu, S. H. Liu, *Dyes. Pigm.* **2011**, *90*, 290-296; c) S. C. Pang, H. Hyun, S. Lee, D. Jang, M. J. Lee, S. H. Kang, K. H. Ahn, *Chem. Commun.* **2012**, *48*, 3745-3747.

[48] Y.-C. Jeong, D. G. Park, I. S. Lee, S. I. Yang, K.-H. Ahn, *J. Mater. Chem.* **2009**, *19*,

97.

[49] a) K. Uno, H. Niikura, M. Morimoto, Y. Ishibashi, H. Miyasaka, M. Irie, *J. Am. Chem. Soc.* **2011**, *133*, 13558-13564; b) M. Irie, M. Morimoto, *Bull. Chem. Soc. Jpn.* **2017**, *91*, 237-250.

[50] a) A. T. Bens, J. Ern, K. Kuldova, H. P. Trommsdorff, C. Kryschi, *J. Lumin.* **2001**, *94*, 51-54; b) J. Ern, A. T. Bens, H. D. Martin, K. Kuldova, H. P. Trommsdorff, C. Kryschi, *J. Phys. Chem. A* **2002**, *106*, 1654-1660; c) Y. C. Jeong, S. I. Yang, E. Kim, K. H. Ahn, *Tetrahedron* **2006**, *62*, 5855-5861; d) M. S. Kim, T. Kawai, M. Irie, *Chem. Lett.* **2001**, 702-703; e) K. Yagi, M. Irie, *Chem. Lett.* **2003**, *32*, 848-849.

[51] a) H. H. Liu, Y. Chen, *J. Phys. Chem. A* **2009**, *113*, 5550-5553; b) K. Kasatani, S. Kambe, M. Irie, *J. Photochem. Photobiol. A* **1999**, *122*, 11-15; c) P. D. Patel, I. A. Mikhailov, K. D. Belfield, A. E. Masunov, *Int. J. Quantum Chem.* **2009**, *109*, 3711-3722; d) Y. C. Jeong, S. I. Yang, K. H. Ahn, E. Kim, *Chem. Commun.* **2005**, 2503-2505; e) Y. C. Jeong, S. I. Yang, E. Kim, K. H. Ahn, *Macromol. Rapid Commun.* **2006**, *27*, 1769-1773.

[52] T. Nakagawa, Y. Miyasaka, Y. Yokoyama, *Chem. Commun.* **2018**, *54*, 3207-3210.

[53] a) L. Giordano, T. M. Jovin, M. Irie, E. A. Jares-Erijman, *J. Am. Chem. Soc.* **2002**, *124*, 7481-7489; b) M. Berberich, A. M. Krause, M. Orlandi, F. Scandola, F. Wurthner, *Angew. Chem. Int. Ed.* **2008**, *47*, 6616-6619.

[54] T. Fukaminato, T. Doi, N. Tamaoki, K. Okuno, Y. Ishibashi, H. Miyasaka, M. Irie, *J. Am. Chem. Soc.* **2011**, *133*, 4984-4990.

[55] a) Y. Odo, T. Fukaminato, M. Irie, *Chem. Lett.* **2007**, *36*, 240-241; b) M. Berberich, M. Natali, P. Spenst, C. Chiorboli, F. Scandola, F. Wurthner, *Chem. Eur. J.* **2012**, *18*, 13651-13664; c) M. Berberich, F. Wurthner, *Chem. Sci.* **2012**, *3*, 2771-2777; d) T. Fukaminato, M. Tanaka, T. Doi, N. Tamaoki, T. Katayama, A. Mallick, Y. Ishibashi, H. Miyasaka, M. Irie, *Photochem. Photobiol. Sci.* **2010**, *9*, 181-187.

[56] T. Fukaminato, T. Sasaki, T. Kawai, N. Tamai, M. Irie, *J. Am. Chem. Soc.* **2004**, *126*, 14843-14849.

[57] I. L. Medintz, N. Hildebrandt, *FRET-Förster Resonance Energy Transfer: From Theory to Applications*, John Wiley & Sons, **2013**.

[58] a) A. E. Keirstead, J. W. Bridgewater, Y. Terazono, G. Kodis, S. Straight, P. A. Liddell, A. L. Moore, T. A. Moore, D. Gust, *J. Am. Chem. Soc.* **2010**, *132*, 6588-6595; b) A. Osuka, D. Fujikane, H. Shinmori, S. Kobatake, M. Irie, *J. Org. Chem.* **2001**, *66*, 3913-3923; c) T. B. Norsten, N. R. Branda, *Adv. Mater.* **2001**, *13*, 347-349; d) I. Lee, Y. You, S. J. Lim, S. Y. Park, *Chem. Lett.* **2007**, *36*, 888-889; e) T. A. Golovkova, D. V. Kozlov, D. C. Neckers, *J. Org. Chem.* **2005**, *70*, 5545-5549; f) N.

Soh, K. Yoshida, H. Nakajima, K. Nakano, T. Imato, T. Fukaminato, M. Irie, *Chem. Commun.* **2007**, 5206-5208; g) H. Y. Zheng, W. D. Zhou, M. J. Yuan, X. D. Yin, Z. C. Zuo, C. B. Ouyang, H. B. Liu, Y. L. Li, D. B. Zhu, *Tetrahedron Lett.* **2009**, *50*, 1588-1592; h) S. F. Yan, V. N. Belov, M. L. Bossi, S. W. Hell, *Eur. J. Org. Chem.* **2008**, 2531-2538.

[59] T. Kawai, T. Sasaki, M. Irie, *Chem. Commun.* **2001**, 711-712.

[60] H. Tian, B. Z. Chen, H. Y. Tu, K. Mullen, *Adv. Mater.* **2002**, *14*, 918-923.

[61] W. J. Tan, X. Li, J. J. Zhang, H. Tian, *Dyes Pigm.* **2011**, *89*, 260-265.

[62] C. Li, H. Yan, L. X. Zhao, G. F. Zhang, Z. Hu, Z. L. Huang, M. Q. Zhu, *Nat. Commun.* **2014**, *5*, 5709.

[63] a) J. Folling, S. Polyakova, V. Belov, A. van Blaaderen, M. L. Bossi, S. W. Hell, *Small* **2008**, *4*, 134-142; b) H. Y. Jung, S. You, C. Lee, Y. Kim, *Chem. Commun.* **2013**, *49*, 7528-7530.

[64] a) J. Su, T. Fukaminato, J. P. Placial, T. Onodera, R. Suzuki, H. Oikawa, A. Brosseau, F. Brisset, R. Pansu, K. Nakatani, R. Métivier, *Angew. Chem. Int. Ed.* **2016**, *55*, 3662-3666; b) S. Ishida, T. Fukaminato, S. Kim, T. Ogata, S. Kurihara, *Chem. Lett.* **2017**, *46*, 1182-1185; c) S. Ishida, T. Fukaminato, D. Kitagawa, S. Kobatake, S. Kim, T. Ogata, S. Kurihara, *Chem. Commun.* **2017**, *53*, 8268-8271 ; d) S. J. Lim, B. K. An, S. D. Jung, M. A. Chung, S. Y. Park, *Angew. Chem. Int. Ed.* **2004**, *43*, 6346-6350.

[65] a) J. Bu, K. Watanabe, H. Hayasaka, K. Akagi, *Nat. Commun.* **2014**, *5*, 3799; b) H. Hayasaka, K. Tamura, K. Akagi, *Macromolecules* **2008**, *41*, 2341-2346; c) H. Hayasaka, T. Miyashita, K. Tamura, K. Akagi, *Adv. Funct. Mater.* **2010**, *20*, 1243-1250.

Part I

Effect of Monomer Sequence and Ratio for Fluorescence On/Off Switching Properties in Polymers Bearing Diarylethene and Fluorophore in Side Chains

Chapter 1

Optical Properties and Solvatofluorochromism of Fluorene Derivatives Bearing *S*,*S*-Dioxidized Thiophene

1.1 Introduction

Fluorescence on/off switchable diarylethene systems having efficient fluorescence on/off switching properties, such as high fluorescence on/off contrast and rapid switching speed, are desirable for applications in sensing materials, bioimaging materials for super-resolution microscopy, and single molecule memory materials. As mentioned in General Introduction, effect of monomer sequence and ratio for the fluorescence on/off switching properties in polymers bearing diarylethene and fluorophore in side chains is investigated in Part I. To obtain the fluorophore suitable for the fluorescence on/off switching in the polymers is needed to accomplish the purpose.

A fluorene is one of typical fluorophores showing blue fluorescence. Molecules having a fluorene framework are important materials for organic light-emitting diodes (OLEDs), organic semiconductors and dye-sensitized solar cells due to their high photoluminescence quantum yields, good charge transporting properties and high chemical stability.[1] Dialkylfluorenes and cardofluorenes having alkyl chains and aromatic rings at the 9-position of the fluorene framework are often used as typical fluorene derivatives since they improve solubility and prevent intermolecular π–π stacking.[2] Polymers including these fluorene derivatives are also used as the backbone of π-conjugated polymers.[3] Fluorenes and polyfluorenes are widely investigated in the optoelectronics field.

On the other hand, materials having *S*,*S*-dioxidized thiophene show different optical and electronic properties in comparison with those without *S*,*S*-dioxidization. For example, polythiophenes and fluorene-thiophene copolymers are useful for *p*-type semiconducting materials in photovoltaic cells.[4] Fluorene-thiophene copolymers having a *p*-type nature showed an *n*-type nature on introducing *S*,*S*-dioxidized thiophene.[5] Therefore, such materials can change their properties by oxidation to *S*,*S*-dioxidized thiophene. Additionally, the oxidation from a sulfide group to a sulfonyl group significantly affects photoluminescence properties. The decrease in the lowest unoccupied molecular orbital (LUMO) level by introducing the electron withdrawing *S*,*S*-dioxidized thiophene causes a longer wavelength shift in the fluorescence spectrum and a decrease of the fluorescence quantum yield.[6] On the other hand, there are some examples of fluorescence quantum yield increasing with the introduction of a sulfonyl

group.[7] Park and coworkers have reported that polythiophene bearing alkoxy chains enhances the fluorescence quantum yields by introducing *S*,*S*-dioxidized thiophene.[7a] It is ascribed to the blue shift of the absorption spectrum and the energy gap law.[7b] Furthermore, Swager and co-workers have reported that the oxidation of the thioether side chains of poly(*p*-phenylene-ethynylene) results in an increase in the fluorescence quantum yield.[7c] The increase in the fluorescence quantum yield according to the oxidation has been explained by an increase in the radiative rate due to the molecular orbital overlap. The fluorescence quantum yield also increases with the oxidation of dibenzothiophene.[7d]

As mentioned above, the oxidation from a sulfide group to a sulfonyl group exerts various effects on the electronic and optical properties of the materials. Thus, it is considered that the introduction of *S*,*S*-dioxidized thiophene to the fluorene framework is a promising method to obtain the fluorophore with the high fluorescence quantum yield. In this chapter, two fluorene derivatives having phenylthiophene (**FPT**) and benzothiophene (**FBT**), and their *S*,*S*-dioxidized compounds (**FPTO$_2$**, **FBTO$_2$**, **FPTO$_4$** and **FBTO$_4$**) have been synthesized, as shown in Scheme 1-1. The optical properties of the six fluorene derivatives are discussed in this chapter.[8]

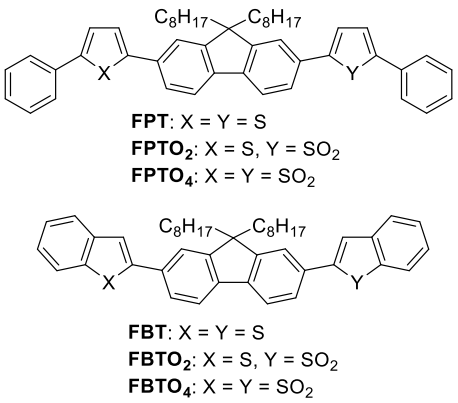

Scheme 1-1. Fluorene derivatives used in this work. Reproduced from ref. 8 with permission from the European Society for Photobiology, the European Photochemistry Association, and The Royal Society of Chemistry.

1.2 Experimental Section

1.2.1 General

Solvents used were spectroscopic grade and purified by distillation before use. ^{1}H NMR spectra were recorded on a Bruker AV-300N spectrometer at 300 MHz. Deuterated chloroform ($CDCl_3$) was used as the solvent and tetramethylsilane (TMS) as an internal standard. Mass spectra were obtained using a JEOL JMS-700/700S mass spectrometer.

High-performance liquid chromatography (HPLC) was carried out using a Hitachi L-7150/L-2400 HPLC system equipped with a Kanto Chemical Mightysil Si60 column. Recycling preparative HPLC was carried out using a JAI LC-908 equipped with JAIGEL-1H and 2H columns using chloroform as the eluent. Absorption spectra were recorded with a JASCO V-560 absorption spectrophotometer. Fluorescence spectra were recorded with a Hitachi F-2700 fluorescence spectrophotometer. All measurements performed in solutions were carried out with optical density around 0.1 at the excitation wavelength in 1 cm path length quartz cells at room temperature (298 K). Furthermore, all samples in solutions were deaerated by bubbling with argon gas for 3 min before the measurements. Theoretical calculations were performed with Gaussian 09.[9] The molecular structures in the ground and excited states were fully optimized at the B3LYP/6-31G* level of theory, and vibrational frequencies for all optimized species were computed at the same level to confirm each stationary point to be a minimum.

1.2.2 Fluorescence Quantum Yield

The fluorescence quantum yields (Φ_f) were determined from the integrated intensity in the fluorescence spectrum of a measurement sample relative to that of a reference solution using eq 1.[10]

$$\Phi_f = \Phi_{f,ref} \frac{A_{ref}}{A} \frac{I_{ref}}{I} \frac{F}{F_{ref}} \frac{n^2}{{n_{ref}}^2} \quad (1)$$

where A and A_{ref} are the optical densities of the solutions at the excitation wavelength, I and I_{ref} are the excitation light intensities at the excitation wavelength, F and F_{ref} are the integrated intensities of the corrected fluorescence spectra, and n and n_{ref} are the refractive indices of the solvents, used for the sample solution and a standard reference solution, respectively. Anthracene (Φ_f = 0.27 excited at 366 nm in ethanol),[11] 9,10-diphenylanthracene (Φ_f = 0.90 excited at 366 nm in cyclohexane), [12] fluorescein (Φ_f = 0.90 excited at 440 nm in 0.1 N NaOHaq)[11a, 13] and 9,10-bis(phenylethynyl)anthracene (Φ_f = 0.64 excited at 440 nm in chloroform)[14] were used as standard references. The Φ_f value was determined as the average of those obtained using two standard references, and the relative experimental error was estimated to be less than 10%.

1.2.3 Fluorescence Lifetime

Fluorescence lifetimes were measured using a time-correlated single-photon-counting (TCSPC) system. The experimental setup for the TCSPC was described

previously.[15] Briefly, a Ti: sapphire oscillator (Spectra-Physics, Tsunami) was utilized as a pulsed light source. The operation wavelength, pulse width and repetition rate were set to 800 nm, 70 fs and 80 MHz, respectively. The fundamental of the laser was converted to the second harmonics (400 nm) using a type I BBO crystal and used to excite samples. The repetition rate was reduced down to 8 MHz by using an electro-optic modulator (Conoptics, Model 350) and the excitation intensity of the samples was typically 2.2 mW at 8 MHz. The detection of the fluorescence at the magic angle configuration was attained by utilizing a film polarizer and a Babinet–Soleil compensator. The fluorescence was detected using a photomultiplier tube (Hamamatsu Photonics, R3809U-50) equipped with a pre-amplifier (Hamamatsu Photonics, C5594) and a TCSPC module (PicoQuant, PicoHarp 300). For the wavelength selection a monochromator (Princeton Instruments, Acton 2150) was placed in front of the photomultiplier tube. The sample solutions were set in 1 cm quartz cells. The typical response time of the system was determined to be 40 ps full-width-at-half-maximum by detecting scattered photons from a colloidal solution.

1.2.4 Materials

Chemicals used for the synthesis were commercially available and used without further purification. The fluorene derivatives were synthesized as follows.

*2,7-Bis(5-phenylthiophen-2-yl)-9,9-dioctylfluorene (**FPT**).* 2,7-Diiodo-9,9-dioctyl-fluorene[16] (780 mg, 1.4 mmol) was dissolved in anhydrous THF (8.0 mL) under argon atmosphere. 1.6 M *n*-BuLi hexane solution (2.0 mL, 3.2 mmol) was slowly added dropwise to the solution at −78 °C, and the mixture was stirred for 1.5 h. Tri-*n*-butyl borate (0.91 mL, 3.4 mmol) was slowly added to the solution at the temperature, and the mixture was stirred for 1.5 h. Adequate amount of distilled water was added to the mixture to quench the reaction. 2-Iodo-5-phenylthiophene[17] (810 mg, 2.8 mmol), tetrakis(triphenylphosphine)palladium(0) (23 mg, 0.020 mmol) and 20 wt% Na_2CO_3 aqueous solution (2.2 mL) were added to the solution, and the mixture was refluxed for 8 h. The reaction mixture was neutralized by HCl aqueous solution, extracted with dichloromethane, washed with brine, dried over $MgSO_4$, filtered, and concentrated in vacuo. The crude product was purified by column chromatography and HPLC on silica gel using *n*-hexane/ethyl acetate (80:20) as the eluent to give 460 mg of **FPT** in 46% yield. **FPT**: ^{1}H NMR (300 MHz, $CDCl_3$, TMS) δ = 0.71 (br, 4H, CH_2), 0.79 (t, *J* = 7 Hz, 6H, CH_3), 1.0-1.2 (m, 20H, CH_2), 2.0-2.1 (m, 4H, CH_2), 7.2-7.5 (m, 10H, Aromatic H), 7.5-7.8 (m, 10H, Aromatic H). ^{13}C NMR (75 MHz, $CDCl_3$) δ = 14.2, 22.7, 23.9, 29.3, 29.4, 30.1, 31.9, 40.5, 55.4, 119.9, 120.3, 124.0, 124.2, 124.8, 125.7, 127.6, 129.0, 133.3, 134.5,

140.4, 143.4, 144.4, 151.9. HR-MS (FAB): *m/z* = 706.3668 (M^+, 100%). Calcd. for $C_{49}H_{54}S_2$ = 706.3667.

*2-(5-Phenyl-S,S-dioxidized thiophen-2-yl)-7-(5-phenylthiophen-2-yl)-9,9-dioctyl-fluorene (**FPTO₂**).* **FPT** (50 mg, 0.071 mmol) and *m*-CPBA (25 mg, 0.14 mmol) were dissolved in dichloromethane (10 mL), and the mixture was stirred at room temperature for 24 h. The reaction mixture was neutralized by $NaHCO_3$ aqueous solution, extracted with dichloromethane, washed with brine, dried over $MgSO_4$, filtered, and concentrated in vacuo. The crude product was purified by column chromatography on silica gel using *n*-hexane/ethyl acetate (85:15) as the eluent and by HPLC using *n*-hexane/ethyl acetate (60:40) as the eluent to give 11 mg of **FPTO₂** in 23% yield. **FPTO₂**: ^{1}H NMR (300 MHz, $CDCl_3$, TMS) δ = 0.69 (br, 4H CH_2), 0.79 (t, *J* = 7 Hz, 6H, CH_3), 1.0-1.2 (m, 20H, CH_2), 2.0-2.1 (m, 4H, CH_2), 7.05 (d, *J* = 5 Hz, 1H, Aromatic H), 7.06 (d, *J* = 5 Hz, 1H, Aromatic H), 7.2-7.5 (m, 8H, Aromatic H), 7.6-7.9 (m, 10H, Aromatic H). ^{13}C NMR (75 MHz, $CDCl_3$) δ = 14.2, 22.7, 23.9, 29.3, 29.4, 30.1, 31.9, 40.4, 55.6, 119.5, 120.0, 120.5, 120.6, 121.0, 124.2, 124.3, 124.3, 124.9, 125.8, 125.8, 125.9, 126.5, 127.5, 127.7, 129.1, 129.4, 130.3, 134.3, 134.4, 139.7, 141.4, 142.4, 143.1, 143.8, 144.2, 152.0, 152.4. HR-MS (FAB): *m/z* = 738.3550 (M^+, 100%). Calcd. for $C_{49}H_{54}O_2S_2$ = 738.3565.

*2,7-Bis(5-phenyl-S,S-dioxidized thiophen-2-yl)-9,9-dioctylfluorene (**FPTO₄**).* **FPT** (100 mg, 0.14 mmol) and *m*-CPBA (250 mg, 1.4 mmol) were dissolved in dichloromethane (50 mL), and the mixture was stirred at room temperature for 24 h. The reaction mixture was neutralized by $NaHCO_3$ aqueous solution, extracted with dichloromethane, washed with brine, dried over $MgSO_4$, filtered, and concentrated in vacuo. The crude product was purified by column chromatography and HPLC on silica gel using *n*-hexane/ethyl acetate (70:30) as the eluent and recycling preparative HPLC using chloroform as the eluent to give 14 mg of **FPTO₄** in 12% yield. **FPTO₄**: ^{1}H-NMR (300 MHz, $CDCl_3$, TMS): δ = 0.67 (br, 4H, CH_2), 0.80 (t, *J* = 7 Hz, 6H, CH_3), 1.0-1.3 (m, 20H, CH_2), 2.0-2.1 (m, 4H, CH_2), 7.07 (d, *J* = 5 Hz, 2H, Aromatic H), 7.11 (d, *J* = 5 Hz, 2H, Aromatic H), 7.4-7.6 (m, 6H, Aromatic H), 7.73 (s, 2H, Aromatic H), 7.8-7.9 (m, 8H, Aromatic H). ^{13}C NMR (75 MHz, $CDCl_3$) δ = 14.2, 22.7, 24.0, 29.3, 29.4, 30.1, 31.9, 40.3, 55.9, 120.1, 120.6, 120.8, 121.3, 125.9, 126.5, 126.8, 127.4, 129.4, 130.4, 141.7, 142.2, 142.3, 152.5. HR-MS (FAB): *m/z* = 770.3463 (M^+, 100%). Calcd. for $C_{49}H_{54}O_4S_2$ = 770.3464

*2,7-Bis(1-benzothiophen-2-yl)-9,9-dioctylfluorene (**FBT**).* 2-Bromo-1-benzo-

thiophene[18] (1.2 g, 5.6 mmol) was dissolved in anhydrous THF (20 mL) under argon atmosphere at −78 °C. 1.6 M *n*-BuLi hexane solution (5.5 mL, 8.4 mmol) was slowly added dropwise to the solution, and the mixture was stirred for 1.5 h. Tri-*n*-butyl borate (2.5 mL, 8.4 mmol) was slowly added to the solution at −78 °C, and the mixture was stirred for 1.5 h. Adequate amount of distilled water was added to the mixture to quench the reaction. 2,7-Dibromo-9,9-dioctylfluorene[19] (1.7 g, 2.8 mmol), tetrakis(triphenyl-phosphine)palladium(0) (320 mg, 0.28 mmol) and 20 wt% Na_2CO_3 aqueous solution (6.0 mL) were added to the solution, and the mixture were refluxed for 12 h. The reaction mixture was neutralized by HCl aqueous solution, extracted with dichloromethane, washed with brine, dried over $MgSO_4$, filtered, and concentrated in vacuo. The crude product was purified by column chromatography on silica gel using hexane 100% as the eluent to give 1.1 g of **FBT** in 60% yield. **FBT**: ^{1}H NMR (300 MHz, $CDCl_3$, TMS): δ = 0.73 (br, 4H CH_2), 0.77 (t, *J* = 7 Hz, 6H, CH_3), 1.0-1.2 (m, 20H, CH_2), 2.0-2.1 (m, 4H, CH_2), 7.2-7.4 (m, 4H, Aromatic H), 7.63 (s, 2H, Aromatic H), 7.6-7.9 (m, 10H, Aromatic H). HR-MS (FAB). ^{13}C NMR (75 MHz, $CDCl_3$) δ = 14.2, 22.7, 23.9, 29.3, 29.3, 30.1, 31.9, 40.5, 55.5, 119.4, 120.5, 120.8, 122.4, 123.6, 124.4, 124.7, 125.8, 133.5, 139.6, 141.0, 141.0, 145.0, 152.0. HR-MS (FAB): *m/z* = 654.3357 (M^+, 100%). Calcd. for $C_{45}H_{50}S_2$ = 654.3354.

*2-(S,S-Dioxidized 1-benzothiophen-2-yl)-7-(benzothiophen-2-yl)-9,9-dioctylfluorene (**FBTO₂**) and 2,7-(S,S-dioxidized 1-benzothiophen-2-yl)-9,9-dioctylfluorene (**FBTO₄**).* **FBT** (50 mg, 0.076 mmol) and *m*-CPBA (27 mg, 0.15 mmol) were dissolved in dichloromethane (5.0 mL), and the mixture was stirred at room temperature for 48 h. The reaction mixture was neutralized by $NaHCO_3$ aqueous solution, extracted with dichloromethane, washed with brine, dried over $MgSO_4$, filtered, and concentrated in vacuo. The crude product was purified by column chromatography on silica gel using ethyl acetate 100% as the eluent and HPLC using hexane/ethyl acetate (75:25) as the eluent to give 10 mg of **FBTO₂** in 18% yield and 28 mg of **FBTO₄** in 51%. **FBTO₂**: ^{1}H NMR (300 MHz, $CDCl_3$, TMS): δ = 0.70 (br, 4H CH_2), 0.77 (t, *J* = 7 Hz, 6H, CH_3), 1.0-1.2 (m, 20H, CH_2), 2.0-2.1 (m, 4H, CH_2), 7.3-7.9 (m, 16H, Aromatic H). ^{13}C NMR (75 Hz, $CDCl_3$) δ = 14.2, 22.7, 24.0, 29.3, 29.3, 30.1, 31.9, 40.4, 55.7, 119.7, 120.7, 120.8, 120.9, 121.0, 121.6, 122.4, 122.9, 123.7, 124.5, 124.7, 125.0, 125.9, 125.9, 126.1, 129.8, 131.6, 133.9, 134.2, 137.3, 139.6, 140.5, 140.9, 143.0, 143.3, 144.7, 152.1, 152.3. HR-MS (FAB): *m/z* = 686.3234 (M^+, 100%). Calcd. for $C_{45}H_{50}O_2S_2$ = 686.3252. **FBTO₄**: ^{1}H NMR (300 MHz, $CDCl_3$, TMS): δ = 0.68 (br, 4H CH_2), 0.76 (t, *J* = 7 Hz, 6H, CH_3), 1.0-2.0 (m, 20H, CH_2), 2.0-2.1 (m, 4H, CH_2), 7.38 (s, 2H, Aromatic H), 7.4-7.6 (m, 6H,

Aromatic H), 7.7-7.9 (m, 6H, Aromatic H), 7.9-8.0 (m, 6H, Aromatic H). ^{13}C NMR (75 MHz, $CDCl_3$) δ = 14.2, 22.7, 24.0, 29.3, 29.3, 30.1, 31.8, 40.2, 55.9, 120.8, 121.2, 121.6, 123.3, 125.1, 126.0, 126.8, 129.9, 131.4, 133.9, 137.2, 142.3, 143.0, 152.4. HR-MS (FAB): *m/z* = 718.3144 (M^+, 100%). Calcd. for $C_{45}H_{50}O_4S_2$ = 718.3151.

1.3 Results and Discussion

1.3.1 Optical Properties

Figure 1-1 shows the absorption and fluorescence spectra of **FPT** and **FBT** in *n*-hexane before and after the oxidation of the thiophene rings. The optical properties are summarized in Table 1-1. Before the oxidation, the absorption maximum wavelength (λ_{abs}) and fluorescence maximum wavelength (λ_{flu}) of **FPT** were observed at 383 and 423 nm, respectively. The Stokes shift was 2470 cm^{-1}. After the oxidation of the thiophene ring from **FPT** to **FPTO₂**, the λ_{abs} and λ_{flu} of **FPTO₂** were observed at 432 and 502 nm,

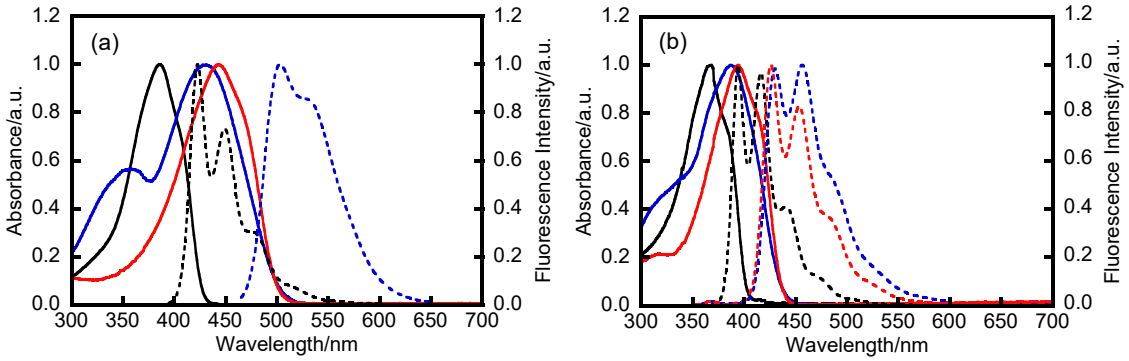

Figure 1-1. Normalized absorption spectra (solid line) and fluorescence spectra (dotted line) in *n*-hexane: (a) **FPT** (black line), **FPTO₂** (blue line), **FPTO₄** (red line), (b) **FBT** (black line), **FBTO₂** (blue line) and **FBTO₄** (red line). Reproduced from ref. 8 with permission from the European Society for Photobiology, the European Photochemistry Association, and The Royal Society of Chemistry.

Table 1-1. Absorption and fluorescence spectroscopic data of the fluorene derivatives in *n*-hexane. Reproduced from ref. 8 with permission from the European Society for Photobiology, the European Photochemistry Association, and The Royal Society of Chemistry.

Compound	λ_{abs}/nm[a]	λ_{flu}/nm[b]	$\Delta\nu$/cm^{-1}[c]	Φ_f[d]	τ_f/ns[e]	χ^2/ns[e]	k_f/ns^{-1}[f]	k_{nr}/ns^{-1}[g]
FPT	383	423, (449)	2470	0.69	0.747	1.06	0.924	0.415
FPTO₂	(356), 432	502	3230	0.25	2.08	1.11	0.120	0.361
FPTO₄	441	—[h]	—	—	—	—	—	—
FBT	366	393, (416)	1880	0.63	1.01	1.12	0.624	0.366
FBTO₂	390	429, (456)	2330	0.63	1.70	1.10	0.371	0.218
FBTO₄	392	426, (453)	2040	0.53	1.45	1.13	0.366	0.324

[a]Absorption maximum wavelength in *n*-hexane. [b]Fluorescence maximum wavelength in *n*-hexane. [c] Stokes shift ($\Delta\nu$). [d]Fluorescence quantum yield (Φ_f) in *n*-hexane. [e]Fluorescence lifetime in *n*-hexane. [f] Radiative rate constant: $k_f = \Phi_f/\tau_f$. [g]Non-radiative rate constant: $k_{nr} = (1 - \Phi_f)/\tau_f$. [h]No fluorescence.

respectively, which were shifted toward a longer wavelength by 49 and 79 nm compared with those of **FPT**. The Stokes shift increased up to 3230 cm^{-1}. In contrast, when **$FPTO_2$** was oxidized to **$FPTO_4$**, the absorption spectrum of **$FPTO_4$** was hardly shifted toward a longer wavelength in comparison with that of **$FPTO_2$**. **$FPTO_4$** showed no fluorescence. These results indicate that the first oxidation of the thiophene ring from **FPT** to **$FPTO_2$** is more effective to the longer wavelength shift of the absorption and fluorescence spectra.

Moreover, the optical properties of the benzothienylfluorene derivatives were also examined. In *n*-hexane, the λ_{abs} and λ_{flu} of **FBT** were observed at 366 and 393 nm, respectively. When **FBT** was oxidized to **$FBTO_2$**, λ_{abs} and λ_{flu} were shifted toward a longer wavelength at 390 nm and 429 nm, respectively. The shifts toward the longer wavelength of λ_{abs} and λ_{flu} were 24 and 36 nm, respectively, which are smaller than those of the phenylthienylfluorene derivatives. Furthermore, when **$FBTO_2$** was oxidized to **$FBTO_4$**, the absorption and fluorescence spectra of **$FBTO_4$** hardly changed. The red shifts of the absorption and fluorescence spectra by the oxidation of the thiophene ring are similar to those of the phenylthienylfluorene derivatives. The red shift of the absorption and fluorescence spectra can be ascribed to the introduction of the strong electron-withdrawing group of the *S*,*S*-dioxidized thienyl group. The introduction of the electron-withdrawing group stabilizes the LUMO level.[20] As a result, the energy gap between the highest occupied molecular orbital (HOMO) and LUMO decreases and the larger red shifts of the absorption and fluorescence spectra can be observed. In addition, the absorption spectra of all the compounds showed non-vibrational structures. However, the fluorescence spectra showed clear-cut vibrational structures in *n*-hexane. This result suggests that the fluorene derivatives are non-planar in the ground state, and the geometrical structure changes from a non-planar structure to a planar structure in the first excited state, which is consistent with the results of TD-DFT calculations as shown in Figure 1-2.

Next, the change in Φ_f by the oxidation of the thiophene rings was focused. The Φ_f value of **FPT** was determined to be 0.69. After the oxidation of the thiophene ring from **FPT** to **$FPTO_2$**, the Φ_f value of **$FPTO_2$** decreased down to 0.25. These results indicate that the Φ_f of **FPT** dramatically decreased with the oxidation of the thiophene rings, which may be ascribed to the decrease in the energy gap between the HOMO and LUMO. The Φ_f tends to decrease when λ_{flu} becomes longer, because of the increase in the deactivation process by the internal conversion, which is well-known as the energy gap law.[7b]

The Φ_f of the benzothienylfluorene derivatives in *n*-hexane was also examined. The Φ_f values of both **FBT** and **$FBTO_2$** were determined to be 0.63. The Φ_f did not decrease

according to the oxidation from **FBT** to **FBTO2**, while the Φ_f values of the phenylthienylfluorene derivatives dramatically decreased with the oxidation. Moreover, even if **FBTO2** was oxidized to **FBTO4**, Φ_f showed no significant difference. These results indicate that the change in Φ_f according to the oxidation of the benzothienylfluorene derivatives is quite different from that of the phenylthienylfluorene derivatives.

The change in optical properties by the oxidation of thiophene rings has also been reported for fluorophores having similar structures. The decrease in Φ_f for the phenylthienylfluorene derivatives according to the oxidation is comparable to that for the oligo/polythiophenes and fluorene–thiophene copolymers.[5, 6c, 21] Their absorption and fluorescence spectra are red-shifted according to the stabilization of the LUMO by introducing the *S*,*S*-dioxidized thienyl group as the electron withdrawing group. In addition, the Φ_f value of the thiophene derivatives often decreases by introducing *S*,*S*-dioxidized thiophene rings.[21b, 21d-f] In contrast, the optical properties of the benzothienylfluorene derivatives can be approximated with that of dibenzothiophene derivatives such as oligo/polymers bearing dibenzothiophene moieties.[7d, 21h, 22] The Φ_f values of the dibenzothiophene derivatives hardly change regardless of the presence of *S*,*S*-dioxidized dibenzothiophene.[21h, 22e] Some reports have described that the decrease in the Φ_f of thiophene derivatives is ascribed to the increase of the non-radiative process.[21a, 21b, 21e] Thereby, it is considered that the Φ_f of the phenylthienylfluorene derivatives decreased with the increase in the non-radiative process.

To further investigate the fluorescence properties of the phenylthienylfluorene derivatives, the fluorescence lifetimes (τ_f) were measured (Figure 1-3). The τ_f of **FPT** in *n*-hexane was determined to be 0.747 ns. After the oxidation of the thiophene ring from

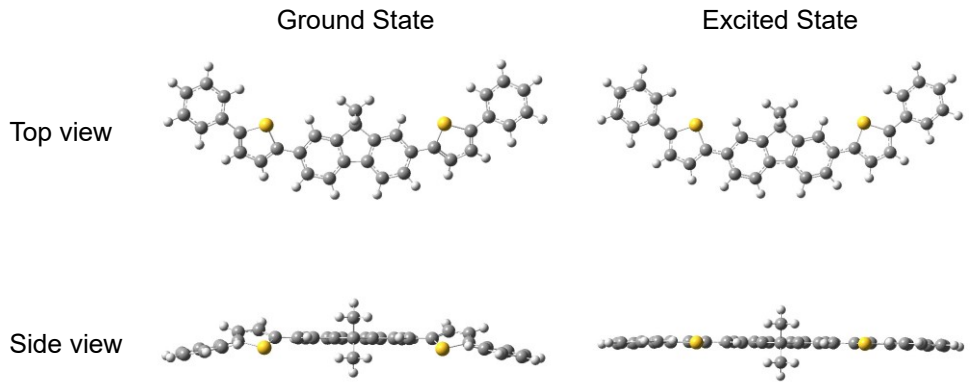

Figure 1-2. Top and side views of **FPT** molecule at the geometry-optimized ground and excited states. Reproduced from ref. 8 with permission from the European Society for Photobiology, the European Photochemistry Association, and The Royal Society of Chemistry.

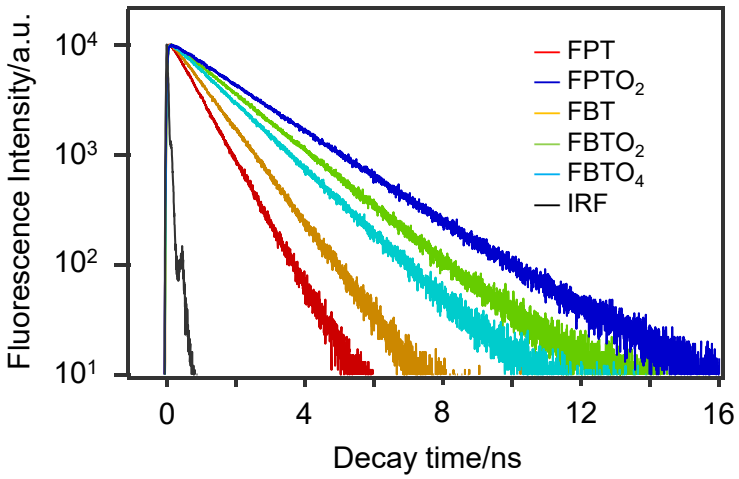

Figure 1-3. Fluorescence decay curves of fluorene derivatives in *n*-hexane. Reproduced from ref. 8 with permission from the European Society for Photobiology, the European Photochemistry Association, and The Royal Society of Chemistry.

FPT to **FPTO₂**, the τ_f of **FPTO₂** increased to 2.08 ns. The radiative rate constant (k_f) and the non-radiative rate constant (k_{nr}) of the phenylthienylfluorene derivatives were calculated from τ_f and Φ_f: $k_f = \Phi_f/\tau_f$, and $k_{nr} = (1 - \Phi_f)/\tau_f$. The k_f values of **FPT** and **FPTO₂** were estimated to be 0.924 and 0.120 ns^{-1}, respectively. By the oxidation of the thiophene ring, the k_f value significantly decreased. In contrast, their k_{nr} values were estimated to be 0.415 and 0.361 ns^{-1}, respectively. The k_{nr} value showed no significant difference compared with the k_f value. The τ_f values of **FBT**, **FBTO₂** and **FBTO₄** in *n*-hexane were determined to be 1.01, 1.70, and 1.45 ns, respectively. The k_f values were calculated to be 0.624, 0.371, and 0.366 ns^{-1}, and the k_{nr} values were calculated to be 0.366, 0.218, and 0.324 ns^{-1} for **FBT**, **FBTO₂** and **FBTO₄**, respectively. The k_f values slightly decreased according to the oxidation of the benzothiophene ring. No significant decrease of k_{nr} was also observed. These results indicate that the Φ_f values of the benzothienylfluorene derivatives are substantially constant because k_f and k_{nr} scarcely changed. In contrast, the results of the phenylthienylfluorene derivatives were different from those of the benzothienylfluorene derivatives. The k_{nr} value hardly changed and the k_f value significantly decreased by the oxidation of thiophene. Therefore, these results indicate that the decrease in Φ_f for the phenylthienylfluorene derivatives is not due to the increase in the non-radiative process but due to the decrease in the radiative process.

1.3.2 Solvent Effect

The solvent effect of the fluorene derivatives was investigated. Figure 1-4 shows the photographs of fluorescence in various solvents upon excitation with 365 nm light. The blue fluorescence was observed for **FPT** and **FBT** in all solvents. In contrast, **FPTO₂** and

FBTO$_2$ exhibited different fluorescence colors depending on the solvent. The absorption spectra, fluorescence spectra and the Φ_f of the fluorene derivatives in various organic solvents are summarized in Figure 1-5, Table 1-2, and Table 1-3. In *n*-hexane, the λ_{flu} of **FPT** was observed at 423 nm. Even if the polarity of the solvent increased, the λ_{flu} of **FPT** hardly changed. In contrast, the fluorescence spectra of **FPTO$_2$** were largely red-

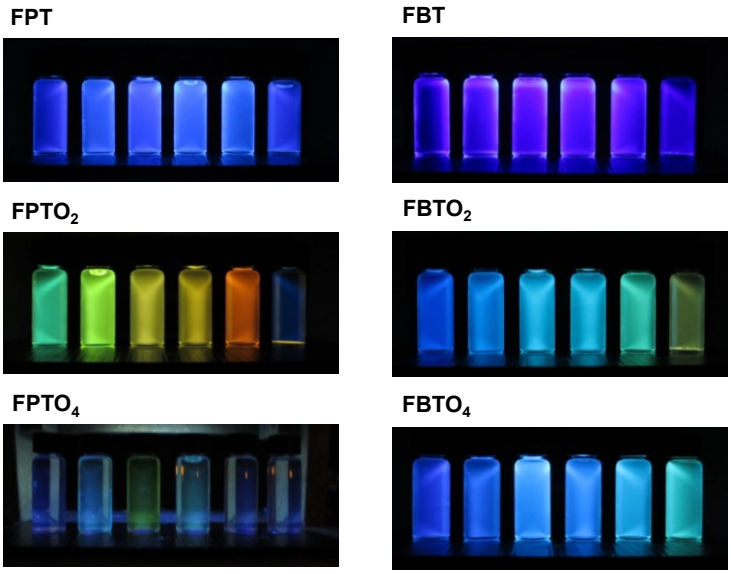

Figure 1-4. Photographs on fluorescence of the fluorene derivatives in various solvents upon excitation with 365 nm light: from the left side, *n*-hexane, toluene, THF, ethyl acetate, chloroform, and methanol as the solvent. Reproduced from ref. 8 with permission from the European Society for Photobiology, the European Photochemistry Association, and The Royal Society of Chemistry.

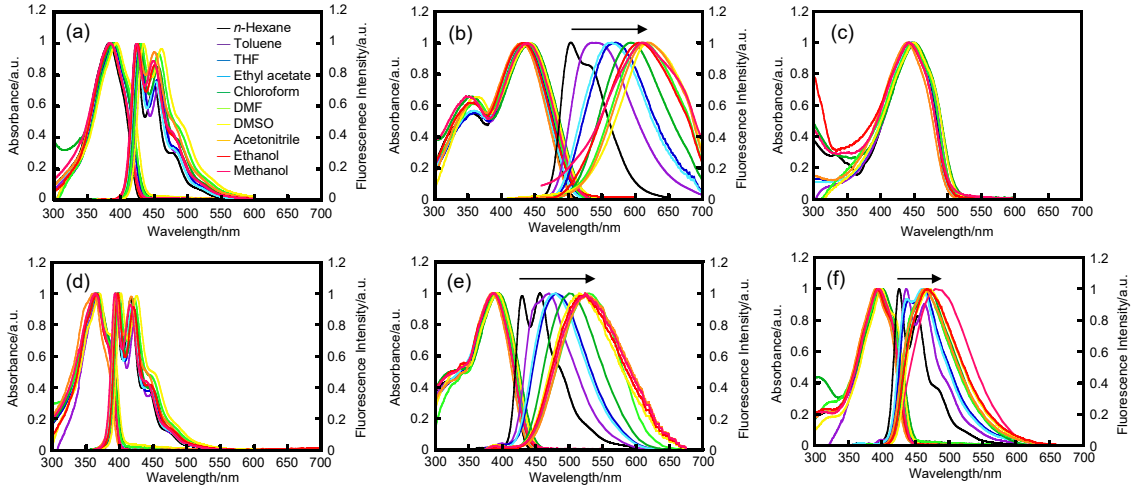

Figure 1-5. Normalized absorption and fluorescence spectra of (a) **FPT**, (b) **FPTO$_2$**, (c) **FPTO$_4$**, (d) **FBT**, (e) **FBTO$_2$**, and (f) **FBTO$_4$** in various organic solvents. Reproduced from ref. 8 with permission from the European Society for Photobiology, the European Photochemistry Association, and The Royal Society of Chemistry.

Table 1-2. Solvent dependence of the optical properties of fluorene derivatives. Reproduced from ref. 8 with permission from the European Society for Photobiology, the European Photochemistry Association, and The Royal Society of Chemistry.

Solvent	$E_T(30)$ /kcal mol^{-1}	Δf	Stokes shift/cm^{-1}					Φ_f				
			FPT	**FPTO$_2$**	**FBT**	**FBTO$_2$**	**FBTO$_4$**	**FPT**	**FPTO$_2$**	**FBT**	**FBTO$_2$**	**FBTO$_4$**
n-Hexane	31.0	0.00	2470	3230	1880	2330	2040	0.69	0.25	0.63	0.63	0.53
Toluene	33.9	0.01	2520	3970	1960	3960	2250	0.75	0.22	0.64	0.67	0.66
THF	37.4	0.20	2340	5390	1910	4720	3700	0.72	0.12	0.66	0.63	0.64
Ethyl acetate	38.1	0.18	2180	5420	1930	4880	3690	0.71	0.11	0.66	0.64	0.63
Chloroform	39.1	0.15	2460	5760	2050	5250	3720	0.70	0.050	0.69	0.61	0.67
DMF	43.2	0.28	2320	6520	2110	6170	3790	0.69	0.026	0.63	0.55	0.69
DMSO	45.1	0.27	2340	6490	2080	6430	3830	0.70	0.011	0.66	0.50	0.68
Acetonitrile	45.6	0.31	2440	7100	2170	6780	4090	0.72	0.013	0.68	0.52	0.69
Ethanol	51.9	0.29	2390	6780	2060	6730	4010	0.74	0.0070	0.62	0.40	0.71
Methanol	55.4	0.31	2400	6280	2030	6970	4570	0.73	0.0018	0.59	0.18	0.62

Table 1-3. Solvent dependence of the optical properties of fluorene derivatives. Reproduced from ref. 8 with permission from the European Society for Photobiology, the European Photochemistry Association, and The Royal Society of Chemistry.

Solvent	λ_{abs}/nm						λ_{flu}/nm					
	FPT	**FPTO$_2$**	**FPTO$_4$**	**FBT**	**FBTO$_2$**	**FBTO$_4$**	**FPT**	**FPTO$_2$**	**FPTO$_4$**	**FBT**	**FBTO$_2$**	**FBTO$_4$**
n-Hexane	383	432	441	366	390	392	423	502	–	393	429	426
Toluene	388	440	448	370	392	397	430	533	–	399	464	436
THF	389	436	446	369	390	396	428	570	–	397	478	464
Ethyl acetate	389	432	443	367	387	394	425	564	–	395	477	461
Chloroform	388	442	450	368	396	400	429	593	–	398	500	470
DMF	391	437	448	368	392	396	430	611	–	399	517	466
DMSO	394	441	450	371	393	399	434	618	–	402	526	471
Acetonitrile	385	429	440	363	385	390	425	617	–	394	521	464
Ethanol	385	428	444	367	388	394	424	603	–	397	525	468
Methanol	384	441	442	364	387	395	423	610	–	393	530	482

shifted as the polarity of the solvents increased: from λ_{flu} = 502 nm in *n*-hexane as apolar solvents to λ_{flu} = 610 nm in methanol as polar solvents.

First, the solvent polarity parameter ($E_T(30)$)[23] was employed in order to correlate the solvent dependence of the absorption and fluorescence spectra. $E_T(30)$ is known as a probe depending on solvent dipolarity and solvent acidity,[24] and the $E_T(30)$ approach is useful as a simple method for understanding the solvent effect. The absorption and

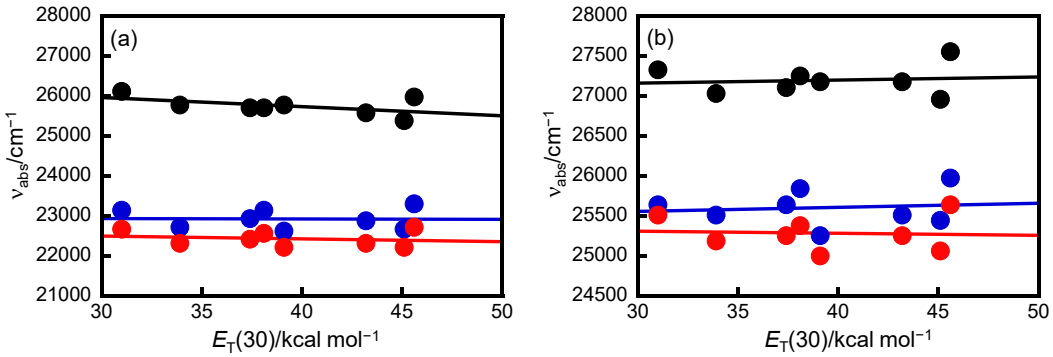

Figure 1-6. Absorption peak energy (ν_{abs}/cm^{-1}) of **FPT** (a: black), **FPTO$_2$** (a: blue), **FPTO$_4$** (a: red), **FBT** (b: black), **FBTO$_2$** (b: blue) and **FBTO$_4$** (b: red) versus the solvent polarity parameter, E_T(30). The slopes of the linear relationship are −3.19 for **FPT**, 1.24 for **FPTO$_2$**, 3.85 for **FPTO$_4$**, 9.35 for **FBT**, 10.91 for **FBTO$_2$** and −1.53 for **FBTO$_4$**. Reproduced from ref. 8 with permission from the European Society for Photobiology, the European Photochemistry Association, and The Royal Society of Chemistry.

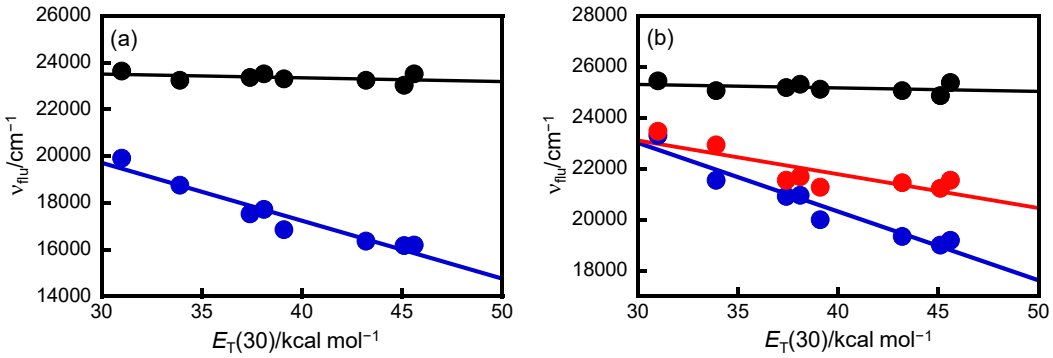

Figure 1-7. Fluorescence peak energy (ν_{flu}/cm^{-1}) of **FPT** (a: black), **FPTO$_2$** (a: blue), **FBT** (b: black), **FBTO$_2$** (b: blue) and **FBTO$_4$** (b: red) versus the solvent polarity parameter, E_T(30). The slopes of the linear relationship are 5.0 for **FPT**, −247 for **FPTO$_2$**, 1.65 for **FBT**, −269 for **FBTO$_2$** and −133 for **FBTO$_4$**. In the case of **FPTO$_2$**, **FBTO$_2$** and **FBTO$_4$**, the slope of the linear relationship was calculated except in methanol and ethanol. Reproduced from ref. 8 with permission from the European Society for Photobiology, the European Photochemistry Association, and The Royal Society of Chemistry.

fluorescence peak energies (ν_{abs} and ν_{flu}, respectively) relative to E_T(30) are plotted, as shown in Figures 1-6 and 1-7. The absorption and fluorescence maximum wavelengths of **FPT** and **FBT** hardly depended on the solvent. In contrast, the fluorescence spectra of **FPTO$_2$**, **FBTO$_2$** and **FBTO$_4$** largely depended on the solvent. ν_{flu} was well correlated to E_T(30) except in protonic solvents, such as methanol and ethanol. The linear relationship is considered to be ascribed to the solvent dipolarity.

Figure 1-8a shows the Stokes shifts ($\Delta\nu$) of the phenylthienylfluorene derivatives versus E_T(30). As shown in Figure 1-5, the changes in the absorption spectra of the fluorene derivatives by the solvent were much smaller than those in the fluorescence spectra. Therefore, the changes in the Stokes shifts are mainly due to those in the

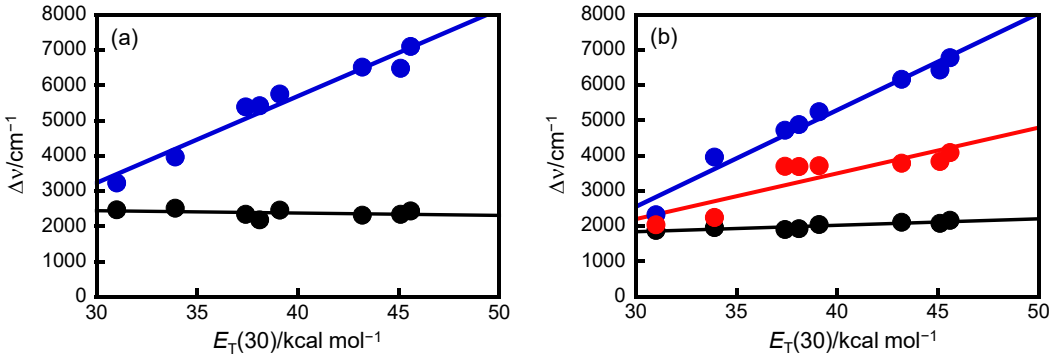

Figure 1-8. Stokes shift ($\Delta\nu$/cm^{-1}) of **FPT** (a: black), **FPTO$_2$** (a: blue), **FBT** (b: black), **FBTO$_2$** (b: blue) and **FBTO$_4$** (b: red) versus the solvent polarity, $E_T(30)$. The slopes of the linear relationship are −1.89 for **FPT**, 246 for **FPTO$_2$**, 7.72 for **FBT**, 274 for **FBTO$_2$** and 130 for **FBTO$_4$**. In the case of **FPTO$_2$**, **FBTO$_2$** and **FBTO$_4$**, the slope of the linear relationship was calculated except in methanol and ethanol. Reproduced from ref. 8 with permission from the European Society for Photobiology, the European Photochemistry Association, and The Royal Society of Chemistry.

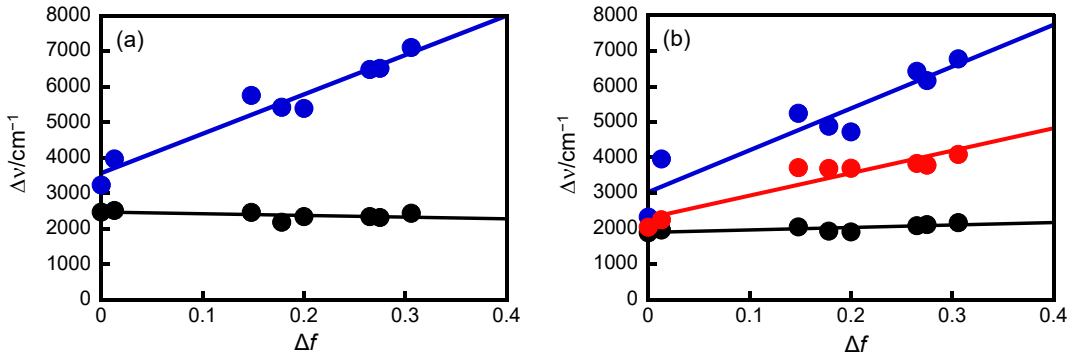

Figure 1-9. Stokes shift ($\Delta\nu$/cm^{-1}) of **FPT** (a: black), **FPTO$_2$** (a: blue), **FBT** (b: black), FBTO2 (b: blue) and **FBTO$_4$** (b: red) versus orientation polarizability function (Δf). Only aprotic solvent was used. The slopes of the linear relationship are −470 ± 337 for **FPT** (r = 0.495), 11102 ± 1102 for **FPTO$_2$** (r = 0.972), 684 ± 243 for **FBT** (r = 0.754), 11794 ± 1855 for **FBTO$_2$** (r = 0.933) and 6342 ± 956 for **FBTO$_4$** (r = 0.938). Reproduced from ref. 8 with permission from the European Society for Photobiology, the European Photochemistry Association, and The Royal Society of Chemistry.

fluorescence spectra. The slopes of the linear relationship for **FPTO$_2$**, **FBTO$_2$** and **FBTO$_4$** were larger than those of **FPT** and **FBT**. This is considered to be ascribed to the difference in dipole moments at the excited and ground states ($\Delta\mu$).

The Stokes shift can be related to $\Delta\mu$ by the Mataga–Lippert equation (eq 2).[25]

$$\Delta\nu = \nu_{\mathrm{abs}} - \nu_{\mathrm{flu}} = \frac{1}{4\pi\varepsilon_0}\frac{2\Delta\mu^2}{hca^3}\Delta f + constant \tag{2}$$

where $\Delta\nu$ is the Stokes shift in wavenumber (cm^{-1}), ν_{abs} and ν_{flu} are the wavenumbers of the absorption and fluorescence maximum wavelengths, respectively, ε_0 is the dielectric

constant of vacuum, h is the Planck constant, c is the light velocity, α is the cavity radius, and Δf is the orientation polarizability of the solvent defined as follows (eq 3):

$$\Delta f = \frac{\varepsilon - 1}{2\varepsilon + 1} - \frac{n^2 - 1}{2n^2 + 1} \tag{3}$$

where ε and n are the dielectric constant and refractive index of the solvent, respectively. Therefore, Δf depends on the solvent dipolarity and polarizability, while $E_T(30)$ depends on the solvent dipolarity and acidity. The cavity radius α for **FPTO₂** was estimated by using eq 4 and taken as 6.64 Å.[26]

$$a = \left(\frac{3M}{4N\pi d}\right)^{1/3} \tag{4}$$

where M is the molecular weight, N is Avogadro's number, and d is an assumed molecular density of 1 g cm^{-3}. The Mataga–Lippert plot for the phenylthienylfluorene derivatives is shown in Figure 1-9a. The data in protonic solvents were excluded to avoid specific solute–solvent interactions such as hydrogen bonding and the acidity and basicity of solvents. The linear relationships for the $\Delta\mu$ of **FPTO₂**, **FBTO₂** and **FBTO₄** versus Δf were obtained. These results indicate that the Stokes shift, i.e. the fluorescence spectra of **FPTO₂**, **FBTO₂** and **FBTO₄** depended on the solvent dipolarity and/or polarizability.

The $\Delta\mu$ value was estimated to be 18.0 D for **FPTO₂** from the slope of the Mataga–Lippert plot (11102 ± 1102 cm^{-1}, r = 0.972). The $\Delta\mu$ value between S_0 and S_1 states for **FPTO₂** was also calculated using the TD-DFT method. The calculated ground and excited state dipole moments (μ_g and μ_e) were 2.55 and 23.3 D, respectively. Thus, the calculated $\Delta\mu$ value was determined to be 20.8 D, which is in reasonably good agreement with that obtained from the Mataga–Lippert plot. These results suggest that **FPTO₂** has a larger dipole moment in the excited state in comparison with **FPT**. Thereby, **FPTO₂** showed strong solvatofluorochromism based on charge transfer (CT).

The $\Delta\mu$ value of **FBTO₂** can also be estimated from the Mataga–Lippert plot. The cavity radius α was taken as 6.48 Å for **FBTO₂** by the method described above. The $\Delta\mu$ value was determined to be 17.9 D for **FBTO₂** from the slope of the Mataga–Lippert plot (11794 ± 1855 cm^{-1}, r = 0.933). Th μ_g, μ_e and $\Delta\mu$ values calculated by TD-DFT were determined to be 4.40, 20.2 and 15.8 D. The calculated $\Delta\mu$ value is in reasonably good agreement with that obtained from the Mataga–Lippert plot. As with **FPTO₂** in the phenylthienylfluorene derivatives, **FBTO₂** has the largest $\Delta\mu$ among the

Table 1-4. Estimated coefficients (y_0, a_{SA}, b_{SB}, c_{SP} and d_{SdP} for ν_{abs}, ν_{flu}) and correlation coefficients (r) for regression analysis of the fluorene derivatives according to the Catalán solvent parameters (SA, SB, SP and SdP)[a] Reproduced from ref. 8 with permission from the European Society for Photobiology, the European Photochemistry Association, and The Royal Society of Chemistry.

Compound	Observable	y_0	a_{SA}	b_{SB}	c_{SP}	d_{SdP}	r
FPT	ν_{abs}	27355 ± 215	331 ± 129	−483 ± 116	−1967 ± 314	−18 ± 94	0.980
	ν_{flu}	25098 ± 123	78 ± 74	−118 ± 66	−2313 ± 179	−26 ± 53	0.992
FPTO₂	ν_{abs}	25242 ± 728	−874 ± 436	249 ± 391	−3394 ± 1061	138 ± 316	0.831
	ν_{flu}	20502 ± 922	−802 ± 553	749 ± 495	−1175 ± 1343	−3892 ± 401	0.988
FPTO₄	ν_{abs}	24249 ± 215	−246 ± 129	−117 ± 116	−2563 ± 313	136 ± 93	0.970
	ν_{flu}	–	–	–	–	–	–
FBT	ν_{abs}	28758 ± 108	−75 ± 65	−495 ± 58	−2299 ± 157	440 ± 47	0.992
	ν_{flu}	26879 ± 224	−76 ± 134	−261 ± 120	−2292 ± 326	86 ± 97	0.967
FBTO₂	ν_{abs}	27396 ± 439	−313 ± 263	109 ± 236	−2738 ± 639	241 ± 191	0.906
	ν_{flu}	24720 ± 1050	−2315 ± 629	856 ± 564	−2632 ± 1529	−4025 ± 456	0.988
FBTO₄	ν_{abs}	27171 ± 343	−515 ± 205	−93 ± 184	−2724 ± 499	209 ± 149	0.927
	ν_{flu}	23813 ± 1576	−1119 ± 944	−70 ± 847	−889 ± 2296	−1913 ± 685	0.916

benzothienylfluorene derivatives and showed significant solvatofluorochromism. It is considered that these properties are also caused by CT from the donor to the acceptor by bearing a benzothienyl group as a donor and an *S*,*S*-dioxidized benzothienyl group as an acceptor. From the $E_T(30)$ approach and the Mataga–Lippert approach, the solvatofluorochromism of **FPTO₂**, **FBTO₂** and **FBTO₄** is considered to be mainly affected by solvent dipolarity. However, other factors such as the solvent polarizability, acidity and basicity cannot be neglected as minor contributors.

Next, a multiparametric method is employed to discuss about the solvent effect in more detail. Recently, Catalán developed an empirical methodology to explain the experimental solvatochromic properties of organic compounds from theoretical solvent characteristics. The solvent effect of ν_{abs} and ν_{flu} can be described by using the multilinear expression (eq 5).[24]

$$\mathrm{y} = y_0 + a_{\mathrm{SA}}\mathrm{SA} + b_{\mathrm{SB}}\mathrm{SB} + c_{\mathrm{SP}}\mathrm{SP} + d_{\mathrm{SdP}}\mathrm{SdP} \quad (5)$$

where y is the solvent dependent physicochemical properties (ν_{abs} and ν_{flu}) in a given solvent, and y_0 is the value of the physicochemical properties in the gas phase. SA, SB, SP and SdP are the solvent acidity, basicity, polarizability, and dipolarity properties, respectively. The coefficients, a_{SA}, b_{SB}, c_{SP} and d_{SdP}, represent the contribution of each type of interaction. SA, SB, SP and SdP parameters for each solvent were taken from the

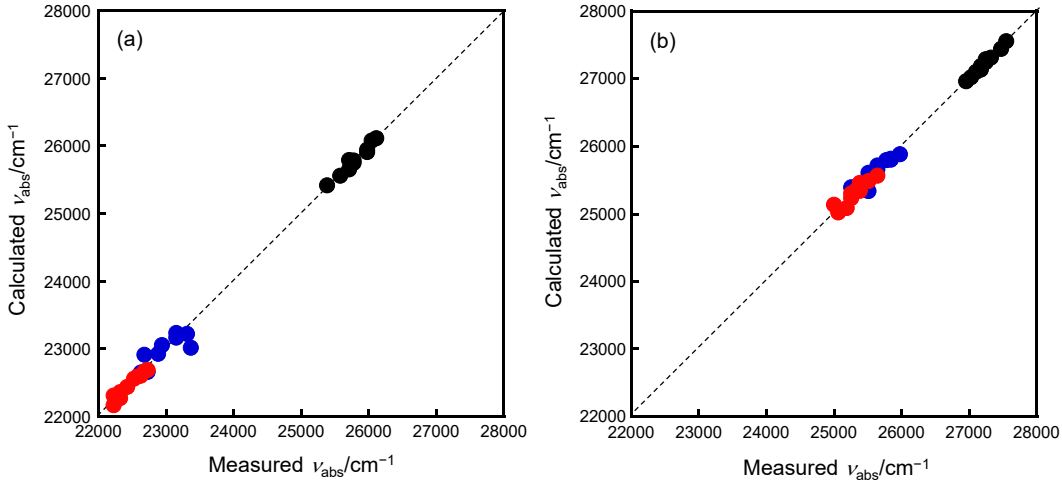

Figure 1-10. Relationship between the measured and calculated ν_{abs} values according to the Catalán equation for **FPT** (a: black), **FPTO$_2$** (a: blue), **FPTO$_4$** (a: red), **FBT** (b: black), **FBTO$_2$** (b: blue) and **FBTO$_4$** (b: red). Reproduced from ref. 8 with permission from the European Society for Photobiology, the European Photochemistry Association, and The Royal Society of Chemistry.

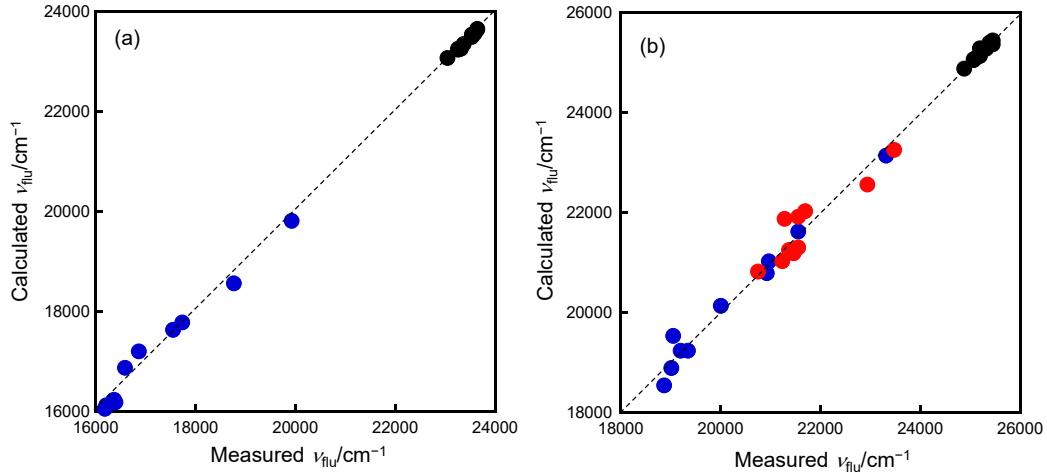

Figure 1-11. Relationship between the measured and calculated ν_{flu} values according to the Catalán equation for **FPT** (a: black), **FPTO$_2$** (a: blue), **FBT** (b: black), **FBTO$_2$** (b: blue) and **FBTO$_4$** (b: red). Reproduced from ref. 8 with permission from the European Society for Photobiology, the European Photochemistry Association, and The Royal Society of Chemistry.

literature.[24] By using the Catalán's model, it is possible to estimate the magnitude of acidity, basicity, dipolarity and polarizability of the solvents for the solvent effect. The coefficients, y_0, a_{SA}, b_{SB}, c_{SP} and d_{SdP}, their standard deviations and the multiple linear correlation coefficient r for the fluorene derivatives are summarized in Table 1-4. The experimental data are shown in Figures 1-10 and 1-11. In the case of ν_{flu} for the phenylthienylfluorene derivatives, a good r value was obtained. The largest contribution for **FPT** was the solvent polarizability (c_{SP} = −2313), which indicates that the dominant factor influencing the solvatochromic changes in ν_{flu} is the solvent polarizability. The

dominant factor of **FPTO₂** in ν_{flu} was the solvent dipolarity (d_{SdP} = −3892). However, the polarizability, acidity and basicity factors should not be neglected since c_{SP}, a_{SA} and b_{SB} are also relatively large. These results are consistent with those obtained from the $E_T(30)$ approach and the Mataga–Lippert approach. On the other hand, the largest value was c_{SP} in the case of ν_{abs}, which indicates that the dominant factor influencing the solvatochromic changes in ν_{abs} is the solvent polarizability, and the solvent acidity, basicity and dipolarity hardly influenced the solvatochromic changes in ν_{abs} in comparison with the solvent polarizability. Less contribution of the solvent dipolarity is consistent with the result obtained from the $E_T(30)$ approach.

In the case of ν_{abs} for the benzothienylfluorene derivatives, the dominant factor influencing the solvatochromic changes is the solvent polarizability as well as the phenylthienylfluorene derivatives. Moreover, although the dominant factor of **FBTO₂** and **FBTO₄** in ν_{flu} was the solvent dipolarity (d_{SdP} = −4025 for **FBTO₂** and −1913 for

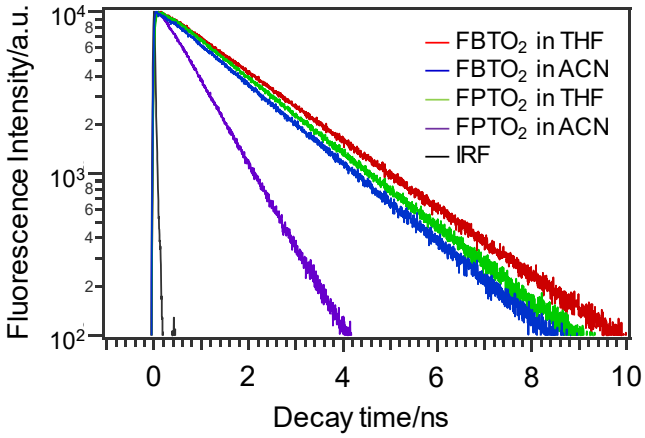

Figure 1-12. Fluorescence decay curves of **FPTO₂** and **FBTO₂** in THF and acetonitrile. Reproduced from ref. 8 with permission from the European Society for Photobiology, the European Photochemistry Association, and The Royal Society of Chemistry.

Table 1-5. Fluorescence lifetime, fluorescence quantum yield, radiative and non-radiative rate constants of **FPTO₂** and **FBTO₂** in several solvents. Reproduced from ref. 8 with permission from the European Society for Photobiology, the European Photochemistry Association, and The Royal Society of Chemistry.

	Solvent	τ_f/ns	χ^2	Φ_f	k_f/ns^{-1}	k_{nr}/ns^{-1}
	n-Hexane	2.08	1.11	0.25	0.120	6.24
FPTO₂	THF	1.88	1.13	0.11	0.0585	15.2
	Acetonitirle	0.845	1.46	0.013	0.0154	64.2
	n-Hexane	1.70	1.10	0.63	0.371	1.00
FBTO₂	THF	2.06	1.03	0.63	0.306	1.21
	Acetonitirle	1.79	1.10	0.52	0.291	1.65

FBTO4), the ν_{flu} values were also influenced by the solvent acidity (a_{SA} = −2315 for **FBTO2** and −1119 for **FBTO4**) and polarizability (c_{SP} = −2632 for **FBTO2** and −889 for **FBTO4**) as minor contributors.

The solvent dependence of Φ_f was also investigated. In *n*-hexane, the Φ_f of **FPTO2** was 0.25. However, it gradually decreased with the polarity of the solvents and was found to be 0.0018 in methanol. **FPTO4** showed no fluorescence. These results can also be explained by the energy gap law.[7b] The red shift of the fluorescence spectra caused an increase in internal conversion and a decrease in Φ_f. The solvent effect is ascribed to the asymmetric structure of the fluorene derivatives. **FPTO2** has a large polarity in the excited state because it has the *S*,*S*-dioxidized thienyl group as the electron withdrawing character and the thienyl group as the electron donating character. Therefore, **FPTO2** at the singlet excited state is stabilized because of the solvent reorientation caused by interaction with the solvents. Table 1-5 summarizes the τ_f, Φ_f, k_f and k_{nr} of **FPTO2** and **FBTO2** in several solvents (in *n*-hexane, THF and acetonitrile). Their fluorescence decays are shown in Figures 1-3 and 1-12. As mentioned above, the Φ_f of **FPTO2** decreased with the increasing polarity of the solvents based on the energy gap law.

In addition, although τ_f in *n*-hexane was 2.08 ns, the τ_f values in THF and acetonitrile were 1.88 and 0.845 ns, respectively. τ_f also decreased with the increasing polarity of the solvents. By estimating k_f and k_{nr} from these values, k_f decreased and k_{nr} increased with the increasing polarity of the solvents. These results support that the decrease in Φ_f is based on the energy gap law.

The Φ_f of **FBTO2** decreased with the polarity of the solvents from *n*-hexane (Φ_f = 0.63) to methanol (Φ_f = 0.18). In addition, as shown in Table 1-4, k_f slightly decreased and k_{nr} slightly increased with the increasing polarity of the solvents. Therefore, the solvatofluorochromism of **FBTO2** is also due to the energy gap law.

1.3.3 Theoretical Study

The absorption maximum wavelength corresponds to the energy gap between the ground state and the singlet excited state. Additionally, this energy gap can be related to the HOMO–LUMO gap. Therefore, the absorption maximum wavelength of the fluorene derivatives can be evaluated by using the HOMO–LUMO gap. The molecular structures of the fluorene derivatives in the ground state were fully optimized at the B3LYP/6-31G* level of theory, which can determine their HOMO and LUMO levels. The results are shown in Table 1-6. In the calculation, the octyl groups in the fluorene derivatives were replaced with the methyl groups to simplify the calculation. The HOMO and LUMO levels were decreased with the increasing *S*,*S*-dioxidized thiophene moiety. In particular,

Table 1-6. HOMO and LUMO level data of the fluorene derivatives calculated by the density functional theory (DFT) (B3LYP/6-31G*)[a]. Reproduced from ref. 8 with permission from the European Society for Photobiology, the European Photochemistry Association, and The Royal Society of Chemistry.

Compound	E_{LUMO}/eV	E_{HOMO}/eV	$E_{HOMO\text{-}LUMO\ gap}$/eV
FPT	−1.68	−5.06	−3.38
$FPTO_2$	−2.48	−5.26	−2.78
$FPTO_4$	−2.70	−5.56	−2.86
FBT	−1.69	−5.30	−3.61
$FBTO_2$	−2.24	−5.45	−3.22
$FBTO_4$	−2.41	−5.72	−3.31

[a]The octyl groups in the fluorene derivatives were replaced with the methyl groups to simplify the calculation.

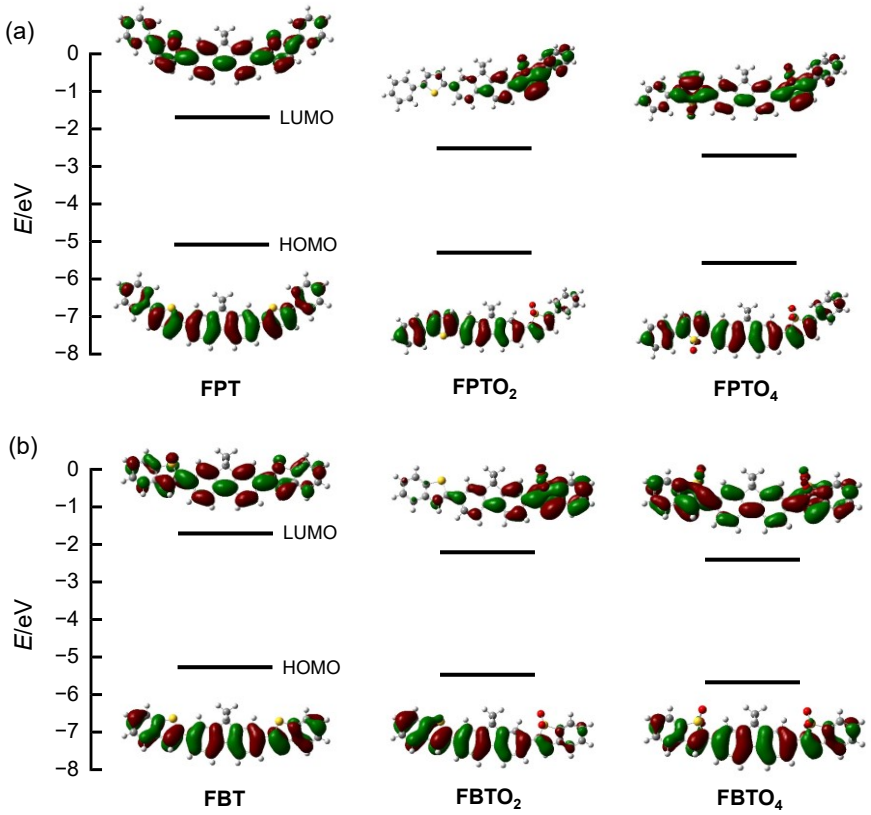

Figure 1-13. Molecular orbitals and energies of (a) the phenylthienylfluorene derivatives and (b) the benzothienylfluorene derivatives. The octyl groups in the fluorene derivatives were replaced with the methyl groups to simplify the calculation. Reproduced from ref. 8 with permission from the European Society for Photobiology, the European Photochemistry Association, and The Royal Society of Chemistry.

the LUMO level was significantly decreased. This was ascribed to the stabilization of the LUMO by introducing the *S*,*S*-dioxidized thienyl and benzothienyl groups as strong

electron withdrawing groups. As a result, the HOMO–LUMO gap was reduced, and the absorption maximum wavelength was redshifted. The decreasing HOMO–LUMO gap from **FPTO$_2$** to **FPTO$_4$** was smaller than that from **FPT** to **FPTO$_2$**. The benzothienylfluorene derivatives also showed similar results.

Next, the electron density distributions of the fluorene derivatives used in this work were calculated by using the optimized molecular structures, and the energies of the HOMO and LUMO levels are shown in Figure 1-13. The electron densities of the HOMO and LUMO levels for **FPT** and **FBT** were delocalized. **FPTO$_4$** and **FBTO$_4$** also exhibited a similar tendency. In contrast, the electron densities of **FPTO$_2$** and **FBTO$_2$** bearing asymmetric structures significantly change between the HOMO and LUMO levels. The electron density of the LUMO level was localized on the *S*,*S*-dioxidized thiophene moiety, while that of the HOMO level was localized on the thiophene and fluorene moieties. The HOMO–LUMO transition of **FPTO$_2$** and **FBTO$_2$** exhibited a significant CT character. Therefore, it is considered that **FPTO$_2$** and **FBTO$_2$** also have a CT character. Thereby, **FPTO$_2$** and **FBTO$_2$** in excited states interacted with polar solvents, and solvent reorientation was caused. The fluorescence maximum wavelength was shifted toward a longer wavelength because the excited states were stabilized with the increasing polarity of the solvents. Few changes of the electron density distribution between the HOMO and LUMO levels for **FPT**, **FBT**, **FPTO$_4$**, and **FBTO$_4$** bearing symmetric structures were confirmed.

1.4 Summary

9,9-Dioctylfluorenes connected phenylthiophene (**FPT**) or benzothiophene (**FBT**), and their thiopheneoxidized derivatives (**FPTO$_2$**, **FPTO$_4$**, **FBTO$_2$**, and **FBTO$_4$**) were synthesized, and their optical properties were examined. The absorption and fluorescence maximum wavelengths of their fluorene derivatives were shifted toward a longer wavelength by oxidation of the thiophene rings. This is due to the decrease of the HOMO–LUMO energy gap with the stabilization of the LUMO energy by oxidation of the thiophene ring. The fluorescence quantum yields of the phenylthienylfluorene derivatives drastically decreased with the increasing number of the *S*,*S*-dioxidized thiophene rings. This is due to the decrease in the radiative process. On the other hand, the benzothienylfluorene derivatives maintained the fluorescence quantum yields even in the fluorene having *S*,*S*-dioxidized thiophene rings at both sides. Moreover, the solvent effects on the absorption and fluorescence spectra and the fluorescence quantum yields of the fluorene derivatives were observed in **FPTO$_2$** and **FBTO$_2$**. Although there were no changes in **FPT** and **FBT**, the Stokes shifts of the oxidized compounds increased and the

fluorescence quantum yields decreased with the increasing polarity of the solvent. This is due to the CT effect caused by the electron withdrawing sulfonyl groups.

1.5 References

[1] a) M. Leclerc, *J. Polym. Sci., Part A: Polym. Chem.* **2001**, *39*, 2867-2873; b) U. Scherf, E. J. W. List, *Adv. Mater.* **2002**, *14*, 477-487; c) A. C. Grimsdale, K. Leok Chan, R. E. Martin, P. G. Jokisz, A. B. Holmes, *Chem. Rev.* **2009**, *109*, 897-1091; d) S. Beaupré, P.-L. T. Boudreault, M. Leclerc, *Adv. Mater.* **2010**, *22*, E6-E27; e) L. Xiao, Z. Chen, B. Qu, J. Luo, S. Kong, Q. Gong, J. Kido, *Adv. Mater.* **2010**, *23*, 926-952.

[2] a) J. Y. Kim, T. Yasuda, Y. S. Yang, N. Matsumoto, C. Adachi, *Chem. Commun.* **2014**, *50*, 1523-1526; b) J. Xu, A. Takai, Y. Kobayashi, M. Takeuchi, *Chem. Commun.* **2013**, *49*, 8447-8449.

[3] A. Yokoyama, H. Suzuki, Y. Kubota, K. Ohuchi, H. Higashimura, T. Yokozawa, *J. Am. Chem. Soc.* **2007**, *129*, 7236-7237.

[4] A. Facchetti, *Chem. Mater.* **2011**, *23*, 733-758.

[5] S. Destri, M. Pasini, W. Porzio, G. Gigli, D. Pisignano, C. Capolupo, *Synth. Met.* **2003**, *138*, 289-293.

[6] a) G. Barbarella, O. Pudova, C. Arbizzani, M. Mastragostino, A. Bongini, *J. Org. Chem.* **1998**, *63*, 1742-1745; b) L. S. Miguel, A. J. Matzger, *J. Org. Chem.* **2008**, *73*, 7882-7888; c) S. Wei, J. Xia, E. J. Dell, Y. Jiang, R. Song, H. Lee, P. Rodenbough, A. L. Briseno, L. M. Campos, *Angew. Chem. Int. Ed.* **2014**, *53*, 1832-1836.

[7] a) M. H. M. Cativo, A. C. Kamps, J. Gao, J. K. Grey, G. R. Hutchison, S.-J. Park, *J. Phys. Chem. B* **2013**, *117*, 4528-4535; b) N. J. Turro, V. Ramamurthy, V. Ramamurthy, J. C. Scaiano, *Principles of Molecular Photochemistry: An Introduction*, University Science Books, **2009**; c) E. L. Dane, S. B. King, T. M. Swager, *J. Am. Chem. Soc.* **2010**, *132*, 7758-7768; d) L. Yao, S. Sun, S. Xue, S. Zhang, X. Wu, H. Zhang, Y. Pan, C. Gu, F. Li, Y. Ma, *J. Phys. Chem. C* **2013**, *117*, 14189-14196.

[8] T. Nakahama, D. Kitagawa, H. Sotome, S. Ito, H. Miyasaka, S. Kobatake, *Photochem. Photobiol. Sci.* **2016**, *15*, 1254-1263.

[9] M. Frisch, G. Trucks, H. Schlegel, G. Scuseria, M. Robb, J. Cheeseman, G. Scalmani, V. Barone, B. Mennucci, G. J. I. Petersson *et al*., Gaussian 09, Revision C.01, Gaussian, Inc., Wallingford CT, **2009**.

[10] C. A. Parker, W. T. Rees, *Analyst* **1960**, *85*, 587-600.

[11] a) W. R. Dawson, M. W. Windsor, *J. Phys. Chem.* **1968**, *72*, 3251-3260; b) W. H. Melhuish, *J. Phys. Chem.* **1961**, *65*, 229-235.

[12] a) S. Hamai, F. Hirayama, *J. Phys. Chem.* **1983**, *87*, 83-89; b) S. R. Meech, D. Phillips, *J. Photochem.* **1983**, *23*, 193-217.

[13] G. A. Crosby, J. N. Demas, *J. Phys. Chem.* **1971**, *75*, 991-1024.

[14] C. V. Suneesh, M. V. Vinayak, K. R. Gopidas, *J. Phys. Chem. C* **2010**, *114*, 18735-18744.

[15] Y. Nagasawa, T. Itoh, M. Yasuda, Y. Ishibashi, S. Ito, H. Miyasaka, *J. Phys. Chem. B* **2008**, *112*, 15758-15765.

[16] M. S. Maji, T. Pfeifer, A. Studer, *Chem. Eur. J.* **2010**, *16*, 5872-5875.

[17] S. Kobatake, M. Irie, *Chem. Lett.* **2003**, *32*, 1078-1079.

[18] L. Qiu, X. Zhang, W. Yang, Y. Wang, G. P. Simon, D. Li, *Chem. Commun.* **2011**, *47*, 5810-5812.

[19] H. Chi, S. L. Lim, F. Wang, X. Wang, C. He, W. S. Chin, *Macromol. Rapid Commun.* **2014**, *35*, 801-806.

[20] J. L. Jellison, C.-H. Lee, X. Zhu, J. D. Wood, K. N. Plunkett, *Angew. Chem. Int. Ed.* **2012**, *51*, 12321-12324.

[21] a) G. Barbarella, L. Favaretto, G. Sotgiu, M. Zambianchi, A. Bongini, C. Arbizzani, M. Mastragostino, M. Anni, G. Gigli, R. Cingolani, *J. Am. Chem. Soc.* **2000**, *122*, 11971-11978; b) M. M. Oliva, J. Casado, J. T. L. Navarrete, S. Patchkovskii, T. Goodson, M. R. Harpham, J. S. Seixas de Melo, E. Amir, S. Rozen, *J. Am. Chem. Soc.* **2010**, *132*, 6231-6242; c) E. Busby, J. Xia, J. Z. Low, Q. Wu, J. Hoy, L. M. Campos, M. Y. Sfeir, *J. Phys. Chem. B* **2015**, *119*, 7644-7650; d) G. Barbarella, L. Favaretto, G. Sotgiu, M. Zambianchi, V. Fattori, M. Cocchi, F. Cacialli, G. Gigli, R. Cingolani, *Adv. Mater.* **1999**, *11*, 1375-1379; e) M. Pasini, S. Destri, W. Porzio, C. Botta, U. Giovanella, *J. Mater. Chem.* **2003**, *13*, 807-813; f) A. Charas, J. Morgado, J. M. G. Martinho, L. Alcácer, F. Cacialli, *Chem. Commun.* **2001**, 1216-1217; g) S. M. Fonseca, J. Pina, L. G. Arnaut, J. Seixas de Melo, H. D. Burrows, N. Chattopadhyay, L. Alcácer, A. Charas, J. Morgado, A. P. Monkman, U. Asawapirom, U. Scherf, R. Edge, S. Navaratnam, *J. Phys. Chem. B* **2006**, *110*, 8278-8283; h) Z. H. Li, M. S. Wong, H. Fukutani, Y. Tao, *Chem. Mater.* **2005**, *17*, 5032-5040.

[22] a) W. Yang, Q. Hou, C. Liu, Y. Niu, J. Huang, R. Yang, Y. Cao, *J. Mater. Chem.* **2003**, *13*, 1351-1355; b) F. B. Dias, S. Pollock, G. Hedley, L.-O. Pålsson, A. Monkman, I. I. Perepichka, I. F. Perepichka, M. Tavasli, M. R. Bryce, *J. Phys. Chem. B* **2006**, *110*, 19329-19339; c) S. M. King, I. I. Perepichka, I. F. Perepichka, F. B. Dias, M. R. Bryce, A. P. Monkman, *Adv. Funct. Mater.* **2009**, *19*, 586-591; d) I. I.

Perepichka, I. F. Perepichka, M. R. Bryce, L.-O. Pålsson, *Chem. Commun.* **2005**, 3397-3399; e) J. A. Mikroyannidis, H. A. Moshopoulou, J. A. Anastasopoulos, M. M. Stylianakis, L. Fenenko, C. Adachi, *J. Polym. Sci., Part A: Polym. Chem.* **2006**, *44*, 6790-6800.

[23] C. Reichardt, *Chem. Rev.* **1994**, *94*, 2319-2358.

[24] J. Catalán, *J. Phys. Chem. B* **2009**, *113*, 5951-5960.

[25] a) N. Mataga, Y. Kaifu, M. Koizumi, *Bull. Chem. Soc. Jpn.* **1955**, *28*, 690-691; b) N. Mataga, Y. Kaifu, M. Koizumi, *Bull. Chem. Soc. Jpn.* **1956**, *29*, 465-470; c) E. Lippert, in *Z. Naturforsch., A: Phys. Sci.,* **1955**, *10*, 541-545; d) E. Lippert, *Z. Elektrochem.* **1957**, *61*, 962-975.

[26] L. Onsager, *J. Am. Chem. Soc.* **1936**, *58*, 1486-1493.

Chapter 2

Fluorescence On/Off Switching in Polymers Bearing Diarylethene and Fluorene in Their Side Chains

2.1 Introduction

As mentioned in General Introduction, the fluorescence on/off switching of various photochromic diarylethenes has been reported. Diarylethenes linked to fluorophores exhibit fluorescence on/off switching upon alternating irradiation with UV and visible light. When diarylethenes are in their open-ring forms, the fluorophores exhibit fluorescence. When diarylethenes are converted to their closed-ring forms, the fluorescence is quenched by an energy transfer from the fluorophore moiety to the diarylethene closed-ring form.[1] Fluorescence-switchable diarylethenes exhibit properties, such as high fluorescence on/off contrast and rapid switching speed, which are desirable for applications in the field of optoelectronics and bioimaging.[2]

When the photocyclization conversion of diarylethenes linked to fluorophores does not reach 100% at the photostationary state (PSS), residual fluorescence occurs, which results in low fluorescence on/off contrast. To improve their fluorescence on/off contrast, molecules bearing one fluorophore and multiple diarylethenes have been reported. Bis-(phenylethynyl)anthracene,[3] porphyrin,[4] and perylenediimide[5] linked to multiple diarylethenes have been investigated for their fluorescence on/off switching properties. Moreover, aggregates such as silica nanoparticles,[6] organic nanoparticles,[7] and polymers[8] have been proposed as alternative approaches to improve fluorescence on/off switching properties.

However, there are few reports on the effect of polymer structures such as a monomer sequence for the fluorescence on/off switching properties, such as the fluorescence on/off contrast and switching speed, although various systems of polymers containing diarylethenes and fluorophores have been proposed for the applications described above. Clarifying this effect is expected to lead to systems bearing more efficient fluorescence on/off switching properties even if the same diarylethene and fluorophore moieties are used.

In this chapter, developing molecules with efficient fluorescent on/off switching properties, such as high speed switching and high fluorescence on/off contrast, have been focused. The introduction of diarylethene and fluorene derivatives into the side chains of polymers was proposed. First, a diarylethene-fluorene dyad (**DE-FL**) connected by an ester bond was synthesized, as shown in Scheme 2-1. Next, random and alternative

copolymers bearing diarylethene and fluorene derivatives in their side chains [**poly(DE1$_x$-*co*-FL1$_y$)** and **poly(DE1-*alt*-FL2)**] were synthesized to investigate the effects of the molar fractions of diarylethene and fluorene and the monomer sequence of the copolymers on their fluorescence on/off switching properties.[9]

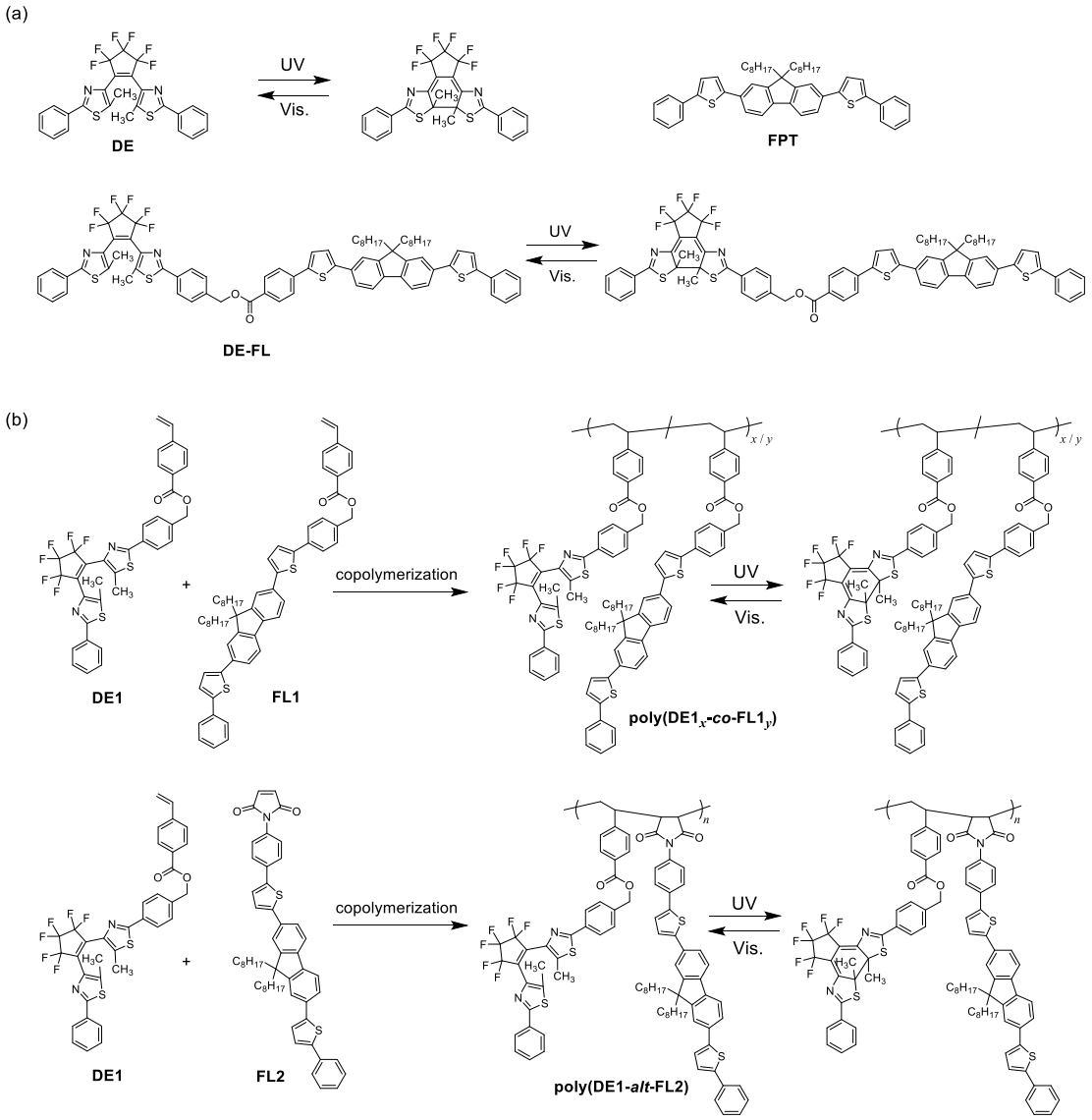

Scheme 2-1. (a) Molecular structures of diarylethene derivative (**DE**), fluorene derivative (**FPT**), and diarylethene-fluorene dyad (**DE-FL**); (b) synthesis and photochromic reaction of **poly(DE1$_x$-*co*-FL1$_y$)** and **poly(DE1-*alt*-FL2).** Reprinted with permission from ref. 9. Copyright 2017 American Chemical Society.

2.2 Experimental Section

2.2.1 General

^{1}H NMR spectra were recorded on a Bruker AV- 300N spectrometer at 300 MHz. Deuterated chloroform ($CDCl_3$) was used as the solvent, and tetramethylsilane (TMS)

was used as an internal standard. Mass spectra were obtained using a Bruker FT-ICR/solariX mass spectrometer. Gel-permeation chromatography (GPC) was performed using a Tosoh 8000 series GPC system equipped with TSK-gel columns at 40 °C in tetrahydrofuran (THF) as the eluent. Standard polystyrenes were used as the calibration standard. Differential scanning calorimetry (DSC) was performed using a Hitachi DSC7000X instrument at a heating rate of 10 °C min^{-1}. The glass transition temperature (T_g) was determined from an initial inflection point of temperature dependence on DSC. High-performance liquid chromatography (HPLC) was conducted using a Hitachi L-7150/L-2400 HPLC system equipped with a Kanto Chemical Mightysil Si60 column. Recycling preparative HPLC was conducted using a JAI LC-908 equipped with JAIGEL-1H and 2H columns using chloroform as the eluent. Absorption spectra were measured with a JASCO V-560 absorption spectrophotometer. Fluorescence spectra were measured with a Hitachi F-2700 fluorescence spectrophotometer.

2.2.2 Materials

2,2'-Azobis(isobutyronitrile) (AIBN) was purified by recrystallization from methanol. Toluene and styrene (St) were purified by distillation. All other reagents were commercially available and were used without further purification. For preparing 1,2-bis(5-methyl-2-phenylthiazol-4-yl)perfluorocyclopentene (**DE**),[10] 2,7-bis(5-phenyl-thiophen-2-yl)-9,9-dioctylfluorene (**FPT**),[11] and 1-(5-methyl-2-(4-(4-vinylbenzoyloxy-methyl)phenyl)thiazol-4-yl)-2-(5-methyl-2-phenylthiazol-4-yl)perfluorocyclopentene (**DE1**),[12] a method described in previous papers was used; as for 2-(5-(4-(4-vinylbenzoyloxymethyl)phenyl)thiophen-2-yl)-7-(5-phenylthiophen-2-yl)-9,9-dioctyl-fluorene (**FL1**), *N*-4-(5-(7-(5-phenylthiophen-2-yl)-9,9-dioctylfluoren-2-yl)thiophen-2-yl)phenylmaleimide (**FL2**), and 1-(5-methyl-2-(4-(5-(7-(5-phenylthiophen-2-yl)-9,9-dioctylfluoren-2-yl)thiophen-2-yl)benzoyloxymethyl)phenylthiazol-4-yl)-2-(5-methyl-2-phenylthiazol-4-yl)perfluorocyclopentene (**DE-FL**), as described as below.

*Synthesis of Fluorene Monomer (**FL1**).* **FL1** were prepared according to the synthetic routes as shown in Scheme 2-2.

*2-Bromo-7-(5-phenylthiophen-2-yl)-9,9-dioctylfluorene (**3**).* 2-Bromo-5-phenyl-thiophene (**1**)[13] (3.0 g, 13 mmol) was dissolved in anhydrous tetrahydrofuran (THF) (50 mL) under argon atmosphere. 1.6 M *n*-BuLi hexane solution (11 mL, 19 mmol) was slowly added dropwise to the solution at −78 °C, and the mixture was stirred for 1.5 h. Tri-*n*-butyl borate (5.0 mL, 19 mmol) was slowly added to the solution at the temperature,

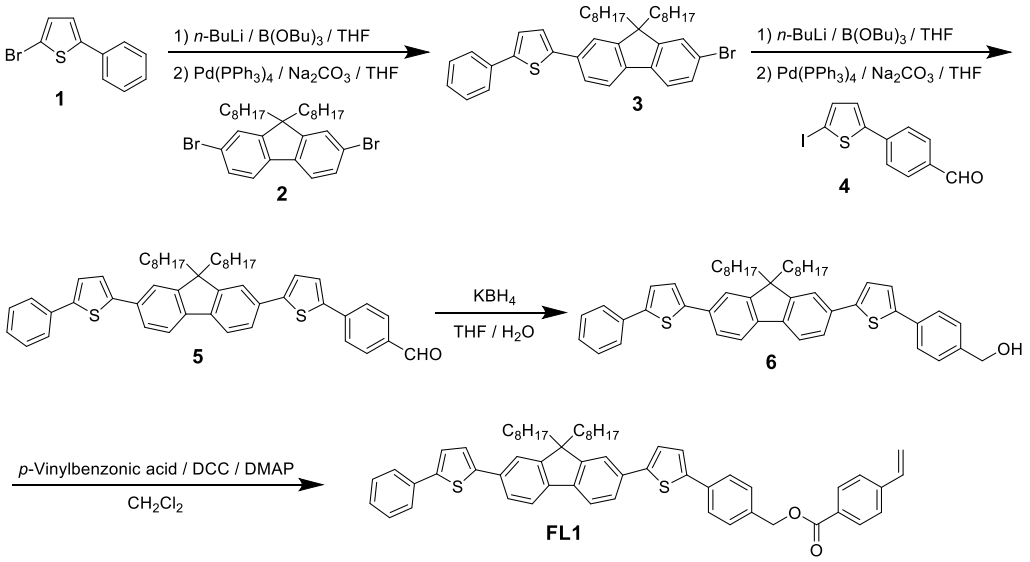

Scheme 2-2. Synthetic scheme of **FL1**. Reprinted with permission from ref. 9. Copyright 2017 American Chemical Society.

and the mixture was stirred for 1.5 h. Adequate amount of distilled water was added to the mixture to quench the reaction. 2,7-Dibromo-9,9-dioctylfluorene (**2**)[14] (10 g, 19 mmol), tetrakis(triphenylphosphine)palladium(0) (720 mg, 0.63 mmol), and 20 wt% Na_2CO_3 aqueous solution (13 mL) were added to the solution, and the mixture was refluxed for 8 h. The reaction mixture was neutralized by HCl aqueous solution, extracted with ether, washed with brine, dried over $MgSO_4$, filtered, and concentrated in vacuo. The crude product was purified by column chromatography on silica gel using *n*-hexane as the eluent to give 3.7 g of **3** in 45% yield. **3**: ^{1}H NMR (300 MHz, $CDCl_3$, TMS) δ = 0.64 (br, 4H, CH_2), 0.81 (t, J = 7 Hz, 6H, CH_3), 1.0-1.2 (m, 20H, CH_2), 1.9-2.0 (m, 4H, CH_2), 7.2-7.5 (m, 7H, Aromatic H), 7.5-7.8 (m, 6H, Aromatic H). ^{13}C NMR (75 MHz, $CDCl_3$) δ = 14.1, 22.6, 23.7, 29.2, 29.2, 29.9, 31.8, 40.3, 55.5, 119.8, 120.2, 121.0, 123.9, 124.0, 124.7, 125.6, 126.1, 127.5, 128.9, 130.0, 133.5, 134.3, 139.6, 139.6, 143.5, 144.1, 151.2, 153.1. HR-MS (MALDI) *m/z* = 626.2575 (M^+). Calcd. for $C_{39}H_{47}BrS^+$ = 626.2576.

*2-(5-(4-Formylphenyl)thiophen-2-yl)-7-(5-phenylthiophen-2-yl)-9,9-dioctylfluorene (**5**)*. Compound **3** (2.0 g, 3.2 mmol) was dissolved in anhydrous THF (50 mL) under argon atmosphere. 1.6 M *n*-BuLi hexane solution (3.0 mL, 4.8 mmol) was slowly added dropwise to the solution at −78 °C, and the mixture was stirred for 1.5 h. Tri-*n*-butyl borate (1.3 mL, 4.8 mmol) was slowly added to the solution at the temperature, and the mixture was stirred for 1.5 h. Adequate amount of distilled water was added to the mixture to quench the reaction. 2-Iodo-5-(4-formylphenyl)thiophene (**4**)[15] (1.0 g, 3.2 mmol), tetrakis(triphenylphosphine)palladium(0) (180 mg, 0.016 mmol), and 20 wt% Na_2CO_3

aqueous solution (3.4 mL) were added to the solution, and the mixture was refluxed for 6 h. The reaction mixture was neutralized by HCl aqueous solution, extracted with ether, washed with brine, dried over $MgSO_4$, filtered, and concentrated in vacuo. The crude product was purified by column chromatography on silica gel using *n*-hexane/ethyl acetate (80:20) as the eluent to give 1.5 g of **5** in 61% yield. **5**: ^{1}H NMR (300 MHz, $CDCl_3$, TMS) δ = 0.71 (br, 4H, CH_2), 0.78 (t, *J* = 7 Hz, 6H, CH_3), 1.0-1.2 (m, 20H, CH_2), 2.0-2.1 (m, 4H, CH_2), 7.2-7.5 (m, 7H, Aromatic H), 7.5-7.8 (m, 8H, Aromatic H), 7.8-8.0 (m, 4H, Aromatic H), 10.0 (s, 1H, CHO). ^{13}C NMR (75 MHz, $CDCl_3$) δ = 14.0, 22.6, 23.7, 29.2, 29.2, 31.8, 40.4, 55.3, 119.8, 119.9, 120.2, 120.3, 123.9, 124.0, 124.2, 124.7, 124.8, 125.6, 126.1, 127.5, 128.9, 130.5, 132.6, 133.4, 134.3, 134.9, 140.0, 140.8, 141.3, 143.4, 144.2, 146.7, 151.8, 151.8, 191.4. HR-MS (MALDI) *m/z* = 734.3609 (M^+). Calcd. for $C_{50}H_{54}OS_2^+$ = 734.3611.

*2-(5-(4-Hydroxymethylphenyl)thiophen-2-yl)-7-(5-phenylthiophen-2-yl)-9,9-dioctyl-fluorene (**6**)*. Compound **5** (550 mg, 0.74 mmol) was dissolved in anhydrous THF (50 mL). A solution of potassium borohydride (40 mg, 0.74 mmol) in THF (2.0 mL) and water (2.0 mL) was slowly added to the solution, and the mixture was stirred for 2 h at room temperature. The reaction mixture was extracted with ether, washed with brine, dried over $MgSO_4$, filtered, and concentrated in vacuo to give 510 mg of **6** in 94% yield. **6**: ^{1}H NMR (300 MHz, $CDCl_3$, TMS) δ = 0.71 (br, 4H, CH_2), 0.79 (t, *J* = 7 Hz, 6H, CH_3), 1.0-1.2 (m, 20H, CH_2), 1.66 (t, *J* = 6 Hz, 1H, CH_2OH), 2.0-2.1 (m, 4H, CH_2), 4.74 (d, *J* = 6 Hz, 2H, CH_2OH), 7.2-7.5 (m, 9H, Aromatic H), 7.5-7.8 (m, 10H, Aromatic H). ^{13}C NMR (75 MHz, $CDCl_3$) δ = 14.0, 22.6, 23.7, 29.1, 29.2, 30.0, 31.2, 40.4, 55.3, 65.0, 119.7, 120.1, 123.8, 125.0, 124.6, 125.6, 125.7, 127.4, 127.5, 128.9, 133.1, 133.2, 133.7, 134.3, 140.1, 140.2, 140.3, 142.9, 143.3, 144.3, 144.3, 151.7. HR-MS (MALDI) *m/z* = 736.3765 (M^+). Calcd. for $C_{50}H_{56}OS_2^+$ = 736.3767.

*2-(5-(4-(4-Vinylbenzoyloxymethyl)phenyl)thiophen-2-yl)-7-(5-phenylthiophen-2-yl)-9,9-dioctylfluorene (**FL1**)*. Compound **6** (1.4 g, 1.9 mmol) was dissolved in dichloromethane (50 mL). *p*-Vinylbenzoic acid (300 mg, 1.9 mmol), 4-dimethylaminopyridine (DMAP) (290 g, 1.9 mmol), and dicyclohexylcarbodiimide (DCC) (390 mg, 1.9 mmol) were added to the solution at 0 °C, and the mixture was stirred for 10 h. The reaction mixture was extracted with dichloromethane, washed with brine, dried over $MgSO_4$, filtered, and concentrated in vacuo. The crude product was purified by column chromatography on silica gel and HPLC using *n*-hexane/ethyl acetate (70:30) as the eluent to give 1.3 g of **FL1** in 77% yield. **FL1**: ^{1}H NMR (300 MHz, $CDCl_3$, TMS)

δ = 0.71 (br, 4H, CH_2), 0.78 (t, J = 7 Hz, 6H, CH_3), 1.0-1.2 (m, 20H, CH_2), 2.0-2.1 (m, 4H, CH_2), 5.38 (s, 2H, CH_2), 5.39 (dd, 1H, J_1 = 11 Hz, J_2 = 1 Hz, Vinyl H), 5.87 (dd, 1H, J_1 = 18 Hz, J_2 = 1 Hz, Vinyl H), 6.76 (dd, 1H, J_1 = 18 Hz, J_2 = 11 Hz, Vinyl H), 7.2-7.8 (m, 21H, Aromatic H), 8.0-8.1 (m, 2H, Aromatic H). ^{13}C NMR (75 MHz, $CDCl_3$) δ = 14.0, 22.3, 23.7, 29.1, 29.2, 29.9, 31.8, 40.4, 55.3, 66.3, 116.5, 119.7, 120.1, 123.3, 123.8, 123.8, 124.0, 124.3, 126.0, 124.6, 125.0, 125.5, 125.7, 126.0, 126.1, 127.4, 128.0, 128.7, 128.8, 128.9, 129.1, 130.0, 133.0, 133.2, 134.3, 135.2, 135.9, 140.2, 140.3, 142.0, 142.6, 143.3, 144.2, 144.5, 151.7. 166.1. HR-MS (MALDI) *m/z* = 866.4188 (M^+, 100%). Calcd. for $C_{59}H_{62}O_2S_2^+$ = 866.4186.

*Synthesis of Fluorene Monomer (**FL2**).* **FL2** was prepared according to the synthetic routes as shown in Scheme 2-3.

*N-(4-(Thien-2-yl)phenyl)maleimide (**8**).* 2-(4-Aminophenyl)thiophene (**7**) (540 mg, 2.9 mmol)[16] was dissolved in chloroform (15 mL). A solution of maleic anhydride (300 mg, 2.9 mmol) in chloroform (5.0 mL) was slowly added to the solution at room temperature, and the mixture was stirred at 1 h. The solution was concentrated. Acetic anhydride (10 mL) and sodium acetate (500 mg, 5.7 mmol) were added to the residue, and the mixture was heated for 3 h at 120 °C. The mixture was cooled to room temperature. The precipitate was washed with a large amount water, and filtered to give 410 mg of **8** in 57% yield. **8**: ^{1}H NMR (300 MHz, $CDCl_3$, TMS) δ = 6.88 (s, 2H, CH), 7.09 (dd, J_1 = 5 Hz, J_2 = 4 Hz, 1H, Thienyl H), 7.31 (d, J = 5 Hz, 1H, Thienyl H), 7.33 (d, J = 4 Hz, 1H,

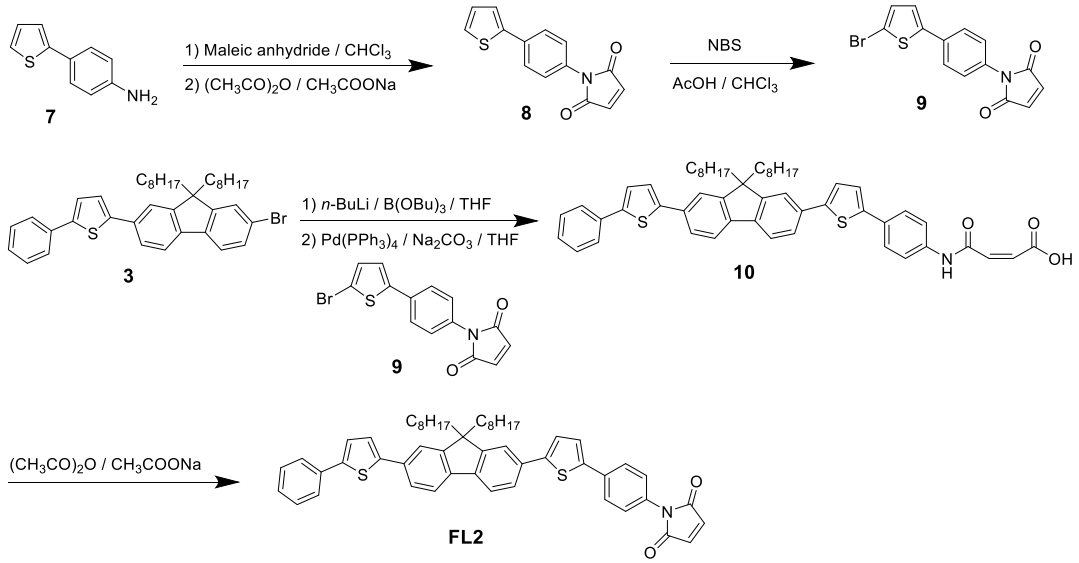

Scheme 2-3. Synthetic scheme of **FL2**. Reprinted with permission from ref. 9. Copyright 2017 American Chemical Society.

Thienyl H), 7.38 (d, J = 9 Hz, 2H, Aromatic H), 7.70 (d, J = 9 Hz, 2H, Aromatic H). ^{13}C NMR (75 MHz, $CDCl_3$) δ = 123.7, 125.4, 126.3, 126.5, 128.1, 130.2, 134.0, 134.2, 143.2, 169.4. HR-MS (MALDI) m/z = 255.0348 (M^+). Calcd. for $C_{14}H_9NO_2S^+$ = 255.0349.

*N-(4-(5-Bromothien-2-yl)phenyl)maleimide (**9**).* Compound **8** (410 mg, 1.6 mmol) was dissolved in acetic acid (10 mL) and chloroform (10 mL). *N*-Bromosuccinimide (NBS) (290 mg, 1.6 mmol) was added to the solution at room temperature, and the mixture was stirred at 12 h. The reaction mixture was neutralized by $NaHCO_3$ aqueous solution, extracted with chloroform, washed with brine, dried over $MgSO_4$, filtered, and concentrated in vacuo. The crude product was purified by column chromatography on silica gel using chloroform as the eluent to give 430 mg of **9** in 80% yield. **9**: ^{1}H-NMR (300 MHz, $CDCl_3$, TMS) δ = 6.88 (s, 2H, CH), 7.04 (d, J = 4 Hz, 1H, Thienyl H), 7.09 (d, J = 4 Hz, 1H, Thienyl H), 7.38 (d, J = 9 Hz, 2H, Aromatic H), 7.60 (d, J = 9 Hz, 2H, Aromatic H). ^{13}C NMR (75 MHz, $CDCl_3$) δ = 107.2, 112.2, 125.9, 129.6, 131.5, 133.8, 134.3, 138.7, 169.2. HR-MS (MALDI) m/z = 332.9455 (M^+). Calcd. for $C_{14}H_8BrNO_2S^+$ = 332.9454.

*N-4-(5-(7-(5-Phenylthiophen-2-yl)-9,9-dioctylfluoren-2-yl)thiophen-2-yl)phenyl-maleimide (**FL2**).* Compound **3** (840 mg, 1.3 mmol) was dissolved in anhydrous THF (30 mL) under argon atmosphere. 1.6 M *n*-BuLi hexane solution (1.3 mL, 2.0 mmol) was slowly added dropwise to the solution at −78 °C, and the mixture was stirred for 1.5 h. Tri-*n*-butyl borate (0.5 mL, 2.0 mmol) was slowly added to the solution at the temperature, and the mixture was stirred for 1.5 h. Adequate amount of distilled water was added to the mixture to quench the reaction. Compound **9** (400 mg, 1.2 mmol), tetrakis(triphenylphosphine)palladium(0) (80 mg, 0.067 mmol), and 20 wt% Na_2CO_3 aqueous solution (10 mL) were added to the solution, and the mixture was refluxed for 3 h. The reaction mixture was neutralized by HCl aqueous solution, extracted with chloroform, washed with brine, dried over $MgSO_4$, filtered, and concentrated in vacuo. The solid product of **10** was obtained by recrystallization from acetone in 620 mg yield. 270 mg of **10** was used for the next reaction without further purification. Compound **10** (270 mg, 0.33 mmol) and sodium acetate (54 mg, 0.66 mmol) were added to acetic anhydride (5.0 mL), and the mixture was heated for 3 h at 120 °C. The mixture was cooled to room temperature. The reaction mixture was neutralized by $NaHCO_3$ aqueous solution, extracted with chloroform, washed with brine, dried over $MgSO_4$, filtered, and concentrated in vacuo. The crude product was purified by column chromatography on silica gel using chloroform as the eluent to give 190 mg of **FL2** in 45% yield based on

compound **3**. **FL2**: ^{1}H NMR (300 MHz, $CDCl_3$, TMS) δ = 0.70 (br, 4H, CH_2), 0.79 (t, *J* = 7 Hz, 6H, CH_3), 1.0-1.2 (m, 20H, CH_2), 2.0-2.1 (m, 4H, CH_2), 6.88 (s, 2H, CH), 7.2-7.5 (m, 9H, Aromatic H), 7.5-7.8 (m, 10H, Aromatic H). ^{13}C NMR (75 MHz, $CDCl_3$) δ = 14.0, 22.6, 23.7, 29.1, 29.2, 29.9, 31.8, 40.3, 55.3, 119.7, 120.2, 123.8, 124.0, 124.6, 124.7, 125.5, 126.1, 126.3, 127.4, 128.9, 130.2, 132.9, 133.2, 134.0, 134.2, 134.3, 140.2, 140.4, 142.0, 143.3, 144.3, 145.0, 151.7, 169.4. HR-MS (MALDI): *m/z* = 801.3665 (M^+, 100%). Calcd. for $C_{53}H_{55}NO_2S_2^+$ = 801.3669.

Synthesis of diarylethene-fluorene dyad (**DE-FL**). **DE-FL** was prepared according to the synthetic routes as shown in Scheme 2-4.

*1-(5-Methyl-2-(4-(4-(5-(7-(5-phenylthiophen-2-yl)-9,9-dioctylfluoren-2-yl)-thiophen-2-yl)benzoyloxymethyl)phenyl)thiazol-4-yl)-2-(5-methyl-2-phenylthiazol-4-yl)-perfluorocyclopentene (**DE-FL**).* Compound **3** (1.0 g, 1.6 mmol) was dissolved in anhydrous THF (30 mL) under argon atmosphere. 1.6 M *n*-BuLi hexane solution (1.5 mL, 2.4 mmol) was slowly added dropwise to the solution at −78 °C, and the mixture was stirred for 1.5 h. Tri-*n*-butyl borate (0.65 mL, 2.4 mmol) was slowly added to the solution at the temperature, and the mixture was stirred for 1.5 h. Adequate amount of distilled water was added to the mixture to quench the reaction. 4-(5-Bromothiophen-2-yl)benzoic acid (**11**)[17] (450 mg, 1.6 mmol), tetrakis(triphenylphosphine)palladium(0) (92 mg, 0.080 mmol), and 20 wt% Na_2CO_3 aqueous solution (2.0 mL) were added to the solution, and the mixture was refluxed for 6 h. The reaction mixture was neutralized by HCl aqueous solution, extracted with ether, washed with brine, dried over $MgSO_4$, filtered, and concentrated in vacuo. The solid product of **12** was obtained by column chromatography

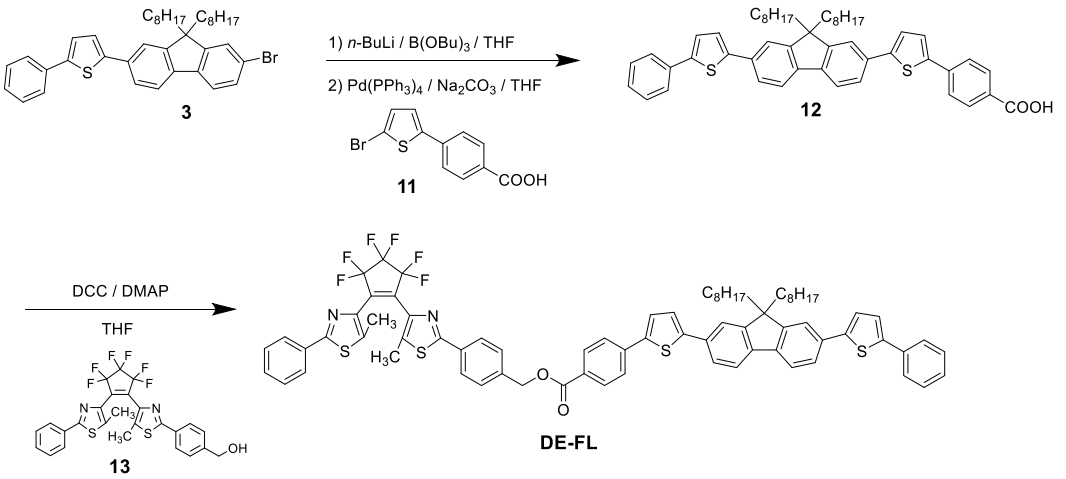

Scheme 2-4. Synthetic scheme of **DE-FL**. Reprinted with permission from ref. 9. Copyright 2017 American Chemical Society.

on silica gel using *n*-hexane/ethyl acetate (50:50) as the eluent in 800 mg yield. 144 mg of **12** was used for the next reaction without further purification. Compound **12** (144 mg, 0.19 mmol) was dissolved in THF (10 mL). 1-(5-Methyl-2-(4-hydroxymethyl)-phenyl)thiazol-4-yl)-2-(5-methyl-2-phenylthiazol-4-yl)perfluorocyclopentene (**13**)[12] (100 mg, 0.19 mmol), DMAP (35 g, 0.29 mmol), and DCC (59 mg, 0.29 mmol) were added to the solution at 0 °C, and the mixture was stirred at room temperature for 48 h. The reaction mixture was extracted with dichloromethane, washed with brine, dried over $MgSO_4$, filtered, and concentrated in vacuo. The crude product was purified by column chromatography on silica gel and HPLC using *n*-hexane/ethyl acetate (70:30) as the eluent to give 140 mg of **DE-FL** in 37% yield based on compound **3**. **DE-FL**: ^{1}H NMR (300 MHz, $CDCl_3$, TMS) δ = 0.71 (br, 4H, CH_2), 0.78 (t, J = 7 Hz, 6H, CH_3), 1.0-1.2 (m, 20H, CH_2), 2.0-2.1 (m, 4H, CH_2), 2.10 (s, 3H, CH_3), 2.11 (s, 3H, CH_3), 5.41 (s, 2H, CH_2), 7.2-7.8 (m, 22H, Aromatic H), 7.8-8.0 (m, 4H, Aromatic H), 8.0-8.2 (m, 2H, Aromatic H). ^{13}C NMR (75 MHz, $CDCl_3$) δ = 12.2, 14.0, 22.6, 23.7, 29.2, 29.2, 29.6, 31.8, 40.4, 55.3, 66.1, 119.8, 119.9, 120.2, 120.2, 123.9, 124.0, 124.1, 124.7, 124.8, 125.1, 125.6, 125.6, 126.4, 126.7, 127.5, 128.3, 128.6, 128.9, 129.0, 130.3, 130.4, 132.7, 132.8, 132.9, 133.3, 134.3, 137.1, 137.3, 138.4, 138.8, 140.1, 140.7, 141.6, 143.4, 144.2, 146.1, 151.8, 151.6, 165.2, 165.8, 165.9. HR-MS (MALDI) *m/z* = 1284.4216 (M^+). Calcd. for $C_{76}H_{70}F_6N_2O_2S_4^+$ = 1284.4219.

2.2.3 Polymerization

Radical polymerization was conducted in a sealed glass tube under vacuum. Monomer, AIBN, and toluene were placed in a glass tube. The tube was degassed by several freeze−pump−thaw cycles and sealed under vacuum. After polymerization for a prescribed time at 60 °C, the resulting polymers were obtained by precipitation in methanol. The number- and weight-average molecular weights (M_n and M_w, respectively) of the polymers were determined by GPC calibrated with standard polystyrenes. The copolymer compositions were determined from the ^{1}H NMR spectra of the copolymers.

2.2.4 Photochemical Reaction

The photocyclization and cycloreversion quantum yields were determined in *n*-hexane relative to **DE**, whose quantum yield has been previously determined ([**DE**] = 1.1 × 10^{-5} M and [**DE-FL**] = 7.0 × 10^{-6} M).[18] Photoirradiation was conducted using a 200 W mercury−xenon lamp (Moritex MUV-202) or a 300 W xenon lamp (Asahi Spectra MAX-301) as the light source. Monochromatic light was obtained by passing the light through a monochromator (Jobin Yvon H10 UV). Photocyclization conversions of **DE-**

FL and the polymers were determined by ^{1}H NMR spectroscopy and absorption spectroscopic analysis.

2.2.5 Fluorescence Quantum Yield.

All measurements performed in solution were conducted with an optical density of approximately 0.1 at the excitation wavelength in 1 cm path length quartz cells at room temperature (298 K). All samples in a solution were deaerated by bubbling with argon gas for 5 min before the measurements. The fluorescence quantum yields (Φ_f) were determined from the integrated intensity in the fluorescence spectrum of a measurement sample relative to that of a reference solution using eq 1.[19]

$$\Phi_f = \Phi_{f,ref} \frac{A_{ref}}{A} \frac{I_{ref}}{I} \frac{F}{F_{ref}} \frac{n^2}{{n_{ref}}^2} \quad (1)$$

where A and A_{ref} are the optical densities of the solutions at the excitation wavelength, I and I_{ref} the excitation light intensities at the excitation wavelength, F and F_{ref} the integrated intensities of the corrected fluorescence spectra, and n and n_{ref} the refractive indices of the solvents used for the sample solution and a standard reference solution, respectively. Coumarin 102 (Φ_f = 0.76 in ethanol excited at 390 nm) and Coumarin 153 (Φ_f = 0.54 in ethanol excited at 390 nm) were used as standard references.[20] The Φ_f value was determined as the average of the values obtained using two standard references, and the relative experimental error was estimated to be less than 10%.

2.2.6 Fluorescence Lifetime

Fluorescent dynamics of polymers with fluorene and diarylethene units were measured by means of the time-correlated single-photon-counting (TCSPC) method. The experimental setup of our TCSPC system was described in a previous report.[21] Briefly, the output of a Ti:sapphire laser (Spectra-Physics, Tsunami, 800 nm, 1.8 W, 70 fs, 80 MHz) was divided into two portions. The small portion was detected by a photodiode as a starting signal of TCSPC measurements. The remaining major portion was converted into the second harmonics (400 nm) using a type I barium borate (BBO) crystal and then used for the excitation of the sample. The repetition rate was reduced to 8 MHz by using an electro-optic modulator (Conoptics, Model 350). The excitation power at the sample position was typically 16 μW (8 MHz). Polarization of the excitation pulses was set to the magic angle with respect to that of the fluorescence detection by using a film polarizer and Babinet−Soleil compensator. A monochromator (Princeton Instruments, Acton SP-

2150) was placed before the photomultiplier-tube (Hamamatsu Photonics, R3809U-50) equipped with a combination of a preamplifier (Hamamatsu Photonics, C5594) and a TCSPC module (PicoQuant, PicoHarp 300). Sample solutions were put in 1 cm quartz cells. Typical response time of the system was ca. 40 ps fwhm, which was determined by the scattering signal of the colloidal solution.

2.3 Results and Discussion

2.3.1 Molecular Design

First, the effect of the monomer sequence and ratio for the fluorescence on/off switching properties in the copolymers was simulated by a simple model. As shown in Figure 2-1a, the model of random or alternating copolymers was prepared by linearly

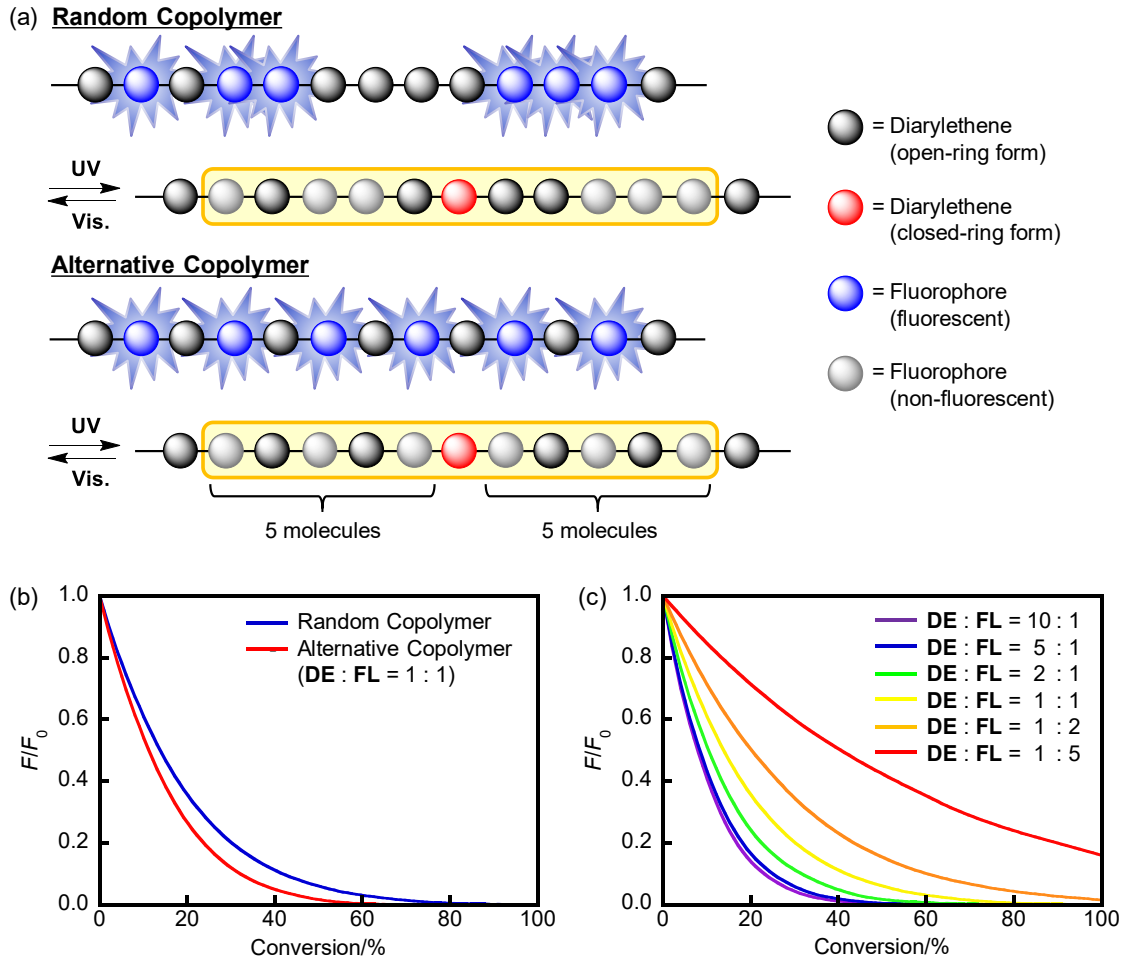

Figure 2-1. (a) Illustration of simulation model of random and alternative copolymers by linearly arranging diarylethenes and fluorophores randomly or alternately in an arbitrary ratio. (b,c) Relative fluorescence intensities (F/F_0) of random and alternative copolymers bearing diarylethene (**DE**) and fluorophore (**FL**) at the same ratio (b), and random copolymers bearing **DE** and **FL** at various ratios (c) relative to the photocyclization conversion of diarylethene.

arranging the diarylethenes and the fluorophores randomly or alternately in an arbitrary ratio. It was assumed that a single diarylethene closed-ring form completely quenched the fluorophores existing within ten adjacent molecules. Figure 2-1b shows the results of the simulation for the relative fluorescence intensities (F/F_0) relative to the photocyclization conversion of the diarylethene. The F/F_0 value of alternative copolymer significantly decreased with increasing photocyclization conversion of the diarylethene in comparison with that of random copolymer. In addition, the quenching of random copolymer relative to the photocyclization conversion increased with increasing ratio of diarylethene, as shown in Figure 2-1c. Therefore, the theoretical results by the simulation model suggest that the monomer sequence and ratio of the copolymer greatly affects the fluorescence

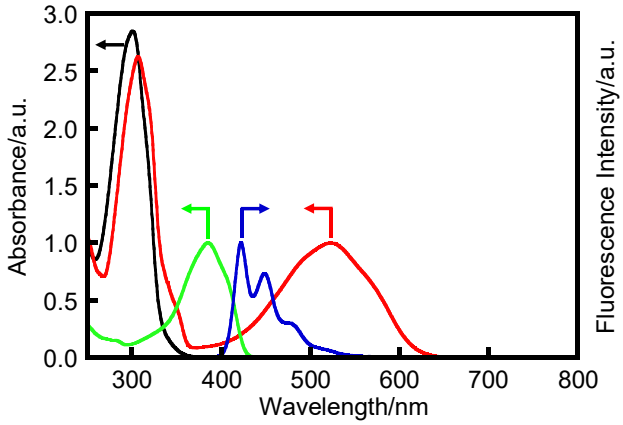

Figure 2-2. Normalized absorption spectra of the open-ring form (black line) and the photostationary solution upon irradiation with 313 nm light (red line) of **DE** in *n*-hexane and normalized absorption spectrum (green line) and fluorescence spectrum under excitation at 366 nm (blue line) of **FPT** in *n*-hexane. Reprinted with permission from ref. 9. Copyright 2017 American Chemical Society.

Table 2-1. Radical polymerization initiated with AIBN (0.020 M) in toluene for 10 h at 60 °C and characterization of the resulting polymers. Reprinted with permission from ref. 9. Copyright 2017 American Chemical Society.

Entry	[**DE1**] /M	[**St**] /M	[**FL1**] /M	[**FL2**] /M	Yield /%	M_n	M_w/M_n	Molar fraction of **FL**/mol%[a]	T_g/°C
1[b]	0.37	–	0	–	79	41900	2.24	0	102
2	0.38	–	0.062	–	66	43500	2.28	12[d]	96
3	0.31	–	0.12	–	62	43500	2.19	25[d]	90
4	0.19	–	0.19	–	—[c]	41100	2.77	52[d]	81
5	0.12	–	0.25	–	77	42900	2.40	65[d]	74
6	0.062	–	0.31	–	76	41900	2.92	86[d]	71
7	0.034	–	0.34	–	77	49700	2.71	90[d]	69
8	0	–	0.37	–	64	57200	2.83	100	64
9	0.19	–	–	0.19	85	53400	3.00	48[e]	78
10	–	0.19	–	0.19	79	61100	3.06	49[e]	60

[a]Molar fraction of **FL1** or **FL2** in the polymer. [b]ref. 11. [c]Not determined. [d]Determined by absorption spectroscopic analysis. [e]Determined by ^{1}H NMR spectroscopic analysis.

on/off switching properties.

Next, **DE** and **FPT** were employed as the photochromic and fluorophore units of the diarylethene-fluorene dyad and copolymers. **DE** is a diarylethene derivative, and both its open- and closed-ring forms have high thermal stability. **FPT** shows blue fluorescence with high Φ_f (Φ_f = 0.69). Because the fluorescence on/off switching in this chapter is based on the Förster resonance energy transfer (FRET) from the fluorophore to the diarylethene closed-ring form, an overlap between the absorption spectrum of the diarylethene closed-ring form and the fluorescence spectrum of the fluorophore is required to quench the excited energy of the fluorophore with high efficiency. As shown in Figure 2-2, the fluorescence spectrum of **FPT** properly overlaps the absorption spectrum of the closed-ring form of **DE**. Therefore, the fluorescence of **FPT** is expected to be quenched when **DE** isomerizes from the open-ring form to the closed-ring form. Contrastingly, when **DE** is in the open-ring form, fluorescence quenching does not occur because the excited-state energy level of **DE** is higher than that of **FPT**.

In **DE-FL**, **DE** is covalently connected with **FPT** through an ester spacer. St and maleimide monomers connected with **FL** (**FL1** and **FL2**) were synthesized. Random copolymers bearing **DE** and **FL** in their side chains (**poly(DE1$_x$-*co*-FL1$_y$)**) were

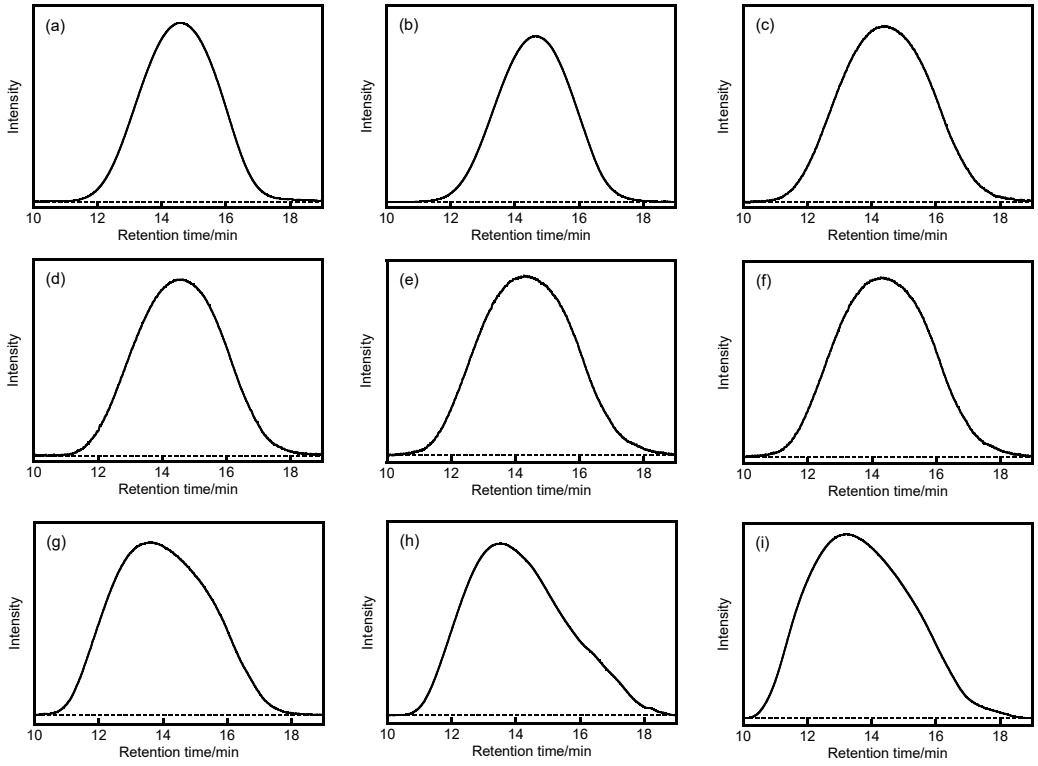

Figure 2-3. GPC elution curves of **poly(DE1$_{88}$-*co*-FL1$_{12}$)** (a), **poly(DE1$_{75}$-*co*-FL1$_{25}$)** (b), **poly(DE1$_{48}$-*co*-FL1$_{52}$)** (c), **poly(DE1$_{35}$-*co*-FL1$_{65}$)** (d), **poly(DE1$_{14}$-*co*-FL1$_{86}$)** (e), **poly(DE1$_{10}$-*co*-FL1$_{90}$)** (f), **poly(FL1)** (g), **poly(DE1-*alt*-FL2)** (h), and **poly(St-*alt*-FL2)** (i). Reprinted with permission from ref. 9. Copyright 2017 American Chemical Society.

synthesized by copolymerization of **DE1** and **FL1** in an arbitrary ratio, where *x* and *y* are the molar fractions of **DE1** and **FL1** in the copolymer, respectively. In addition, alternative copolymers (**poly(DE1-*alt*-FL2)**) were also synthesized by copolymerization

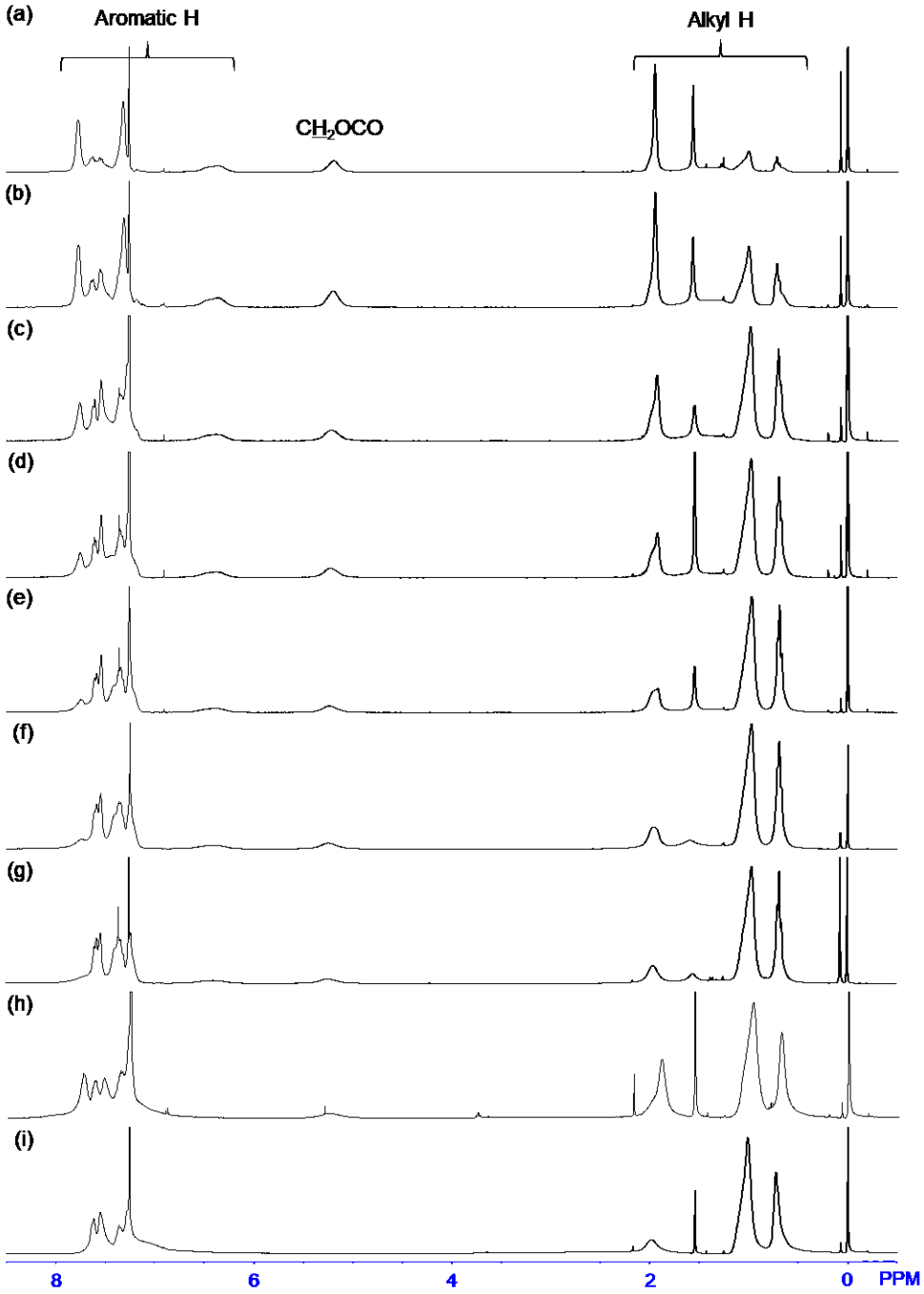

Figure 2-4. ^{1}H NMR spectra of **poly(DE1$_{88}$-*co*-FL1$_{12}$)** (a), **poly(DE1$_{75}$-*co*-FL1$_{25}$)** (b), **poly(DE1$_{48}$-*co*-FL1$_{52}$)** (c), **poly(DE1$_{35}$-*co*-FL1$_{65}$)** (d), **poly(DE1$_{14}$-*co*-FL1$_{86}$)** (e), **poly(DE1$_{10}$-*co*-FL1$_{90}$)** (f), **poly(FL1)** (g), **poly(DE1-*alt*-FL2)** (h), and **poly(St-*alt*-FL2)** (i). Reprinted with permission from ref. 9. Copyright 2017 American Chemical Society.

of **DE1** and **FL2** with the same molar fractions. Because St and *N*-phenylmaleimide show a charge transfer complex in the copolymerization process due to their electron-donating and electron-accepting characters, respectively, this copolymerization process leads to alternative copolymers with low monomer reactivity ratios ($r_1 \ll 0.1$ and $r_2 \ll 0.1$).[22]

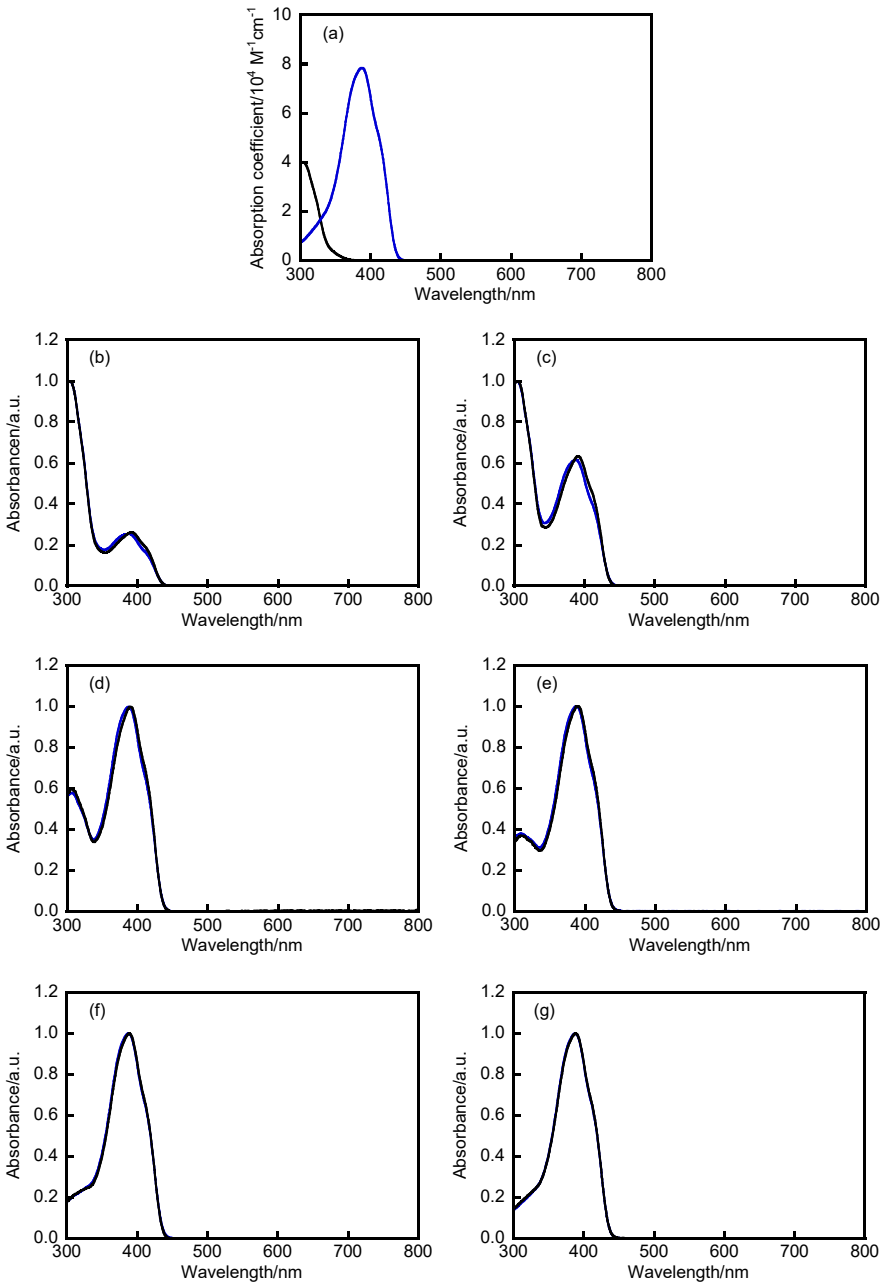

Figure 2-5. (a) Absorption spectra of **poly(DE1)** (black line) and **poly(FL1)** (blue line) in THF. (b-g) Normalized and simulated absorption spectra (black and blue lines, respectively) of **poly(DE1$_{88}$-*co*-FL1$_{12}$)** (b), **poly(DE1$_{75}$-*co*-FL1$_{25}$)** (c), **poly(DE1$_{48}$-*co*-FL1$_{52}$)** (d), **poly(DE1$_{35}$-*co*-FL1$_{65}$)** (e), **poly(DE1$_{14}$-*co*-FL1$_{86}$)** (f), **poly(DE1$_{10}$-*co*-FL1$_{90}$)** (g). Reprinted with permission from ref. 9. Copyright 2017 American Chemical Society.

2.3.2 Polymerization

Table 2-1 shows the polymerization conditions, yields, M_n, M_w/M_n, and T_g of the studied polymers. GPC elution curves and ^{1}H NMR spectra of the polymers are shown in Figures 2-3 and 2-4, respectively. The compositions of **poly(DE1$_x$-*co*-FL1$_y$)** were estimated from absorption spectroscopic analysis. It was hypothesized that the absorption spectra of **poly(DE1$_x$-*co*-FL1$_y$)** are consistent with the summation of a content of **poly(DE1)** and **poly(FL1)** in the composition of **poly(DE1$_x$-*co*-FL1$_y$)**, as shown in Figure 2-5. The molar fraction of **FL1** in all **poly(DE1$_x$-*co*-FL1$_y$)** was determined as shown in Table 2-1. Next, the composition of alternating copolymers was calculated from ^{1}H NMR spectroscopic analysis. The molar fraction of **FL2** in **poly(DE1-*alt*-FL2)** and **poly(St-*alt*-FL2)** was estimated to be 48 and 49%, respectively, by comparing the integral intensities of alkyl, CH_2OCO, and aromatic proton peaks. The composition curve for the copolymerization of **FL1** with **DE1** exhibited a linear relationship, as shown in Figure 2-6. Therefore, the composition of **FL1** in the copolymers was almost the same as that in the feed. In addition, the yields, M_n, and M_w/M_n of the copolymers were similar. These results indicate that the introduction of **DE** and **FL** to the *p*-position of St did not affect the polymerization reactivity. The T_g values of **poly(DE1)** and **poly(FL1)** were determined to be 102 °C[11] and 64 °C by DSC, respectively. The lower T_g of **poly(FL1)** is ascribed to the two octyl groups. The T_g values of **poly(DE1$_x$-*co*-FL1$_y$)** were determined to be 69-96 °C; these values decreased with increasing molar fraction of **FL1** in the copolymer. Moreover, the compositions of **FL2** in **poly(DE1-*alt*-FL2)** and **poly(St-*alt*-FL2)** were determined to be ca. 50 mol %. Thus, copolymers consisting of **DE** and

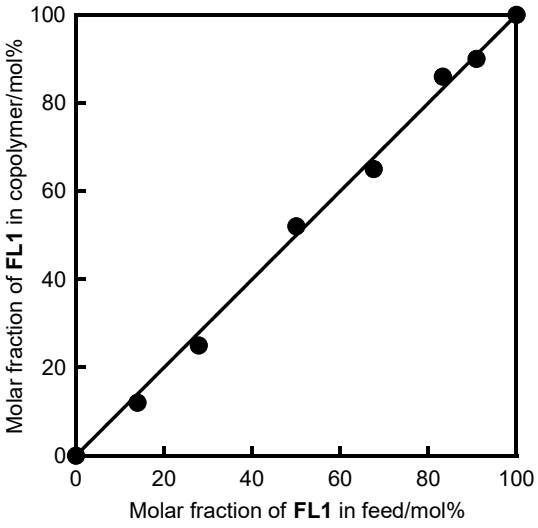

Figure 2-6. Composition curve for copolymerization of **FL1** with **DE1** in toluene at 60 °C. Reprinted with permission from ref. 9. Copyright 2017 American Chemical Society.

FL in an arbitrary ratio could be fabricated.

2.3.3 Photochromism

The optical properties of **DE-FL** and the polymers are summarized in Tables 2-2 and 2-3. Figure 2-7a-c shows the absorption spectral changes of **DE-FL** in *n*-hexane, **poly(DE1$_{48}$-*co*-FL1$_{52}$)** in THF, and **poly(DE1-*alt*-FL2)** in THF upon irradiation with 313 nm light. The absorption maximum wavelengths (λ_{abs}) were observed at 393, 390, and 390 nm (ε = 79900, 78500, and 78200 M^{-1} cm^{-1}) for **DE-FL**, **poly(DE1$_{48}$-*co*-FL1$_{52}$)**, and **poly(DE1-*alt*-FL2)**, respectively; these correspond to the band for the fluorene moiety. Upon irradiation with 313 nm light, the colorless solution became red, and new absorption

Table 2-2. Optical properties of **DE**, **FPT**, and **DE-FL** in *n*-hexane. Reprinted with permission from ref. 9. Copyright 2017 American Chemical Society.

compound	λ_{abs}/nm (ε/$M^{-1}cm^{-1}$)	conv./%	$\Phi_{o\rightarrow c}$	$\Phi_{c\rightarrow o}$	λ_{flu}/nm	Φ_f	contrast[a]
DE[b]	524 (14900)[c]	87	0.48	0.018	—	—	—
FPT[d]	383 (80100)	—	—	—	423, (449)	0.69	—
DE-FL	393 (79900)[c] 524 (15200)[c]	88	0.25	0.016	436, (464)	0.69	5.6

[a]Contrast is defined as initial fluorescence intensity relative to fluorescence intensity at the PSS. [b]ref. 9. [c]λ_{abs} and ε for the closed-ring form of **DE**. [d]ref. 10. [e]λ_{abs} and ε for **FPT**.

Table 2-3. Optical properties of the studied polymers in THF. Reprinted with permission from ref. 9. Copyright 2017 American Chemical Society.

polymer	λ_{abs}/nm (ε/$M^{-1}cm^{-1}$)	conv./%	λ_{flu}/nm	Φ_f	contrast[a]
poly(DE1$_{88}$-*co*-FL1$_{12}$)	391 (78500)[b] 534 (13900)[c]	87	433, (461)	0.16	133
poly(DE1$_{75}$-*co*-FL1$_{25}$)	391 (80700)[b] 534 (13200)[c]	87	434, (463)	0.13	106
poly(DE1$_{48}$-*co*-FL1$_{52}$)	390 (78500)[b] 534 (14300)[c]	87	434, (462)	0.15	71
poly(DE1$_{35}$-*co*-FL1$_{65}$)	390 (78600)[b] 534 (14600)[c]	87	434, (462)	0.20	36
poly(DE1$_{14}$-*co*-FL1$_{86}$)	389 (78000)[b] 534 (14600)[c]	88	434, (463)	0.37	11
poly(DE1$_{10}$-*co*-FL1$_{90}$)	389 (80700)[b] 534 (14100)[c]	88	435, (463)	0.42	5.1
poly(FL1)	388 (78800)[b]	—	436, (463)	0.66	—
poly(DE1-*alt*-FL2)	391 (78200)[b] 534 (15500)[c]	88	436, (464)	0.21	76
poly(St-*alt*-FL2)	390 (79100)[b]	—	436, (463)	0.69	—

[a]Contrast is defined as initial fluorescence intensity relative to fluorescence intensity at the PSS. [b]λ_{abs} and ε for the **FL1** or **FL2** unit in the polymers. [c]λ_{abs} and ε for the closed-ring form of the **DE1** unit in the polymers.

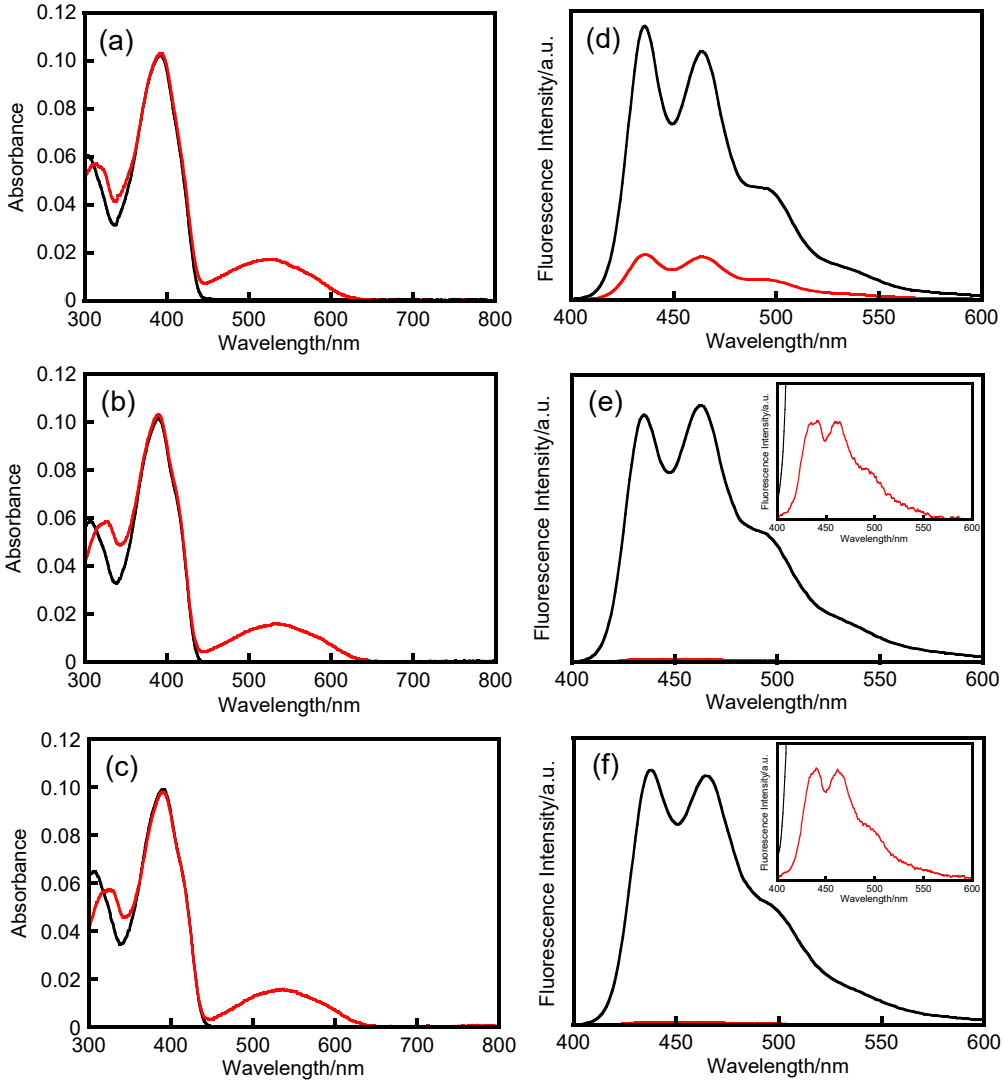

Figure 2-7. Absorption and fluorescence spectra of **DE-FL** in *n*-hexane (a, d), **poly(DE1$_{48}$-*co*-FL1$_{52}$)** in THF (b, e), and **poly(DE1-*alt*-FL2)** in THF (c, f) (1.3×10^{-6} M for **DE** or **DE1** moiety): open-ring form (black line) and photostationary solution upon irradiation with 313 nm light (red line). The fluorescence spectra were recorded upon excitation at 390 nm. Reprinted with permission from ref. 9. Copyright 2017 American Chemical Society.

bands appeared at 524, 534, and 534 nm for **DE-FL**, **poly(DE1$_{48}$-*co*-FL1$_{52}$)**, and **poly(DE1-*alt*-FL2)**, respectively. The ε values for the closed-ring forms of **DE** in **DE-FL**, **poly(DE1$_{48}$-*co*-FL1$_{52}$)**, and **poly(DE1-*alt*-FL2)** were determined to be 15200, 14300, and 15500 $M^{-1}cm^{-1}$, respectively. λ_{abs} and ε of **poly(DE1$_x$-*co*-FL1$_y$)** were almost constant regardless of the molar fraction of **FL1** in the copolymer. These spectral changes are ascribed to photoisomerization from the open- to the closed-ring forms. Upon irradiation with visible light (>500 nm), the solution colors and absorption spectra returned to their initial states. Thus, **DE-FL** and the copolymers exhibited reversible photochromic reactions upon alternating irradiation with UV and visible light. Their photocyclization

conversions upon irradiation with 313 nm light were determined to be approximately 88%.

2.3.4 Fluorescence Properties

Figure 2-7d-f shows the fluorescence spectral changes of **DE-FL** in *n*-hexane, **poly(DE1$_{48}$-*co*-FL1$_{52}$)** in THF, and **poly(DE1-*alt*-FL2)** in THF upon excitation at 390 nm. The fluorescence maximum wavelengths (λ_{flu}) of the blue fluorescence for the fluorene moiety were observed at 436, 434, and 436 nm, respectively. λ_{flu} changed only slightly regardless of the molar fraction of **FL1** in **poly(DE1$_x$-*co*-FL1$_y$)**. The Φ_f of **DE-FL** was determined to be 0.69, which is similar to that of **FPT**. The Φ_f values for **poly(DE1$_{48}$-*co*-FL1$_{52}$)** and **poly(DE1-*alt*-FL2)** were determined to be 0.15 and 0.21, respectively; these values are much smaller than those of **DE-FL** and **FL**. The Φ_f values for **poly(DE1$_x$-*co*-FL1$_y$)** decreased from 0.42 to 0.13 with increasing molar fraction of **DE** in the copolymer. The low Φ_f values of **poly(DE1$_x$-*co*-FL1$_y$)** and **poly(DE1-*alt*-FL2)** are due to the presence of the **DE1** unit in the copolymers; this will be discussed in more detail later.

2.3.5 Fluorescence On/Off Switching

The fluorescence intensity gradually decreased upon irradiation with 313 nm light, as shown in Figure 2-8a. This is ascribed to the energy transfer from the fluorene moiety to the diarylethene closed-ring form. Upon irradiation with visible light, the fluorescence intensity returned to its initial one. These results indicate that **DE-FL** and the copolymers demonstrate fluorescence on/off switching properties upon alternating irradiation with UV and visible light. Figure 2-8b shows the F/F_0 value related to the photocyclization

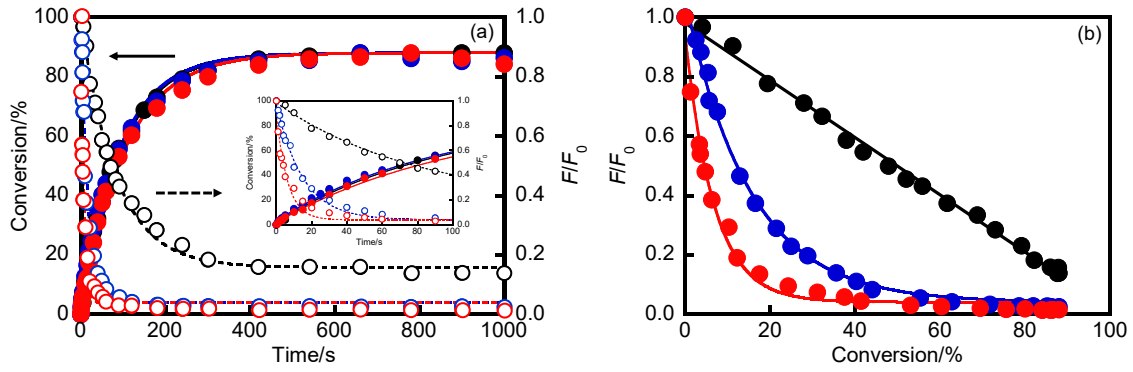

Figure 2-8. (a) Photocyclization conversion and normalized fluorescence intensity excited at 390 nm relative to irradiation time with 313 nm light (0.24 mW cm^{-2}) of **DE-FL** in *n*-hexane (open and closed black circles), **poly(DE1$_{48}$-*co*-FL1$_{52}$)** in THF (open and closed blue circles), and **poly(DE1-*alt*-FL2)** in THF (open and closed red circles). (b) Normalized fluorescence intensity excited at 390 nm relative to the photocyclization conversion of **DE-FL** in *n*-hexane (black circles), **poly(DE1$_{48}$-*co*-FL1$_{52}$)** in THF (blue circles), and **poly(DE1-*alt*-FL2)** in THF (red circles). Reprinted with permission from ref. 9. Copyright 2017 American Chemical Society.

conversion of the diarylethene. The F/F_0 value of **DE-FL** linearly decreased with increasing photocyclization conversion of the diarylethene. This result indicates that the fluorescence of the fluorene moiety in **DE-FL** was quenched by one diarylethene moiety in the closed-ring form. However, the residual fluorescence was observed at the PSS, although the fluorescence intensity of **DE-FL** decreased upon irradiation with UV light. The residual fluorescence is ascribed to two factors: one is the fluorescence of **DE-FL** in the open-ring form at the PSS, while the other is the fluorescence of **DE-FL** in the closed-ring form, which did not completely quench the fluorescence of the fluorene moiety. If the fluorescence of the fluorene moiety is completely quenched by the diarylethene closed-ring form, the slope of F/F_0 versus the photocyclization conversion should be $-0.01\%^{-1}$. The slope for **DE-FL** is $-0.0093\%^{-1}$ ($r^2 = 0.99$), which indicates that about 93% of the fluorescence of the fluorene moiety is quenched by the diarylethene close-ring form. Thus, the strong residual fluorescence and the linear fluorescence decay versus the photocyclization conversion indicate that **DE-FL** does not have efficient fluorescence on/off properties. Moreover, the fluorescence on/off switching properties of **DE-FL** in THF was also investigated, as shown in Figure 2-9. The fluorescence spectrum was red-shifted from λ_{flu} = 436 nm in *n*-hexane to λ_{flu} = 474 nm in THF, which is due to the

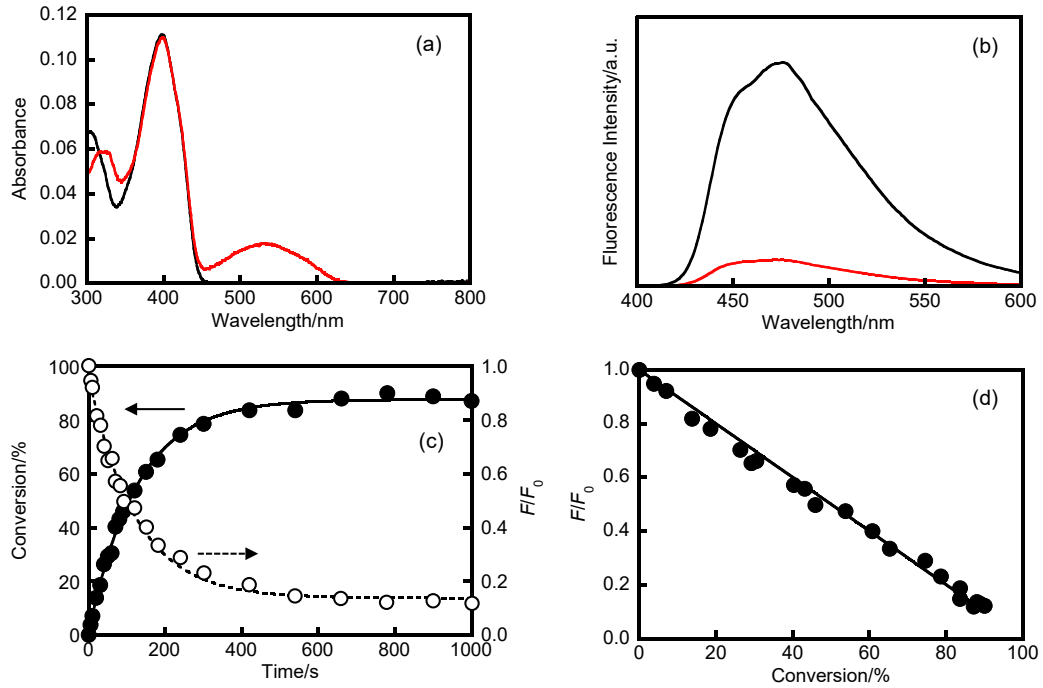

Figure 2-9. Absorption and fluorescence spectra of **DE-FL** (ε_{398nm} = 81800 $M^{-1}cm^{-1}$, 1.4 × 10^{-6} M) in THF (a and b): open-ring form (black line) and the photostationary solution upon irradiation with 313 nm light (red line). Photocyclization conversion and normalized fluorescence intensity excited at 390 nm (● and ○, respectively) relative to irradiation time with 313 nm light (0.24 mW cm^{-2}) (c). Normalized fluorescence intensity excited at 390 nm relative to the photocyclization conversion (d). Reprinted with permission from ref. 9. Copyright 2017 American Chemical Society.

electron withdrawing effect of the carbonyl group of the fluorene moiety. The Φ_f value in THF was determined to be 0.79. Upon irradiation with UV and visible light, the fluorescence on/off switching was observed in THF as well as in *n*-hexane. The slope of F/F_0 versus the photocyclization conversion is $-0.0099\%^{-1}$ ($r^2 = 0.99$), which is slightly larger than that in *n*-hexane because the overlap integral between the absorption spectrum of the diarylethene closed-ring form and the fluorescence spectrum in THF is larger than that in *n*-hexane. To investigate the fluorescence on/off switching of **DE-FL** in more detail, the Förster distance (R_0) and FRET efficiency (E) were estimated as follows. The R_0 values of **DE-FL** in *n*-hexane and THF were determined to be 4.31 and 4.47 nm, respectively, based on the Förster equation.[23] Furthermore, the E values of **DE-FL** in *n*-hexane and THF were calculated to be 99.0 and 99.2%, respectively, when the distance between diarylethene and fluorene moieties was assumed to be 2.0 nm.[23] These results support that the slope in THF is slightly larger than that in *n*-hexane.

Upon irradiation with 313 nm light (0.24 mW cm^{-2}) for 60 s, the fluorescence of **poly(DE1$_{48}$-*co*-FL$_{52}$)** was almost quenched although the fluorescence intensity of **DE-FL** in *n*-hexane decreased upon irradiation for 400 s. The photocyclization reaction speed of **DE-FL** and **poly(DE1$_{48}$-*co*-FL$_{52}$)** versus UV irradiation time hardly changed. These results indicate that the fluorescence on/off switching of **poly(DE1$_{48}$-*co*-FL1$_{52}$)** was speedier than that of **DE-FL**. The fluorescence on/off contrast is defined as the value of the initial fluorescence intensity divided by the fluorescence intensity at the PSS. Contrasts for **DE-FL** and **poly(DE1$_{48}$-*co*-FL1$_{52}$)** were determined to be 5.6 and 71, respectively. The contrast for **poly(DE$_{48}$-*co*-FL1$_{52}$)** is much larger than that for **DE-FL**. Thus, the fluorescence on/off switching property of **poly(DE1$_{48}$-*co*-FL1$_{52}$)** is superior to that of **DE-FL**, although **DE** and **FL** in **DE-FL** and **poly(DE1$_{48}$-*co*-FL1$_{52}$)** have the same

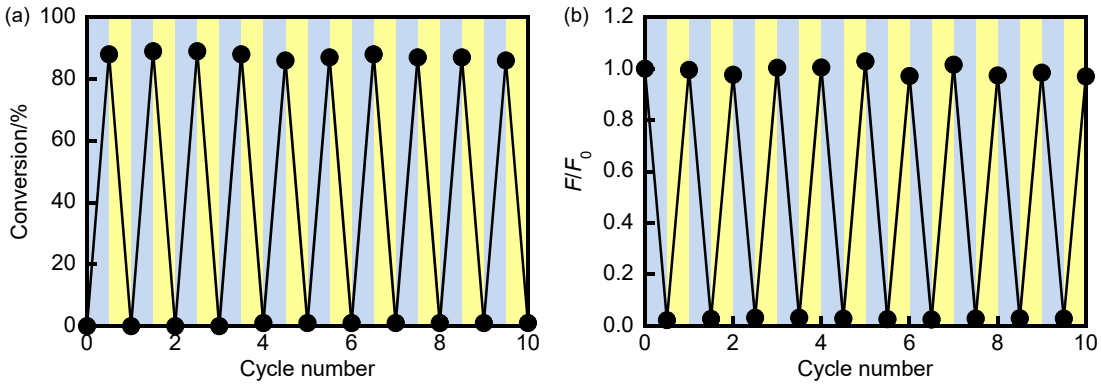

Figure 2-10. Reversible photochromic reactions (a) and fluorescence on/off switching (b) of **poly(DE1-*alt*-FL2)** in THF upon alternating irradiation with 313 nm light for 12 min (0.23 mW cm^{-2}, blue region) (a) and 60 s (0.22 mW cm^{-2}, blue region) (b) and visible light for 3 min (>500 nm, yellow region). Reprinted with permission from ref. 9. Copyright 2017 American Chemical Society.

molecular structures and the same molar fractions. As shown in Figure 2-8b, the F/F_0 value of **poly(DE1$_{48}$-*co*-FL1$_{52}$)** greatly decreased with increasing photocyclization

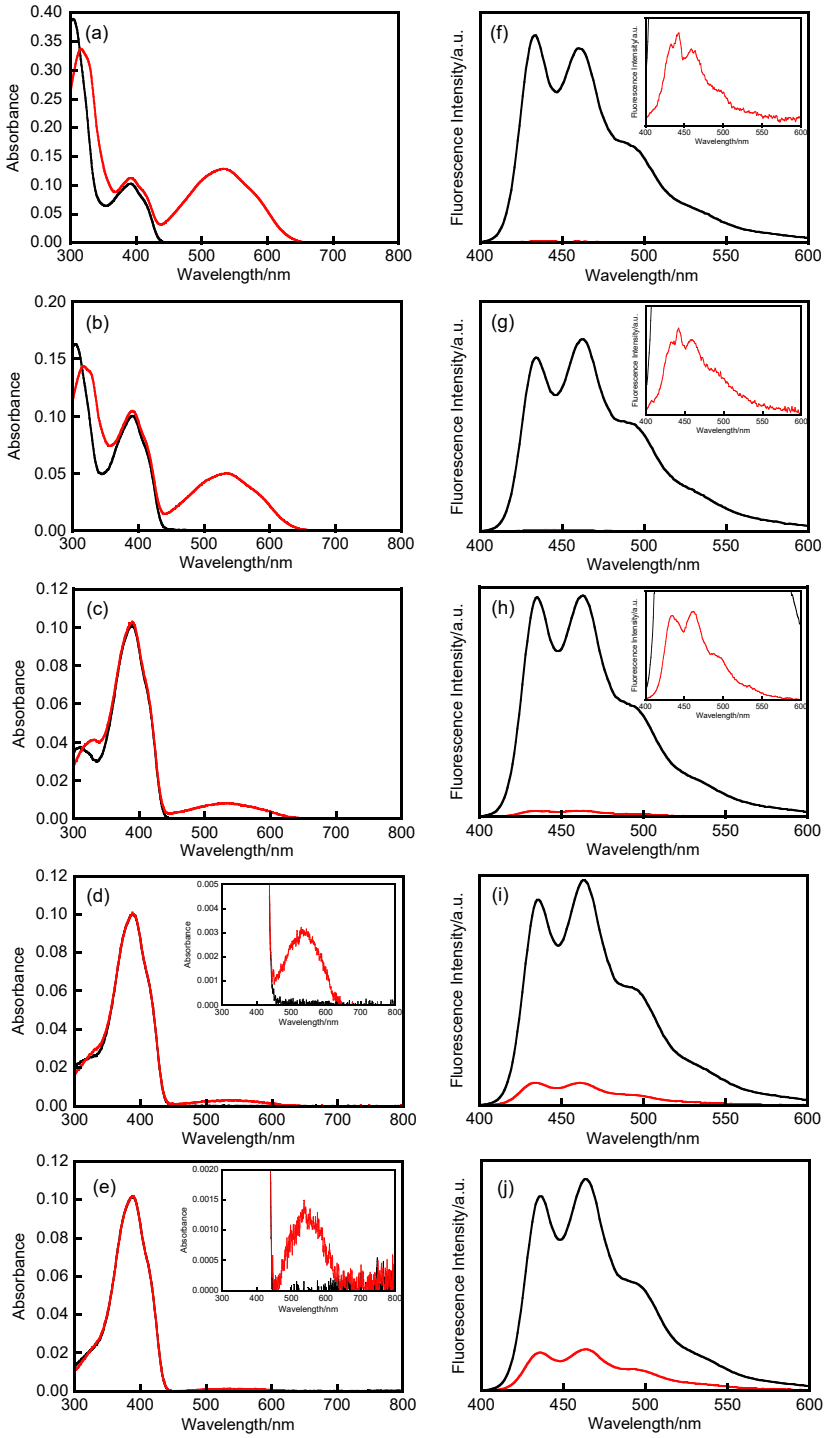

Figure 2-11. Absorption spectra and fluorescence spectra of (a,f) **poly(DE1$_{88}$-*co*-FL1$_{12}$)**, (b,g) **poly(DE1$_{75}$-*co*-FL1$_{25}$)**, (c,h) **poly(DE1$_{35}$-*co*-FL1$_{65}$)**, (d,i) **poly(DE1$_{14}$-*co*-FL1$_{86}$)**, and (e,j) **poly(DE1$_{10}$-*co*-FL1$_{90}$)** in the open-ring form (black line) and at the photostationary state upon irradiation with 313 nm light (red line) in THF. Reprinted with permission from ref. 9. Copyright 2017 American Chemical Society.

conversion of the diarylethene. This is because a large number of fluorene moieties are quenched by a single closed-ring diarylethene in the copolymer. These results indicate that the introduction of **DE** and **FL** into the side chains of the polymers improved their fluorescence on/off switching properties.

Moreover, the fluorescence on/off switching of **poly(DE1-*alt*-FL2)** was speedier than that of **poly(DE1$_{48}$-*co*-FL1$_{52}$)** although their photocyclization reaction rates hardly changed. The F/F_0 value of **poly(DE1-*alt*-FL2)** significantly decreased with increasing photocyclization conversion of the diarylethene in comparison with that of **poly(DE1$_{48}$-*co*-FL1$_{52}$)**. The number of fluorene moieties quenched by a single closed-ring diarylethene of **poly(DE1$_{48}$-*co*-FL1$_{52}$)** and **poly(DE1-*alt*-FL2)** is almost the same. Thus, the monomer sequence of the copolymer greatly affects its fluorescence on/off switching properties.

Figure 2-10 shows repeating cycles of the photochromic reactions and fluorescence on/off switching of **poly(DE1-*alt*-FL2)** upon alternating irradiation with UV and visible light, which could be repeated 10 times without a significant decrease of the absorbance in their closed-ring form and the fluorescence intensity in their open-ring form.

Next, the dependence of the fluorescence on/off switching properties on the molar fraction of **DE1** and **FL1** in **poly(DE1$_x$-*co*-FL1$_y$)** was investigated. Figure 2-11 shows the absorption and fluorescence spectral changes of **poly(DE1$_x$-*co*-FL1$_y$)** with various molar fractions of **FL1**. The F/F_0 values for **poly(DE1$_x$-*co*-FL1$_y$)** versus the photocyclization conversion are shown in Figure 2-12. All the copolymers showed

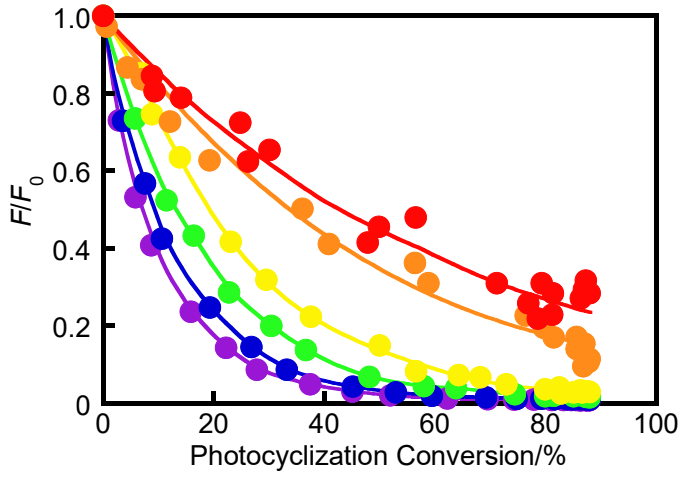

Figure 2-12. Normalized fluorescence intensity excited at 390 nm as a function of the photocyclization conversion of **poly(DE1$_{88}$-*co*-FL1$_{12}$)** (purple), **poly(DE1$_{75}$-*co*-FL1$_{25}$)** (blue), **poly(DE1$_{48}$-*co*-FL1$_{52}$)** (green), **poly(DE1$_{35}$-*co*-FL1$_{65}$)** (yellow), **poly(DE1$_{14}$-*co*-FL1$_{86}$)** (orange), and **poly(DE1$_{10}$-*co*-FL1$_{90}$)** (red) in THF (1.3-1.4 × 10^{-6} M for fluorene moiety). Reprinted with permission from ref. 9. Copyright 2017 American Chemical Society.

fluorescence on/off switching upon irradiation with UV and visible light. The change in the F/F_0 value relative to the photoisomerization conversion decreased with increasing molar fraction of **FL1** in the copolymer. The fluorescence on/off contrast for **poly(DE1$_{10}$-*co*-FL1$_{90}$)** was determined to be 5.1, and 30% of the initial fluorescence was observed as the residual fluorescence even at the PSS. These results are ascribed to the increase in the number of fluorene moieties outside the area where the diarylethene closed-ring form in the copolymer can quench their excited energies. On the other hand, the changes in the F/F_0 value versus the photocyclization conversion increased with decreasing molar fraction of **FL1** in the copolymer. The contrast for **poly(DE1$_{88}$-*co*-FL1$_{12}$)** with the smallest molar fraction of **FL1** in this chapter was determined to be 133, and the fluorescence of **poly(DE1$_{88}$-*co*-FL1$_{12}$)** was almost quenched at the PSS. **poly(DE1$_{88}$-*co*-FL1$_{12}$)** showed the most efficient fluorescence on/off switching properties among the **poly(DE1$_x$-*co*-FL1$_y$)** polymers. These results revealed that the fluorescence on/off switching properties of **poly(DE1$_x$-*co*-FL1$_y$)** improved as the molar fraction of **FL1**

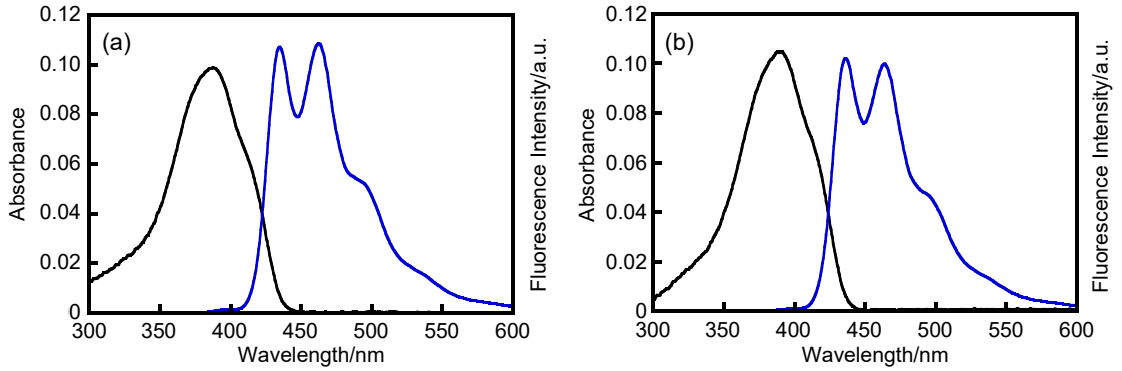

Figure 2-13. Absorption spectra (black line) and fluorescence spectra (blue line) of **poly(FL1)** (a) and **poly(St-*alt*-FL2)** (b) in THF. The fluorescence spectra was excited at 390 nm. Reprinted with permission from ref. 9. Copyright 2017 American Chemical Society.

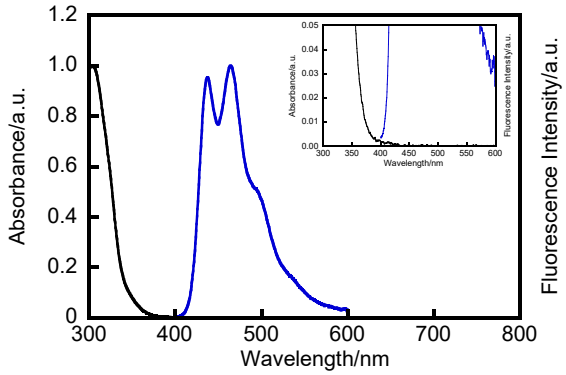

Figure 2-14. Absorption spectrum of **poly(DE1)** in the open-ring form (black line) in THF and fluorescence spectrum of **poly(FL1)** (blue line) in THF upon excitation at 390 nm. Reprinted with permission from ref. 9. Copyright 2017 American Chemical Society.

decreased.

2.3.6 Fluorescence Quantum Yield and Fluorescence Lifetime

As mentioned above, the Φ_f values of **poly(DE1$_x$-*co*-FL1$_y$)** and **poly(DE1-*alt*-FL2)** are lower than those of **DE-FL** and **FL**. The absorbance and fluorescence properties of **poly(FL1)** and **poly(St-*alt*-FL2)** in THF were investigated to reveal the reason for the decrease of Φ_f (Figure 2-13). The Φ_f values of **poly(FL1)** and **poly(St-*alt*-FL2)** were determined to be 0.66 and 0.69, respectively. These values are almost the same as those of **DE-FL** and **FL**. This result reveals that introduction of the fluorene moiety into the side chains of the polymer only slightly affects its fluorescence properties; it also indicates that the lower Φ_f values of **poly(DE1$_x$-*co*-FL1$_y$)** and **poly(DE1-*alt*-FL2)** are not due to intermolecular interactions between the fluorene moieties.

Next, the intermolecular interactions between the diarylethene open-ring form and the fluorene moiety were examined. There is a slight overlap between the absorption spectrum of **poly(DE1)** in the open-ring form and the fluorescence spectrum of **poly(FL1)** in THF (Figure 2-14), which indicates that an energy transfer from the fluorene moiety to the diarylethene open-ring form can occur. Moreover, it is considered that the energy transfer is enhanced in the copolymers because the fluorescence of multiple

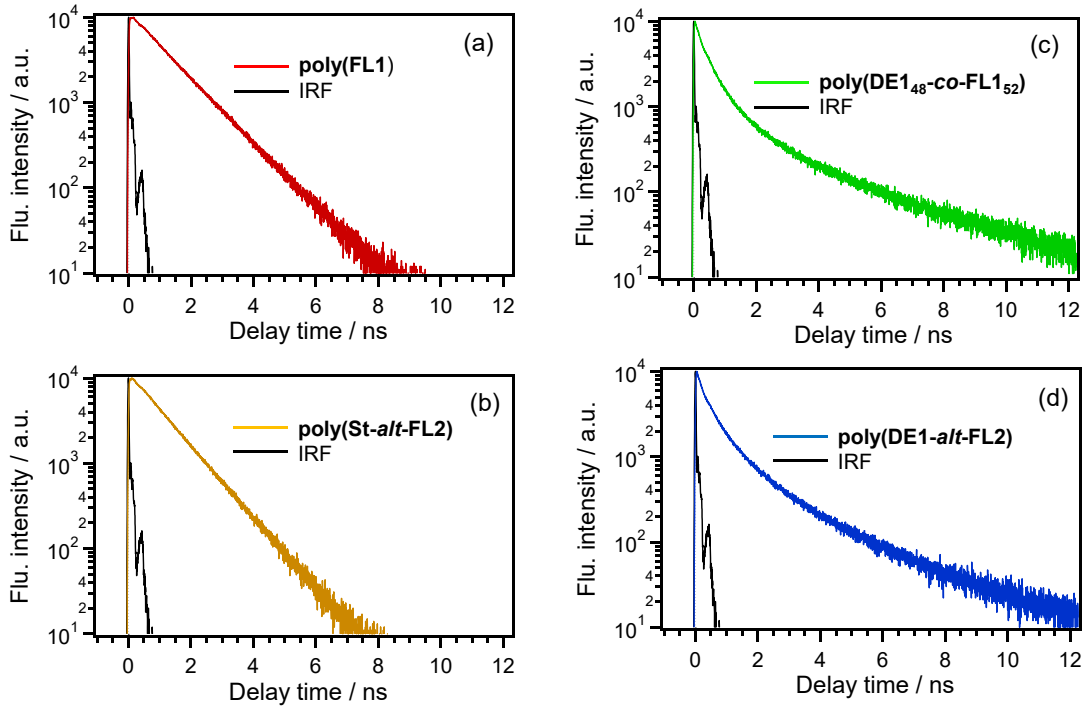

Figure 2-15. Fluorescence decay curves of **poly(FL1)** (a), **poly(St-*alt*-FL2)** (b), **poly(DE1$_{48}$-*co*-FL1$_{52}$)** (c) and **poly(DE1-*alt*-FL2)** (d) monitored at 435 nm. Reprinted with permission from ref. 9. Copyright 2017 American Chemical Society.

Table 2-4. Fluorescence lifetimes, fluorescence quantum yields, and radiative and non-radiative rate constants in THF. Reprinted with permission from ref. 9. Copyright 2017 American Chemical Society.

compound	τ_1/ns	τ_2/ns	τ_3/ns	τ_4/ns	τ_{ave}/ns[a]	χ^2	Φ_f	k_f/ns^{-1}	k_{nr}/ns^{-1}
FPT[b]	0.75	—	—	—	—	1.06	0.69	0.92	0.42
DE-FL	0.22 (17%, rise)	0.89 (83%)	—	—	—	1.00	0.69	0.98	0.44
poly(DE1$_{48}$-*co*-FL1$_{52}$)	0.10 (59%)	0.43 (31%)	1.1 (7%)	3.6 (2%)	0.34	1,06	0.15	0.44	2.49
poly(FL1)	0.32 (16%)	1.1 (84%)	—	—	0.98	1.16	0.66	0.68	0.35
poly(DE1-*alt*-FL2)	0.091 (61%)	0.44 (27%)	1.2 (10%)	3.5 (2%)	0.29	1.07	0.21	0.71	2.68
poly(St-*alt*-FL2)	0.22 (12%)	1.0 (88%)	—	—	0.91	1.14	0.69	0.76	0.34

[a] $\tau_{ave} = \Sigma\ (\tau_i \times \%)$. [b]ref. 10.

fluorene moieties is quenched by one diarylethene moiety in the open-ring form. Moreover, because the distance between diarylethene and fluorene moieties is short, other energy-transfer processes through the exchange interaction such as Dexter mechanism may contribute to some extent. As a result, the Φ_f values of **poly(DE1$_x$-*co*-FL1$_y$)** and **poly(DE1-*alt*-FL2)** decreased because of the increase in the non-radiative energy transfer process by the intermolecular interactions between the diarylethene open-ring form and the fluorene moiety.

To further investigate the fluorescence properties of the copolymers, their fluorescence lifetimes were measured (Figure 2-15). The results are summarized in Table 2-4. **FL** showed τ of 0.75 ns with a single component. **DE-FL** showed τ of 0.89 ns accompanied by a rise component of 0.20 ns. The component of ca. 0.8 ns is due to the fluorescence of the fluorene moiety. The rise component of ca. 0.2 ns may be due to an energy transfer from the diarylethene open-ring form at the excited state to the fluorene moiety. **DE-FL** at the photostationary state showed the same values as that in the open-ring form, while Φ_f decreased at the PSS. This means that the energy transfer from the fluorene moiety at the excited state to the diarylethene closed-ring form is fast enough not to detect the fluorescent lifetime and that the diarylethene closed-ring form efficiently quenches the fluorescence of the fluorene moiety. On the other hand, the studied polymers showed fluorescence lifetimes with multiple components: 0.10 (59%), 0.43 (31%), 1.1 (7%), and 3.6 ns (2%) for **poly(DE1$_{48}$-*co*-FL1$_{52}$)** and 0.091 (61%), 0.44 (27%), 1.2 (10%), and 3.5 ns (2%) for **poly(DE1-*alt*-FL2)** in the open-ring form in THF. Average fluorescence lifetimes (τ_{ave}) were calculated from these values according to $\tau_{ave} = (\tau \times \%)$; they were determined to be 0.34 ns for **poly(DE1$_{48}$-*co*-FL1$_{52}$)** and 0.29 ns for **poly(DE1-*alt*-FL2)**. The radiative rate constants (k_f) and the non-radiative rate constants (k_{nr}) were

calculated from Φ_f according to τ_{ave}: $k_f = \Phi_f / \tau_{ave}$ and $k_{nr} = (1 - \Phi_f) / \tau_{ave}$. The k_f values were calculated to be 0.44 and 0.71 ns^{-1}, and the k_{nr} values were calculated to be 2.5 and 2.7 ns^{-1} for **poly(DE1$_{48}$-*co*-FL1$_{52}$)** and **poly(DE1-*alt*-FL2)**, respectively, in the open-ring form in THF. The same method was used to calculate τ_{ave}, k_f, and k_{nr} for **poly(FL1)** and **poly(St-*alt*-FL2)**. Two components for τ in both **poly(FL1)** and **poly(St-*alt*-FL2)** were observed, which may be ascribed to the difference in the conformation in the polymers. The τ_1 values of ca. 0.1 ns for **poly(DE1$_{48}$-*co*-FL1$_{52}$)** and **poly(DE1-*alt*-FL$_2$)** do not exist in **poly(FL1)** and **poly(St-*alt*-FL2)**, which correspond to the energy transfer from the fluorene moiety to the diarylethene open-ring form. This result supports the presence of the intermolecular interactions between the diarylethene open-ring form and the fluorene moiety in **poly(DE1$_{48}$-*co*-FL1$_{52}$)** and **poly(DE1-*alt*-FL2)**. As a result, the apparent k_{nr} values for **poly(DE1$_{48}$-*co*-FL1$_{52}$)** and **poly(DE1-*alt*-FL2)** are much larger than those for **poly(FL1)** and **poly(St-*alt*-FL2)**.

2.4 Summary

In this chapter, a diarylethene-fluorene dyad connected by an ester bond (**DE-FL**) and random and alternative copolymers bearing **DE** and **FPT** in their side chains [**poly(DE1$_x$-*co*-FL1$_y$)** and **poly(DE1-*alt*-FL2)**] were synthesized to develop materials with highly efficient fluorescence on/off switching properties. Although the fluorescence intensity of **DE-FL** linearly decreased with increasing photocyclization conversion of the diarylethene, the fluorescence intensities of the copolymers significantly decreased with increasing photocyclization conversion of the diarylethene because the fluorescence of many fluorene moieties was quenched by one closed-ring diarylethene moiety. In addition, the fluorescence intensity of **poly(DE1-*alt*-FL2)** significantly decreased with increasing photocyclization conversion of the diarylethene in comparison with that of **poly(DE1$_{48}$-*co*-FL1$_{52}$)**, which revealed that the monomer sequence affects the fluorescence on/off switching properties of the copolymers. Moreover, the fluorescence on/off switching properties, such as the switching speed and contrast, of **poly(DE1$_x$-*co*-FL1$_y$)** were improved by decreasing molar fraction of **FL1** in the copolymer. The Φ_f values of the copolymers were smaller than those of **DE-FL** and **FL**. This is ascribed to the energy transfer from the fluorene moiety to the diarylethene moiety in the open-ring form.

2.5 References

[1] a) L. Giordano, T. M. Jovin, M. Irie, E. A. Jares-Erijman, *J. Am. Chem. Soc.* **2002**, *124*, 7481-7489; b) R. Metivier, S. Badre, R. Meallet-Renault, P. Yu, R. B. Pansu, K. Nakatani, *J. Phys. Chem. C* **2009**, *113*, 11916-11926.

[2] C. Li, H. Yan, L. X. Zhao, G. F. Zhang, Z. Hu, Z. L. Huang, M. Q. Zhu, *Nat. Commun.* **2014**, *5*, 5709.
[3] T. Kawai, T. Sasaki, M. Irie, *Chem. Commun.* **2001**, 711-712.
[4] H. Tian, B. Z. Chen, H. Y. Tu, K. Mullen, *Adv. Mater.* **2002**, *14*, 918-923.
[5] W. J. Tan, X. Li, J. J. Zhang, H. Tian, *Dyes. Pigm.* **2011**, *89*, 260-265.
[6] J. Folling, S. Polyakova, V. Belov, A. van Blaaderen, M. L. Bossi, S. W. Hell, *Small* **2008**, *4*, 134-142.
[7] J. Su, T. Fukaminato, J. P. Placial, T. Onodera, R. Suzuki, H. Oikawa, A. Brosseau, F. Brisset, R. Pansu, K. Nakatani, R. Métivier, *Angew. Chem. Int. Ed.* **2016**, *55*, 3662-3666.
[8] a) K. Watanabe, H. Hayasaka, T. Miyashita, K. Ueda, K. Akagi, *Adv. Funct. Mater.* **2015**, *25*, 2794-2806; b) J. Bu, K. Watanabe, H. Hayasaka, K. Akagi, *Nat. Commun.* **2014**, *5*, 3799; c) C. Li, Z. Hu, M. P. Aldred, L. X. Zhao, H. Yan, G. F. Zhang, Z. L. Huang, A. D. Q. Li, M. Q. Zhu, *Macromolecules* **2014**, *47*, 8594-8601; d) H. Hayasaka, K. Tamura, K. Akagi, *Macromolecules* **2008**, *41*, 2341-2346.
[9] T. Nakahama, D. Kitagawa, H. Sotome, S. Ito, H. Miyasaka, S. Kobatake, *J. Phys. Chem. C* **2017**, *121*, 6272-6281.
[10] a) K. Uchida, T. Ishikawa, M. Takeshita, M. Irie, *Tetrahedron* **1998**, *54*, 6627-6638; b) S. Takami, S. Kobatake, T. Kawai, M. Irie, *Chem. Lett.* **2003**, *32*, 892-893.
[11] T. Nakahama, D. Kitagawa, H. Sotome, S. Ito, H. Miyasaka, S. Kobatake, *Photochem. Photobiol. Sci.* **2016**, *15*, 1254-1263.
[12] H. Nishi, T. Namari, S. Kobatake, *J. Mater. Chem.* **2011**, *21*, 17249-17258.
[13] T. Inouchi, T. Nakashima, T. Kawai, *Chem. Asian. J.* **2014**, *9*, 2542-2547.
[14] M. S. Maji, T. Pfeifer, A. Studer, *Chem. Eur. J.* **2010**, *16*, 5872-5875.
[15] E. R. Leonard, H. D. M. Bernadette, I. R. John, L. C. Andrew, P. I. Leo, S. S. Allen, *PCT Int. Appl.* **2002**, 77 pp, WO 2002030911 A2002030911 2020020418.
[16] Y. Fan, W. Wan, G. Ma, W. Gao, H. Jiang, S. Zhu, J. Hao, *Chem. Commun.* **2014**, *50*, 5733-5736.
[17] C. A. Axton, M. E. J. Billingham, P. M. Bishop, P. T. Gallagher, T. A. Hicks, E. A. Kitchen, G. W. Mullier, W. M. Owton, M. G. Parry, S. Scott, D. J. Steggles, *J. Chem. Soc., Perkin Trans. 1* **1992**, 2203-2213.
[18] Y. Yokoyama, Y. Kurita, *J. Synth. Org. Chem. Jpn.* **1991**, *49*, 364-372.
[19] C. A. Parker, W. T. Rees, *Analyst* **1960**, *85*, 587-600.
[20] K. Rurack, M. Spieles, *Anal. Chem.* **2011**, *83*, 1232-1242.
[21] Y. Nagasawa, T. Itoh, M. Yasuda, Y. Ishibashi, S. Ito, H. Miyasaka, *J. Phys. Chem. B* **2008**, *112*, 15758-15765.

[22] A. A. Mohamed, F. H. Jebrael, M. Z. Elsabee, *Macromolecules* **1986**, *19*, 32-37.
[23] I. L. Medintz, N. Hildebrandt, *FRET-Förster Resonance Energy Transfer: From Theory to Applications*, John Wiley & Sons, **2013**.

Part II

Fabrication of Nanoparticles Consisting of Diarylethene and Fluorophore with Highly Efficient Fluorescence On/ Off Switching Properties by a Simple and Convenient Method

Chapter 3

Aggregation-Induced Emission of 1,2-Bis(3-methyl-5-phenyl-2-thienyl)perfluorocyclopentene: Direct Visualization of Polymorphic Phase Transition Process by Fluorescence Color Change

3.1 Introduction

In Part I, it was revealed that polymers bearing diarylethene and fluorene in their side chains exhibit the highly efficient fluorescence on/off switching with the high on/off contrast and rapid switching speed compared with the diarylethene-fluorene dyad. In addition to this research, the various reports suggest that the fluorescence on/off switching properties are improved by forming a molecular structure aggregated at a high density. However, a complicated multistep synthesis is required to construct the fluorescence switchable systems. In Part II, a more convenient system with the highly efficient fluorescence on/off switching properties is constructed.

However, the fluorescence intensity of most fluorophores including the fluorene derivatives is often decreased in the solid state as compared with in the solution due to the aggregation-caused quenching. To accomplish the purpose in Part II, it is necessary to use a fluorophore showing strong fluorescence even in aggregated states such as crystal. Many researchers have reported several types of organic molecules that exhibit strong fluorescence even in the solid state.[1] Especially, molecules that exhibit aggregation-induced emission (AIE) have been widely investigated.[2] They exhibit weak or no emission in solution, but exhibit strong emission in the solid state. Many researchers have worked on the design and synthesis of new AIE molecules, which has resulted in the development of various molecules with AIE character, such as tetraphenylethylene[3] and cyanostilbene.[4] To investigate a new type of molecules having AIE character is one of the important tasks for improving the fluorescence on/off switching properties.

As mentioned in General Introduction, photochromic diarylethenes have attracted much attention for application to optical memory media, switching devices, and display materials. Although there are many studies on the photochromic reaction in the crystalline phase and its applications,[5] there is little research that focuses on the fluorescence property of diarylethenes in the solid state.[6] In the course of study on photochromic diarylethene crystals, polymorphism of a diarylethene, 1,2-bis(3-methyl-5-phenyl-2-thienyl)perfluorocyclopentene (**14a**) was found (Scheme 3-1). In *n*-hexane solution, diarylethene **14a** undergoes reversible photochromic reactions with photocyclization

quantum yield of 0.17 and photocycloreversion quantum yield of 0.48 and emits fluorescence in the open-ring isomer with fluorescence quantum yield of 0.017.[7] On the other hand, the diarylethene does not undergo photochromism in the crystalline state and the polymorphic crystals exhibit strong emission with different fluorescence colors. In this chapter, it was observed that the diarylethene exhibits AIE in the crystalline state and the phase transition between polymorphs accompanying fluorescence color change.[8]

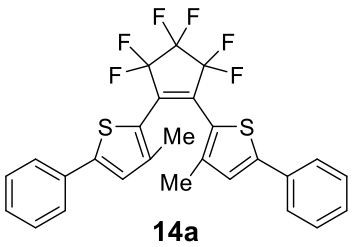

14a

Scheme 3-1. Molecular structure of diarylethene **14a**. Reprinted with permission from ref. 8. Copyright 2017 Elsevier.

3.2 Experimental Section

3.2.1 General

Polymorphic crystals were observed using a Keyence VHX-500 digital microscope. Excitation in fluorescence observation was carried out using a Keyence UV-LED UV-400 (365-nm light) or a super high pressure mercury lamp (100 W; UV-19a filter (365-nm light excitation)). Diffuse reflectance spectra were measured using a JASCO V-560 absorption spectrophotometer equipped with a JASCO ISV-469 integrating sphere. Fluorescence spectra were measured with a JASCO FP-8300 fluorescence spectrometer. Fluorescence quantum yields were also determined with a JASCO FP- 8300 fluorescence spectrometer equipped with a JASCO ILF-835 integrate sphere. Polymorphic phase transition of crystals was observed using a Nikon ECLIPSE E600POL polarizing optical microscope, equipped with a Mettler-Toledo FP82HT hot stage and FP90 central processor. Differential scanning calorimetry (DSC) was run using a HITACHI DSC-7000X. Thermogravimetric analysis (TGA) was run using a SII TG/DTA 6200. Powder X-ray diffraction profiles were recorded on a Rigaku RINT-2100 diffractometer employing CuK_α radiation (λ = 1.54184 Å). Single crystal X-ray crystallographic analysis was carried out using a Rigaku AFC/Mercury CCD diffractometer with MoK_α radiation (λ = 0.71073 Å) monochromated by graphite. The crystal structures were solved by a direct method using SIR92 and refined by the full-matrix least-squares method on F^2 with anisotropic displacement parameters for non-hydrogen atoms using SHELXL-97.

3.2.2 Fluorescence Lifetime Measurement

Time profiles of the fluorescence of polymorphic crystals were measured using a time-correlated single-photon-counting (TCSPC) system with a Ti:sapphire laser as a pulsed light source (Spectra-Physics, Tsunami, 80 MHz, ca. 100-fs fwhm). An experimental setup of the TCSPC system was described elsewhere.[9] The fundamental output at 870 nm of the Ti:sapphire laser was converted into the 540 nm pulse by using a photonic crystal fiber (NKT Photonics, FemtoWHITE800). The excitation beam was introduced into the samples after removing the remaining near-infrared light by a bandpass filter. The repetition rate was reduced to 8 MHz by an electro-optic modulator (Conoptics, Model 350). The excitation power at the sample position was typically 4.4 mW at 8 MHz. Fluorescence signal was detected at the magic angle configuration with a film polarizer and Babinet-Soleil compensator. A photomultiplier-tube (Hamamatsu Photonics, R3809U-50) equipped with a pre-amplifier (Hamamatsu Photonics, C5594) and a TCSPC module (PicoQuant, PicoHarp 300) were used. A monochromator (Princeton Instruments, Acton SP-2150) was placed in front of the photomultiplier-tube. The crystalline samples were retained using a pair of glass plates. The typical response time of the system was 100 ps (fwhm), which was determined by detecting scattered photons from a scratched glass plate.

3.2.3 Materials

Diarylethene **14a** was synthesized by the method described in the literature.[7]

3.3 Results and Discussion

Figure 3-1 shows the photographs of single crystals of diarylethene **14a** observed under normal view. When diarylethene **14a** was recrystallized from acetone, the orange needle crystal, called crystal **14a-α**, can be obtained.[7] On the other hand, the yellow platelet crystal, called crystal **14a-β**, can be obtained when diarylethene **14a** was recrystallized from *n*-hexane. To clarify the polymorphic forms of these crystals, single

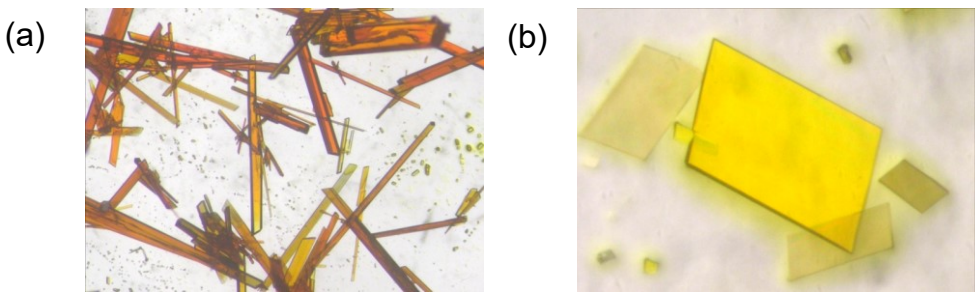

Figure 3-1. Optical microscopic photographs of single crystals of diarylethene **14a**: (a) crystal **14a-α** and (b) crystal **14a-β**. Reprinted with permission from ref. 8. Copyright 2017 Elsevier.

crystal X-ray crystallographic analysis was performed. Molecular packing diagrams of crystals **14a-α** and **14a-β** are shown in Figures 3-2 and 3-3, respectively. The crystallographic data are summarized in Table 3-1. The crystal systems and space groups of crystals **14a-α** and **14a-β** were monoclinic $P2_1/c$ and triclinic $P\bar{1}$, respectively. The crystal **14a-α** consists of eight diarylethene molecules in the unit cell and two diarylethene molecules in the asymmetric unit, while the crystal **14a-β** has two diarylethene molecules and one hexane molecule in the unit cell and one diarylethene molecule and a half of hexane molecule in the asymmetric unit. These results indicate that crystals **14a-α** and **14a-β** are evidently polymorphic forms.

Next, optical properties of crystals **14a-α** and **14a-β** were examined. Figure 3-4 shows the diffuse reflection and fluorescence spectra of powder crystals **14a-α** and **14a-β**. The optical properties are summarized in Table 3-2. In the diffuse reflection spectra,

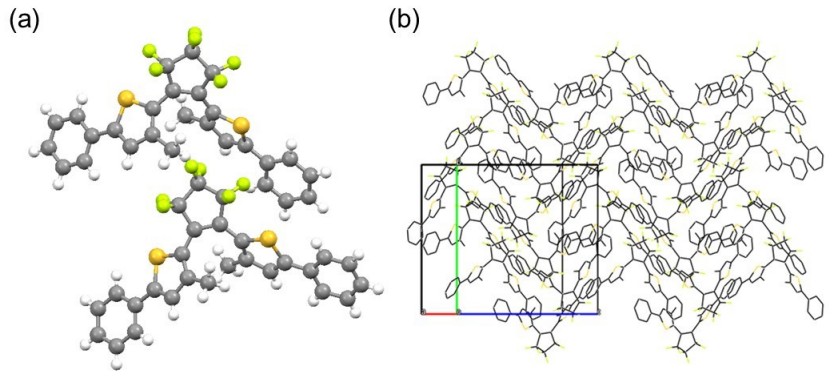

Figure 3-2. Crystal structure of crystal **14a-α** (a) in the asymmetric unit and (b) molecular packing viewed from $(\bar{1}00)$. Reprinted with permission from ref. 8. Copyright 2017 Elsevier.

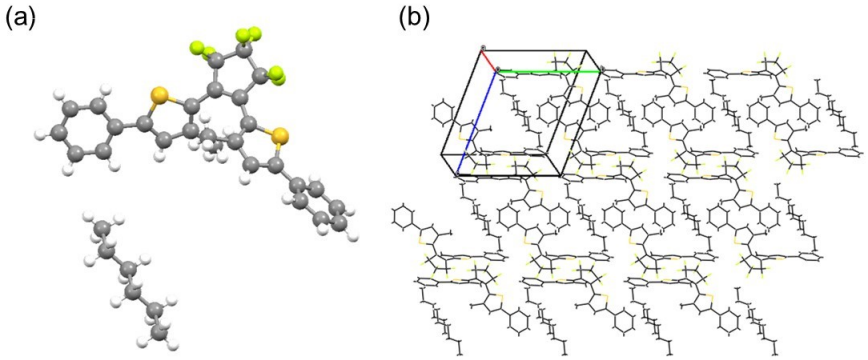

Figure 3-3. Crystal structure of crystal **14a-β** (a) in the asymmetric unit and (b) molecular packing viewed from $(\bar{1}00)$. Although there is a half of hexane molecule in the asymmetric unit, whole hexane molecule was illustrated for clarity. Reprinted with permission from ref. 8. Copyright 2017 Elsevier.

both crystals had a strong band around 400 nm and a broad and structureless band in the 450-600 nm region. The absorption edge wavelength of crystal **14a-α** was slightly longer than that of crystal **14a-β**. The difference in the absorption edge wavelength is due to the intermolecular interaction in the crystalline phase. The diarylethene molecules in crystal **14a-α** are packed more closely than that in crystal **14a-β**. On the other hand, the absorption maximum wavelength and the absorption edge wavelength of **14a** in *n*-hexane were observed at 370 and 450 nm, respectively.[7] Although diarylethene **14a** undergoes photochromic reactions in *n*-hexane[7], it does not exhibit photochromism in the crystalline state. Moreover, both crystals exhibited strong fluorescence. The fluorescence maximum wavelength (λ_{flu}) of crystal **14a-β** was observed at 570 nm. On the other hand, λ_{flu} of crystal **14a-α** was observed at 601 nm, which was shifted toward longer wavelength by 31 nm as compared with that of crystal **14a-β**. This is consistent with the difference in the absorption edge wavelength between crystals **14a-α** and **14a-β**. Furthermore, the fluorescence quantum yields (Φ_f) and fluorescence lifetime (τ) of crystals **14a-α** and **14a-β** were determined as shown in Table 3-2 and Figure 3-5. The Φ_f values of crystals **14a-α** and **14a-β** were 0.52 and 0.50, respectively, which drastically

Table 3-1. X-ray crystallographic data for crystals **14a-α** and **14a-β**. Reprinted with permission from ref. 8. Copyright 2017 Elsevier.

	crystal **14a-α**	crystal **14a-β**
Formula	$C_{27}H_{18}F_6S_2$	$C_{27}H_{18}F_6S_2$, C_3H_7
Formula weight	520.53	563.62
Temperature/K	200(2)	200(2)
Crystal system	Monoclinic	Triclinic
Space group	$P2_1/c$	$P\bar{1}$
a/Å	17.8941(46)	8.7527(17)
b/Å	16.9519(5)	12.902(3)
c/Å	15.9772(5)	13.709(3)
α/deg	90	110.982(2)
β/deg	102.933(2)	101.756(2)
γ/deg	90	101.938(1)
Volume/Å^3	4723.6(3)	1347.24(5)
Z	8	2
Density/g cm^{-3}	1.464	1.389
Goodness-of-fit on F^2	1.166	1.055
$R1$ [$I > 2\sigma(I)$]	0.0582	0.0528
$wR2$ (all data)	0.149	0.1425
CCDC No.	1509478	1509479

increased in comparison with that in *n*-hexane ($\Phi_f = 0.017$).[7]. This result clearly indicates that diarylethene has the AIE character. It is a new type of molecules that exhibit AIE. The reason why diarylethene **14a** shows a strong fluorescence in the crystalline phase may be related to the fact that diarylethene **14a** cannot undergo photochromic reactions in the crystalline phase.

In the course of this study, a polymorphic phase transition from crystal **14a-β** to crystal **14a-α** was found. Figure 3-6a-b shows the optical microscopic photographs

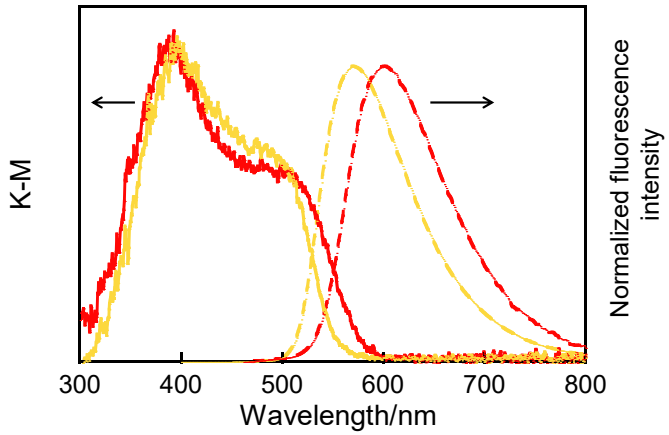

Figure 3-4. Normalized diffuse reflection spectra (solid line) and fluorescence spectra (dashed line) of powder crystals **14a-α** (orange) and **14a-β** (yellow). Reprinted with permission from ref. 8. Copyright 2017 Elsevier.

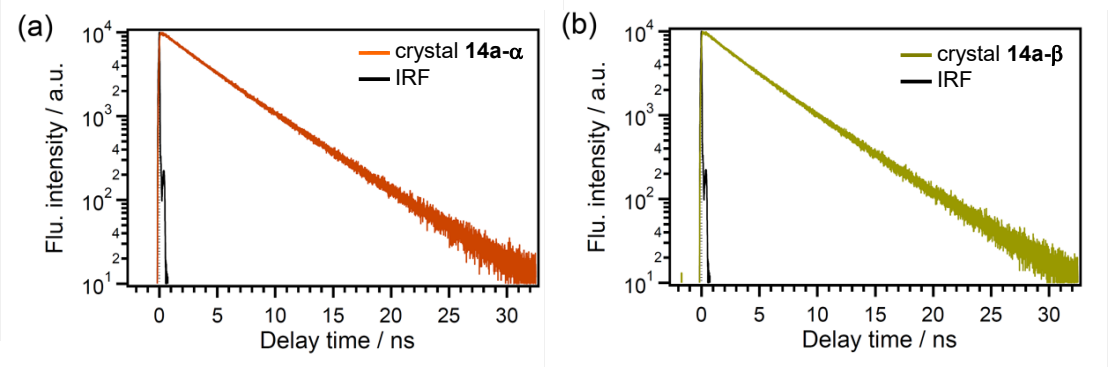

Figure 3-5. Fluorescence decay curves of crystals **14a-α** (a) and **14a-β** (b) monitored at 600 nm. Reprinted with permission from ref. 8. Copyright 2017 Elsevier.

Table 3-2. Absorption and fluorescence spectroscopic data of crystals **14a-α** and **14a-β**. Reprinted with permission from ref. 8. Copyright 2017 Elsevier.

	λ_{abs}/nm	λ_{flu}/nm	Φ_f[a]	τ_1/ns[b]	τ_2/ns[b]
crystal **14a-α**	394, 509	601	0.52	4.6 (89%)	1.9 (11%)
crystal **14a-β**	398, 505	570	0.50	4.5 (86%)	1.9 (14%)

[a]Excited at 365 nm. [b]Excited at 540 nm and observed at 600 nm.

observed in reflection mode under irradiation with white light. When the powder crystals **14a-β** were heated up from 30 °C to 120 °C at a heating rate of 10 °C min^{-1}, the color of the powder crystals changed from yellow to orange. The fluorescence color also changed from yellow to orange, as shown in Figure 3-6c-d. This color change is not due to isomerization. These results suggest that powder crystals **14a-β** can undergo a

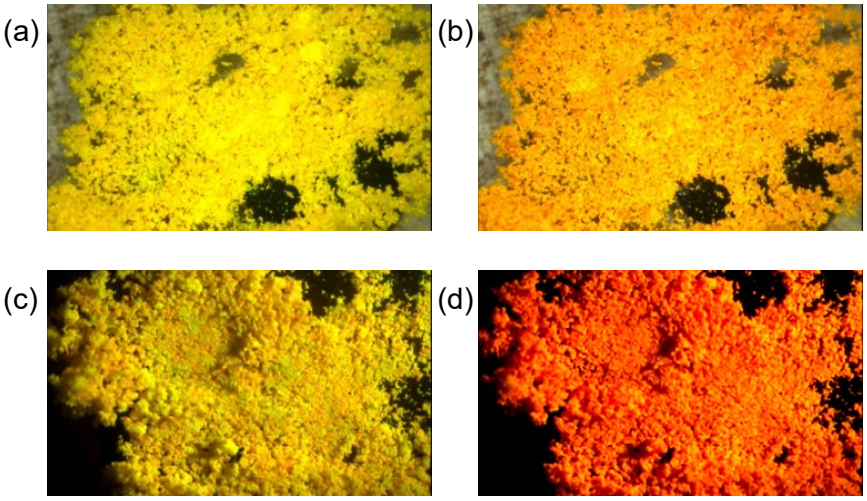

Figure 3-6. Optical microscopic photographs of powder crystals **14a-β** observed in reflection mode under irradiation with white light at (a) 30 and (b) 120 °C, and under excitation with 365 nm light at (c) 30 and (d) 120 °C. Reprinted with permission from ref. 8. Copyright 2017 Elsevier.

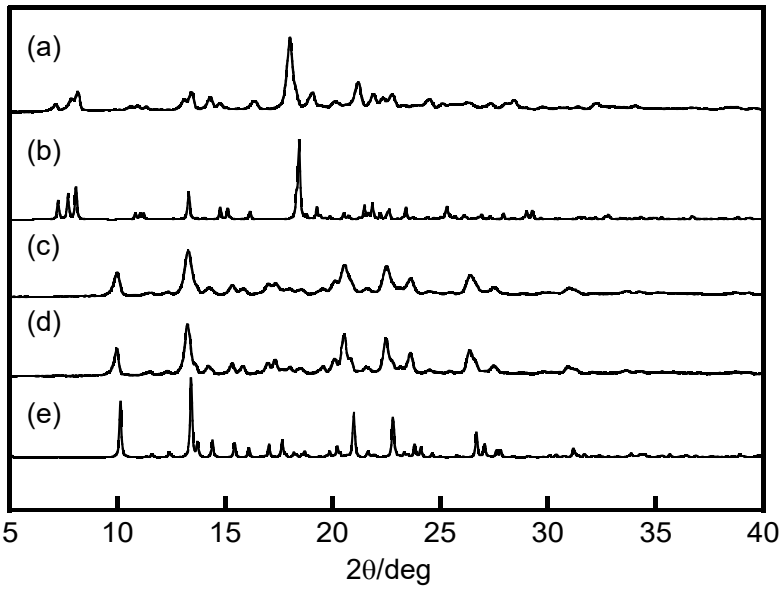

Figure 3-7. Powder X-ray diffraction patterns: (a) the pattern of powder crystals **14a-β**, (b) the calculated pattern of crystal **14a-β**, (c) the pattern of after the phase transition of powder crystals **14a-β**, (d) the pattern of powder crystals **14a-α**, and (e) the calculated pattern of crystal **14a-α**. The calculated patterns were obtained using parameters determined from single-crystal X-ray crystallographic analysis of crystals **14a-α** and **14a-β**. Reprinted with permission from ref. 8. Copyright 2017 Elsevier.

polymorphic phase transition to powder crystals **14a-α**. In order to confirm the phase transition from crystal **14a-β** to crystal **14a-α**, powder X-ray diffraction measurement was performed. Figure 3-7 shows X-ray powder diffraction patterns of the powder crystals **14a-β** before and after heating, and the calculated patterns of crystals **14a-α** and **14a-β** obtained from single crystal X-ray crystallographic analysis. The diffraction profile after heating was consistent with that of crystal **14a-α**. This result clearly indicates that the phase transition occurs from crystal **14a-β** to crystal **14a-α**.

Next, the phase transition from crystal **14a-β** to crystal **14a-α** was performed in a single crystal. Figure 3-8 shows the optical microscopic photographs observed at 50 °C under crossed Nicols. The single crystal **14a-β** emitted yellow (Figure 3-8a). After that, the yellow emission became weak (dark state) and the polymorphic phase transition started from the upper right and lower right side, which resulted in the orange emission (Figure 3-8b). Finally, the phase transition spread throughout the crystal (Figure 3-8c-d). The dark state can be assigned to a low crystallinity state like an amorphous state because the fluorescence quantum yield in the amorphous state ($\Phi_f = 0.17$) is quite smaller than that in the crystalline state ($\Phi_f > 0.5$). These results suggest that the polymorphic phase transition from crystal **14a-β** to crystal **14a-α** includes the collapse of the β-crystalline phase accompanying the exclusion of the hexane molecules and the crystallization of the crystal **14a-α**. To clarify the exclusion of the hexane molecules, thermogravimetric analysis (TGA) of crystal **14a-β** was performed as shown in Figure 3-9. When the crystal

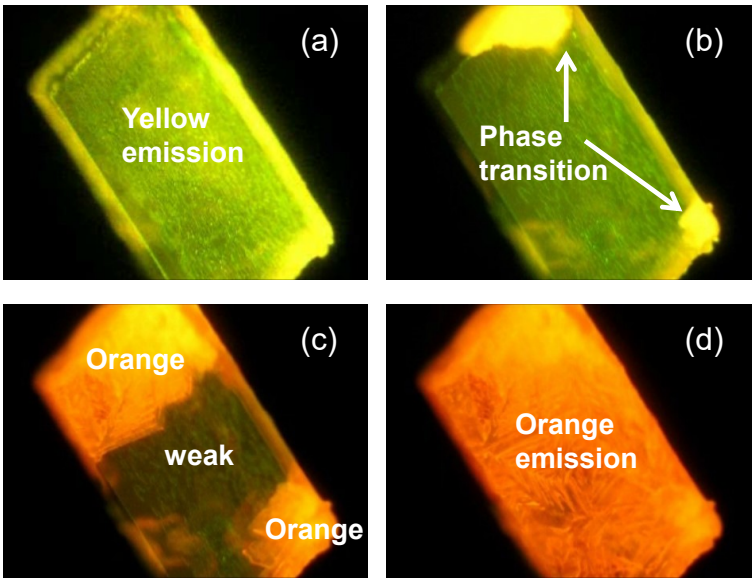

Figure 3-8. Optical microscopic photographs of crystal **14a-β** observed in reflection mode under excitation with 365 nm light at 50 °C, (a) 0, (b) 20, (c) 47, and (d) 80 min later. Reprinted with permission from ref. 8. Copyright 2017 Elsevier.

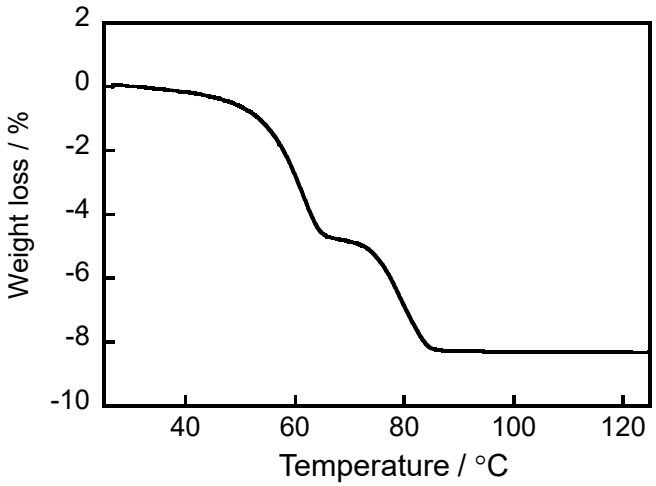

Figure 3-9. TGA trace of crystal **14a-β** at a heating rate of 10 °C min^{-1}. Reprinted with permission from ref. 8. Copyright 2017 Elsevier.

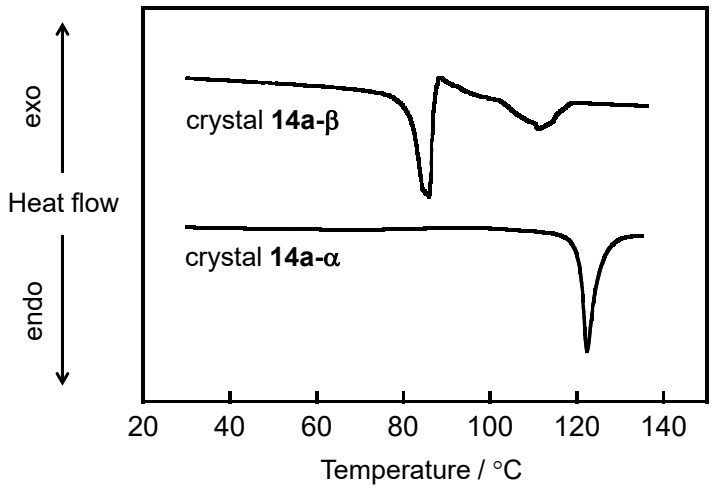

Figure 3-10. DSC traces of crystals **14a-α** (a) and **14a-β** (b) at a heating rate of 2 °C min^{-1}. Reprinted with permission from ref. 8. Copyright 2017 Elsevier.

14a-β was heated up at a rate of 10 °C min^{-1}, the weight of the crystal sample decreased in stepwise. The hexane molecules in the vicinity of the crystal surface were easily excluded around 60 °C. On the other hand, the hexane molecules inside the crystal were excluded at 70-85 °C. The weight loss by the exclusion of the hexane molecules was estimated to be 8%, which is consistent with the amount of the hexane molecules contained in the crystal **14a-β**. Figure 3-10 shows the differential scanning calorimetry (DSC) traces of crystals **14a-α** and **14a-β**. When the crystal **14a-β** was heated up at a rate of 2 °C min^{-1}, the crystal showed a small and broad endothermic behavior at 60-80 °C due to the exclusion of the *n*-hexane molecules as shown in Figure 3-11. After that, a large endothermic and a small exothermic behavior due to the collapse of the *β*-crystalline

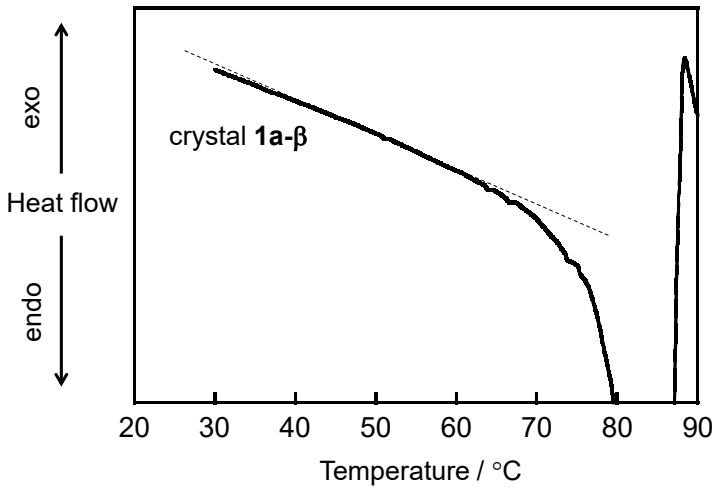

Figure 3-11. Enlarged view of DSC trace of crystal **14a-β**. Reprinted with permission from ref. 8. Copyright 2017 Elsevier.

phase and crystallization of crystal **14a-α** and a small endothermic behavior due to the crystal melting were observed at 86-90 °C and around 110 °C, respectively. The crystal **14a-α** exhibited only a large endothermic behavior corresponding to the crystal melting at 120 °C. The melting point of crystal **14a-α** obtained by the phase transition is lower than that of crystal **14a-α** prepared by recrystallization. This is ascribed to a low crystallinity or a presence of the amorphous phase. Thus, the results of TGA and DSC measurements are consistent with that observed by fluorescence color change.

3.4 Summary

The polymorphism and the phase transition for crystal of diarylethene **14a** have been demonstrated. Diarylethene **14a** has two polymorphic forms, α- and β-forms. It was revealed that both crystals show strong emission in the crystalline phase as compared with in hexane solution, which means that diarylethene **14a** has the AIE character. It has been first observed that the diarylethene exhibits AIE in the crystalline state. This result provides a new perspective for design of diarylethenes that work as luminescent solid-state materials. Furthermore, the polymorphic phase transition from *β*-form to *α*-form was found and the phase transition process was directly observed by fluorescence color change. In the phase transition process, the fluorescence color changed from yellow to orange via dark state, which means that the phase transition includes the collapse of the *β*-crystalline phase accompanying the exclusion of the *n*-hexane molecules and the crystallization of the *α*-form. This mechanism is successfully supported by TGA and DSC measurements. Thus, the polymorphic phase transition process was completely visualized

by fluorescence color change.

3.5 References

[1] a) T. Mutai, H. Shono, Y. Shigemitsu, K. Araki, *CrystEngComm* **2014**, *16*, 3890-3895; b) A. Wakamiya, K. Mori, S. Yamaguchi, *Angew. Chem. Int. Ed.* **2007**, *46*, 4273-4276; c) Y. Hong, J. W. Y. Lam, B. Z. Tang, *Chem. Soc. Rev.* **2011**, *40*, 5361-5388.

[2] a) Y. Hong, J. W. Lam, B. Z. Tang, *Chem. Soc. Rev.* **2011**, *40*, 5361-5388; b) Z. Zhang, B. Xu, J. Su, L. Shen, Y. Xie, H. Tian, *Angew. Chem. Int. Ed.* **2011**, *50*, 11654-11657.

[3] a) W. Z. Yuan, S. Chen, J. W. Lam, C. Deng, P. Lu, H. H. Sung, I. D. Williams, H. S. Kwok, Y. Zhang, B. Z. Tang, *Chem. Commun.* **2011**, *47*, 11216-11218; b) C. Y. K. Chan, Z. Zhao, J. W. Y. Lam, J. Liu, S. Chen, P. Lu, F. Mahtab, X. Chen, H. H. Y. Sung, H. S. Kwok, Y. Ma, I. D. Williams, K. S. Wong, B. Z. Tang, *Adv. Funct. Mater.* **2011**, *22*, 378-389; c) W. Wang, T. Lin, M. Wang, T.-X. Liu, L. Ren, D. Chen, S. Huang, *J. Phys. Chem. B* **2010**, *114*, 5983-5988.

[4] a) B.-K. An, S.-K. Kwon, S.-D. Jung, S. Y. Park, *J. Am. Chem. Soc.* **2002**, *124*, 14410-14415; b) B.-K. An, D.-S. Lee, J.-S. Lee, Y.-S. Park, H.-S. Song, S. Y. Park, *J. Am. Chem. Soc.* **2004**, *126*, 10232-10233; c) S.-J. Yoon, J. W. Chung, J. Gierschner, K. S. Kim, M.-G. Choi, D. Kim, S. Y. Park, *J. Am. Chem. Soc.* **2010**, *132*, 13675-13683.

[5] a) D. Kitagawa, I. Yamashita, S. Kobatake, *Chem. Commun.* **2010**, *46*, 3723-3725; b) D. Kitagawa, S. Kobatake, *Chem. Sci.* **2012**, *3*, 1445-1449; c) D. Kitagawa, H. Nishi, S. Kobatake, *Angew. Chem. Int. Ed.* **2013**, *52*, 9320-9322; d) D. Kitagawa, S. Kobatake, *J. Phys. Chem. C* **2013**, *117*, 20887-20892; e) S. Kobatake, M. Irie, *Bull. Chem. Soc. Jpn.* **2004**, *77*, 195-210.

[6] T. Fukaminato, S. Kobatake, T. Kawai, M. Irie, *Proc. Japan Acad., Ser. B* **2001**, *77*, 30-35.

[7] K. Uchida, T. Matsuoka, S. Kobatake, T. Yamaguchi, M. Irie, *Tetrahedron* **2001**, *57*, 4559-4565.

[8] D. Kitagawa, T. Nakahama, K. Mutoh, Y. Kobayashi, J. Abe, H. Sotome, S. Ito, H. Miyasaka, S. Kobatake, *Dyes Pigm.* **2017**, *139*, 233-238.

[9] Y. Nagasawa, T. Itoh, M. Yasuda, Y. Ishibashi, S. Ito, H. Miyasaka, *J. Phys. Chem. B* **2008**, *112*, 15758-15765.

Chapter 4

Solid-State Fluorescence Behavior Induced by Photochemical Ring-Opening Reaction of 1,2-Bis(3-methyl-5-phenyl-2-thienyl)perfluorocyclopentene

4.1 Introduction

As mentioned in Chapter 3, a convenient molecular system with highly efficient fluorescence on/off switching properties is constructed in Part II. To accomplish the purpose, the fluorophore with AIE characteristics is needed. 1,2-Bis(3-methyl-5-phenyl-2-thienyl)perfluorocyclopentene undergoes reversible photochromic reactions from the open-ring isomer (**14a**) to the closed-ring isomer (**14b**) in *n*-hexane and exhibits turn-off mode fluorescence switching with a fluorescence quantum yield (Φ_f) of 0.017 in the open-ring form in *n*-hexane (Scheme 4-1).[1] In Chapter 3, it was found that **14a** has two polymorphic forms (crystals **14a-α** and **14a-β**), which exhibit strong orange and yellow fluorescence (Φ_f = 0.52 and 0.50, respectively).[2] However, crystals **14a-α** and **14a-β** do not undergo photocyclization reaction. Thus, **14a** has attractive solid-state luminescence properties and can be expected as a new AIE molecular skeleton. The results suggest that **14a** has potential as fluorophore to develop the more efficient fluorescence on/off switching system. The further investigation of the fluorescence properties of **14a** in the solid states was performed.

In this chapter, the photochemical reactivity of crystal **14b** and the characteristic fluorescence emission induced by the photochemical ring-opening reaction of crystal **14b** upon irradiation with visible light (>500 nm) have been investigated. The fluorescence colors, quantum yields, and lifetimes in various states are discussed here.[3]

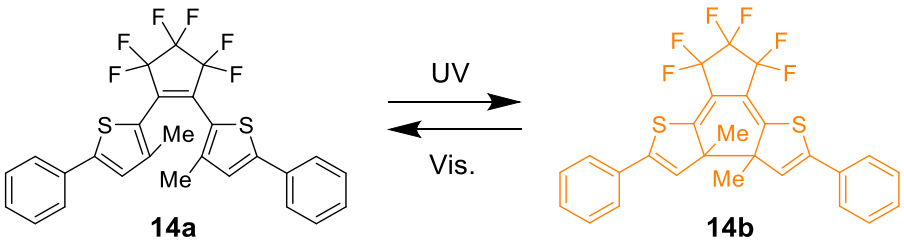

Scheme 4-1. Photochromic reaction of diarylethene **14a**/**14b**. Reprinted with permission from ref. 3. Copyright 2018 The Chemical Society of Japan.

4.2 Experimental Section

4.2.1 General

^{1}H NMR spectra were conducted using a Bruker AV-300N spectrometer at 300 MHz. Deuterated chloroform ($CDCl_3$) was used as the solvent and tetramethylsilane (TMS) as an internal standard. High-performance liquid chromatography (HPLC) was performed using a Hitachi L-7150/L-2400 HPLC system equipped with a Kanto Chemical Mightysil Si 60 column. Powder X-ray diffraction profiles were recorded on a Rigaku MiniFlex II diffractometer using CuK_α radiation (λ = 1.54184 Å). Single crystal X-ray crystallographic analysis was conducted using a Rigaku AFC/Mercury CCD diffractometer with MoK_α radiation (λ = 0.71073 Å) monochromated by graphite. The crystal structures were solved by a direct method using SIR92 and refined by the full-matrix least-squares method for F^2 with anisotropic displacement parameters for nonhydrogen atoms using SHELXL-97. Absorption spectra were measured with a JASCO V-560 absorption spectrophotometer. Photoirradiation in solution was conducted using a 200W mercury-xenon lamp (Moritex MUV-202) as a light source. Monochromatic light was obtained by passing the light through a monochromator (Jobin Yvon H10 UV) and glass filters. Fluorescence spectra were measured with a JASCO FP-8300 fluorescence spectrophotometer. Fluorescence quantum yields were also determined with a JASCO FP-8300 fluorescence spectrometer equipped with a JASCO ILF-835 integrating sphere.

4.2.2 Fluorescence Lifetime

Fluorescence lifetimes were measured using a time-correlated single-photon-counting (TCSPC) system. The experimental setup for the TCSPC has been described previously.[4] Briefly, a Ti:sapphire oscillator (Spectra-Physics, Tsunami) was utilized as a pulsed light source. The operation wavelength, pulse width, and repetition rate were set to 800 nm, 70 fs, and 80 MHz, respectively. The fundamental frequency of the laser was converted to the second harmonic (400 nm) using a type I beta barium borate (BBO) crystal and this was used to excite the samples. The repetition rate was reduced down to 8MHz using an electrooptic modulator (Conoptics, Model 350) and the excitation intensity to the sample was typically 2.2 μW at 8 MHz. The detection of fluorescence at the magic angle configuration was attained by utilizing a film polarizer and a Babinet-Soleil compensator. The fluorescence was detected using a photomultiplier tube (Hamamatsu Photonics, R3809U-50) equipped with a preamplifier (Hamamatsu Photonics, C5594) and a TCSPC module (PicoQuant, PicoHarp 300). For wavelength selection, a monochromator (Princeton Instruments, Acton 2150) was placed in front of the photomultiplier tube. Crystalline sample was retained with a pair of glass plates. For solution samples, 1 cm path length quartz cells were used. The typical response time of

the system was determined to be 40 ps full width at half maximum by detecting scattered photons from a colloidal solution and scratched glass plate.

4.2.3 Materials

1,2-Bis(3-methyl-5-phenyl-2-thienyl)perfluorocyclopentene (**14a**) was prepared by the method described previously.[1] The diarylethene closed-ring form (**14b**) was isolated by HPLC (silica-gel column) using *n*-hexane/ethyl acetate (97:3) as the eluent.

4.3 Results and Discussion

4.3.1 Characterization of Crystal

Single crystal **14b** was fabricated by recrystallization from *n*-hexane/acetone. Single crystal X-ray crystallographic analysis was successfully performed and the results are summarized in Table 4-1. Crystal **14b** is monoclinic and belongs to the $P2_1/c$ space group. The crystal structure of crystal **14b** in an asymmetric unit and the molecular packing diagram are shown in Figure 4-1. Crystal **14b** has four molecules in a unit cell and one molecule in the asymmetric unit. Molecule **14b** has a relatively planar structure compared

Table 4-1. X-ray crystallographic data for crystal **14b**. Reprinted with permission from ref. 3. Copyright 2018 The Chemical Society of Japan.

Formula	$C_{27}H_{18}F_6S_2$
Formula weight	520.53
Temperature/K	150(2)
Crystal system	Monoclinic
Space group	$P2_1/c$
Unit cell dimensions	
a/Å	8.4417(8)
b/Å	13.9459(12)
c/Å	19.7795(19)
α/deg	90
β/deg	91.572(6)
γ/deg	90
Volume/Å^3	2327.7(4)
Z	4
Density/g cm^{-3}	1.485
Goodness-of-fit on F^2	1.023
$R1$ [$I > 2\sigma(I)$]	0.0551
$wR2$ (all data)	0.1248

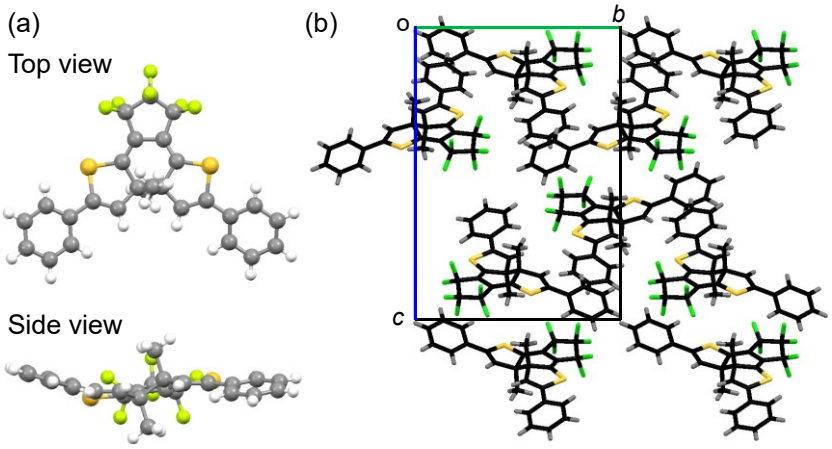

Figure 4-1. (a) Molecular structure and (b) packing diagram of **14b** in crystalline **14b**. Reprinted with permission from ref. 3. Copyright 2018 The Chemical Society of Japan.

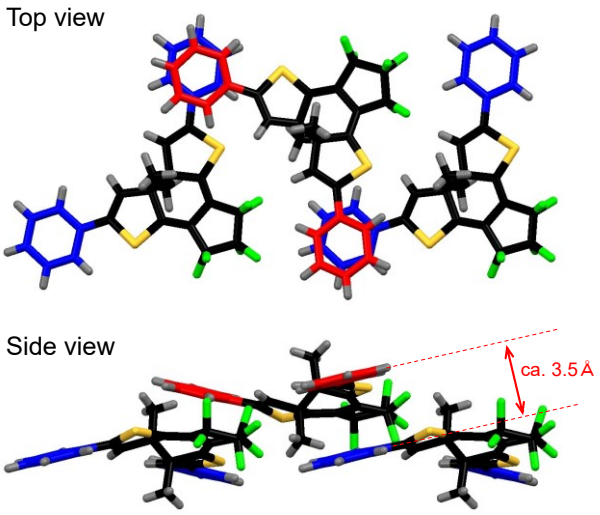

Figure 4-2. Molecular packing of crystal **14b** viewed from the top and side. The phenyl rings shown in red and blue indicate π-π intermolecular interaction. Reprinted with permission from ref. 3. Copyright 2018 The Chemical Society of Japan.

with molecule **14a** in crystals **14a-α** and **14a-β**. In the crystal, two phenyl rings of adjacent molecules have parallel face-to-face stacking and the face-to-face distance is approximately 3.5 Å, which is sufficiently short for π-π intermolecular interaction, as shown in Figure 4-2.

4.3.2 Ring-Opening Reaction in Crystal

Figure 4-3 shows optical micrographs of crystal **14b** before and after irradiation with visible light. Crystal **14b** is orange colored before photoirradiation, whereas upon irradiation with visible light, the color became yellow. The photogenerated yellow solid material was confirmed to consist of the open-ring isomer **14a** from measurement of the

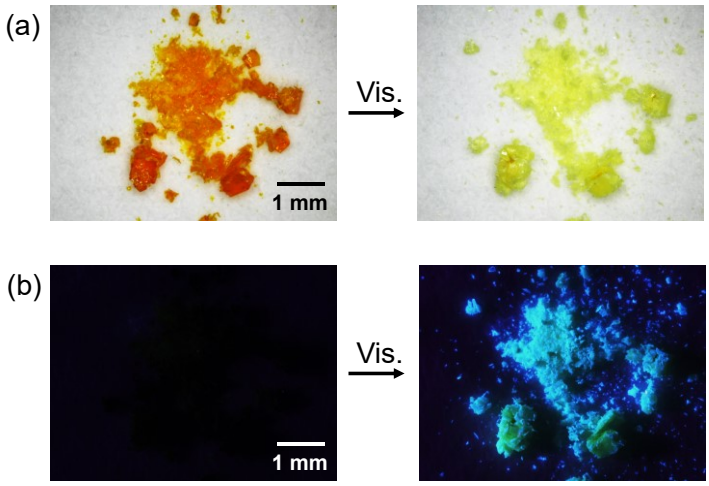

Figure 4-3. Optical micrographs of crystal **14b** observed (a) under white light and (b) under excitation at 365 nm before and after irradiation with visible light. Reprinted with permission from ref. 3. Copyright 2018 The Chemical Society of Japan.

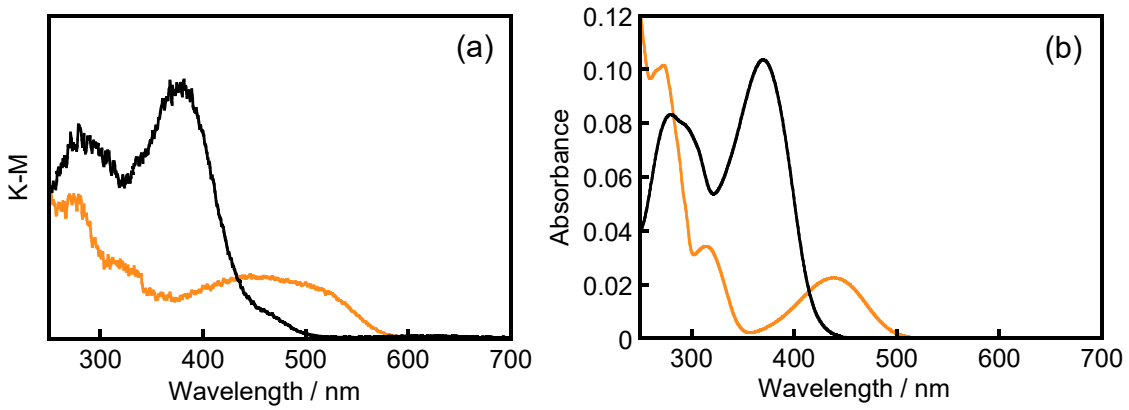

Figure 4-4. (a) Diffuse reflection spectra for powdered crystals of **14b** (orange) and **14a'** (black). (b) Absorption spectra of **14a** (black) and **14b** (orange) in *n*-hexane (4.5×10^{-6} M). Reprinted with permission from ref. 3. Copyright 2018 The Chemical Society of Japan.

absorption spectrum of a solution in *n*-hexane. Here, the photogenerated open-ring form crystal is called crystal **14a'**. In addition, crystal **14b** was rapidly fragmented simultaneously, as shown in Figure 4-3a. The fragmentation is ascribed to the strain generated by the geometrical structure change of diarylethene molecules due to the photochemical ring-opening reaction from the closed-ring form to the open-ring form in the crystalline phase.[5] The molecules in crystal **14b** have face-to-face π-π intermolecular interaction. The movement of the phenylthienyl groups by the photochemical ring-opening reaction may result in the loss of π-π intermolecular interaction. Consequently, the photochemical ring-opening reaction of **14b** in the crystal generates strain in the crystal.

Figure 4-4 shows diffuse reflection spectra for the powdered crystals of **14b** before

and after irradiation with visible light. Before irradiation with visible light, a broad band was observed in the region of 400-600 nm. The band disappeared by the ring-opening reaction upon irradiation with visible light and a band around 400 nm appeared. The absorption bands are similar to those of **14a** and **14b** in *n*-hexane. Crystal **14a'** produced by the ring-opening reaction of **14b** in the crystal did not undergo the photocyclization reaction from the open-ring form to the closed-ring form upon irradiation with UV light. No reaction has yet been observed for **14a** crystals produced by recrystallization from acetone (crystal **14a-α**) and *n*-hexane (crystal **14a-β**), which gives two polymorphic crystals,[2] whereas **14a** undergoes reversible photochromic reactions in *n*-hexane.[1]

4.3.3 X-Ray Diffraction

Single-crystal X-ray crystallographic analysis of crystal **14a'** was performed. However, it could not be accomplished due to the lack of crystallinity after the ring-opening reaction. The crystal may contain invisible cracking by the photoinduced crystal fragmentation. Therefore, powder X-ray diffraction measurement was performed. Figures 4-5a and b show X-ray powder diffraction patterns for crystals **14b** and **14a'**. For

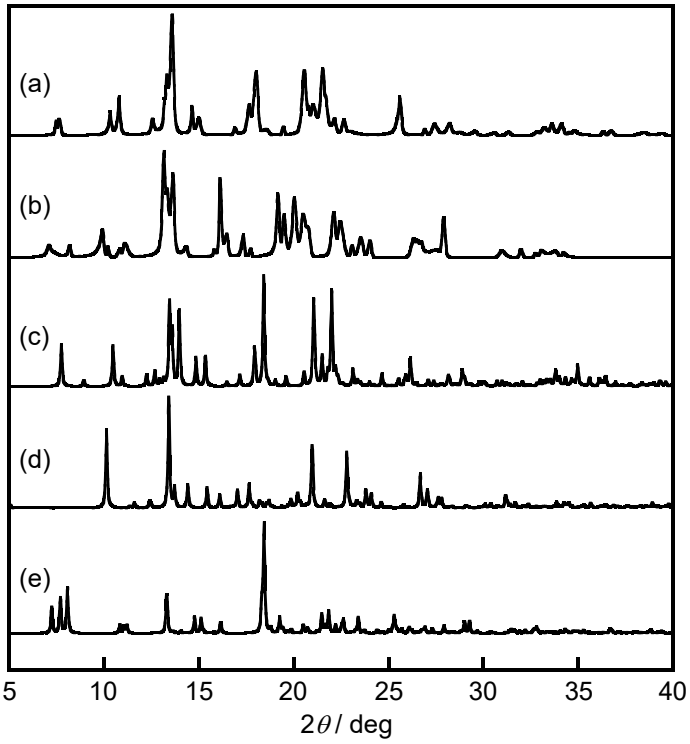

Figure 4-5. Powder X-ray diffraction patterns for (a) crystal **14b** at 27 °C and (b) crystal **14a'** at 27 °C, and calculated patterns for (c) crystal **14b** at −123 °C, (d) **14a-α** at −73 °C, and (e) **14a-β** at −73 °C. The calculated patterns were obtained using parameters determined from single-crystal X-ray crystallographic analysis of **14b**, **14a-α**, and **14a-β**. Reprinted with permission from ref. 3. Copyright 2018 The Chemical Society of Japan.

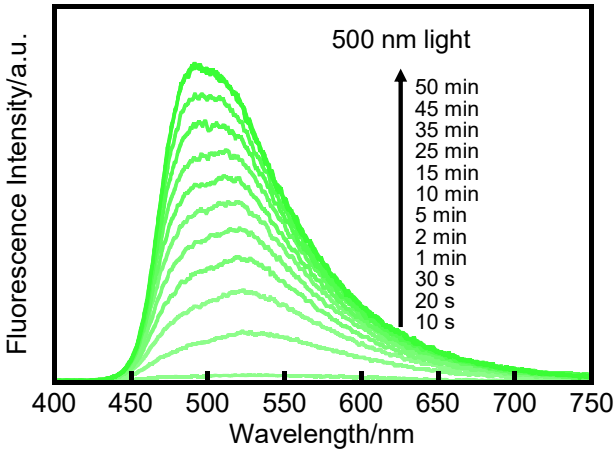

Figure 4-6. Fluorescence spectral change of **14a** in crystal **14b** upon irradiation with 500 nm light. Reprinted with permission from ref. 3. Copyright 2018 The Chemical Society of Japan.

Table 4-2. Absorption and fluorescence spectroscopic data for crystalline **14b**, **14a'**, **14a-α**, and **14a-β** and **14a** in *n*-hexane. Reprinted with permission from ref. 3. Copyright 2018 The Chemical Society of Japan.

	λ_{abs}/nm	λ_{flu}/nm	Φ_f[a]	τ_1/ns	τ_2/ns	τ_3/ns
crystal **14b**	445	—	—	—	—	—
crystal **14a'**[b]	377	491	0.15	0.19 (53%)[c]	0.40 (46%)[c]	3.8 (1%)[c]
				0.38 (80%)[d]	1.4 (8%)[d]	4.7 (1.2%)[d]
crystal **14a-α**[e]	394, 509	601	0.52	1.9 (11%)[f]	4.6 (89%)[f]	—
crystal **14a-β**[e]	398, 505	570	0.50	1.9 (14%)[f]	4.5 (86%)[f]	—
14a in *n*-hexane	370[g]	480[g]	0.017[g]	0.14 (93%)[h]	0.42 (7%)[h]	—

[a]Excited at 365 nm. [b]A sample after the ring-opening reaction in 100% conversion in crystal **14b**. [c] Excited at 400 nm and monitored at 540 nm. [d]Excited at 400nm and monitored at 600 nm. [e]ref. 2. [f] Excited at 540 nm and monitored at 600 nm. [g]ref. 1. [h][**14a**] = 2.6×10^{-5} M. Excited at 400 nm and monitored at 500 nm.

comparison, Figures 4-5c-e show the patterns calculated for crystals **14b**, **14a-α**, and **14a-β**.[2] The diffraction pattern of crystal **14b** was consistent with that calculated for a single crystal of **14b**. In contrast, the diffraction pattern of crystal **14a'** was not consistent with those of crystals **14b**, **14a-α**, and **14a-β**, which indicates that crystal **14a'** has a crystal structure that is different from those of crystals **14a-α** and **14a-β**. Thus, a new polymorphic form of **14a** was produced by the ring-opening reaction of crystal **14b**.

4.3.4 Fluorescence Spectra

As shown in Figure 4-3b, crystal **14b** exhibited no fluorescence upon excitation at 365 nm. On the contrary, after irradiation with visible light, the crystal exhibited green fluorescence (Figure 4-3b). In the initial process upon irradiation with visible light, the

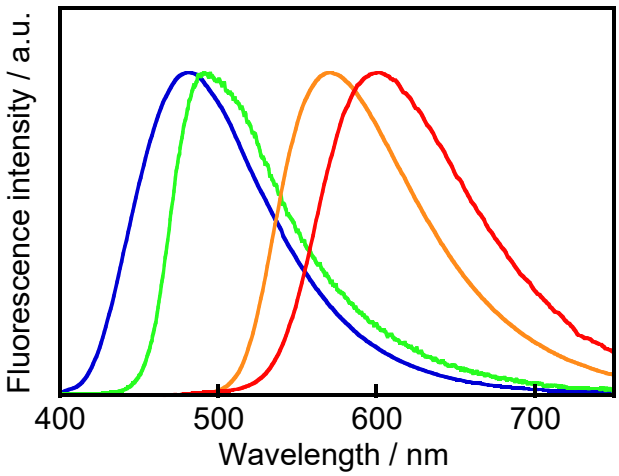

Figure 4-7. Fluorescence spectra of **14a** in *n*-hexane (4.5×10^{-6} M) (blue), crystal **14a'** (green), crystal **14a-α** (red), and crystal **14a-β** (orange). Reprinted with permission from ref. 3. Copyright 2018 The Chemical Society of Japan.

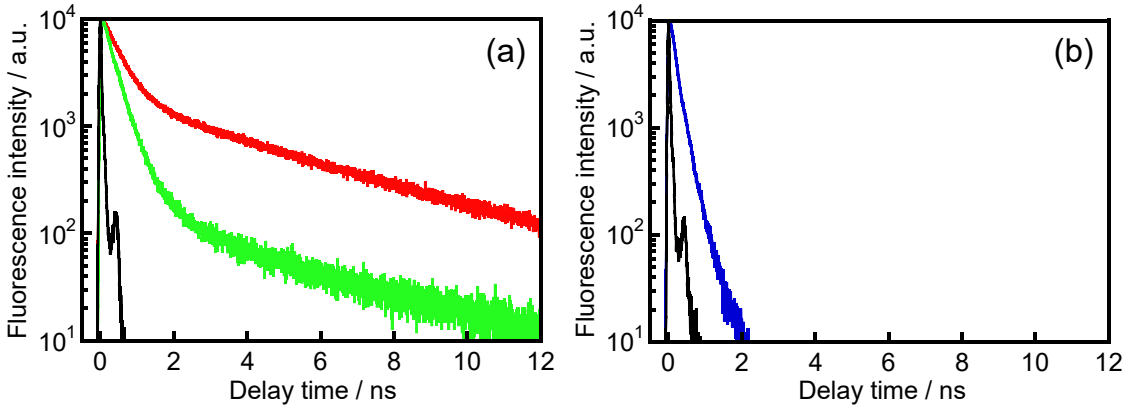

Figure 4-8. Fluorescence decay curve for (a) crystal **14a'** monitored at 540 nm ($\chi^2 = 1.16$) (green) and 600 nm ($\chi^2 = 1.17$) (red) and for (b) **14a** in *n*-hexane monitored at 500 nm ($\chi^2 = 1.16$) (blue). Reprinted with permission from ref. 3. Copyright 2018 The Chemical Society of Japan.

fluorescence spectrum was observed around 530 nm (Figure 4-6). Upon continuous irradiation with visible light, the fluorescence maximum wavelength (λ_{flu}) was shifted to the shorter wavelength. Finally, λ_{flu} was observed at 491 nm with Φ_f of 0.15. The shift of λ_{flu} is ascribed to quenching by reabsorption to **14b** in the low photoreaction conversion. The influence of the reabsorption decreased in the higher photoreaction conversion. Table 4-2 summarizes the optical properties of crystals **14b** and **14a'**. For comparison, the optical properties of **14a** in the crystal (crystals **14a-α** and **14a-β**) and in *n*-hexane are also shown in Table 4-2. Φ_f for crystal **14a'** was larger than that in *n*-hexane. This indicates that **14a** in crystal **14a'** also has AIE character as well as **14a** in crystals **14a-α** and **14a-β**. λ_{flu} of crystal **14a'** is different from those of crystals **14a-α** (λ_{flu} = 601 nm) and **14a-β** (λ_{flu} = 570 nm) and that in *n*-hexane (λ_{flu} = 480 nm). These results indicate that diarylethene **14a** exhibits four different fluorescence colors, i.e. blue, green, yellow, and

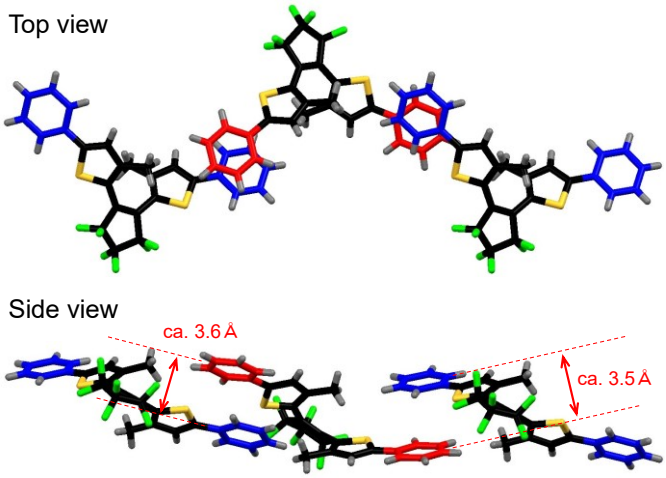

Figure 4-9. Molecular packing of crystal **14a-α** viewed from top and side. The phenyl rings shown in blue and red indicate face to face π-π intermolecular interaction. Reprinted with permission from ref. 3. Copyright 2018 The Chemical Society of Japan.

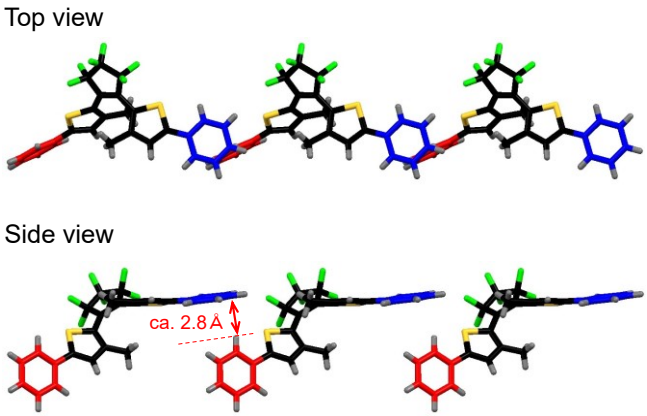

Figure 4-10. Molecular packing of crystal **14a-β** viewed from top and side. The phenyl rings shown in blue and red indicate edge to face π-π intermolecular interaction. Reprinted with permission from ref. 3. Copyright 2018 The Chemical Society of Japan.

orange, depending on the crystalline state or the solvent solution, as shown in Figure 4-7. This is the first example in which the diarylethene itself exhibits multiple fluorescent colors when in the different states.

The fluorescence lifetimes of **14a** in crystal **14a'** and *n*-hexane were compared. Figure 4-8 shows the fluorescence decay curves of **14a** in crystal **14a'** and in *n*-hexane. The fluorescence lifetime (τ) of **14a** in crystal **14a'** consisted of 0.19 ns (53%), 0.40 ns (46%), and 3.8 ns (1%) when the fluorescence was monitored at 540 nm. On the other hand, when the fluorescence was monitored at 600 nm, τ was observed to be 0.38 ns (80%), 1.4 ns (8%), and 4.7 ns (12%). These results indicate that the fluorescence consists of mainly two components, <1 ns and 1-5 ns. **14a** in *n*-hexane also showed a decay curve with multiple components: 0.14 ns (93%) and 0.42 ns (7%). The components of τ for **14a** in *n*-hexane were consistent with the faster decay component for crystal **14a'**. These

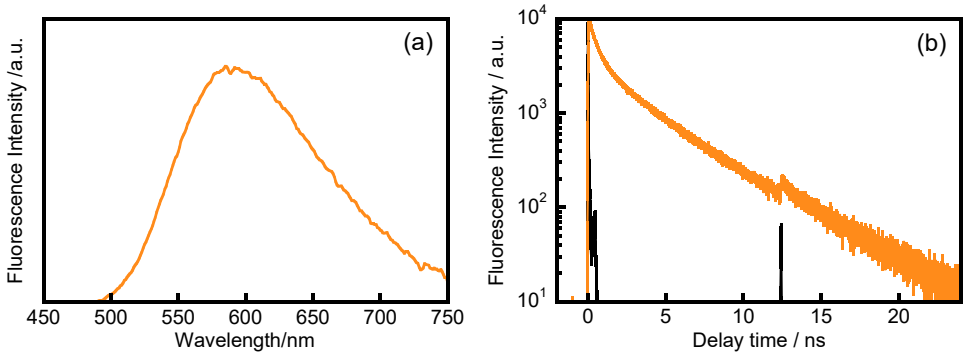

Figure 4-11. (a) Fluorescence spectrum of **14a** in the amorphous phase excited at 365 nm, and (b) fluorescence decay curve for **14a** in the amorphous phase monitored at 600 nm ($\chi^2 = 1.15$). The sample was prepared by melting crystal **14a** followed by cooling to room temperature. Reprinted with permission from ref. 3. Copyright 2018 The Chemical Society of Japan.

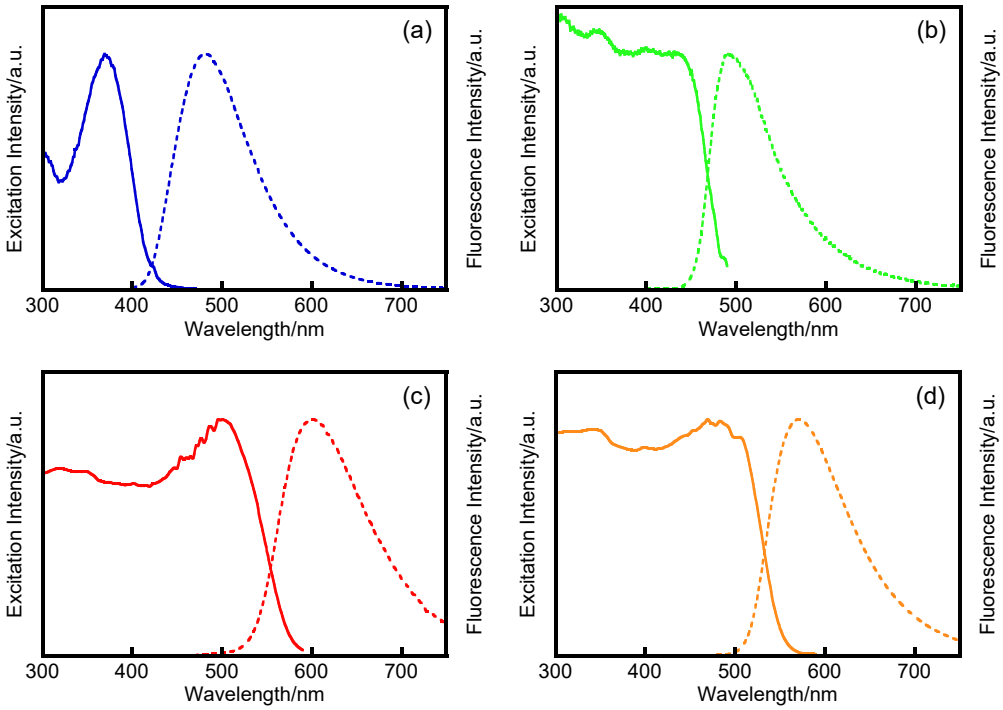

Figure 4-12. Excitation (solid line) and fluorescence spectra (dashed line) of **14a** in *n*-hexane (a), crystal **14a'** (b), crystal **14a-α** (c), and crystal **14a-β** (d). The excitation spectra were monitored at 480, 500, 600, and 600 nm for **14a** in *n*-hexane, crystal **14a'**, crystal **14a-α**, and crystal **14a-β**, respectively. The fluorescence spectra were recorded upon excitation at 365 nm. Reprinted with permission from ref. 3. Copyright 2018 The Chemical Society of Japan.

results indicate that the faster decay component in crystal **14a'** is due to the fluorescence of a single molecule. On the other hand, the lifetime of 1-5 ns does not exist for **14a** in *n*-hexane. The longer lifetime of 1-5 ns is close to those of crystals **14a-α** and **14a-β**. The molecules in the **14a-α** crystal have face-to-face π-π intermolecular interaction between phenyl rings (Figure 4-9). In crystals **14a-β** the molecules have edge-to-face π-π intermolecular interaction between phenyl rings (Figure 4-10). In spite of the different π-

π intermolecular interactions, τ in crystals **14a-α** and **14a-β** are similar. It was previously reported that 1,2-bis(3-methyl-2-thienyl)perfluorocyclopentene showed two components of τ in a low concentration solution and in the crystalline phase. It was revealed that the longer τ was attributed to molecular aggregations, which exhibited a red-shifted fluorescence spectrum in comparison with that of monomer.[6] It is possible that similar phenomena occurred with **14a** in *n*-hexane and with crystal **14a'**. τ of **14a** in the amorphous phase was observed to be 0.30 ns (46.4%), 0.84 ns (25.1%), 3.1 ns (21.6%), and 5.6 ns (6.9%) when the fluorescence was monitored at 600 nm (Figure 4-11). The longer lifetime of 1-5 ns was observed even in the amorphous phase. Therefore, the slower decay component is ascribed to the condensed state.

In the excitation spectra, crystals **14a-α** and **14a-β** have a band from 500 to 600 nm (Figure 4-12). On the other hand, the excitation band of crystal **14a'** was not observed in the region of 500-600 nm, but was slightly shifted to a longer wavelength than that of **14a** in *n*-hexane. Thus, the large red-shifted fluorescence for crystals **14a-α** and **14a-β** is ascribed to the intermolecular π-π interactions. Contrastively, crystal **14a'** exhibited the slightly red-shifted fluorescence in comparison with **14a** in *n*-hexane, but it is not the major characteristics in crystal **14a'** compared with those in crystals **14a-α** and **14a-β**.

4.4 Summary

Crystals of diarylethene closed-ring form **14b** have been fabricated and the change in the solid-state luminescence of the crystal induced by irradiation with visible light was demonstrated. Upon irradiation with visible light, **14b** in the crystal underwent a photochemical ring-opening reaction accompanying crystal fragmentation. The **14b** crystal exhibited no fluorescence at the initial state. However, after the ring-opening reaction, green fluorescence was observed with higher Φ_f than that in solution. This fluorescence color is different from those in crystals **14a-α** and **14a-β** and in *n*-hexane, which is ascribed to the difference in the intermolecular interaction between **14a** molecules.

4.5 References

[1] K. Uchida, T. Matsuoka, S. Kobatake, T. Yamaguchi, M. Irie, *Tetrahedron* **2001**, *57*, 4559-4565.

[2] D. Kitagawa, T. Nakahama, K. Mutoh, Y. Kobayashi, J. Abe, H. Sotome, S. Ito, H. Miyasaka, S. Kobatake, *Dyes Pigm.* **2017**, *139*, 233-238.

[3] T. Nakahama, D. Kitagawa, H. Sotome, S. Ito, H. Miyasaka, S. Kobatake, *Bull. Chem. Soc. Jpn.* **2018**, *91*, 153-157.

[4] Y. Nagasawa, T. Itoh, M. Yasuda, Y. Ishibashi, S. Ito, H. Miyasaka, *J. Phys. Chem. B* **2008**, *112*, 15758-15765.

[5] a) D. Kitagawa, T. Okuyama, R. Tanaka, S. Kobatake, *Chem. Mater.* **2016**, *28*, 4889-4892; b) E. Hatano, M. Morimoto, K. Hyodo, N. Yasuda, S. Yokojima, S. Nakamura, K. Uchida, *Chem. Eur. J.* **2016**, *22*, 12680-12683.

[6] T. Fukaminato, T. Kawai, S. Kobatake, M. Irie, *J. Phys. Chem. B* **2003**, *107*, 8372-8377.

Chapter 5

Crystallization-Induced Emission of 1,2-Bis(3-methyl-5-(4-alkylphenyl)-2-thienyl)perfluorocyclopentenes: A Mechanical and Thermal Recording System

5.1 Introduction

As mentioned in Chapters 3 and 4, the purpose in Part II is to realize the molecular system, which shows the highly efficient fluorescence on/off switching, by a simple and convenient method. It is considered that the fluorophore with aggregation-induced emission (AIE) characteristics is suitable as the fluorophore moiety in the molecular system.

Many researchers have tried to search AIE molecules, which has resulted in discovering of various AIE molecules.[1] During the studies of the AIE phenomenon, some luminescent dyes which exhibit strong emission in the crystalline phase compared with those in dilute solution and in the amorphous phase were found. The phenomenon is expressed as crystallization-induced emission (CIE).[2] Most of the molecules having CIE characteristics exhibit the red-shifted and weak emission in the concentrated amorphous states due to strong intermolecular interactions, such as π-π stacking by random conformations and disorderly packing in the amorphous states. On the other hand, CIE molecules exhibit the blue-shifted and strong emission in the crystalline phase. They adopt a twisted conformation in the crystal, which prevents strong intermolecular interactions. In addition, there are weak intermolecular interactions such as C-H…π and C-H···O in the crystal, which reduces the non-radiative decay caused by intramolecular vibrations and rotations.[1, 3]

In Chapter 3, it was found that 1,2-bis(3-methyl-5-phenyl-2-thienyl)perfluorocyclopentene **(14a)** has two polymorphic forms (crystals **14a-α** and **14a-β**), which exhibit strong orange and yellow fluorescence (Φ_f = 0.52 and 0.50), respectively, although **14a** does not undergo the photocyclization reaction in the solid states.[4] In addition, the open-ring form crystal (crystal **14a'**) which is produced by the photochemical ring-opening reaction in the crystal of **14b** exhibits green fluorescence (Φ_f = 0.15), as shown in Chapter 4.[5] The red-shifted fluorescence of **14a** in crystals **14a-α** and **14a-β** compared with that in *n*-hexane is ascribed to the intermolecular π-π interactions between the phenyl rings. Introduction of alkyl substituents to the phenyl rings may modulate the intermolecular π-π interactions to result in a dramatic change in the solid-state luminescence properties.

In this chapter, diarylethenes **15a**-**18a**, 1,2-bis(3-methyl-5-(4-alkylphenyl)-2-thienyl)perfluorocyclopentenes having methyl, ethyl, *n*-propyl, and *n*-butyl substituents at *p*-position of the phenyl ring, have been synthesized as shown in Scheme 5-1, and the photochromic and fluorescence properties were investigated in *n*-hexane and in the solid states. In the solid states, **15a**-**18a** exhibited optical properties significantly different from **14a**, i.e. different fluorescence color and crystallization-induced emission characteristics depending on alkyl chain length. Moreover, it was found that the amorphous solid of **15a** crystallizes after mechanical scratching followed by heating to result in strong emission.[6]

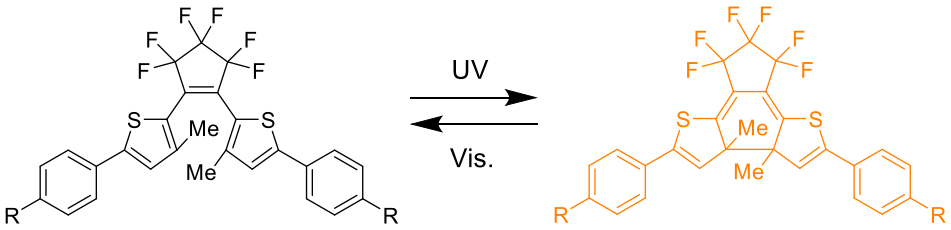

14a : R = H
15a : R = Me
16a : R = Et
17a : R = *n*-Pr
18a : R = *n*-Bu

14b : R = H
15b : R = Me
16b : R = Et
17b : R = *n*-Pr
18b : R = *n*-Bu

Scheme 5-1. Molecular structure of diarylethenes used in this chapter. Reprinted with permission from ref. 6. Copyright 2019 Elsevier.

5.2 Experimental Section

5.2.1 General

^{1}H NMR spectra were recorded on a Bruker AV-300N spectrometer at 300 MHz. Deuterated chloroform ($CDCl_3$) was used as the solvent and tetramethylsilane (TMS) as an internal standard, respectively. High resolution mass spectra (HRMS) were obtained on a Bruker FT-ICR/solariX mass spectrometer. The matrix-assisted laser desorption/ionization (MALDI) was used as an ionization technique. *trans*-2-[3-(4-*tert*-Butylphenyl)-2-methyl-2-propenylidene]malononitrile (DCTB) was used as matrix. High-performance liquid chromatography (HPLC) was carried out using a Hitachi L-7150/L-2400 HPLC system equipped with a Kanto Chemical Mightysil Si 60 column. Differential scanning calorimetry (DSC) was performed using a Hitachi DSC7000X instrument. Powder X-ray diffraction profiles were recorded on a Rigaku MiniFlex 600 diffractometer employing CuKα radiation (λ = 1.54184 Å). Single crystal X-ray crystallographic analysis was carried out using a Rigaku AFC/Mercury CCD diffractometer with MoKα radiation (λ = 0.71073 Å) monochromated by graphite. The crystal structures were solved by a direct method using SIR92 and refined by the full-matrix least-squares method on F^2 with anisotropic displacement parameters for non-

hydrogen atoms using SHELXL-97. Absorption spectra were measured with a JASCO V-560 absorption spectrophotometer. Photoirradiation in solution was conducted using a 200 W mercury−xenon lamp (Moritex MUV-202) as a light source. Monochromatic light was obtained by passing the light through a monochromator (Jobin Yvon H10 UV) and glass filters. Fluorescence spectra were measured with a JASCO FP-8300 fluorescence spectrophotometer. Fluorescence quantum yields were also determined with a JASCO FP-8300 fluorescence spectrometer equipped with a JASCO ILF-835 integrate sphere.

5.2.2 Photochemical Reaction

The photocyclization and cycloreversion quantum yields were determined in *n*-hexane relative to **14a**,[7] whose quantum yield had been previously determined.[8] Photoirradiation was conducted using a 200 W mercury−xenon lamp (Moritex MUV-202) or a 300 W xenon lamp (Asahi Spectra MAX-301) as the light source. Monochromatic light was obtained by passing the light through a monochromator (Jobin Yvon H10 UV).

5.2.3 Fluorescence Lifetime

Fluorescence lifetimes were measured using a time-correlated single-photon-counting (TCSPC) system. The experimental setup for the TCSPC has been described previously.[9] Briefly, a Ti:sapphire oscillator (Spectra-Physics, Tsunami) was utilized as a pulsed light source. The operation wavelength, pulse width, and repetition rate were set to 800 nm, 70 fs, and 80 MHz, respectively. The fundamentals of the laser were converted to the second harmonics (400 nm) using a type I beta barium borate crystal and used to excite the samples. The repetition rate was reduced down to 8 MHz by using an electro-optic modulator (Conoptics, model 350), and the excitation intensity to the samples was typically 17 μW at 8 MHz. The detection of fluorescence at the magic-angle configuration was attained by utilizing a film polarizer and a Babinet-Soleil compensator. The fluorescence was detected using a photomultiplier tube (Hamamatsu Photonics, R3809U-50) equipped with a preamplifier (Hamamatsu Photonics, C5594) and a TCSPC module (PicoQuant, PicoHarp 300). For wavelength selection, a monochromator (Princeton Instruments, Acton 2150) was placed in front of the photomultiplier tube. The sample solutions were set in 1 cm path length of the quartz cells. The typical response time of the system was determined to be 40 ps full width at half maximum by detecting the scattered photons from a colloidal solution.

5.2.4 Materials

Chemicals used for synthesis were commercially available and used without further

purification. Diarylethenes **15a**-**18a** were synthesized as shown below.

*Synthesis of **15a**.* Diarylethene **15a** was prepared according to the synthetic route in Scheme 5-2.

*1,2-Bis(3-methyl-5-(4-methylphenyl)-2-thienyl)perfluorocyclopentene (**15a**)*. 2-(4-Methylphenyl)-4-methylthiophene (**19**)[10] (1.0 g, 5.3 mmol) was dissolved in anhydrous ether (10 mL) under argon atmosphere. 1.6 M *n*-BuLi hexane solution (3.7 mL, 5.9 mmol) was slowly added dropwise to the solution at 0 °C, and the mixture was refluxed for 1.5 h. Octafluorocyclopentene (0.36 mL, 2.7 mmol) was slowly added to the solution at the temperature, and the mixture was stirred for 3 h. Adequate amount of distilled water was added to the mixture to quench the reaction. The reaction mixture was neutralized by HCl aqueous solution, extracted with ether, washed with brine, dried over $MgSO_4$, filtered, and concentrated in vacuo. The crude product was purified by column chromatography on silica gel using *n*-hexane as the eluent and recrystallization from *n*-hexane/acetone to give 570 mg of **15a** in 39% yield as a yellow crystal. mp = 134-135 °C. **15a**: ^{1}H NMR (300 MHz, $CDCl_3$, TMS) δ = 1.82 (s, 6H, CH_3), 2.36 (s, 6H, CH_3), 7.03 (s, 2H, Thienyl H), 7.18 (d, 4H, *J* = 8 Hz, Aromatic H), 7.47 (d, 4H, *J* = 8 Hz, Aromatic H). ^{13}C NMR (75 MHz, $CDCl_3$) δ = 15.7, 21.4, 122.2, 125.9, 126.2, 129.8, 130.5, 138.7, 142.4, 148.3. HR-MS (MALDI) *m/z* = 548.1061 (M^+, 100%). Calcd. for $C_{29}H_{22}F_6S_2^+$ = 548.1062.

*Synthesis of **16a**.* Diarylethene **16a** was prepared according to the synthetic route in Scheme 5-3.

*2-Bromo-3-methyl-5-(4-ethylphenyl)thiophene (**21**)*. 3-Methylthiophene (2.0 mL, 21 mmol) was dissolved in anhydrous ether (40 mL) under argon atmosphere. 1.6 M *n*-BuLi hexane solution (14 mL, 22 mmol) was slowly added dropwise to the solution at 0 °C, and the mixture was refluxed for 1.5 h. Tri-*n*-butyl borate (6.0 mL, 22 mmol) was slowly added to the solution at −78 °C, and the mixture was stirred for 1.5 h. Adequate amount

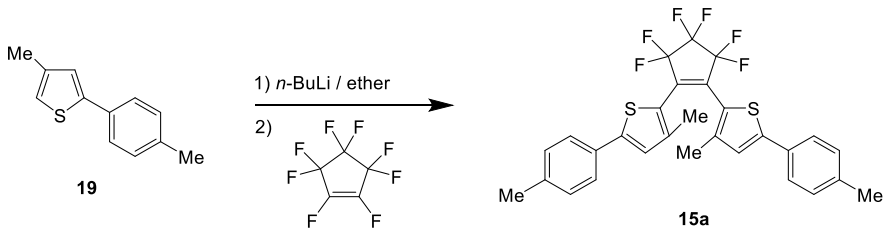

Scheme 5-2. Synthetic scheme of diarylethene **15a**. Reprinted with permission from ref. 6. Copyright 2019 Elsevier.

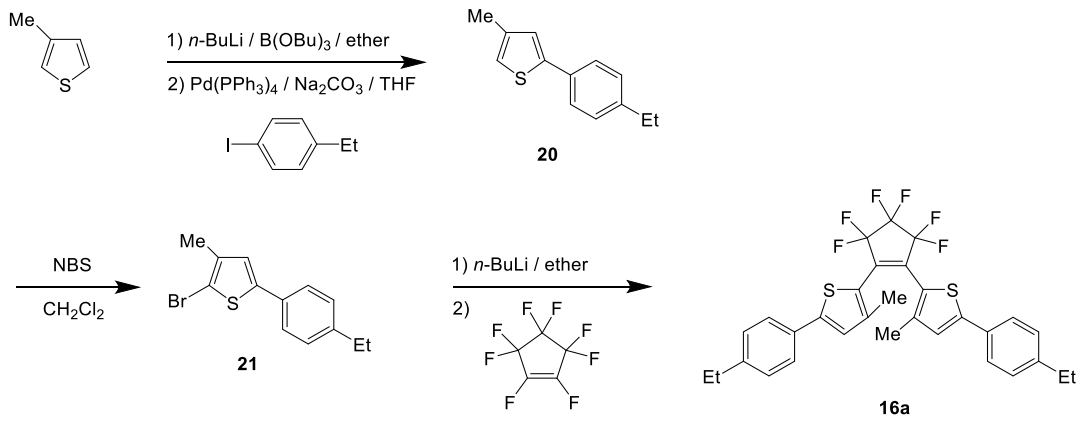

Scheme 5-3. Synthetic scheme of diarylethene **16a**. Reprinted with permission from ref. 6. Copyright 2019 Elsevier.

of distilled water was added to the mixture to quench the reaction. *p*-Iodoethylbenzene (4.3 g, 19 mmol), tetrakis(triphenylphosphine)palladium(0) (120 mg 0.10 mmol), 20 wt% Na_2CO_3 aqueous solution (24 mL), and THF (40 mL) were added to the solution, and the mixture was refluxed for 6 h. The reaction mixture was neutralized by HCl aqueous solution, extracted with ether, washed with brine, dried over $MgSO_4$, filtered, and concentrated in vacuo. The clear oil of mixture of 4-methyl-2-(4-ethylphenyl)thiophene (**20**) and 3-methyl-2-(4-ethylphenyl)thiophene (**20'**) (**20** : **20'** = 1 : 0.18) was obtained by column chromatography on silica gel using *n*-hexane as the eluent in 3.5 g yield. 2.0 g of the mixture was used for the following reaction without further purification. The mixture was dissolved in chloroform (20 mL). *N*-Bromosuccinimide (NBS) (1.8 g, 10 mmol) was added to the solution at room temperature, and the mixture was stirred for 48 h. The reaction mixture was neutralized by $NaHCO_3$ aqueous solution, extracted with chloroform, washed with brine, dried over $MgSO_4$, filtered, and concentrated in vacuo. The crude product was purified by column chromatography on silica gel using *n*-hexane as the eluent to give 1.7 g of **21** in 51% yield based on 3-methylthiphene. **21**: ^{1}H NMR (300 MHz, $CDCl_3$, TMS) δ = 1.23 (t, 3H, J = 8 Hz, CH_3), 2.18 (s, 3H, CH_3), 2.63 (q, 2H, J = 8 Hz, CH_2), 6.92 (s, 1H, Thienyl H), 7.17 (d, 2H, J = 8 Hz, Aromatic H), 7.39 (d, 2H, J = 8 Hz, Aromatic H). ^{13}C NMR (75 MHz, $CDCl_3$) δ = 15.5, 15.6, 28.7, 108.1, 124.6, 125.5, 128.6, 131.4, 138.2, 143.8, 144.2. HR-MS (MALDI) *m/z* = 279.9916 (M^+, 100%). Calcd. for $C_{13}H_{13}BrS^+$ = 279.9916.

1,2-Bis(3-methyl-5-(4-ethylphenyl)-2-thienyl)perfluorocyclopentene ***(16a)***. Compound **21** (1.0 g, 3.6 mmol) was dissolved in anhydrous THF (20 mL) under argon atmosphere. 1.6 M *n*-BuLi hexane solution (2.4 mL, 3.8 mmol) was slowly added dropwise to the solution at −78 °C, and the mixture was stirred for 1.5 h at the temperature.

Octafluorocyclopentene (0.24 mL, 1,8 mmol) was slowly added to the solution at the temperature, and the mixture was stirred for 6 h. Adequate amount of distilled water was added to the mixture to quench the reaction. The reaction mixture was neutralized by HCl aqueous solution, extracted with ether, washed with brine, dried over $MgSO_4$, filtered, and concentrated in vacuo. The crude product was purified by column chromatography on silica gel using *n*-hexane as the eluent and recrystallization from *n*-hexane/acetone to give 730 mg of **16a** in 71% yield as a yellow crystal. mp = 133-134 °C. **16a**: ^{1}H NMR (300 MHz, $CDCl_3$, TMS) δ = 1.24 (t, 6H, *J* = 8 Hz, CH_3), 1.81 (s, 6H, CH_3), 2.65 (q, 4H, *J* = 8 Hz, CH_2),7.03 (s, 2H, Thienyl H), 7.21 (d, 4H, *J* = 8 Hz, Aromatic H), 7.49 (d, 4H, *J* = 8 Hz, Aromatic H). ^{13}C NMR (75 MHz, $CDCl_3$) δ = 15.6, 15.7, 28.8, 122.2, 126.0, 126.2, 128.7, 130.8, 142.4, 145.1, 148.3. HR-MS (MALDI) *m/z* = 576.1373 (M^+, 100%). Calcd. for $C_{31}H_{26}F_6S_2^+$ = 576.1375.

*Synthesis of **17a**.* Diarylethene **17a** was prepared according to the synthetic route in Scheme 5-4.

*2-Bromo-3-methyl-5-(4-propylphenyl)thiophene (**23**).* 3-Methylthiophene (2.0 mL, 21 mmol) was dissolved in anhydrous ether (40 mL) under argon atmosphere. 1.6 M *n*-BuLi hexane solution (14 mL, 22 mmol) was slowly added dropwise to the solution at 0 °C, and the mixture was refluxed for 1.5 h. Tri-*n*-butyl borate (6.0 mL, 22 mmol) was slowly added to the solution at −78 °C, and the mixture was stirred for 1.5 h. Adequate amount of distilled water was added to the mixture to quench the reaction. *p*-Bromopropylbenzene (3.7 g, 19 mmol), tetrakis(triphenylphosphine)palladium(0) (120 mg 0.10 mmol), 20 wt% Na_2CO_3 aqueous solution (20 mL), and THF (40 mL) were added to the solution, and the mixture was refluxed for 6 h. The reaction mixture was neutralized

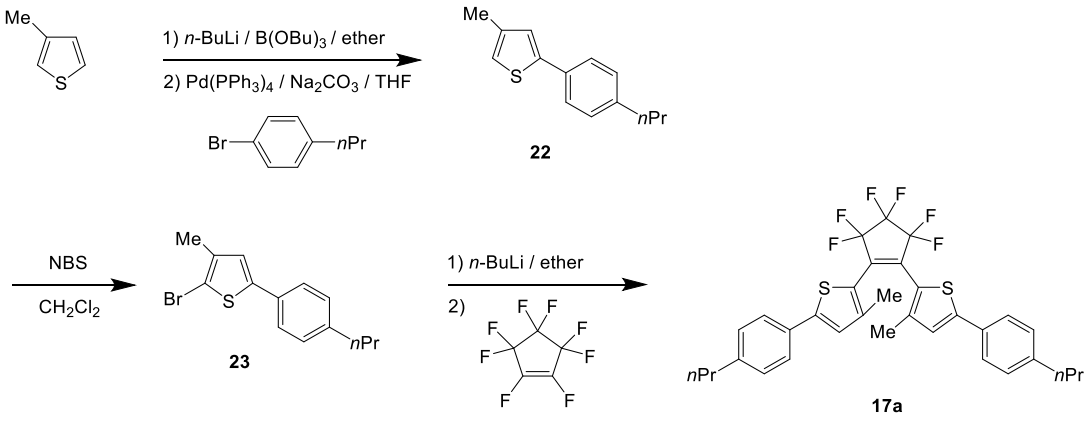

Scheme 5-4. Synthetic scheme of diarylethene **17a**. Reprinted with permission from ref. 6. Copyright 2019 Elsevier.

by HCl aqueous solution, extracted with ether, washed with brine, dried over $MgSO_4$, filtered, and concentrated in vacuo. The clear oil of mixture of 4-methyl-2-(4-propylphenyl)thiophene (**22**) and 3-methyl-2-(4-propylphenyl)thiophene (**22'**) (**22** : **22'** = 1 : 0.19) was obtained by column chromatography on silica gel using *n*-hexane as the eluent in 2.7 g yield. 2.0 g of the mixture was used for the next reaction without further purification. The mixture was dissolved in chloroform (20 mL). NBS (1.8 g, 10 mmol) was added to the solution at room temperature, and the mixture was stirred for 48 h. The reaction mixture was neutralized by $NaHCO_3$ aqueous solution, extracted with chloroform, washed with brine, dried over $MgSO_4$, filtered, and concentrated in vacuo. The crude product was purified by column chromatography on silica gel using *n*-hexane as the eluent to give 1.7 g of **23** in 29% yield based on 3-methylthiphene. **23**: ^{1}H NMR (300 MHz, $CDCl_3$, TMS) δ = 0.94 (t, 3H, *J* = 7 Hz, CH_3), 1.58-1.70 (m, 2H, CH_2), 2.19 (s, 3H, CH_3), 2.58 (t, 2H, *J* = 8 Hz, CH_2), 6.93 (s, 1H, Thienyl H), 7.16 (d, 2H, *J* = 8 Hz, Aromatic H), 7.39 (d, 2H, *J* = 8 Hz, Aromatic H). ^{13}C NMR (75 MHz, $CDCl_3$) δ = 13.9, 15.5, 24.6, 37.9, 108.1, 124.6, 125.5, 129.2, 131.4, 138.2, 142.6, 143.8. HR-MS (MALDI) *m/z* = 294.0072 (M^+, 100%). Calcd. for $C_{14}H_{15}BrS^+$ = 294.0072.

1,2-Bis(3-methyl-5-(4-propylphenyl)-2-thienyl)perfluorocyclopentene ***(17a)***. Compound **23** (1.0 g, 3.4 mmol) was dissolved in anhydrous THF (20 mL) under argon atmosphere. 1.6 M *n*-BuLi hexane solution (2.3 mL, 3.7 mmol) was slowly added dropwise to the solution at −78 °C, and the mixture was stirred for 1.5 h at the temperature. Octafluorocyclopentene (0.23 mL, 1,7 mmol) was slowly added to the solution at the temperature, and the mixture was stirred for 5 h. Adequate amount of distilled water was added to the mixture to quench the reaction. The reaction mixture was neutralized by HCl aqueous solution, extracted with ether, washed with brine, dried over $MgSO_4$, filtered, and concentrated in vacuo. The crude product was purified by column chromatography on silica gel using *n*-hexane as the eluent and recrystallization from *n*-hexane/acetone to give 780 mg of **17a** in 76% yield as a yellow crystal. mp = 115-116 °C. **17a**: ^{1}H NMR (300 MHz, $CDCl_3$, TMS) δ = 0.94 (t, 6H, *J* = 7 Hz, CH_3), 1.58-1.70 (m, 4H, CH_2), 1.81 (s, 6H, CH_3), 2.59 (t, 4H, *J* = 8 Hz, CH_2), 7.03 (s, 2H, Thienyl H), 7.18 (d, 4H, *J* = 8 Hz, Aromatic H), 7.49 (d, 4H, *J* = 8 Hz, Aromatic H). ^{13}C NMR (75 MHz, $CDCl_3$) δ = 13.9, 15.7, 24.6, 37.9, 122.2, 125.8, 126.2, 129.3, 130.8, 142.4, 143.5, 148.3. HR-MS (MALDI) *m/z* = 604.1686 (M^+, 100%). Calcd. for $C_{33}H_{30}F_6S_2^+$ = 604.1688.

Synthesis of ***18a***. Diarylethene **18a** was prepared according to the synthetic route in Scheme 5-5.

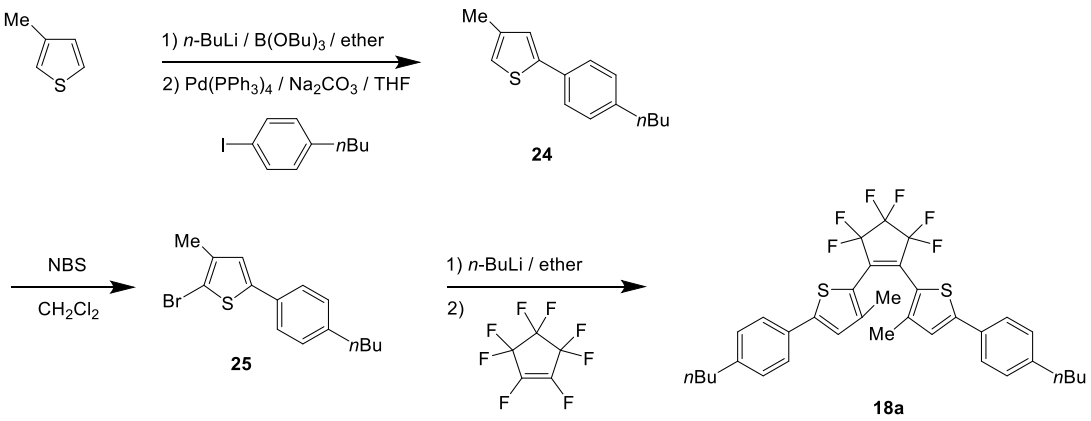

Scheme 5-5. Synthetic scheme of diarylethene **18a**. Reprinted with permission from ref. 6. Copyright 2019 Elsevier.

*2-Bromo-3-methyl-5-(4-butylphenyl)thiophene (**25**).* 3-Methylthiophene (3.6 mL, 37 mmol) was dissolved in anhydrous ether (60 mL) under argon atmosphere. 1.6 M *n*-BuLi hexane solution (26 mL, 42 mmol) was slowly added dropwise to the solution at 0 °C, and the mixture was refluxed for 1.5 h. Tri-*n*-butyl borate (11 mL, 41 mmol) was slowly added to the solution at −78 °C, and the mixture was stirred for 1.5 h. Adequate amount of distilled water was added to the mixture to quench the reaction. *p*-Bromobutylbenzene (7.9 g, 37 mmol), tetrakis(triphenylphosphine)palladium(0) (210 mg 0.18 mmol), 20 wt% Na_2CO_3 aqueous solution (40 mL), and THF (40 mL) were added to the solution, and the mixture was refluxed for 5 h. The reaction mixture was neutralized by HCl aqueous solution, extracted with ether, washed with brine, dried over $MgSO_4$, filtered, and concentrated in vacuo. The clear oil of mixture of 4-methyl-2-(4-butylphenyl)thiophene (**24**) and 3-methyl-2-(4-butylphenyl)thiophene (**24'**) (**24** : **24'** = 1 : 0.16) was obtained by column chromatography on silica gel using *n*-hexane as the eluent in 5.1 g yield. 5.0 g of the mixture was used for the next reaction without further purification. The mixture was dissolved in chloroform (60 mL). NBS (4.4 g, 25 mmol) was added to the solution at room temperature, and the mixture was stirred at 15 h. The reaction mixture was neutralized by $NaHCO_3$ aqueous solution, extracted with chloroform, washed with brine, dried over $MgSO_4$, filtered, and concentrated in vacuo. The crude product was purified by column chromatography on silica gel and recrystallization from *n*-hexane/acetone as the eluent to give 5.3 g of **25** in 47% yield based on 3-methylthiphene. **25**: ^{1}H NMR (300 MHz, $CDCl_3$, TMS) δ = 0.93 (t, *J* = 7 Hz, 3H, CH_3), 1.30-1.42 (m, 2H, CH_2), 1.54-1.65 (m, 2H, CH_2), 2.19 (s, 3H, CH_3), 2.60 (t, *J* = 8 Hz, 2H, CH_2), 6.93 (s, 1H, Thienyl H), 7.16 (d, *J* = 8 Hz, 2H, Aromatic H), 7.39 (d, *J* = 8 Hz, 2H, Aromatic H). ^{13}C NMR (75 MHz, $CDCl_3$) δ = 14.1, 15.4, 22.5, 33.6, 35.5, 108.0, 124.5, 125.4, 129.1, 131.3, 138.1,

142.8, 143.8. HR-MS (MALDI) *m/z* = 308.0229 (M^+, 100%). Calcd. for $C_{15}H_{17}BrS^+$ = 308.0229.

1,2-Bis(3-methyl-5-(4-butylphenyl)-2-thienyl)perfluorocyclopentene ***(18a)***. Compound **25** (1.5 g, 4.9 mmol) was dissolved in anhydrous THF (15 mL) under argon atmosphere. 1.6 M *n*-BuLi hexane solution (3.3 mL, 5.3 mmol) was slowly added dropwise to the solution at −78 °C, and the mixture was stirred for 1.5 h at the temperature. Octafluorocyclopentene (0.33 mL, 2.5 mmol) was slowly added to the solution at the temperature, and the mixture was stirred for 3 h. Adequate amount of distilled water was added to the mixture to quench the reaction. The reaction mixture was neutralized by HCl aqueous solution, extracted with ether, washed with brine, dried over $MgSO_4$, filtered, and concentrated in vacuo. The crude product was purified by column chromatography on silica gel using *n*-hexane as the eluent and recrystallization from *n*-hexane/acetone to give 1.2 g of **18a** in 78% yield as a yellow crystal. mp = 106-107 °C. **18a**: ^{1}H NMR (300 MHz, $CDCl_3$, TMS) δ = 0.93 (t, *J* = 7 Hz, 6H, CH_3), 1.30-1.42 (m, 4H, CH_2), 1.55-1.65 (m, 4H, CH_2), 1.81 (s, 6H, CH_3), 2.61 (t, *J* = 8 Hz, 4H, CH_2), 7.03 (s, 2H, Thienyl H), 7.18 (d, *J* = 8 Hz, 4H, Aromatic H), 7.48 (d, *J* = 8 Hz, 4H, Aromatic H). ^{13}C NMR (75 MHz, $CDCl_3$) δ = 14.1, 15.7, 22.5, 33.6, 35.5, 122.2, 125.9, 126.2, 129.2, 130.7, 142.4, 143.8, 148.3. HR-MS (MALDI) *m/z* = 632.2000 (M^+, 100%). Calcd. for $C_{35}H_{34}F_6S_2^+$ = 632.2001.

5.3 Results and Discussion

5.3.1 Photochromic and Fluorescence Properties in *n*-Hexane

Diarylethenes **15a**-**18a** underwent reversible photochromic reactions in *n*-hexane upon alternating irradiation with ultraviolet (UV) and visible light. Figure 5-1 shows absorption spectra of **15a**-**18a** in *n*-hexane. The optical properties of **15a**-**18a** in *n*-hexane are summarized in Table 5-1. For comparison, the optical properties of **14a** in *n*-hexane are also shown in Table 5-1. The absorption maximum wavelengths (λ_{abs}) of **15a**-**18a** were observed at 376-377 nm. Upon irradiation with 365 nm light, new absorption bands appeared around 440 nm. The absorption spectral changes are ascribed to the photocyclization reaction from the open-ring form to the closed-ring form. The photocyclization conversions upon irradiation with 365 nm were determined to be 91–95% for **15a**-**18a**. Upon irradiation with visible light (> 450 nm), the absorption bands disappeared and the absorption spectra returned to the initial ones. The photocyclization and photocycloreversion quantum yields ($\Phi_{o\rightarrow c}$ and $\Phi_{c\rightarrow o}$) were determined to be 0.10-0.11 and 0.51-0.53 for **15a**-**18a**, respectively. The $\Phi_{o\rightarrow c}$ values decreased slightly in

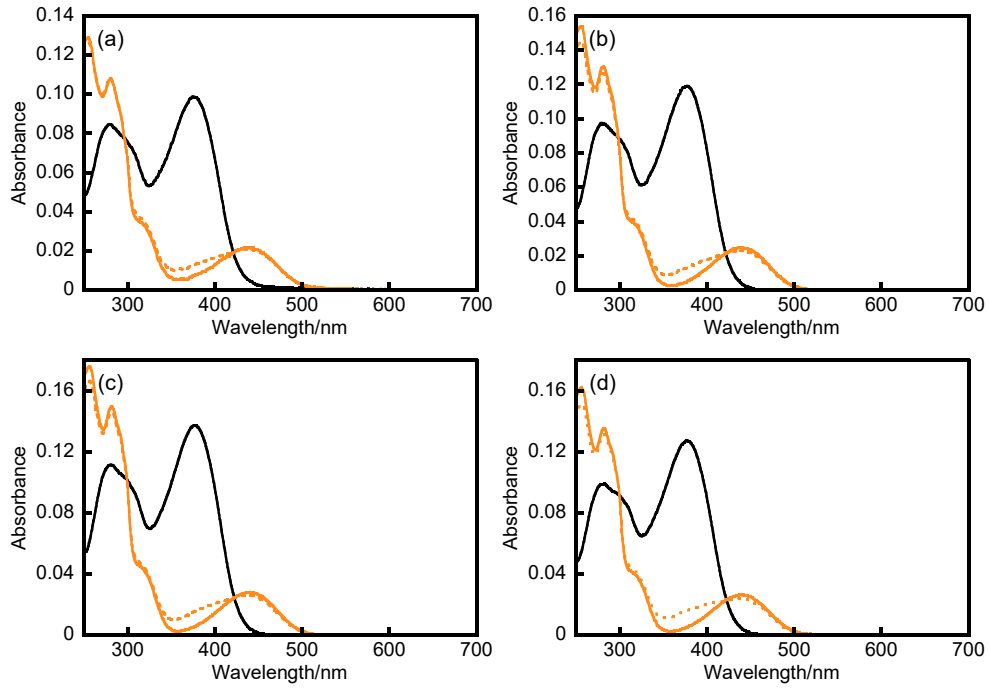

Figure 5-1. Absorption spectra of (a) **15a** (3.8×10^{-6} M), (b) **16a** (4.7×10^{-6} M), (c) **17a** (5.2×10^{-6} M), and (d) **18a** (4.8×10^{-6} M) in *n*-hexane: the open-ring isomer (black solid line), the closed-ring isomer (orange solid line), and the photostationary solution upon irradiation with 365 nm light (orange dashed line). Reprinted with permission from ref. 6. Copyright 2019 Elsevier.

Table 5-1. Optical properties of **14a-18a** in *n*-hexane. Reprinted with permission from ref. 6. Copyright 2019 Elsevier.

	Open-ring form		Closed-ring form		Quantum yield		Conv. /%[a]	λ_{flu} /nm	Φ_f[c]	τ_1 /ns[d]	τ_2 /ns[d]
	λ_{abs} /nm	ε /$M^{-1}cm^{-1}$	λ_{abs} /nm	ε /$M^{-1}cm^{-1}$	$\Phi_{o\rightarrow c}$[a]	$\Phi_{c\rightarrow o}$[b]					
14a	370[e]	22800[e]	438[e]	5250[e]	0.17[e]	0.48[e]	95	480[f]	0.017[e]	0.14 (93.0%)[f]	0.4 (7.0%)[f]
15a	376	25800	438	5410	0.11	0.53	94	485	0.056	0.20 (98.8%)	0.47 (1.2%)
16a	377	25400	439	5280	0.11	0.53	93	486	0.059	0.22 (98.8%)	0.43 (1.2%)
17a	377	26500	440	5320	0.10	0.51	92	486	0.059	0.22 (99.5%)	0.55 (0.5%)
18a	377	26400	438	5430	0.11	0.52	91	487	0.058	0.22 (91.8%)	0.35 (8.2%)

a) Photocyclization quantum yield upon irradiation at 365 nm. b) Photocycloreversion quantum yield upon irradiation at 440 nm. c) Fluorescence quantum yield excited at 365 nm. d) Fluorescence lifetime excited at 400 nm and monitored at 500 nm. e) ref. 7. f) ref. 5.

comparison with that of **14a** ($\Phi_{o\rightarrow c}$ = 0.17),[7] which indicates that the electron-donating property of alkyl substituents at the *p*-positions of phenyl rings reduces the $\Phi_{o\rightarrow c}$ value.

Figure 5-2 shows fluorescence spectral changes of **15a-18a** in *n*-hexane. Diarylethenes **15a-18a** exhibited blue fluorescence with the fluorescence maximum wavelength (λ_{flu}) of 485-487 nm. The fluorescence quantum yields (Φ_f) were determined

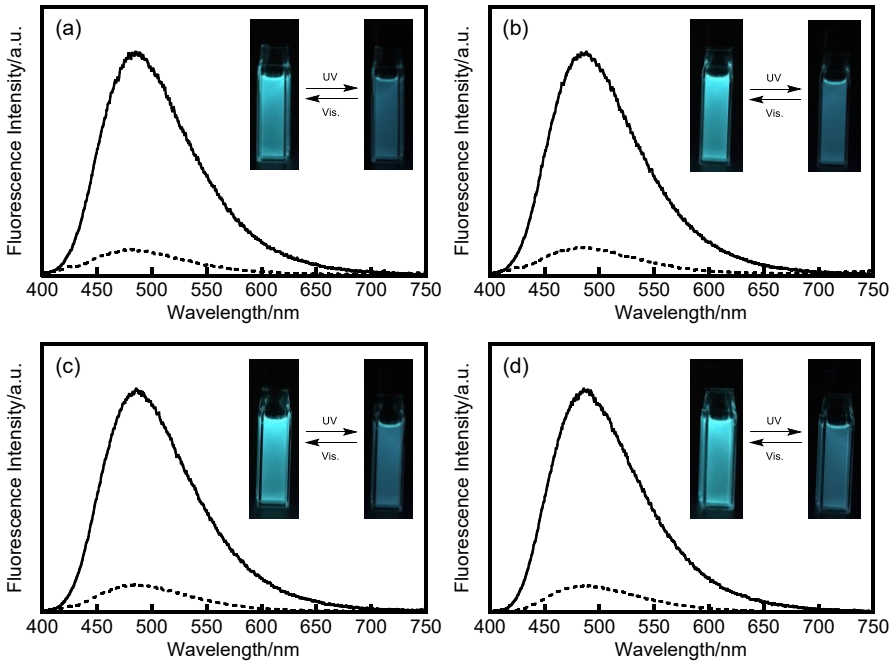

Figure 5-2. Fluorescence spectra of (a) **15a** (3.8×10^{-6} M), (b) **16a** (4.7×10^{-6} M), (c) **17a** (5.2×10^{-6} M), and (d) **18a** (4.8×10^{-6} M) in *n*-hexane: the open-ring isomer (solid line) and the photostationary solution upon irradiation with 365 nm light (dashed line). The fluorescence spectra were recorded upon excitation at 365 nm. Reprinted with permission from ref. 6. Copyright 2019 Elsevier.

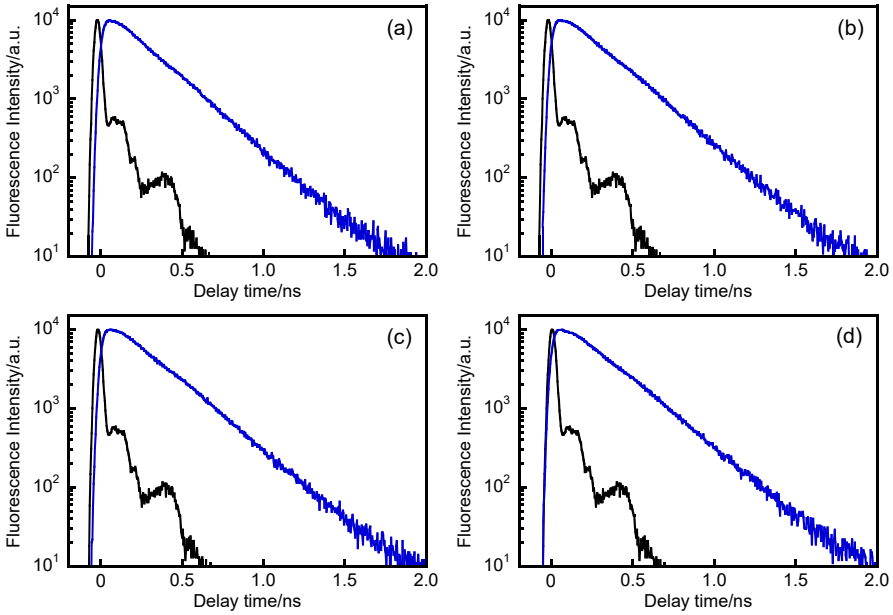

Figure 5-3. Fluorescence decay curves of (a) **15a**, (b) **16a**, (c) **17a**, and (d) **18a** in *n*-hexane monitored at 500 nm. Reprinted with permission from ref. 6. Copyright 2019 Elsevier.

to be 5-6% for **15a**-**18a**. Upon irradiation with 365 nm, the fluorescence intensities decreased. They returned to the initial ones upon irradiation with visible light.

Diarylethenes **15a**-**18a** showed fluorescence lifetimes with two components: τ_1 = ca. 200 ps and τ_2 = ca. 400 ps (Figure 5-3). This indicates that fluorescence consists of two components as well as **14a**.[5] No large difference in the fluorescence properties by alkyl chain length was observed in *n*-hexane.

5.3.2 Characterization of Crystals

Yellow block crystals of **15a**-**18a** were fabricated by recrystallization from *n*-hexane. Single crystal X-ray crystallographic analysis of **15a**-**18a** was performed. The results are summarized in Table 5-2. The crystal systems are monoclinic for **15a**, **17a**, and **18a** and orthorhombic for **16a**. The space groups of **15a**-**18a** are *C*2/*c*, *Pbcn*, *C*2/*c*, and $P2_1/c$, respectively. The crystals have a half molecule for **15a** and **16a**, and one molecule for **17a** and **18a** in the asymmetric unit. The diarylethenes exist in the anti-parallel conformation in all crystals. The distances between the reactive carbons of the molecules in the crystalline phase are 3.577, 3.636, 3.613, and 3.456 Å for **15a**-**18a**, respectively, which

Table 5-2. X-ray crystallographic data for **15a**-**18a**. Reprinted with permission from ref. 6. Copyright 2019 Elsevier.

	15a	**16a**	**17a**	**18a**
Formula	$C_{29}H_{22}F_6S_2$	$C_{31}H_{26}F_6S_2$	$C_{33}H_{30}F_6S_2$	$C_{35}H_{34}F_6S_2$
Formula weight	548.60	576.66	604.69	632.74
Temperature/K	200(2)	150(2)	180(2)	180(2)
Crystal system	Monoclinic	Orthorhombic	Monoclinic	Monoclinic
Space group	*C*2/*c*	*Pbcn*	*C*2/c	$P2_1$/c
Unit cell dimensions				
a/Å	25.525(10)	13.179(5)	31.7131(19)	11.4644(5)
b/Å	8.652(3)	8.339(3)	9.5637(3)	14.6927(6)
c/Å	11.627(5)	24.977(10)	22.8582(12)	18.4739(8)
α/deg	90	90	90	90
β/deg	94.966(5)	90	123.078(2)	95.908(2)
γ/deg	90	90	90	90
Volume/ Å^3	2558.0(17)	2745.2(18)	5809.2(5)	3095.3(2)
Z	4	4	8	4
Density/g cm^{-3}	1.424	1.395	1.383	1.358
Goodness-of-fit on F^2	1.062	1.076	1.092	1.107
$R1$ [$I > 2\sigma(I)$]	0.0404	0.0625	0.0429	0.0564
$wR2$ (all data)	0.1025	0.1796	0.1077	0.1329

are sufficiently short for the photocyclization reaction to take place in the crystalline phase.[11] However, all the crystals did not undergo any photocyclization reaction as well as **14a** in the crystalline phase although the reason is not clear yet.

5.3.3 Fluorescence Properties in Solid States

Crystals **15a**-**18a** exhibited slight red-shifted fluorescence (λ_{flu} = 493-506 nm) compared with those in *n*-hexane, as shown in Figure 5-4. Their fluorescence properties in the solid states are summarized in Table 5-3. The fluorescence properties of crystals **15a**-**18a** were significantly different from those of crystals **14a-α** and **14a-β**, which suggests that introduction of the alkyl chains to *p*-position of the phenyl rings affects the fluorescence properties in the crystalline phase. The molecules in crystals **14a-α** and **14a-β** have face-to-face and edge-to-face π-π intermolecular interactions between the phenyl rings, which result in the large red-shifted fluorescence in the crystalline phase.[4] On the other hand, the molecules in crystals **15a**-**18a** have no π-π intermolecular interaction and only van der Waals interaction (Figures 5-5, 5-6, 5-7, and 5-8). These results indicate that the alkyl chains prevent the formation of the strong π-π interaction between the phenyl rings to result in only slight red-shifted fluorescence.

The Φ_f values for crystals **15a**-**18a** were determined to be 0.12-0.20, which are higher

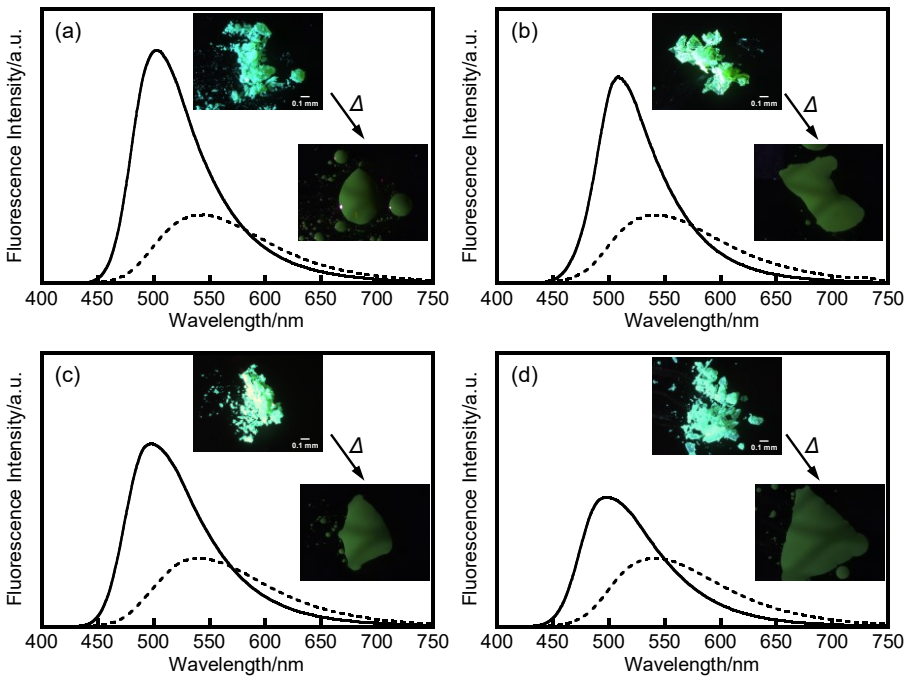

Figure 5-4. Fluorescence spectra of (a) **15a**, (b) **16a**, (c) **17a**, and (d) **18a** in the crystalline phase (solid line) and in the amorphous phase (dashed line). The fluorescence spectra were recorded upon excitation at 365 nm. Reprinted with permission from ref. 6. Copyright 2019 Elsevier.

than those in *n*-hexane. To reveal whether the enhanced emission is induced by aggregation or crystallization, the fluorescence properties of **15a**-**18a** in the amorphous solid state were examined. The amorphous solid was prepared by melting crystals followed by cooling to room temperature. The amorphous solids also did not undergo any photocyclization reaction as well as the crystals. The amorphous solid exhibited yellow-green fluorescence with λ_{flu} of ca. 540 nm, which was shifted toward a longer wavelength compared with those of the crystals. It may be due to the intermolecular π-π interaction.[4] The Φ_f values were determined to be ca. 6%, which decreased significantly in comparison with those in the crystalline phase and were almost the same as those in *n*-hexane. The results indicate that the strong fluorescence of crystals **15a**-**18a** is due to not AIE but CIE.

The dependence of the fluorescence properties on the alkyl chain length is described here. There is no difference in the fluorescence properties of **15a**-**18a** in the amorphous phase. On the other hand, the Φ_f values for crystals **15a**-**18a** decreased from 0.20 for **15a** having methyl group to 0.12 for **18a** having butyl group with increasing alkyl chain length. As shown in Table 5-2, **15a** has the most remarkable CIE characteristics among **15a**-**18a**.

Table 5-4. Fluorescence properties of **14a**-**18a** in the solid states. Reprinted with permission from ref. 6. Copyright 2019 Elsevier.

	State	λ_{flu}/nm	Φ_f[a]	τ_1/ns	τ_2/ns	τ_3/ns	τ_4/ns	τ_{ave}/ns[b]	k_f/ns^{-1}	k_{nr}/ns^{-1}
	Crystal **14a-α**[c]	601	0.52	1.9 (11%)	4.6 (89%)	-	-	4.3	0.12	0.11
14a	Crystal **14a-β**[c]	570	0.50	1.9 (14%)	4.5 (86%)	-	-	4.1	0.12	0.12
	Crystal **14a'**[d]	491	0.15	0.19 (53%)	0.40 (46%)	3.8 (1%)	-	0.32	0.46	2.63
15a	Crystal	505	0.20	0.48 (68.0%)[e]	0.65 (32.0%)[e]	-	-	0.53	0.36	1.51
16a	Crystal	506	0.16	0.39 (7.3%)[e]	0.51 (92.7%)[e]	-	-	0.50	0.31	1.68
17a	Crystal	499	0.15	0.27 (24.5%)[e]	0.40 (75.5%)[e]	-	-	0.37	0.42	2.30
18a	Crystal	493	0.12	0.31 (83.6%)[e]	0.40 (16.4%)[e]	-	-	0.32	0.36	2.72
14a[d]	Amorphous	596	0.20	0.30 (46.4%)	0.84 (25.1%)	3.1 (21.6%)	5.6 (6.9%)	1.41	0.14	0.57
15a	Amorphous	546	0.064	0.028 (42.0%)[f]	0.28 (27.4%)[f]	0.59 (28.5%)[f]	1.3 (2.1%)[f]	0.28	0.22	3.30
16a	Amorphous	545	0.069	0.027 (45.0%)[f]	0.25 (29.6%)[f]	0.62 (24.4%)[f]	2.8 (1.0%)[f]	0.27	0.26	3.51
17a	Amorphous	536	0.068	0.021 (50.6%)[f]	0.26 (19.9%)[f]	0.56 (27.8%)[f]	1.4 (1.7%)[f]	0.24	0.28	3.85
18a	Amorphous	543	0.066	0.13 (34.2%)[f]	0.46 (57.6%)[f]	0.99 (8.2%)[f]	-	0.39	0.17	2.39

a) Fluorescence quantum yield excited at 365 nm. b) Average fluorescence lifetime: $\tau_{ave} = \Sigma(\tau_i \times \%)$. c) ref. 4. d) ref. 5. e) Excited at 400 nm and monitored at 500 nm. f) Excited at 400 nm and monitored at 550 nm.

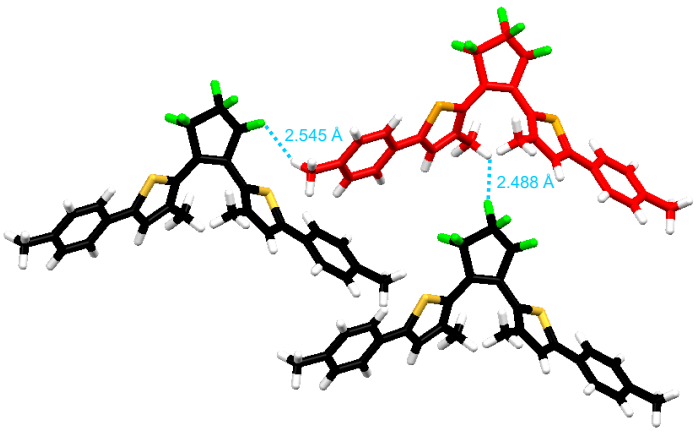

Figure 5-5. Perspective view of **15a** in the crystal. The distance between intermolecular neighboring atoms are denoted by dotted lines. Reprinted with permission from ref. 6. Copyright 2019 Elsevier.

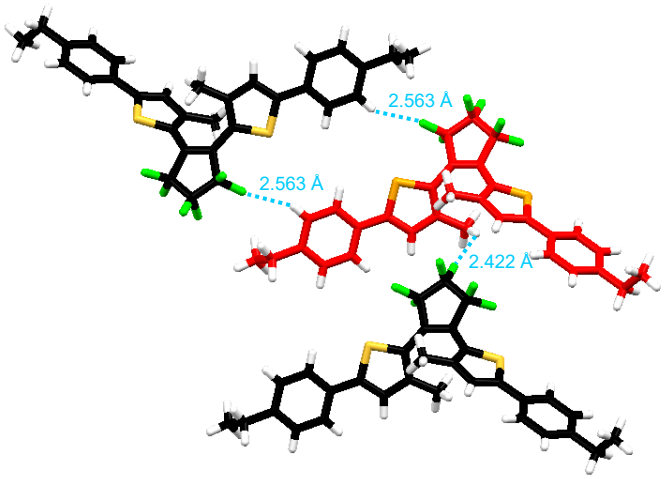

Figure 5-6. Perspective view of **16a** in the crystal. The distance between intermolecular neighboring atoms are denoted by dotted lines. Reprinted with permission from ref. 6. Copyright 2019 Elsevier.

To further investigate the fluorescence properties of **15a**-**18a** in the solid states, their fluorescence lifetimes (τ_i) were measured as shown in Figures 5-9 and 5-10. Amorphous solids of **15a**-**18a** exhibited fluorescence lifetimes with multi components. The faster component of <1 ns is attributed to the fluorescence of a single molecule. On the other hand, the slower component of 1-5 ns is ascribed to the condensed state.[5] The average fluorescence lifetimes (τ_{ave}) were calculated according to $\tau_{ave} = \Sigma(\tau_i \times \%)$. Moreover, the radiative rate constants (k_f) and the non-radiative rate constants (k_{nr}) were calculated from Φ_f and τ_{ave}; $k_f = \Phi_f/\tau_{ave}$ and $k_{nr} = (1 - \Phi_f)/\tau_{ave}$. The k_{nr} values for the crystals increased from 1.51 ns^{-1} to 2.72 ns^{-1} with increasing alkyl chain length. On the other hand, the k_f values for the crystals were hardly changed. These results indicate that the decrease in the

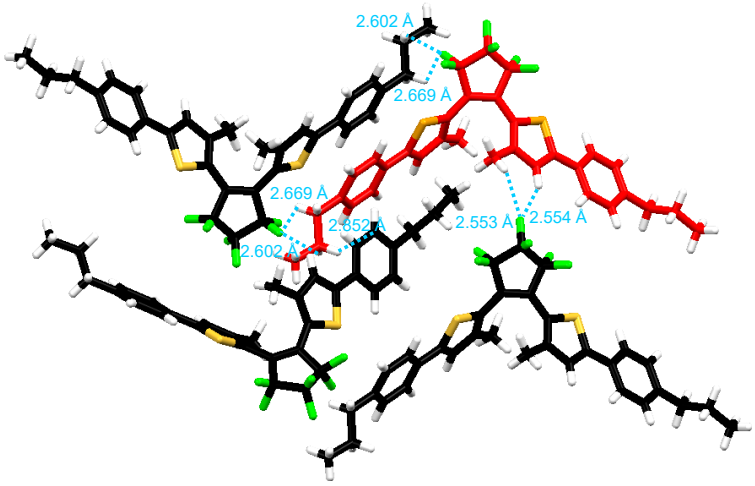

Figure 5-7. Perspective view of **17a** in the crystal. The distance between intermolecular neighboring atoms are denoted by dotted lines. Reprinted with permission from ref. 6. Copyright 2019 Elsevier.

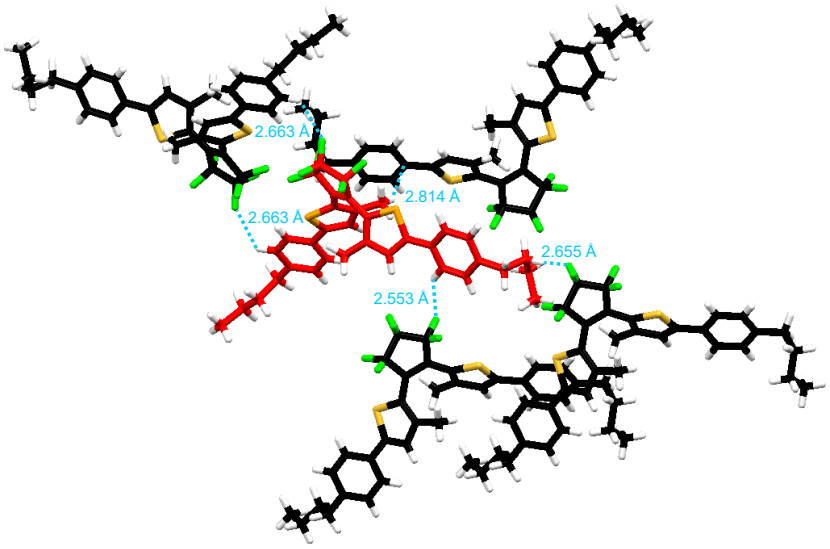

Figure 5-8. Perspective view of **18a** in the crystal. The distance between intermolecular neighboring atoms are denoted by dotted lines. Reprinted with permission from ref. 6. Copyright 2019 Elsevier.

Φ_f values for the crystals with increasing alkyl chain length is due to the increase in the rate constant of the non-radiative decay. As shown in Table 5-2, the density of the molecules in crystals decreased with increasing alkyl chain length. Therefore, the presence of the longer alkyl chain makes the molecules loosely packed in the crystalline phase, which results in the increase of the non-radiative decay, the decrease of the average fluorescence lifetime, and the low Φ_f value.

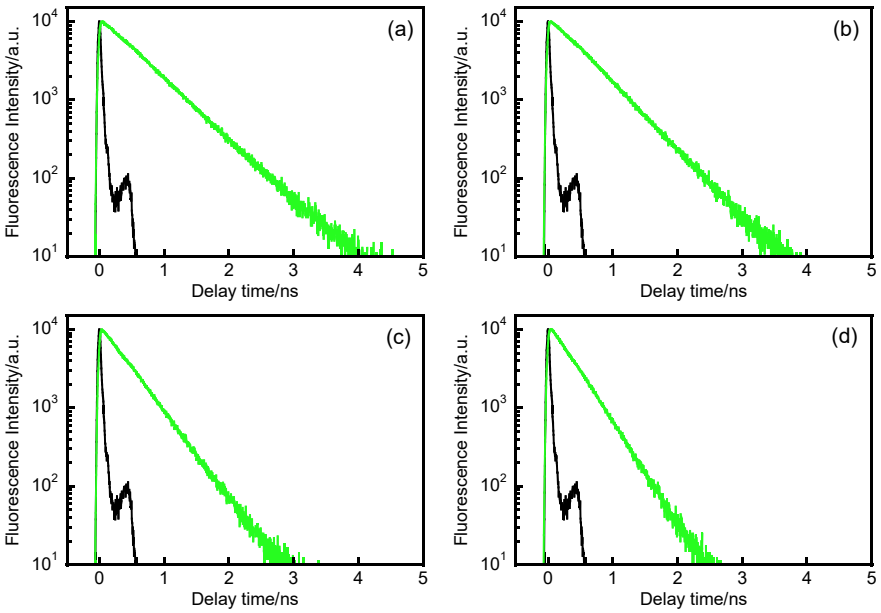

Figure 5-9. Fluorescence decay curves of (a) **15a**, (b) **16a**, (c) **17a**, and (d) **18a** in the crystalline phase monitored at 500 nm. Reprinted with permission from ref. 6. Copyright 2019 Elsevier.

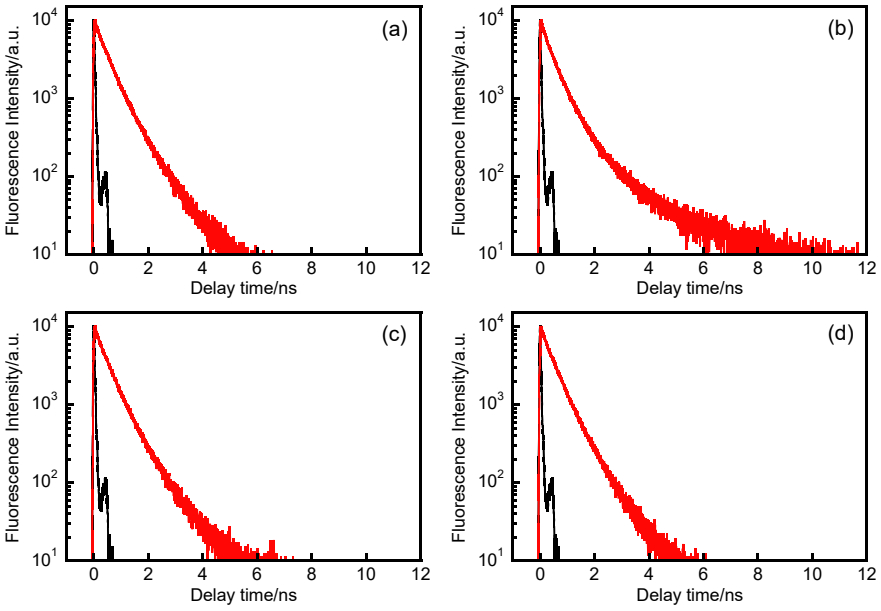

Figure 5-10. Fluorescence decay curves of (a) **15a**, (b) **16a**, (c) **17a**, and (d) **18a** in the amorphous phase monitored at 550 nm. Reprinted with permission from ref. 6. Copyright 2019 Elsevier.

5.3.4 Mechanical Scratching and Heating Induced Crystallization

Mechanical scratching and heating response for the fluorescence properties of **15a**, which has the most remarkable CIE characteristics among **15a**-**18a**, have been investigated in the solid states. In the course of study, it was found that the amorphous solid was crystallized with scratching followed by heating at 90 °C. The green fluorescence in the crystalline phase was observed around 500 nm, as shown in Figure 5-

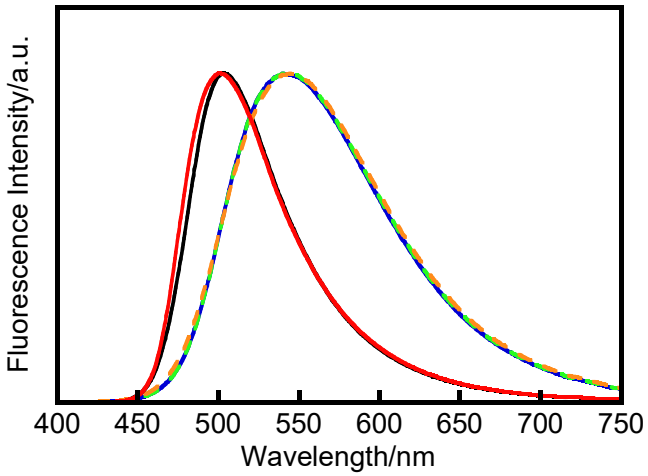

Figure 5-11. Normalized fluorescence spectra of **15a** in the crystalline phase (black), in the amorphous phase (blue), in the amorphous phase after only heating at 90 °C for 10 min (green), in the amorphous phase after only scratching (orange), and in the amorphous phase after scratching and heating at 90 °C for 10 min (red). Reprinted with permission from ref. 6. Copyright 2019 Elsevier.

11, although the amorphous solid after only scratching or heating exhibited the yellow-green fluorescence around 540 nm.

To investigate the mechanical scratching and heating process in detail, differential scanning calorimetry (DSC) measurement was performed. Figure 5-12 shows the DSC traces of **15a** in the crystalline phase, in the amorphous phase, and in the amorphous phase after scratching. When the crystal was heated at a rate of 10 °C min^{-1}, the crystal exhibited a large endothermic behavior due to the crystal melting at 135-150 °C. In addition, the amorphous solid exhibited only a glass transition temperature (T_g) at 33 °C (Figure 5-13). On the other hand, the amorphous solid after scratching exhibited not only T_g at 33 °C but also the crystallization with exothermic at 80-100 °C and the crystal melting with endothermic at 134-150 °C. Thus, the amorphous solid after scratching was crystallized in the region from 80 °C to 100 °C, although the amorphous solid without scratching was stable to heating.

Next, powder X-ray diffraction measurement was performed as shown in Figure 5-14. The diffraction pattern of crystal **15a** was consistent with that calculated from X-ray diffraction of a single crystal of **15a**. The amorphous solid showed only halo pattern, which did not change even after heating at 90 °C for 10 min. On the other hand, the amorphous solid after scratching showed small and sharp peaks due to the partial crystallization in addition to the halo pattern. Moreover, the diffraction pattern which is consistent with that calculated for a single crystal of **15a** was observed by heating the amorphous solid with scratching at 90 °C for 10 min. Thus, the small crystal nuclei were fabricated by scratching and the growth of the crystal nuclei was performed by heating.

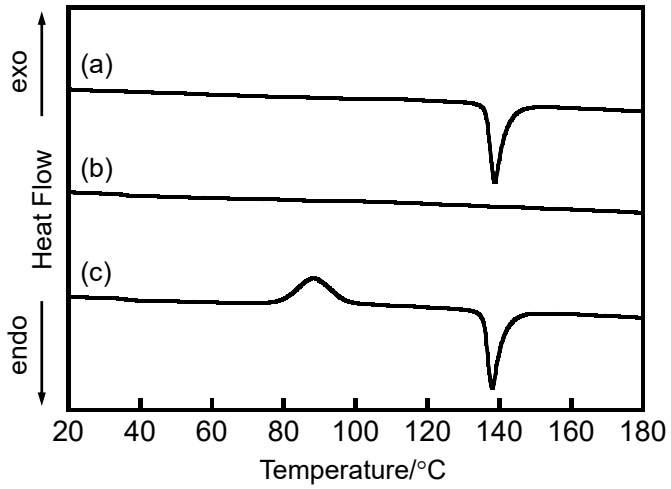

Figure 5-12. DSC traces of **15a** (a) in the crystalline phase, (b) in the amorphous phase, and (c) in the amorphous phase after scratching. All profiles were measured at a heating rate of 10 °C min^{-1}. Reprinted with permission from ref. 6. Copyright 2019 Elsevier.

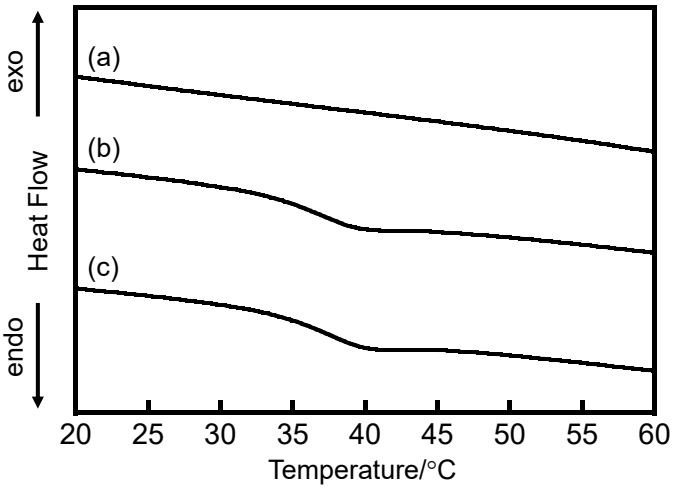

Figure 5-13. Enlarged view for DSC traces of **15a** (a) in the crystalline phase, (b) in the amorphous phase, and (c) in the amorphous phase with scratching at a heating rate of 10 °C min^{-1}. Reprinted with permission from ref. 6. Copyright 2019 Elsevier.

5.3.5 Reversible Fluorescence Recording

Fluorescence recording based on the mechanical scratching and heating induced crystallization from the amorphous solid have been tried. As shown in Figure 5-15a, powder crystals of **15a** were set on a glass substrate. After that, the crystals were heated at 150 °C to result in the amorphous solid at room temperature (Figure 5-15b). By partly scratching and heating at 90 °C for 3 min, green fluorescent letter of "D" was clearly written (Figure 5-15c). The letter was completely erased by heating at 150 °C for 30 s. After re-scratching and heating, new letter of "E" was written, and it could be erased

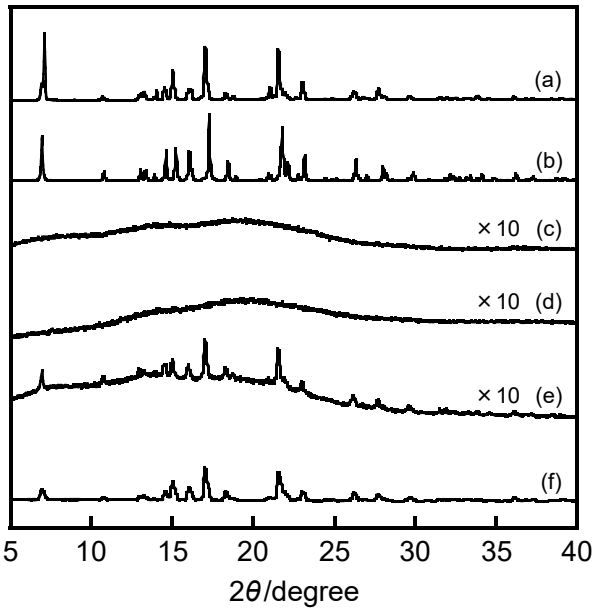

Figure 5-14. Powder X-ray diffraction patterns for **15a** at 27 °C: (a) powder crystals of **15a**, (c) amorphous state of **15a**, (d) amorphous state of **15a** after heating at 90 °C for 10 min followed by cooling, (e) amorphous state of **15a** after mechanical scratching, and (f) state of **15a** after heating of sample (e) at 90 °C for 10 min followed by cooling. (b) shows the pattern calculated from single crystal X-ray diffraction for **15a** at −93 °C. Reprinted with permission from ref. 6. Copyright 2019 Elsevier.

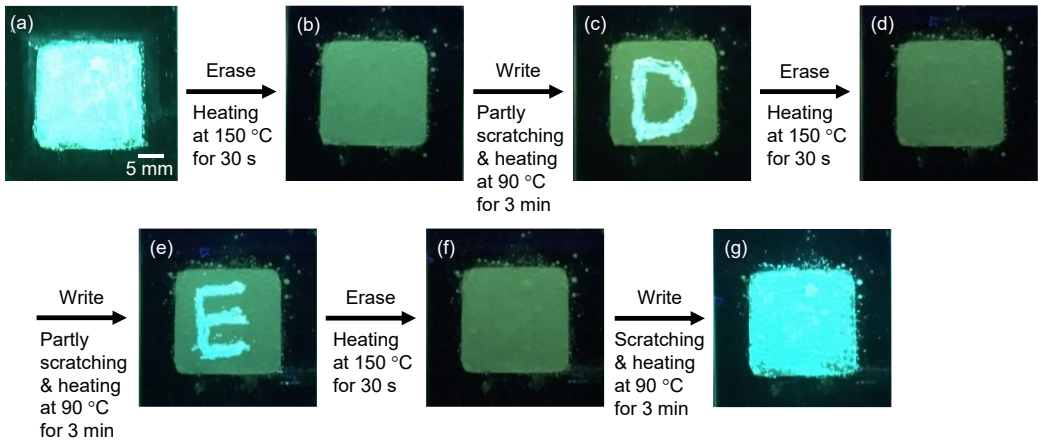

Figure 5-15. Reversible fluorescence recording of **15a** observed at room temperature upon excitation at 365 nm: (a) powder crystals of **15a**, (b,d,f) amorphous state of **15a** prepared by melting crystals at 150 °C for 30 s, (c) crystalline recording "D" prepared by partly mechanical scratching and heating at 90 °C for 3 min, (e) crystalline recording "E" prepared by partly mechanical scratching and heating at 90 °C for 3 min, (g) microcrystals of **15a** prepared by mechanical scratching on the whole area and heating at 90 °C for 3 min. Reprinted with permission from ref. 6. Copyright 2019 Elsevier.

again (Figure 5-15e and f). In addition, the fluorescence recording returned to its initial state by scratching on whole area and heating. The recorded crystalline part was clearly observed for several hours. As a result, the reversible fluorescence recording based on CIE characteristics and mechanical scratching and heating induced crystallization was

successfully demonstrated. Successful fluorescence recording is due to high contrast of fluorescence intensities between the crystalline phase and the amorphous phase, and low fluorescence quantum yield in amorphous solid at the background. Although there are many reports of the crystallization in response to heating or mechanical scratching,[12] crystallization induced by both stimuli is rare. The CIE molecules with mechanical scratching and heating induced crystallization ability may be useful for potential applications, such as in sensors and security materials.

5.4 Summary

Diarylethenes having various alkyl chains (**15a**-**18a**) were synthesized and their photochromic and fluorescence properties were investigated in *n*-hexane and in the solid states. Diarylethenes **15a**-**18a** underwent reversible photochromic reactions in *n*-hexane upon alternating irradiation with UV and visible light and exhibited weak fluorescence (Φ_f = ca. 0.05) in their open-ring forms in *n*-hexane. However, **15a**-**18a** in the solid states did not undergo the photocyclization reaction as well as **14a**. It was revealed that **15a**-**18a** have CIE characteristics to result in strong fluorescence in the crystalline phase compared in *n*-hexane and in the amorphous phase. Crystal **15a** had the largest Φ_f value among crystals **15a**-**18a**. In addition, it was found that amorphous solid of **15a** was crystallized with mechanical scratching followed by heating. The crystallization is ascribed to the growth of microcrystals produced by scratching. Finally, the reversible fluorescence recording based on the mechanical scratching and heating induced crystallization was successfully demonstrated.

5.5 References

[1] Y. Hong, J. W. Lam, B. Z. Tang, *Chem. Soc. Rev.* **2011**, *40*, 5361-5388.

[2] a) Y. Dong, J. W. Lam, A. Qin, J. Sun, J. Liu, Z. Li, J. Sun, H. H. Sung, I. D. Williams, H. S. Kwok, B. Z. Tang, *Chem. Commun.* **2007**, 3255-3257; b) Y. Dong, J. W. Y. Lam, Z. Li, A. Qin, H. Tong, Y. Dong, X. Feng, B. Z. Tang, *J. Inorg. Organomet. Polym. Mater.* **2005**, *15*, 287-291.

[3] J. Tong, Y. J. Wang, Z. Wang, J. Z. Sun, B. Z. Tang, *J. Phys. Chem. C* **2015**, *119*, 21875-21881.

[4] D. Kitagawa, T. Nakahama, K. Mutoh, Y. Kobayashi, J. Abe, H. Sotome, S. Ito, H. Miyasaka, S. Kobatake, *Dyes Pigm.* **2017**, *139*, 233-238.

[5] T. Nakahama, D. Kitagawa, H. Sotome, S. Ito, H. Miyasaka, S. Kobatake, *Bull. Chem. Soc. Jpn.* **2018**, *91*, 153-157.

[6] T. Nakahama, D. Kitagawa, H. Sotome, S. Ito, H. Miyasaka, S. Kobatake, *Dyes*

Pigm. **2019**, *160*, 450-456.
[7] K. Uchida, T. Matsuoka, S. Kobatake, T. Yamaguchi, M. Irie, *Tetrahedron* **2001**, *57*, 4559-4565.
[8] Y. Yokoyama, Y. Kurita, *J. Synth. Org. Chem. Jpn.* **1991**, *49*, 364-372.
[9] Y. Nagasawa, T. Itoh, M. Yasuda, Y. Ishibashi, S. Ito, H. Miyasaka, *J. Phys. Chem. B* **2008**, *112*, 15758-15765.
[10] S. Tanaka, D. Tanaka, G. Tatsuta, K. Murakami, S. Tamba, A. Sugie, A. Mori, *Chem. Eur. J.* **2012**, *19*, 1658-1665.
[11] S. Kobatake, K. Uchida, E. Tsuchida, M. Irie, *Chem. Commun.* **2002**, 2804-2805.
[12] Z. Chi, X. Zhang, B. Xu, X. Zhou, C. Ma, Y. Zhang, S. Liu, J. Xu, *Chem. Soc. Rev.* **2012**, *41*, 3878-3896.

Chapter 6

Fluorescence On/Off Switching in Nanoparticles Consisting of Two Types of Diarylethenes

6.1 Introduction

Diarylethene derivatives linked to fluorophore exhibit reversible fluorescence on/off switching accompanying the photochromic reactions.[1] In the case of dyad systems consisting of a diarylethene derivative and a fluorophore, a low on/off contrast is often observed in a solution because the system remains still at a few of diarylethene open-ring forms at the photostationary state (PSS). In addition, high photocyclization conversion upon UV irradiation is required to quench the fluorescence completely because the fluorescence intensity decreases in proportion with the photocyclization conversion of diarylethene.[2] The fluorescence switchable diarylethene systems having the efficient fluorescence on/off switching properties, such as high fluorescence on/off contrast and rapid switching speed, are desirable for applications in sensing materials,[3] bioimaging materials for superresolution microscopy,[4] and single molecule memory materials.[5]

Recently, Fukaminato, Métivier, and co-workers achieved extremely rapid and high fluorescence on/off contrast with full reversibility and high fatigue resistance using nanoparticles consisting of a diarylethene linked to a benzothiadiazole derivative.[6] In the nanoparticles, a large number of the excited state fluorophores are quenched by a single diarylethene closed-ring form because of the close intermolecular distance in high density. As a result, the fluorescence intensity dramatically decreased even in low photocyclization conversion of diarylethenes, which resulted in highly efficient fluorescence on/off switching properties. Although highly efficient fluorescence on/ off switchable systems consisting of diarylethenes and fluorophores, such as dyad,[4d] polymers,[7] silica nanoparticles,[8] and organic nanoparticles,[9] have been reported, a complicated multistep synthesis is required to construct the fluorescence switchable systems. If a more convenient system with highly efficient fluorescence on/off switching properties can be constructed, it will lead to the development of the fluorescence on/off switchable system and a great contribution to the applications as described above.

Here, nanoparticles consisting of two types of diarylethenes, 1,2-bis(3-methyl-5-phenyl-2-thienyl)perfluorocyclopentene (**14a**), and 1,2-bis(2-methyl-5-phenyl-3-thienyl)perfluorocyclopentene (**26a**), have been focused as shown in Scheme 6-1. With respect to the orientation of the two five-membered heterocyclic rings, diarylethenes can be categorized into two groups, normal type and inverse type, which are 1,2-bis(3-

thienyl)ethene and 1,2-bis(2-thienyl)ethene, respectively. Inverse type diarylethene **14a** undergoes reversible photochromic reactions in *n*-hexane and exhibits blue fluorescence in the open-ring form with a fluorescence quantum yield (Φ_f) of 0.017.[10] The closed-ring form (**14b**) exhibits no fluorescence. On the other hand, crystals consisting of diarylethene **14a** exhibit strong fluorescence as shown in Chapter 3. Crystal **14a** has two polymorphic forms (crystals **14a-α** and **14a-β**), which exhibit orange and yellow fluorescence (Φ_f = 0.52 and 0.50), respectively.[11] In addition, the open-ring form of crystal which is produced by the photochemical ring opening reaction in the crystal of **14b** exhibits green fluorescence (Φ_f = 0.15) as shown in Chapter 4.[12] However, all crystals do not undergo photocyclization reaction. Normal type diarylethene **26a** undergoes reversible photochromic reactions in solution and the crystalline phase.[13] Therefore, diarylethenes **14a** and **26a** are expected to behave as a fluorophore and a photochromic compound in the nanoparticles, respectively. Because **14a** and **26a** have similar geometrical structures, it is expected that the fabricated nanoparticles are evenly space-distributed spheres consisting of **14a** and **26a** at an arbitrary ratio, even if there is no covalent bonding between them. In addition, it is easy to prepare their diarylethenes from commercially available reagents in two or three steps.[10, 13] Therefore, the fluorescence switchable system in this work is much more convenient as compared with those proposed previously.

In this work, first, the photochromic and fluorescence properties of single-component nanoparticles consisting of **14a**, **14b**, **26a**, or **26b** (**NP$_{14a}$**, **NP$_{14b}$**, **NP$_{26a}$**, or **NP$_{26b}$**) were investigated to reveal the optical properties of **14** and **26** in the nanoparticles. Next, double-component nanoparticles consisting of **14a**, **14b**, **26a**, and **26b** (**NP$_{14a/26a}$**, **NP$_{14b/26a}$**, **NP$_{14a/26b}$**, and **NP$_{14b/26b}$**) were fabricated to investigate the fluorescence on/off switching properties. The dependence of the fluorescence on/off switching properties of the nanoparticles on Förster distance and the molar fraction was revealed.[14]

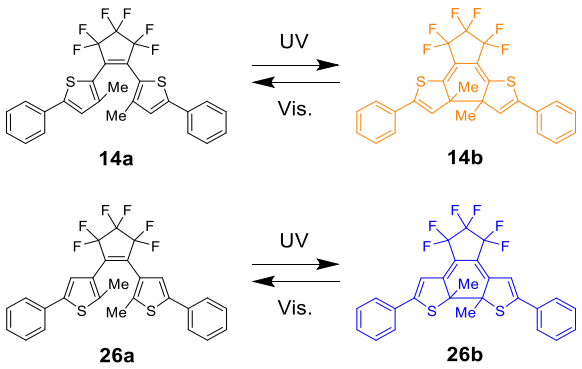

Scheme 6-1. Molecular structures of diarylethenes used in this chapter. Reprinted with permission from ref 14. Copyright 2018 American Chemical Society.

6.2 Experimental Section

6.2.1 General

^{1}H NMR spectra were recorded on a Bruker AV- 300N spectrometer at 300 MHz. Deuterated chloroform ($CDCl_3$) was used as the solvent, and tetramethylsilane as an internal standard. High-performance liquid chromatography (HPLC) was performed using a Hitachi L-7150/L-2400 HPLC system equipped with a Kanto Chemical Mightysil Si 60 column. PXRD profiles were recorded on a Rigaku MiniFlex 600 diffractometer using Cu K_α radiation (λ = 1.54184 Å). The nanoparticle size was determined by the DLS (Sysmex Zetasizer Nano ZS) analysis. DSC was performed using a Hitachi DSC7000X instrument. Absorption spectra were measured with a JASCO V-560 absorption spectrophotometer. Photoirradiation in solution was conducted using a 200 W mercury-xenon lamp (MORITEX MUV-202) as a light source. Monochromatic light was obtained by passing the light through a monochromator (Jobin Yvon H10 UV) and glass filters. Fluorescence spectra were measured with a Hitachi F-2700 fluorescence spectrophotometer. Fluorescence quantum yields were determined with a JASCO FP-8300 fluorescence spectrophotometer equipped with a JASCO ILF-835 integrating sphere. All samples in solutions were deaerated by bubbling with argon gas for 5 min before the measurements.

6.2.2 Fluorescence Lifetime

Fluorescence lifetimes were measured using a time-correlated single-photon-counting (TCSPC) system. The experimental setup for the TCSPC has been described previously.[15] Briefly, a Ti:sapphire oscillator (Spectra-Physics, Tsunami) was utilized as a pulsed light source. The operation wavelength, pulse width, and repetition rate were set to 800 nm, 70 fs, and 80 MHz, respectively. The fundamentals of the laser were converted to the second harmonics (400 nm) using a type I beta barium borate crystal and used to excite the samples. The repetition rate was reduced down to 8 MHz by using an electro-optic modulator (Conoptics, model 350), and the excitation intensity to the samples was typically 2.2 μW at 8 MHz. The detection of fluorescence at the magic-angle configuration was attained by utilizing a film polarizer and a Babinet-Soleil compensator. The fluorescence was detected using a photomultiplier tube (Hamamatsu Photonics, R3809U-50) equipped with a preamplifier (Hamamatsu Photonics, C5594) and a TCSPC module (PicoQuant, PicoHarp 300). For wavelength selection, a monochromator (Princeton Instruments, Acton 2150) was placed in front of the photomultiplier tube. The sample solutions were set in 1 cm path length of the quartz cells. The typical response

time of the system was determined to be 40 ps full width at half maximum by detecting the scattered photons from a colloidal solution.

6.2.3 Materials

1,2-Bis(3-methyl-5-phenyl-2-thienyl)perfluorocyclopentene (**14a**)[10] and 1,2-bis(2-methyl-5-phenyl-3-thienyl)perfluorocyclopentene (**26a**)[13] were prepared by the method described previously. The closed-ring isomers of **14a** and **26a** (**14b** and **26b**) were prepared by irradiation with UV light of the *n*-hexane solution and were isolated by HPLC equipped with a silica-gel column using *n*-hexane as the eluant.

6.2.4 Preparation of Nanoparticles

Nanoparticles were prepared by the reprecipitation method.[16] $\mathbf{NP_{14a}}$ or $\mathbf{NP_{14b}}$ was prepared as follows: THF solution of **14a** or **14b** was prepared by dissolving **14a** or **14b** (1.9 mg) into THF (2.0 mL). The THF solution of **14a** or **14b** (300 μL) was quickly added to 10 mL of distilled water, followed by vigorous stirring for 30 min. The fabricated solution of $\mathbf{NP_{14a}}$ or $\mathbf{NP_{14b}}$ was used for the experiments just as it is. $\mathbf{NP_{26a}}$ or $\mathbf{NP_{26b}}$ was prepared as follows: the THF solution of **26a** or **26b** was prepared by dissolving **26a** or **26b** (3.8 mg) into THF (2.0 mL). The THF solution of **26a** or **26b** (10 μL) was quickly added to 4.0 mL of distilled water, followed by vigorous stirring for 30 min. The fabricated solution of $\mathbf{NP_{26a}}$ or $\mathbf{NP_{26b}}$ was used for the experiments just as it is. Double-component nanoparticles ($\mathbf{NP_{14a/26a}}$, $\mathbf{NP_{14b/26a}}$, $\mathbf{NP_{14a/26b}}$, and $\mathbf{NP_{14b/26b}}$) were prepared as follows: the THF solution of **14a** or **14b** was prepared by dissolving **14a** or **14b** (3.8 mg) into THF (2.0 mL). The THF solution of **26a** or **26b** was prepared by dissolving **26a** or **26b** (3.8 mg) into THF (2.0, 10, and 20 mL). The THF solutions containing **14** and **26** at an arbitrary ratio ([**14**]/[**26**] = 1/1, 1/0.2 and 1/0.1) were prepared by mixing each THF solution (each 1.0 mL) containing **14** and **26**. The THF solution of **14** and **26** (300 μL) was quickly added to 10 mL of distilled water followed by vigorous stirring for 30 min. The fabricated solution of $\mathbf{NP_{14a/26a}}$, $\mathbf{NP_{14b/26a}}$, $\mathbf{NP_{14a/26b}}$, or $\mathbf{NP_{14b/26b}}$ was used for the experiments just as it is.

6.3 Results and Discussion

6.3.1 Photochromic and Fluorescence Properties of Nanoparticles Consisting of Inverse Type Diarylethene

Single-component nanoparticles of **14a** and **14b** were successfully fabricated by the reprecipitation method as described in the Experimental Section. Figure 6-1 shows the absorption and fluorescence spectra of $\mathbf{NP_{14a}}$ and $\mathbf{NP_{14b}}$. The optical properties of $\mathbf{NP_{14a}}$

and **NP$_{14b}$** are summarized in Table 6-1, together with those of diarylethene **14** in *n*-hexane and in the crystalline state. The absorption maximum wavelength (λ_{abs}) for **NP$_{14a}$** was observed at 387 nm, which is almost the same as that of **14a** in *n*-hexane. On the other hand, the fluorescence maximum wavelength (λ_{flu}) for **NP$_{14a}$** was observed at 596 nm, which was shifted toward longer wavelength than that of **14a** in *n*-hexane (λ_{flu} = 480 nm). In addition, the fluorescence quantum yield (Φ_f) of **NP$_{14a}$** was determined to be 0.20. This value was much larger than that of **14a** in *n*-hexane (Φ_f = 0.017).[10] Moreover, **NP$_{14a}$** did not undergo photocyclization reaction from the open-ring form to the closed-ring form upon irradiation with UV light. It was revealed that **14a** in the nanoparticle behaves as a fluorophore.

On the other hand, the optical properties of **NP$_{14b}$** were significantly different from those of **NP$_{14a}$**. **NP$_{14b}$** has the absorption band around 450 nm, as shown in Figure 6-1b. Upon irradiation with visible light (>500 nm), **14b** in **NP$_{14b}$** exhibited the ring-opening reaction from the closed-ring isomer to the open-ring isomer. The absorption band at 450 nm disappeared, and a sharp band around 400 nm appeared. Here, the open-ring isomer photogenerated from the closed-ring isomer is called **14a'**, and the nanoparticle consisting of **14a'** is called **NP$_{14a'}$**. **NP$_{14a'}$** did not undergo photocyclization reaction upon irradiation

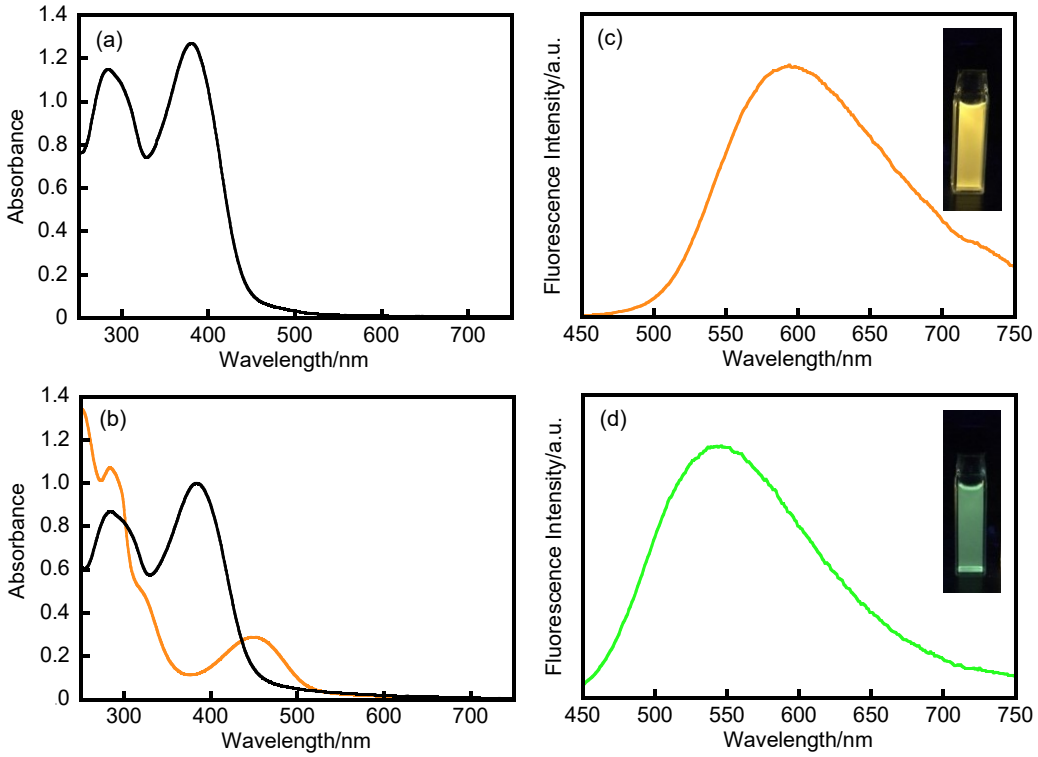

Figure 6-1. Absorption spectra of (a) **NP$_{14a}$** (d = 79 ± 18 nm) and (b) **NP$_{14b}$** (orange solid line) and **NP$_{14a'}$** (black solid line) (d = 148 ± 52 nm), and fluorescence spectra of (c) **NP$_{14a}$** and (d) **NP$_{14a'}$** in water/tetrahydrofuran (THF) (97:3). The fluorescence spectra were recorded upon excitation at 365 nm. Reprinted with permission from ref. 14. Copyright 2018 American Chemical Society.

Table 6-1. Optical properties of diarylethene **14** in various states. Reprinted with permission from ref. 14. Copyright 2018 American Chemical Society.

	λ_{abs}/nm	λ_{flu}/nm	Φ_f[a]	τ_1/ns	τ_2/ns	τ_3/ns	τ_4/ns
NP$_{14a}$	387	595	0.20	0.014 (79%, r[b])[c]	0.55 (6%)[c]	2.4 (10%)[c]	5.5 (5%)[c]
NP$_{14b}$	450	—	—	—	—	—	—
NP$_{14a'}$	389	544	0.05	0.078 (25%)[d]	0.33 (50%)[d]	0.68 (24%)[d]	4.4 (1%)[d]
14a in *n*-hexane	370[e]	480[f]	0.017[e]	0.14 (93%)	0.42 (7%)[f]	—	—
14b in *n*-hexane	438[e]	—	—	—	—	—	—
crystal **14a-α**[g]	394, 509	601	0.52	1.9 (11%)	4.6 (89%)	—	—
crystal **14a-β**[g]	398, 505	570	0.50	1.9 (14%)	4.5 (86%)	—	—
crystal **14b**[f]	445	—	—	—	—	—	—
crystal **14a'**[f]	377	491	0.15	0.19 (53%)	0.40 (46%)	3.8 (1%)	—
amorphous **14a**[f]	407	589	0.17	0.30 (46%)	0.84 (25%)	3.1 (22%)	5.6 (7%)

[a]Excited at 365 nm. [b]Rise component. [c]Excited at 400 nm and monitored at 600 nm. [d]Excited at 400 nm and monitored at 540 nm. [e]ref. 10. [f]ref. 11. [g]ref. 12.

with UV light, as well as **NP$_{14a}$**. At the present work, the reason why **14a** does not undergo photocyclization reaction in the nanoparticle state is not clear yet. Although **NP$_{14b}$** exhibited no fluorescence upon excitation at 365 nm, **NP$_{14a'}$** exhibited green fluorescence, as shown in Figure 6-1d. λ_{flu} was observed at 544 nm with Φ_f of 0.05. The fluorescence properties of **NP$_{14a'}$** are clearly different from those of **NP$_{14a}$**.

As mentioned above, crystal **14a** has two crystalline polymorphic forms (crystals **14a-α** and **14a-β**). Crystals **14a-α** and **14a-β** exhibit the red-shifted strong fluorescence (λ_{flu} = 601 nm, Φ_f = 0.52 for crystal **14a-α** and λ_{flu} = 570 nm, Φ_f = 0.50 for crystal **14a-β**) in comparison with that of **14a** in *n*-hexane (λ_{flu} = 480 nm, Φ_f = 0.017). In addition, crystal **14a'** exhibited green fluorescence with λ_{flu} = 491 nm and Φ_f = 0.15. However, the fluorescence properties of these crystals are slightly different from those of the nanoparticles. This suggests that the nanoparticles are not in the crystalline state.

To reveal the state of the nanoparticles, powder X-ray diffraction (PXRD) measurement was performed. As shown in Figure 6-2, PXRD on **NP$_{14a}$** and **NP$_{14a'}$** showed only a hollow pattern, which indicates that both **NP$_{14a}$** and **NP$_{14a'}$** are in the amorphous state. In the excitation spectrum, **NP$_{14a}$** has a small shoulder band in the region of 450-550 nm, whereas such a shoulder band was not observed in **NP$_{14a'}$**, as shown in Figure 6-3. Crystals **14a-α** and **14a-β** also have the large band in the region of 450-550 nm in the reflection spectra, which is attributed to the aggregates with the intermolecular

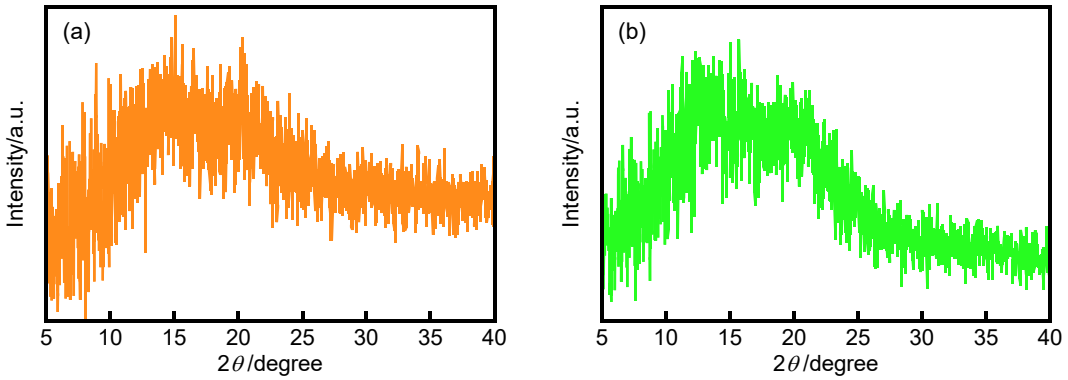

Figure 6-2. Powder X-ray diffraction patterns of (a) **NP$_{14a}$** and (b) **NP$_{14a'}$**. Reprinted with permission from ref 14. Copyright 2018 American Chemical Society.

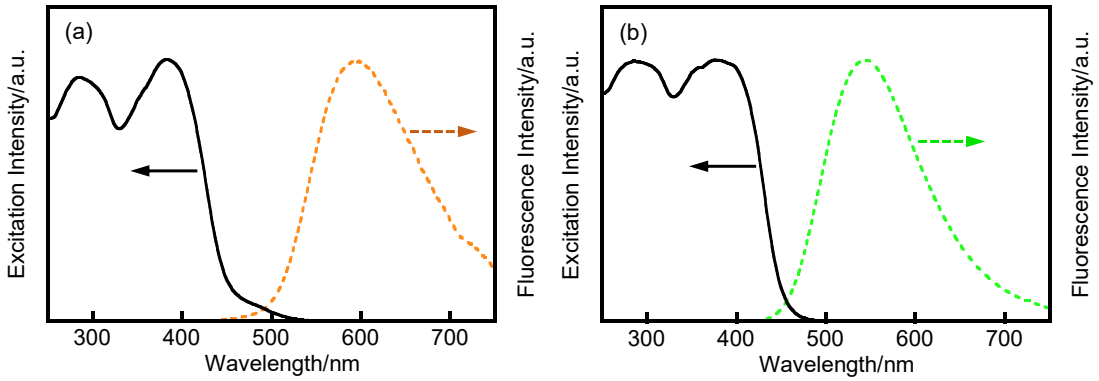

Figure 6-3. Fluorescence spectra (dashed line) and excitation spectra (solid line) of (a) **NP$_{14a}$** (d = 79 ± 18 nm) and (b) **NP$_{14a'}$** (d = 148 ± 52 nm) in water/THF (= 97/3). The fluorescence spectra were recorded under excitation at 365 nm. The excitation spectra were observed at 600 and 550 nm for **NP$_{14a}$** and **NP$_{14a'}$**, respectively. Reprinted with permission from ref 14. Copyright 2018 American Chemical Society.

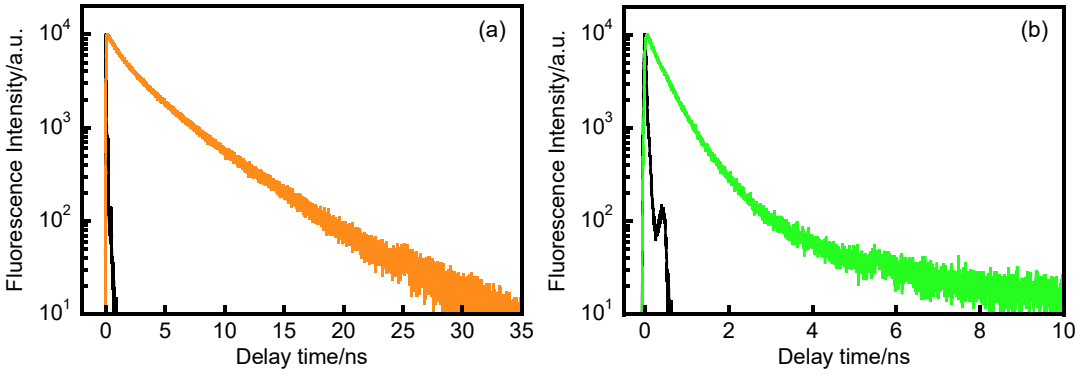

Figure 6-4. Fluorescence decay curve of (a) **NP$_{14a}$** (d = 82 ± 15 nm) monitored at 600 nm (χ^2 = 1.24) and (b) **NP$_{14a'}$** (d = 157 ± 32 nm) monitored at 540 nm (χ^2 = 1.12) in water/THF (= 97/3). Reprinted with permission from ref 14. Copyright 2018 American Chemical Society.

interaction of **14a**. Therefore, **NP$_{14a}$** is in the amorphous state containing a small part of the aggregates, whereas **NP$_{14a'}$** is no aggregate in the amorphous state.

Next, the fluorescence lifetimes of **NP$_{14a}$** and **NP$_{14a'}$** were compared. Figure 6-4

shows the fluorescence decay curves of **NP$_{14a}$** and **NP$_{14a'}$**. Both **NP$_{14a}$** and **NP$_{14a'}$** exhibited fluorescence decay with multiple components. The faster component of <1 ns is attributed to the fluorescence of a single molecule. On the other hand, the slower component of 1-5 ns is ascribed to the condensed state. **NP$_{14a}$** had a rise component of 0.014 ns. The rise component may be because of an energy transfer from the excited energy in the single molecule to the condensed aggregate state. Thus, the nanoparticles consisting of diarylethene **14a** exhibited orange or green fluorescence depending on the fabrication conditions of the nanoparticles.

6.3.2 Photochromism of Nanoparticles Consisting of Normal Type Diarylethene

Figure 6-5 shows the absorption spectral changes of nanoparticles consisting of **26a** (**NP$_{26a}$**) and **26b** (**NP$_{26b}$**) upon photoirradiation. Upon irradiation with 313 nm light, the

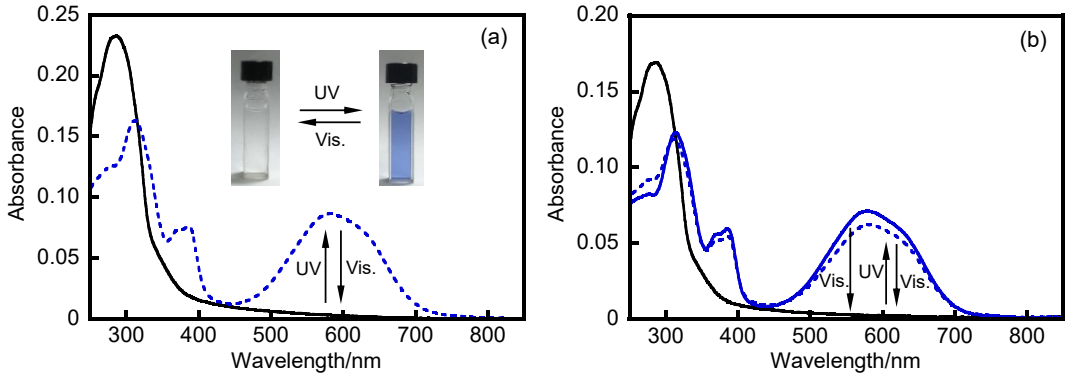

Figure 6-5. Absorption spectral change of (a) **NP$_{26a}$** (d = 146 ± 37 nm) and (b) **NP$_{26b}$** (d = 131 ± 27 nm) in water/THF: the open-ring form (black solid line), the closed-ring form (blue solid line), and the PSS upon irradiation with 313 nm light (blue dashed line). Reprinted with permission from ref 14. Copyright 2018 American Chemical Society.

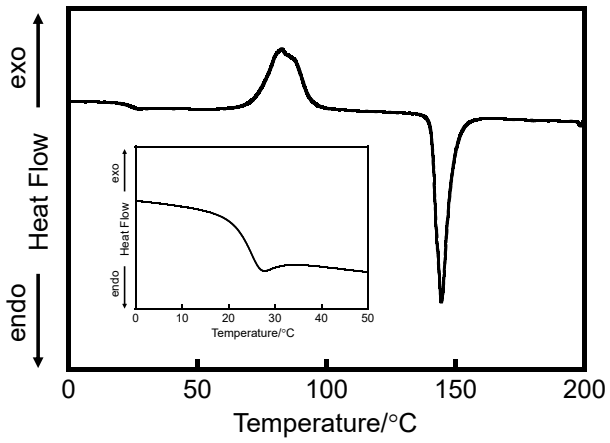

Figure 6-6. Differential scanning calorimetry (DSC) trace of **26a** in the amorphous solid. The rate of heating was 10 °C min^{-1}. Reprinted with permission from ref 14. Copyright 2018 American Chemical Society.

colorless dispersion solution of **NP$_{26a}$** turned blue, and the new absorption band appeared around 579 nm. The spectral change is ascribed to the photocyclization reaction. Upon irradiation with visible light, the solution color and absorption spectrum returned to the initial state. The photocyclization conversion upon irradiation with 313 nm light was determined to be 87%. The value is unexpectedly high although parallel and antiparallel conformers may coexist in **NP$_{26a}$**. Diarylethene nanoparticles fabricated by the reprecipitation method are usually amorphous solids; in some cases, it may crystallize upon irradiation with microwave.[6, 17] To reveal the reason as to why the photocyclization conversion upon irradiation with 313 nm is high, the glass transition temperature of the amorphous solid materials was examined using differential scanning calorimetry (DSC) (Figure 6-6). DSC trace of **26a** in the amorphous solid, which was prepared by melting crystal **26a** followed by cooling to room temperature, exhibited a glass transition temperature at 21 °C, which is lower than room temperature (25 °C). Thus, the photocyclization conversion in the nanoparticles is high because the two conformers can interconvert with each other even in the nanoparticles. In addition, **NP$_{26b}$** exhibited a similar photochromic behavior upon alternating the irradiation with UV and visible light. There was no difference in the spectral changes between **NP$_{26a}$** and **NP$_{26b}$**, which is because the antiparallel conformer can convert to parallel conformer in the nanoparticles, as mentioned above. It was revealed that diarylethene **26** undergoes the reversible photochromic reactions in the nanoparticle upon alternating irradiation with UV and visible light, even if the nanoparticle is fabricated from either of **26a** and **26b**.

6.3.3 Fluorescence On/Off Switching of Nanoparticles Consisting of Inverse Type and Normal Type Diarylethenes

The fluorescence on/off switching accompanying the photochromic reactions of the double-component nanoparticles consisting of **14a**, **14b**, **26a**, and **26b** (**NP$_{14a/26a}$**, **NP$_{14b/26a}$**, **NP$_{14a/26b}$**, and **NP$_{14b/26b}$**) was investigated. The average diameters were determined to be 100-170 nm and the number of the molecules (sum of **14** and **26**) per single nanoparticle to be 8.5×10^5 to 4.2×10^6 was estimated by assuming that the density of the nanoparticles is the same as those of **14** and **26** in the crystalline phase (≈1.4 g cm^{-3}). Figure 6-7a,b shows the absorption spectra of **NP$_{14a/26a}$** and **NP$_{14b/26a}$**, respectively, at the same molar fraction of **14a** and **26a**. Two bands were observed around 385 and 285 nm in the initial absorption spectrum of **NP$_{14a/26a}$**. The band around 385 nm is mainly attributed to **14a**, and the band around 285 nm corresponds to those of **14a** and **26a**. Upon irradiation with 313 nm light, the absorption band of **26b** appeared around 580 nm. On the other hand, **14a** did not undergo photocyclization reaction. The absorption band of

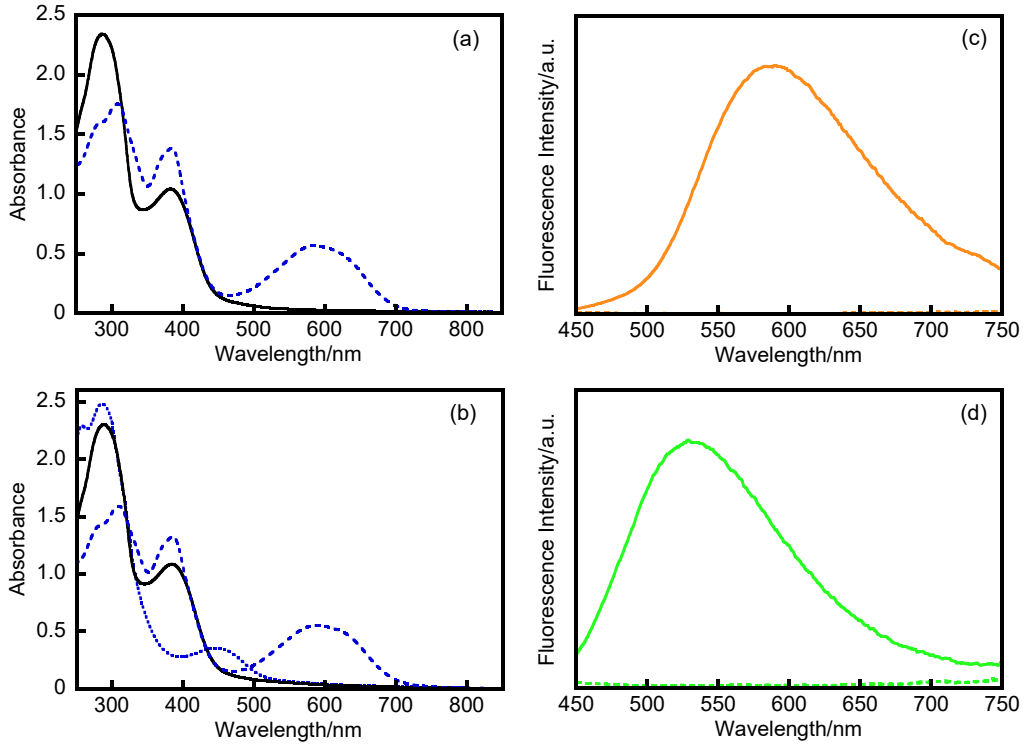

Figure 6-7. Absorption and fluorescence spectra of (a,c) **NP**$_{\mathbf{14a/26a}}$ (**14a**/**26a** = 1:1, d = 107 ± 23 nm) and (b,d) **NP**$_{\mathbf{14b/26a}}$ (**14b**/**26a** = 1:1, d = 175 ± 48 nm) in water/THF (97:3): **14a** and **26a** (solid line), **14b** and **26a** (dotted line), and **14a** and **26** at the PSS upon irradiation with 313 nm light (dashed line). Reprinted with permission from ref 14. Copyright 2018 American Chemical Society.

26b disappeared upon irradiation with visible light. Next, in the initial absorption spectrum of **NP**$_{\mathbf{14b/26a}}$, the absorption band of **14b** was observed around 450 nm. Upon irradiation with visible light, the absorption band disappeared and the band of the photogenerated **14a** (**14a'**) appeared. **14a'** in **NP**$_{\mathbf{14a'/26a}}$ also did not undergo photocyclization reaction, as well as **14a'** in **NP**$_{\mathbf{14a'}}$ upon irradiation with 313 nm light. On the other hand, **26a** underwent the photocyclization reaction upon irradiation with 313 nm. The photocyclization conversions of diarylethene **26a** upon irradiation with 313 nm light were determined to be 83 and 78% for **NP**$_{\mathbf{14a/26a}}$ and **NP**$_{\mathbf{14a'/26a}}$, respectively.

The photochromic properties of **NP**$_{\mathbf{14a/26b}}$ and **NP**$_{\mathbf{14b/26b}}$ (**NP**$_{\mathbf{14a'/26b}}$) were also investigated, as shown in Figures 6-8 and 6-9. They hardly changed in comparison with those of **NP**$_{\mathbf{14a/26a}}$ and **NP**$_{\mathbf{14b/26a}}$ (**NP**$_{\mathbf{14a'/26b}}$). Therefore, it was revealed that the photochromic properties of the double-component nanoparticles can be explained by the summation of those of the single-component nanoparticles.

NP$_{\mathbf{14a/26a}}$ and **NP**$_{\mathbf{14a'/26a}}$ exhibited orange and green fluorescence as shown in Figure 6-7c,d, respectively. The origin of the different color fluorescence between **NP**$_{\mathbf{14a/26a}}$ and **NP**$_{\mathbf{14a'/26a}}$ is the same as that between **NP**$_{\mathbf{14a}}$ and **NP**$_{\mathbf{14a'}}$. The fluorescence intensities quickly decreased upon irradiation with 313 nm light, as shown in Figure 6-10a. The

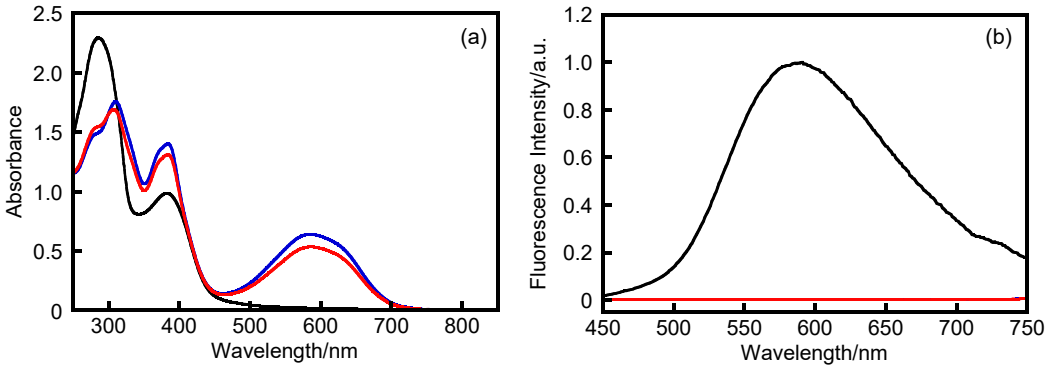

Figure 6-8. (a) Absorption and (b) normalized fluorescence spectra of **NP$_{14a/26b}$** (**14a**:**26b** = 1:1, *d* = 102 ± 24 nm) in water/THF (97:3): **14a** and **26a** (black line), **14a** and **26b** (blue line), and **14a** and **26** at the photostationary state upon irradiation with 313 nm light (red line). Reprinted with permission from ref 14. Copyright 2018 American Chemical Society.

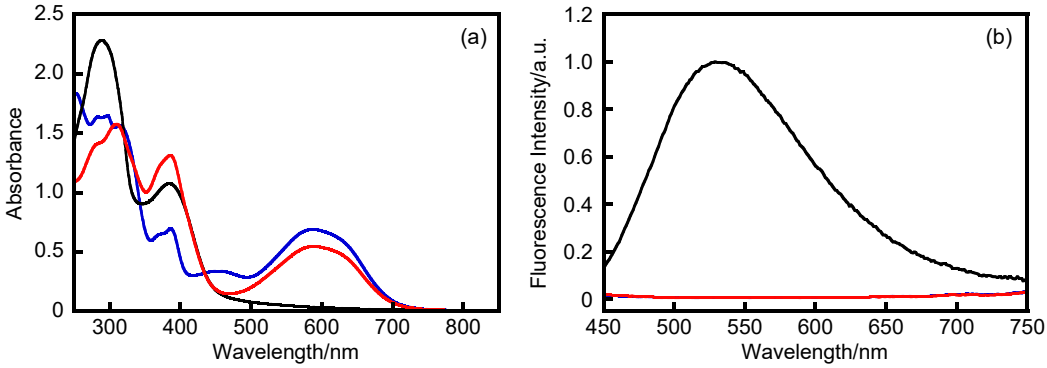

Figure 6-9. (a) Absorption and (b) normalized fluorescence spectra of **NP$_{14b/26b}$** (**14b**:**26b** = 1:1, *d* = 148 ± 32 nm) in water/THF (97:3): **14a** and **26a** (black line), **14b** and **26b** (blue line), and **14a** and **26** at the photostationary state upon irradiation with 313 nm light (red line). Reprinted with permission from ref 14. Copyright 2018 American Chemical Society.

fluorescence was completely quenched at the PSS. This is ascribed to an energy transfer from the excited state **14a** (or **14a'**) to **26b**. Upon irradiation with visible light, the fluorescence intensities returned to their initial ones. Therefore, **NP$_{14a/26a}$** and **NP$_{14a'/26a}$** exhibited the fluorescence on/off switching upon alternating irradiation with UV and visible light. There was no significant difference between **NP$_{14a/26a}$** and **NP$_{14a'/26a}$** in the photocyclization reaction rate. On the other hand, the fluorescence on/off switching of **NP$_{14a/26a}$** was faster than that of **NP$_{14a'/26a}$**. Figure 6-10b shows the relative fluorescence intensity (F/F_0) relative to the photocyclization conversion of **26a**. The F/F_0 values for **NP$_{14a/26a}$** and **NP$_{14a'/26a}$** nonlinearly decreased with the increasing photocyclization conversion of **26a**. This is due to quenching of the excited state energy of a lot of **14a** (or **14a'**) by a single **26b** in the nanoparticles. The fluorescence for **NP$_{14a/26a}$** and **NP$_{14a'/26a}$** was almost quenched when the photocyclization conversion was around 5 and 15%,

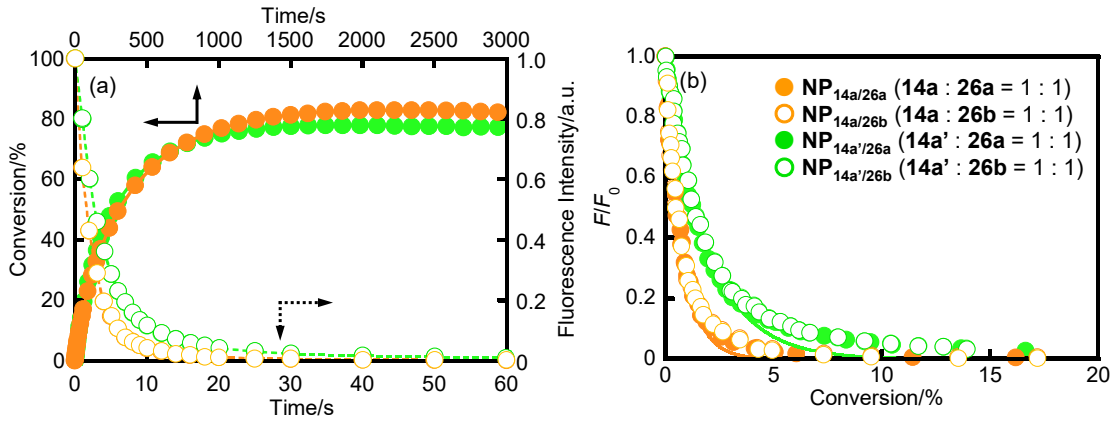

Figure 6-10. (a) Photocyclization conversion and normalized fluorescence intensity excited at 410 nm relative to irradiation time with 313 nm light (0.4 mW cm^{-2}) for **NP$_{14a/26a}$** (**14a**/**26a** = 1:1, d = 131 ± 26 nm) (orange circles) and NP$_{14a'/26a}$ (**14a'**/**26a** = 1:1, d = 167 ± 37 nm) (green circles) in water/THF (97:3). (b) Normalized fluorescence intensity excited at 410 nm relative to the photocyclization conversion for **NP$_{14a/26a}$**, **NP$_{14a/26b}$**, **NP$_{14a'/26a}$**, and **NP$_{14a'/26b}$** in water/THF (97:3). Reprinted with permission from ref 14. Copyright 2018 American Chemical Society.

respectively, which indicates that the number of **14a** quenched by a single **26b** in **NP$_{14a/26a}$** is larger than that in **NP$_{14a'/26a}$**. This is considered to be ascribed to the difference in Förster distance (R_0) between **14a** (or **14a'**) and **26b** in the nanoparticles because the fluorescence on/off switching in this chapter is based on the Förster resonance energy transfer (FRET) from **14a** (or **14a'**) to **26b**.[6] The R_0 value can be described as follows[18]

$$R_0{}^6 = \frac{9Q_0(ln10)\kappa^2 J}{128\pi^5 n^4 N_A} \quad (1)$$

where $Q_0$is the fluorescence quantum yield of donor in the absence of the acceptor, κ^2 is the orientation factor, N_A is the Avogadro constant, and n is the refractive index of the medium. J is an overlap integral and is estimated by using eq 2.

$$J = \int f_D(\lambda)\varepsilon_A(\lambda)\lambda^4 d\lambda \quad (2)$$

where λ is the wavelength of the light, $\varepsilon_A(\lambda)$ is the molar extinction coefficient of the acceptor, and $f_D(\lambda)$ is the normalized fluorescence spectrum of the donor. The R_0 values for **NP$_{14a/26a}$** and **NP$_{14a'/26a}$** were determined to be 4.0 and 3.1 nm, respectively, based on eq 1 using the absorption coefficient of **26b** in THF (λ_{abs} = 587 nm, ε_{abs} = 17800 M^{-1} cm^{-1}) (Figure 6-11), the Φ_f values for **NP$_{14a}$** and **NP$_{14a'}$**, κ^2 = 2/3 of random orientations, and the refractive index of THF. This result indicates that a longer Förster distance results

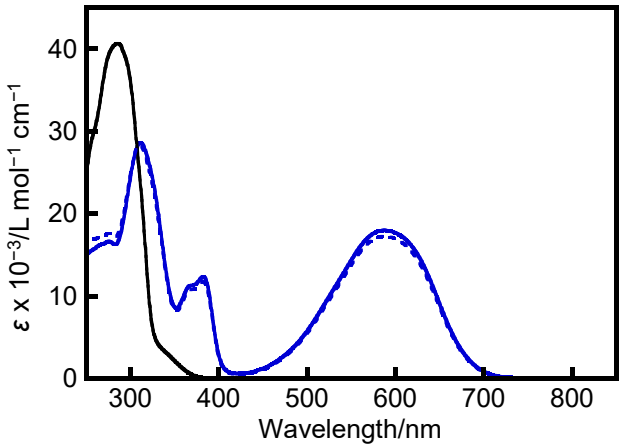

Figure 6-11. Absorption coefficient of **26a** (black solid line), **26b** (blue solid line), and the solution in the photostationary state upon irradiation at 313 nm (dashed line) in THF. Reprinted with permission from ref 14. Copyright 2018 American Chemical Society.

in a larger number of **14a** (or **14a'**) quenched by a single **26b** and the faster fluorescence on/off switching.

Figure 6-12 shows repeating cycles of the fluorescence on/off switching of **NP$_{14a/26a}$** and **NP$_{14a'/26a}$** upon alternating the irradiation with UV and visible light, which could be repeated 50 times although decreases in 38 and 15% of the fluorescence intensity for **NP$_{14a/26a}$** and **NP$_{14a'/26a}$**, respectively, were observed after 50 cycles. To reveal the reason as to why the decrease in the fluorescence intensity of **NP$_{14a/26a}$** was large in comparison with that of **NP$_{14a'/26a}$**, first, the fluorescence intensity changes of **NP$_{14a}$** and **NP$_{14a'}$** upon irradiation with 313 nm light were investigated (Figure 6-13). The fluorescence intensities hardly decreased after irradiation with 313 nm light for 25 min. The result revealed that the reason as to why the fluorescence intensities of **NP$_{14a/26a}$** and **NP$_{14a'/26a}$** decreased upon repeating cycles is not the degradation of **14a** and **14a'**. Next, a stability of **26** was investigated. The absorbance around 285 nm for **NP$_{14a/26a}$**, which is ascribed to **26a**, slightly decreased after 50 repeating cycles (Figure 6-14). In addition, absorbance of **26b** around 580 nm also decreased at the PSS. These results indicate that **26** in **NP$_{14a/26a}$** is degraded upon repeating cycles of the fluorescence on/off switching. A previous study for fatigue resistance of **26** revealed that a photostable byproduct, which has an absorption maximum wavelength at 547 nm, is produced upon repeating the photochromic reactions.[19] The byproduct in the absorption spectra could not be confirmed because the amount of the byproduct produced by repeating the fluorescence on/off switching may be very small. A small amount of byproduct is sufficient to decrease the fluorescence intensity because a large number of the fluorophores are quenched by a single quencher in the nanoparticles. The fact is that the small amount of the byproduct was quenched the

fluorescence of **14a** (or **14a'**) in the nanoparticles was considered. Furthermore, it is considered that the decrease in the fluorescence intensity of $\mathbf{NP_{14a/26a}}$ was large in

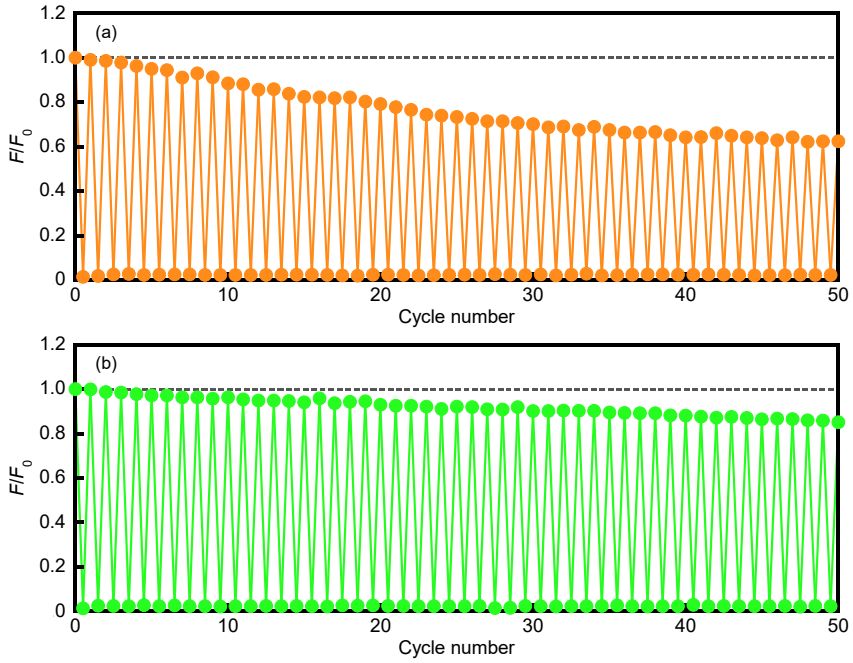

Figure 6-12. Reversible fluorescence on/off switching of (a) $\mathbf{NP_{14a/26a}}$ (**14a**/**26a** = 1:1, d = 131 ± 26 nm) and (b) $\mathbf{NP_{14a'/26a}}$ (**14a'**/**26a** = 1:1, d = 167 ± 37 nm) in water/THF (97:3) upon alternating irradiation with 313 nm light (for 30 s, 0.45 mW cm^{-2} (a) and 60 s, 0.48 mW cm^{-2} (b)) and visible light for 3 min (>500 nm). Reprinted with permission from ref 14. Copyright 2018 American Chemical Society.

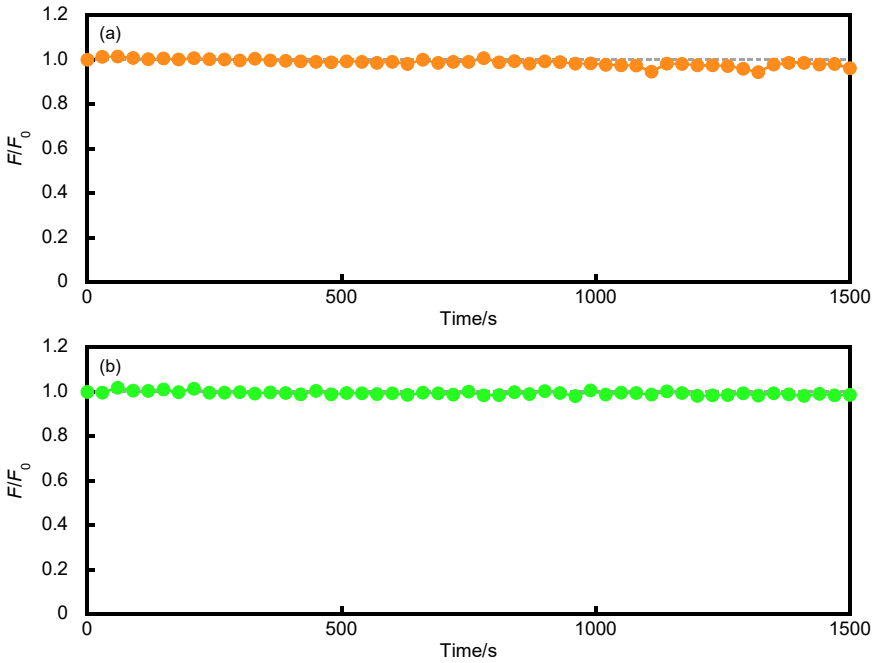

Figure 6-13. Fluorescence intensity changes of (a) $\mathbf{NP_{14a}}$ (d = 71 ± 14 nm) and (b) $\mathbf{NP_{14a'}}$ (d = 145 ± 42 nm) in water/THF (97:3) upon irradiation with 313 nm light (0.47 mWcm^{-2}). Reprinted with permission from ref 14. Copyright 2018 American Chemical Society.

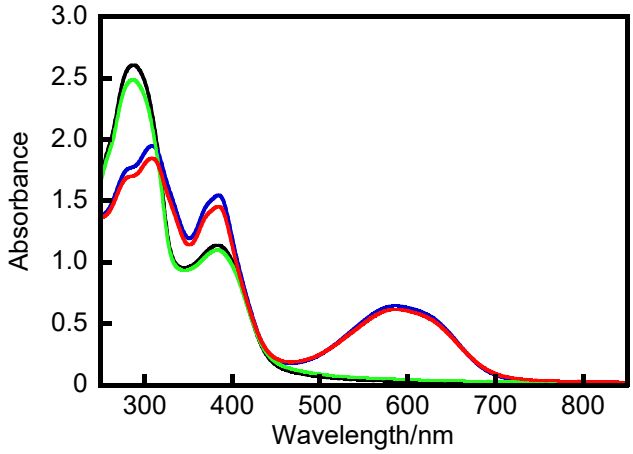

Figure 6-14. Absorption spectra of **NP$_{14a/26a}$** (**14a**:**26a** =1:1, d = 134 ± 44 nm) in water/THF (97:3): **14a** and **26a** before and after 50 cycles of the fluorescence on/off switching (black and green lines), and **14a** and **26** at the photostationary state upon irradiation with 313 nm light before and after 50 cycles of the fluorescence on/off switching (blue and red lines). Reprinted with permission from ref 14. Copyright 2018 American Chemical Society.

comparison with that of **NP$_{14a'/26a}$**, which is because of the high efficiency of energy transfer from **14a** to the byproduct in comparison with that from **14a'** to the byproduct due to the stronger fluorescence of **NP$_{14a/26a}$** in comparison with that of **NP$_{14a'/26a}$**. The fatigue resistance of the fluorescence on/off switching in this chapter is low. However, an important knowledge that it is necessary to select a highly fatigue-resistant diarylethene to improve the fatigue resistance of the fluorescence on/off switching in the aggregated states could be provided.

Next, the dependence of the fluorescence on/off switching properties on the molar fraction of **14** and **26** was investigated. Figures 6-15 and 6-16 show the absorption and fluorescence spectra of **NP$_{14a/26a}$** and **NP$_{14b/26a}$** with various molar fractions of **14** and **26.** All of the nanoparticles underwent reversible photochromism and exhibited the fluorescence on/off switching upon alternating the irradiation with UV and visible light. The change of the F/F_0 value relative to the photocyclization conversion decreased with decreasing molar fraction of **26** as shown in Figure 6-17. In other words, the larger molar fraction of **26** results in the more efficient fluorescence on/off switching properties.

To quantitatively evaluate the dependence of the fluorescence on/off switching of the double-component nanoparticles on Förster distance and molar fraction have been tried. In a previous paper, a simplified model was proposed to quantitatively evaluate the amplified fluorescence on/off switching of the nanoparticles consisting of a diarylethene linked to a benzothiadiazole derivative.[6] This model assumes that the fluorophore is not quenched when all diarylethenes are in their open-ring forms within R_0 and completely

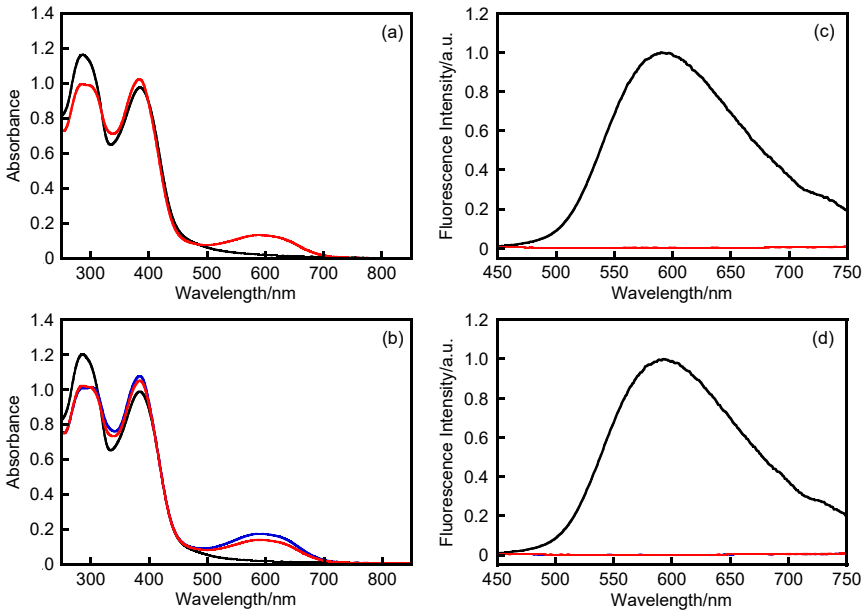

Figure 6-15. Absorption and normalized fluorescence spectra of **NP$_{14a/26a}$** (**14a**:**26a** = 1:0.2, d = 144 ± 23 nm) (a, c) and **NP$_{14a/26b}$** (**14a**:**26b** = 1:0.2, d = 137 ± 26 nm) (b, d) in water/THF (97/3): **14a** and **26a** (black line), **14a** and **26b** (blue line), and **14a** and **26** at the photostationary state upon irradiation with 313 nm light (red line). Reprinted with permission from ref 14. Copyright 2018 American Chemical Society.

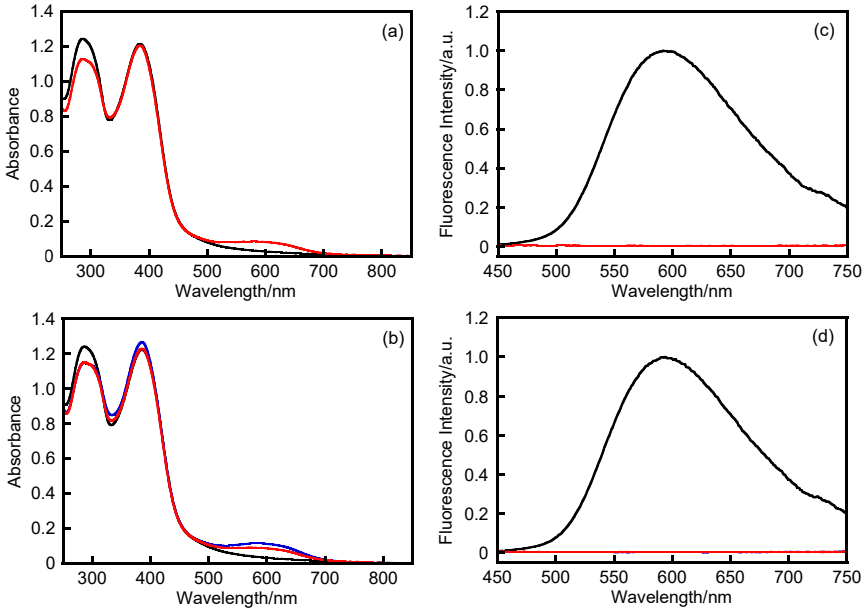

Figure 6-16. Absorption and normalized fluorescence spectra of **NP$_{14a/26a}$** (**14a**:**26a** = 1:0.1, d = 136 ± 18 nm) (a, c) and **NP$_{14a/26b}$** (**14a**:**26b** = 1:0.1, d = 149 ± 31 nm) (b, d) in water/THF (97:3): **14a** and **26a** (black line), **14a** and **26b** (blue line), and **14a** and **26** at the photostationary state upon irradiation with 313 nm light (red line). Reprinted with permission from ref 14. Copyright 2018 American Chemical Society.

quenched in all other cases. In the model, the relative fluorescence intensity (F/F_0) is consistent with $(1 - \alpha_{CF})^n$; where α_{CF} is the photocyclization conversion of diarylethene

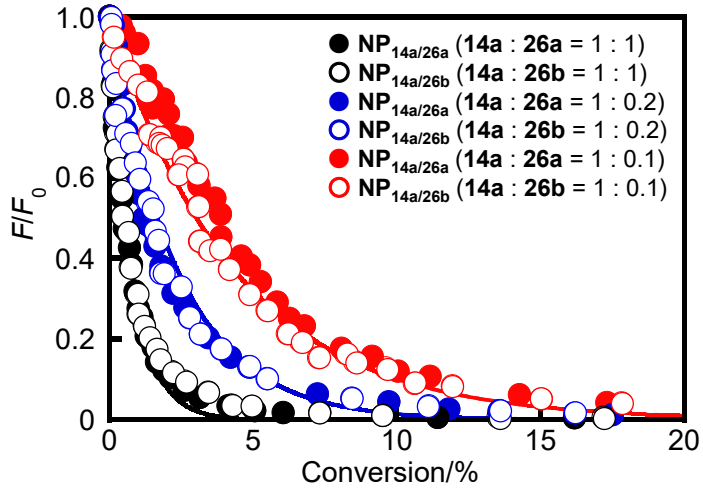

Figure 6-17. Normalized fluorescence intensity excited at 410 nm as a function of the photocyclization conversion of **NP$_{14a/26a}$** in water/THF (97:3). Reprinted with permission from ref 14. Copyright 2018 American Chemical Society.

and n is the number of molecules within R_0. There are two types of molecules, that is, diarylethene open- and closed-ring forms in the model. On the other hand, in this chapter, there are three types of molecules, that is, diarylethenes **14a** (or **14a'**), **26a**, and **26b** at arbitrary ratio in the nanoparticles. Therefore, the model cannot be directly used for the nanoparticles in this chapter. Here, to quantitatively evaluate the dependence of the fluorescence on/off switching of the nanoparticles on Förster distance and molar fraction, the model was modified as follows

$$F/F_0 = (1 - \beta\alpha_{CF})^n \quad (3)$$

where β is molar fraction of diarylethene **26** in the nanoparticles and $(1 - \beta\alpha_{CF})$ is the probability that a molecule in the nanoparticle is not **26b**. The fitted curve based on eq 3 matched the experimental data for **NP$_{14a/26a}$** and **NP$_{14a/26b}$** when the n value was 250, as shown in Figure 6-10b. Therefore, when the molar fraction of **14** and **26** in **NP$_{14a/26a}$** and **NP$_{14a/26b}$** is the same ($\beta = 0.5$), a single **26b** quenched around 125 molecules of **14a** ($= n \times (1 - \beta)$) in the initial fluorescence quenching process. On the other hand, the n value was estimated to be 105 for **NP$_{14a'/26a}$** and **NP$_{14a'/26b}$**, which is smaller than that in **NP$_{14a/26a}$** and **NP$_{14a/26b}$**. Therefore, the fluorescence on/off switching speed of **NP$_{14a/26a}$** and **NP$_{14a/26b}$** is faster than that of **NP$_{14a'/26a}$** and **NP$_{14a'/26b}$** because the number of **14a** quenched by a single **26b** in **NP$_{14a/26a}$** and **NP$_{14a/26b}$** is ca. 2.4 times larger than that in **NP$_{14a'/26a}$** and **NP$_{14a'/26b}$** because of the longer Förster distance. Therefore, the multicolor fluorescence properties of **14a** in the nanoparticles revealed the dependence of the

fluorescence on/off switching of the nanoparticles on Förster distance. Here, it was hypothesized that the density of the nanoparticles is the same as that in the crystalline phase of **14** and **26** (≈1.4 g cm^{-3}), and the nanoparticles are evenly space distributed spheres. By using these hypotheses and the *n* values, the distances that **26b** can quench **14a** (or **14a'**) were calculated to be 3.3 and 2.5 nm for $\mathbf{NP_{14a/26a}}$ (and $\mathbf{NP_{14a/26b}}$) and $\mathbf{NP_{14a'/26a}}$ (and $\mathbf{NP_{14a'/26b}}$), respectively. The values are close to the R_0 values calculated by the Förster equation. This result indicates that the fluorescence on/off switching of the nanoparticles is mainly based on FRET process from **14a** (or **14a'**) to **26b** although various energy-transfer processes, such as FRET, Dexter-type energy transfer, and energy migration, may contribute to the fluorescence quenching because the distance between the molecules is short enough to cause the energy-transfer processes.

FRET efficiency depends on the distance between a donor and an acceptor.[18] However, we used eq 3 for the fluorescence on/off switching analysis of the nanoparticles because it is difficult to make the model in consideration with the distance dependence. To determine if it is appropriate to use the model for the analysis, the fluorescence lifetimes of $\mathbf{NP_{14a/26a}}$ at various photocyclization conversions were measured (Figure 6-18). $\mathbf{NP_{14a/26a}}$ exhibited fluorescence decay with multiple components as well as $\mathbf{NP_{14a}}$ (Table 6-2). The average fluorescence lifetime (τ_{ave}) values, which were calculated from these values according to $\tau_{ave} = \Sigma(\tau_i \times \%)$, decreased with increasing photocyclization conversion. However, the change was much smaller in comparison with that of the fluorescence intensity. This result indicates that **26b** almost quenched the fluorescence of **14a** within R_0 in the nanoparticles and is close to the assumption in the model. Therefore,

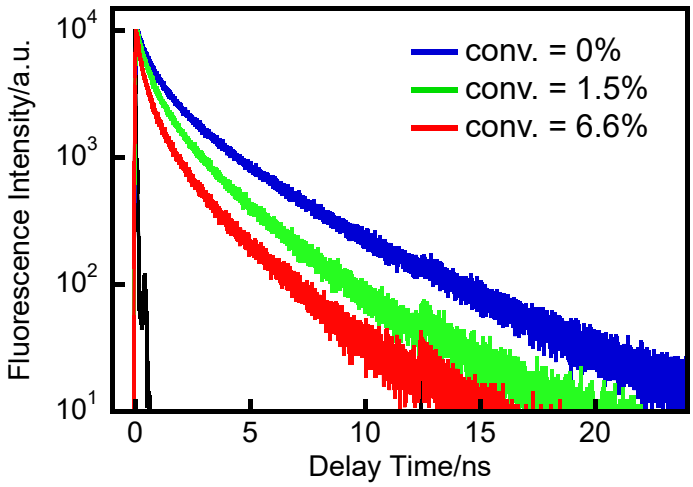

Figure 6-18. Fluorescence decay curve of $\mathbf{NP_{14a/26a}}$ (**14a**:**26a** = 1:1, *d* = 134 ± 44 nm) at various photocyclization conversion (conv.) monitored at 600 nm in water/THF (97:3). Reprinted with permission from ref 14. Copyright 2018 American Chemical Society.

Table 6-2. Fluorescence lifetimes of $\mathbf{NP_{14a/26a}}$ (**14a**:**26a** = 1:1, d = 134 ± 44 nm) at various photocyclization conversions (conv.).[a] Reprinted with permission from ref 14. Copyright 2018 American Chemical Society.

conv.	τ_1/ns	τ_2/ns	τ_3/ns	τ_4/ns	τ_{ave}/ns	χ^2
0%	0.24 (37%)	0.81 (30%)	2.4 (24%)	5.4 (9%)	1.39	1.13
1.5%	0.14 (28%)	0.41 (36%)	1.3 (26%)	3.6 (10%)	0.88	1.15
6.6%	0.046 (38%)	0.26 (36%)	0.96 (19%)	3.0 (7%)	0.50	1.15

a) Excited at 400 nm and monitored at 600 nm.

it was concluded that it is available to use the modified model for the fluorescence on/off switching analysis of the nanoparticles.

In addition, the fitting curves calculated by eq 3 could match the all-experimental data of $\mathbf{NP_{14a/26a}}$ and $\mathbf{NP_{14a/26b}}$ at various molar fractions of **14** and **26** when the n value was constant at 250 and the β value was changed, as shown in Figure 6-17. Therefore, when molar fraction (β) for **26** was 0.5, 0.17, and 0.091, the number of **14a** quenched by a single **26b** was 125, 208, and 227, respectively, in the initial fluorescence-quenching process. This number increased with the decreasing molar fraction of **26**. This is because the probability that other **26b** molecules are present around **26b** decreases with the decreasing molar fraction of **26**. However, the change of the F/F_0 value relative to the photocyclization conversion increased with the increasing molar fraction of **26** as mentioned above. Therefore, a larger number of quencher, that is, **26b**, leads to improve the apparent fluorescence on/off switching properties of the nanoparticles. However, in the case of single molecule in the nanoparticles, the opposite trend was observed. Thus, there is a trade-off relationship between the fluorescence on/off switching properties of the whole nanoparticle solution and the number of **14a** quenched by a single **26b** in the nanoparticles. As a result, the dependence of the fluorescence on/off switching properties of the double-component nanoparticles consisting of **14** and **26** on Förster distance and molar fraction could be quantitatively evaluated by using the modified model. It was considered that **14a** can be replaced by other simple fluorophore if the fluorophore is hydrophobic based on the results in this work. This convenient system with highly efficient fluorescence on/ off switching properties will lead to the development of the fluorescence on/off switchable system and great contribution to the applications.

6.4 Summary

Single- and double-component nanoparticles consisting of diarylethenes **14** and/or **26** were fabricated to develop a convenient system with highly efficient fluorescence

on/off switching properties. The nanoparticles consisting of **14a** exhibited orange fluorescence with Φ_f = 0.20. On the other hand, the nanoparticles consisting of **14b** exhibited no fluorescence, and green fluorescence was observed with Φ_f = 0.05 after irradiation with visible light. It was revealed that the nanoparticles consisting of **14** exhibited multicolor fluorescence depending on the fabrication conditions of the nanoparticles. Moreover, **26** underwent reversible photochromic reactions upon alternating irradiation with UV and visible light in the nanoparticle state. The double-component nanoparticles consisting of **14** and **26** exhibited the fluorescence on/off switching with rapid switching speed and high on/off contrast upon alternating irradiation with UV and visible light. In addition, the fluorescence on/off switching properties of the nanoparticles depended on molar fractions of **14** and **26**, which is ascribed to the Förster distance. The longer Förster distance and larger molar fraction of **26** improved the fluorescence on/off switching properties, which was supported by a simplified model. As a result, to construct the convenient and highly efficient fluorescence on/off switchable system using the double component nanoparticles consisting of two types of diarylethenes was accomplished.

6.5 References

[1] M. Irie, T. Fukaminato, K. Matsuda, S. Kobatake, *Chem. Rev.* **2014**, *114*, 12174-12277.

[2] a) T. Kawai, T. Sasaki, M. Irie, *Chem. Commun.* **2001**, 711-712; b) H. Tian, B. Z. Chen, H. Y. Tu, K. Mullen, *Adv. Mater.* **2002**, *14*, 918-923; c) W. J. Tan, X. Li, J. J. Zhang, H. Tian, *Dyes Pigm.* **2011**, *89*, 260-265.

[3] a) Q. Zou, X. Li, J. J. Zhang, J. Zhou, B. B. Sun, H. Tian, *Chem. Commun.* **2012**, *48*, 2095-2097; b) C. Zhang, S. Pu, Z. Sun, C. Fan, G. Liu, *J. Phys. Chem. B* **2015**, *119*, 4673-4682; c) S. Y. Huang, Z. Y. Li, S. S. Li, J. Yin, S. H. Liu, *Dyes Pigm.* **2012**, *92*, 961-966.

[4] a) Y. Arai, S. Ito, H. Fujita, Y. Yoneda, T. Kaji, S. Takei, R. Kashihara, M. Morimoto, M. Irie, H. Miyasaka, *Chem. Commun.* **2017**, *53*, 4066-4069; b) B. Roubinet, M. L. Bossi, P. Alt, M. Leutenegger, H. Shojaei, S. Schnorrenberg, S. Nizamov, M. Irie, V. N. Belov, S. W. Hell, *Angew. Chem. Int. Ed.* **2016**, *55*, 15429-15433; c) B. Roubinet, M. Weber, H. Shojaei, M. Bates, M. L. Bossi, V. N. Belov, M. Irie, S. W. Hell, *J. Am. Chem. Soc.* **2017**, *139*, 6611-6620; d) C. Li, H. Yan, L. X. Zhao, G. F. Zhang, Z. Hu, Z. L. Huang, M. Q. Zhu, *Nat. Commun.* **2014**, *5*, 5709.

[5] a) T. Fukaminato, S. Kobatake, T. Kawai, M. Irie, *Proc. Japan Acad., Ser. B* **2001**, *77*, 30-35; b) C. C. Corredor, Z. L. Huang, K. D. Belfield, *Adv. Mater.* **2006**, *18*,

2910-2914; c) C. C. Corredor, Z. L. Huang, K. D. Belfield, A. R. Morales, M. V. Bondar, *Chem. Mater.* **2007**, *19*, 5165-5173; d) C. Yun, J. You, J. Kim, J. Huh, E. Kim, *J. Photochem. Photobiol. C* **2009**, *10*, 111-129; e) T. Fukaminato, T. Doi, N. Tamaoki, K. Okuno, Y. Ishibashi, H. Miyasaka, M. Irie, *J. Am. Chem. Soc.* **2011**, *133*, 4984-4990; f) M. Irie, T. Fukaminato, T. Sasaki, N. Tamai, T. Kawai, *Nature* **2002**, *420*, 759-760.

[6] J. Su, T. Fukaminato, J. P. Placial, T. Onodera, R. Suzuki, H. Oikawa, A. Brosseau, F. Brisset, R. Pansu, K. Nakatani, R. Métivier, *Angew. Chem. Int. Ed.* **2016**, *55*, 3662-3666.

[7] a) J. Bu, K. Watanabe, H. Hayasaka, K. Akagi, *Nat. Commun.* **2014**, *5*, 3799; b) H. Hayasaka, K. Tamura, K. Akagi, *Macromolecules* **2008**, *41*, 2341-2346; c) H. Hayasaka, T. Miyashita, K. Tamura, K. Akagi, *Adv. Funct. Mater.* **2010**, *20*, 1243-1250.

[8] J. Folling, S. Polyakova, V. Belov, A. van Blaaderen, M. L. Bossi, S. W. Hell, *Small* **2008**, *4*, 134-142.

[9] a) S. J. Lim, B. K. An, S. D. Jung, M. A. Chung, S. Y. Park, *Angew. Chem. Int. Ed.* **2004**, *43*, 6346-6350; b) S. Ishida, T. Fukaminato, D. Kitagawa, S. Kobatake, S. Kim, T. Ogata, S. Kurihara, *Chem. Commun.* **2017**, *53*, 8268-8271 ; c) S. Ishida, T. Fukaminato, S. Kim, T. Ogata, S. Kurihara, *Chem. Lett.* **2017**, *46*, 1182-1185.

[10] K. Uchida, T. Matsuoka, S. Kobatake, T. Yamaguchi, M. Irie, *Tetrahedron* **2001**, *57*, 4559-4565.

[11] D. Kitagawa, T. Nakahama, K. Mutoh, Y. Kobayashi, J. Abe, H. Sotome, S. Ito, H. Miyasaka, S. Kobatake, *Dyes Pigm.* **2017**, *139*, 233-238.

[12] T. Nakahama, D. Kitagawa, H. Sotome, S. Ito, H. Miyasaka, S. Kobatake, *Bull. Chem. Soc. Jpn.* **2018**, *91*, 153-157.

[13] M. Irie, T. Lifka, S. Kobatake, N. Kato, *J. Am. Chem. Soc.* **2000**, *122*, 4871-4876.

[14] T. Nakahama, D. Kitagawa, H. Sotome, T. Fukaminato, S. Ito, H. Miyasaka, S. Kobatake, *ACS Omega* **2018**, *3*, 2374-2382.

[15] Y. Nagasawa, T. Itoh, M. Yasuda, Y. Ishibashi, S. Ito, H. Miyasaka, *J. Phys. Chem. B* **2008**, *112*, 15758-15765.

[16] K. Hitoshi, N. Hari Singh, O. Hidetoshi, O. Shuji, M. Hiro, M. Nobutsugu, K. Atsushi, O. Katsumichi, M. Akio, N. Hachiro, *Jpn. J. Appl. Phys.* **1992**, *31*, L1132.

[17] a) N. Tagawa, A. Masuhara, H. Kasai, H. Nakanishi, H. Oikawa, *Mol. Cryst. Liq. Cryst.* **2010**, *520*, 521-526; b) N. Tagawa, A. Masuhara, H. Kasai, H. Nakanishi, H. Oikawa, *Cryst. Growth Des.* **2010**, *10*, 2857-2859.

[18] I. L. Medintz, N. Hildebrandt, *FRET-Förster Resonance Energy Transfer: From*

Theory to Applications, John Wiley & Sons, **2013**.

[19] M. Irie, T. Lifka, K. Uchida, S. Kobatake, Y. Shindo, *Chem. Commun.* **1999**, 747-748.

Conclusions

In this thesis, the construction of novel molecular system designs for the highly efficient fluorescence on/off switching using diarylethenes and fluorophores, and the synthesis of novel fluorophores suitable for the molecular systems were described. General Introduction described the backgrounds of the photochromic and fluorescence properties of the diarylethene derivatives and the scope of this thesis.

In Chapter 1, the optical properties and solvatofluorochromism of the fluorene derivatives bearing phenylthiophene or benzothiophene, and their *S*,*S*-dioxidized compounds were investigated. The fluorene derivatives bearing phenylthiophene or benzothiophene exhibited blue fluorescence with the fluorescence quantum yields of 0.6-0.7. The fluorescence spectra of the fluorene derivatives bearing *S*,*S*-dioxidized thiophene or benzothiopehene ring at one side were red-shifted by increasing the solvent polarity. The fluorene derivatives bearing phenylthiophene at both sides show the highest fluorescence quantum yield among the fluorene derivatives synthesized in this chapter at all solvents.

In Chapter 2, the fluorescence on/off switching properties of a diarylethene-fluorene dyad connected by an ester bond and random and alternative copolymers bearing diarylethene and fluorene moieties in their side chains were investigated. The alternative copolymer showed the high fluorescence on/off contrast and rapid switching speed compared with the dyad and random copolymer bearing the diarylethene and the fluorene moieties at the same ratio. In addition, the fluorescence on/off switching properties, such as the switching speed and fluorescence on/off contrast, of the random copolymers were improved by increasing the molar fraction of the diarylethene moiety in the copolymer. It was revealed that the effects of monomer sequence and ratio for the fluorescence on/off switching properties in the polymers bearing the diarylethene and the fluorophore in their side chains.

In Chapter 3, the polymorphism and the phase transition for crystal of 1,2-bis(3-methyl-5-phenyl-2-thienyl)perfluorocyclopentene were described. The diarylethene has two polymorphic forms, α- and β-crystals, which show strong emission as compared with in *n*-hexane solution. A new molecular skeleton of diarylethenes that work as luminescent solid-state materials was found. Furthermore, the polymorphic phase transition from β-crystal to α-crystal was found and the phase transition process was directly observed by fluorescence color change.

In Chapter 4, the change in the solid-state luminescence of the crystal of the diarylethene closed-ring isomer induced by irradiation with visible light was described.

Crystals consisting of the closed-ring isomer underwent a photochemical ring-opening reaction accompanying crystal fragmentation upon irradiation with visible light. The open-ring form crystal produced by the ring-opening reaction exhibited green fluorescence, whereas open-ring form crystals produced by recrystallization exhibit orange or yellow fluorescence depending on the polymorphic forms. It was revealed that the open-ring form exhibits different fluorescence colors depending on the intermolecular interaction in different states.

In Chapter 5, the fluorescence properties of 1,2-bis(3-methyl-5-(4-alkylphenyl)-2-thienyl)perfluorocyclopentenes having methyl, ethyl, *n*-propyl, and *n*-butyl substituents at the *p*-position of phenyl rings were investigated in the solid states. The diarylethenes in the crystalline phase exhibited strong fluorescence with relatively high fluorescence quantum yields of 0.12-0.20 compared with those in the amorphous phase, which indicates that the diarylethenes have crystallization-induced emission (CIE) characteristics. The diarylethene having a methyl group as the alkyl chain exhibited the strongest emission among the diarylethenes that were synthesized in this chapter. It was found that the amorphous solid of the diarylethene having methyl group was crystallized after mechanical scratching followed by heating at 90 °C. The reversible fluorescence recording based on CIE characteristics and mechanical scratching and heating induced crystallization was successfully demonstrated.

In Chapter 6, the fluorescence on/off switching properties of nanoparticles consisting of two types of diarylethenes, 1,2-bis(3-methyl-5-phenyl-2-thienyl)perfluoro-cyclopentene (***i*DE**) and 1,2-bis(2-methyl-5-phenyl-3-thienyl)-perfluorocyclopentene (***n*DE**), fabricated by a reprecipitation method were described. Nanoparticles consisting of ***i*DE** exhibited orange or green fluorescence depending on the fabrication condition and did not undergo any photocyclization reaction. On the other hand, nanoparticles consisting of ***n*DE** underwent photoreversible photochromic reactions upon alternating irradiation with ultraviolet and visible light. Nanoparticles consisting of ***i*DE** and ***n*DE** exhibited fluorescence on/off switching with rapid switching speed and high on/off contrast, accompanying the photochromic reactions of ***n*DE**. The dependence of fluorescence on/off switching properties on Förster distance and the molar fraction was observed and quantitatively evaluated by a simplified model. To contract the molecular system produced by a simple and convenient method with highly efficient fluorescence on/off switching properties was accomplished.

List of Publications

1 Optical Properties and Solvatofluorochromism of Fluorene Derivatives Bearing *S*,*S*-Dioxidized Thiophene
T. Nakahama, D. Kitagawa, H. Sotome, S. Ito, H. Miyasaka, S. Kobatake
Photochem. Photobiol. Sci., **2016**, *15*, 1254-1263.

---------- Chapter 1

2 Fluorescence On/Off Switching in Polymers Bearing Diarylethene and Fluorene in Their Side Chains
T. Nakahama, D. Kitagawa, H. Sotome, S. Ito, H. Miyasaka, S. Kobatake
J. Phys. Chem. C, **2017**, *121*, 6272-6281.

---------- Chapter 2

3 Polymorphs of a Diarylethene that Exhibits Strong Emission and Direct Visualization of Polymorphic Phase Transition Process by Fluorescence Color Change
D. Kitagawa, T. Nakahama, K. Mutoh, Y. Kobayashi, J. Abe, H. Sotome, S. Ito, H. Miyasaka, S. Kobatake
Dyes Pigm., **2017**, *139*, 233-238.

---------- Chapter 3

4 Solid-State Fluorescence Behavior Induced by Photochemical Ring-Opening Reaction of 1,2-Bis(3-methyl-5-phenyl-2-thienyl)perfluorocyclopentene
T. Nakahama, D. Kitagawa, H. Sotome, S. Ito, H. Miyasaka, S. Kobatake
Bull. Chem. Soc. Jpn., **2018**, *91*, 153-157.

---------- Chapter 4

5 Crystallization-Induced Emission of 1,2-Bis(3-methyl-5-(4-alkylphenyl)-2-thienyl)-perfluorocyclopentenes: A Mechanical and Thermal Recording System
T. Nakahama, D. Kitagawa, H. Sotome, S. Ito, H. Miyasaka, S. Kobatake
Dyes Pigm., **2019**, *160*, 450-456.

---------- Chapter 5

6 Fluorescence On/Off Switching in Nanoparticles Consisting of Two Types of Diarylethenes
T. Nakahama, D. Kitagawa, H. Sotome, T. Fukaminato, S. Ito, H. Miyasaka, S.

Kobatake
ACS Omega, **2018**, *3*, 2374-2382.

---------- Chapter 6

Acknowledgments

This thesis work was carried out during the academic years from 2014 to 2018 at Department of Applied Chemistry and Bioengineering, Graduate School of Engineering, Osaka City University. The author is sincerely grateful to Prof. Dr. Seiya Kobatake for his kind direction, helpful suggestion, and cordial consistent encouragement throughout this work.

The author would like to express his deep gratitude to Prof. Dr. Yusuke Yamada and Prof. Dr. Noritsugu Kometani for careful review of this thesis and fruitful suggestion.

The author would like to show his great appreciation to Prof. Dr. Hiroshi Miyasaka, Associate Prof. Dr. Syoji Ito, and Assistant Prof. Dr. Hikaru Sotome at Osaka University for their helpful advice, valuable discussion and collaboration to fluorescence lifetime measurement in Chapters 1-6.

The author would like to offer his special thanks to Prof. Dr. Jiro Abe, Assistant Prof. Dr. Katsuya Mutoh at Aoyama Gakuin University, and Associate Prof. Dr. Yoichi Kobayashi at Ritsumeikan University (in Chapter 3), and Associate Prof. Dr. Tuyoshi Fukaminato at Kumamoto University (in Chapter 6) for their helpful advice, grateful cooperation, and valuable discussion.

The author would like to express the deepest appreciation to Assistant Prof. Dr. Daichi Kitagawa at Osaka City University for his helpful discussion and experimental supports in his Ph. D. course.

The author would like to appreciate Research Fellowship for Young Scientists, Japan Society for the Promotion of Science.

The author also wishes his deep gratitude to all staffs in Department of Applied Chemistry and Bioengineering for their teaching as a useful basis of this thesis work and to all colleagues and graduates in Kobatake Laboratory at Osaka City University for their collaborations, kind help, and friendship.

Finally, the author, Tatsumoto Nakahama, expresses his special thanks to his parents, relatives, and all his friends for their grateful understanding, care, and encouragement.

March 2019

Tatsumoto Nakahama